



KATHOLIEKE UNIVERSITEIT
LEUVEN

Arenberg Doctoral School of Science, Engineering & Technology
Faculty of Engineering
Department of Mechanical Engineering

Dynamic thermal behaviour of buildings with concrete core activation

Maarten SOURBRON

Dissertation presented in partial
fulfilment of the requirements for
the degree of Doctor
in Engineering

September 2012

Dynamic thermal behaviour of buildings with concrete core activation

Maarten SOURBRON

Jury:

Prof. dr. ir. P. Verbaeten, chair

Prof. dr. ir. L. Helsen, promotor

Prof. dr. ir. M. Baelmans, co-promotor

Prof. dr. ir. J. Swevers

Prof. dr. ir. D. Saelens

ing. W. Van Passel

Prof. dr. ir. W. Stephan

(Georg-Simon-Ohm-Hochschule Nürnberg)

Prof. dr. ir. B.W. Olesen

(Technical University of Denmark)

Dissertation presented in partial
fulfilment of the requirements for
the degree of Doctor
in Engineering

September 2012

© Katholieke Universiteit Leuven – Faculty of Engineering
Celestijnenlaan 300A box 2421, B-3001 Heverlee (Belgium)

Alle rechten voorbehouden. Niets uit deze uitgave mag worden vermenigvuldigd en/of openbaar gemaakt worden door middel van druk, fotocopie, microfilm, elektronisch of op welke andere wijze ook zonder voorafgaande schriftelijke toestemming van de uitgever.

All rights reserved. No part of the publication may be reproduced in any form by print, photoprint, microfilm or any other means without written permission from the publisher.

D/2012/7515/106
ISBN 978-94-6018-572-4

Voorwoord

24 juni 2012: Lonesome George is gestorven en een diersoort is uitgestorven. De reuzenschildpad Lonesome George en zijn voorouders hadden een oplossing bedacht om aan de bladeren van bomen te geraken. Zij hadden namelijk de pech dat er op hun Galapagoseiland weinig op de bodem groeide, in tegenstelling tot bij hun collega's van naburige eilanden. Ze ontwikkelden daarom een lange nek en hoge poten. Hoe deden ze dat? Lang wachten en generatie na generatie zichzelf verbeteren. Schildpadden hebben tijd, maar ze verliezen ook geen tijd. Pech voor hen dat er zeevaarders langskwamen die eten nodig hadden voor hun terugreis. Frappant detail over George: "Scientists thought they still had plenty of time to make George providing offspring, because he was assumed to live for at least another 50 years". Ze hadden beter minder hun tijd genomen en nog meer energie aangewend om George aan het paren te krijgen.

Om het energieprobleem op te lossen, lijken we vreemd genoeg dezelfde kortzichtige redenering te volgen als de oppassers van George: we hebben nog tijd. Prof. Boroditsky legt uit dat de meeste mensen op deze wereldbol tijd bekijken ten opzichte van zichzelf: van links naar rechts in onze contreien, op andere plaatsen in de wereld van rechts naar links of van voor naar achter, maar altijd ten opzichte van zichzelf. Misschien moeten we leren om naar tijd te kijken zoals de Pormpuraaw, een aboriginal gemeenschap in Australië: van oost naar west, ongeacht van hoe je staat. Dat zou ons ongetwijfeld een heel ander beeld laten zien. Als schildpadden een lange nek kunnen ontwikkelen, kunnen wij toch wel een energieprobleem oplossen, niet?

Tijd is een vreemd iets, je denkt altijd dat er nog is, maar uiteindelijk is er altijd te weinig (voor mij toch).

Het is in ieder geval nu tijd om een aantal mensen te bedanken die bijgedragen hebben tot dit doctoraat.

Prof. Tine Baelmans en prof. Lieve Helsen, jullie hebben mij de kans geboden om dit doctoraat te starten. Ik besef maar al te goed de waarde hiervan.

Lieve, je doorzettingsvermogen werkt bijzonder aanstekelijk, maar vooral je zin voor verantwoordelijkheid zal ik altijd blijven onthouden. En ondanks al dat vele en harde werk, ook soms in moeilijke omstandigheden, blijf je aandacht hebben voor de persoon in de mensen rondom jou. Het was een plezier om mee te werken in de beginfase van je jonge onderzoeksgroep. Het blijven zoeken tot een figuur of een titel van een artikel echt goed zit, dat ene legendarische conference diner, dat zijn de kleine, maar aangename momenten die ik meeneem. En ik zet nooit meer een spatie voor een dubbele punt!

Tine, ook al werd onze samenwerking minder intens in de loop van het doctoraat, jouw interventies bleven uiterst waardevol en ik verbaasde me telkens weer over de snelheid waarmee je een voorliggend probleem begreep en meedacht naar oplossingen.

In 1999 introduceerden Willy Van Passel en Patrick Van Rymenant me in de wereld van onderzoek naar duurzame energiesystemen. Samen met Kurt Steendam hebben we de jaren daarna mooie onderzoeksresultaten neergezet. Willy, jouw aanvoelen voor wat relevant is in de wereld van de thermotechniek en de mensen die erin rondlopen, heeft mij tot op dit punt gebracht.

Raf en Toon, en ook de andere De Nayer-collega's, jullie hebben met het Thermac-project mee de basis gelegd voor dit doctoraatswerk.

Beste eindwerkstudenten die ik begeleid heb, ook voor jullie een speciaal woordje, want jullie waren vaak mijn volgende horde al aan het verkennen.

Mijn collega's op TME moet ik bedanken voor de fijne en open sfeer die er altijd hangt. Via De Nayer ben ik geleidelijk aan TME binnengeslopen, misschien tot verbazing van een enkeling, maar vooral ben ik in een aangename groep terecht gekomen. Ik bedank mijn bureaugenoten, eerst Tine en dan 'beneden' Filip, Bart, Maarten, Asim, Vladimir, Joris en Tom met de interessante discussies over cultuurverschillen tussen mensen. Ook de Sysi's, Clara, Stefan, Jan, Dieter en Roel, wil ik speciaal vermelden voor de gezamenlijke, maar vooral ook gezellige aanpak van onze wetenschappelijke problemen. Clara, zonder onze behoorlijk intensieve samenwerking ten tijde van de 'Montreal paper', zou m'n doctoraatstekst niet zijn wat het nu is. Moeten er nog koekjes zijn?!

Ivo en Hans, jullie wil ik zeker en vast bedanken voor alle technische ondersteuning. Ivo, het heeft veel zweet gekost en bij momenten ook heel wat lenigheid gevraagd om de testkamer te bouwen. Maar zonder die hulp, daar moet ik eerlijk in zijn, zou er geen testkamer zijn. Ook Chris Vrancken en Gert De Wandeleer dank ik voor het aanleveren van materiaal. En zeker Rudy Vanderheyden, bedankt voor je enthousiaste medewerking, want het is dankzij jouw expertise dat ik de regeling van de testkamer heb kunnen opbouwen.

Ik dank mijn juryleden, prof. Olesen, prof. Stephan, prof. Saelens, prof. Swevers en Willy Van Passel voor het nalezen en becommentariëren van mijn toch wel lijvige tekst. Het geeft een aanzienlijke meerwaarde aan het resultaat. Ook Kathleen en Frieda, jullie houden de boel echt wel draaiende met een ogenschijnlijk gemak waar ik soms toch wel van sta te kijken. En Jan, ik heb nog altijd geen IT-probleem ontdekt dat niet in een handomdraai opgelost was.

Mama, papa, bedankt. Jullie brachten me tot waar ik nu sta, wat een verre van vanzelfsprekende opdracht is, dat kan ik nu ook zelf ten volle ondervinden.

Familie, schoonfamilie en vrienden, van Geste tot de RotteBolstraat: dat af en toe informeren naar de stand van zaken is echt wel fijn, ook al volgde er tegen het einde vaak een blik van “Is dat nu nog altijd niet af?”

En dan zijn er nog die vier andere vrouwen, daar op een tiental kilometer ofwel een half uur fietsen van Heverlee verwijderd. Kaat, Hanne en Lena, ik vind het fantastisch dat jullie er zijn. Hoe heerlijk relatief is alles toch als ik thuiskom of jullie oppik op school.

En Marleen, m'n fantastische vrouw, zonder jou was dit echt allemaal niet gelukt. Bedankt voor alle vanzelfsprekendheden die dat zeker niet altijd waren, en om de zetel in de living te verkiezen boven ons bed ver weg om in slaap te vallen terwijl ik zat te werken. Lj.

Abstract

When using Concrete Core Activation (CCA), the thermal mass of a building is actively heated or cooled. Water tubes are embedded in a concrete slab of a building zone and condition the core of this slab. In office buildings, which are addressed in this work, CCA generally refers to the floor and ceiling slab.

In this work, the dynamic thermal behaviour of CCA integrated in a building is analysed and guidelines for the design of a CCA controller are derived. Combined operation with an additional fast reacting system, such as the air handling unit, is investigated. Furthermore, simplified dynamic thermal models of CCA and of a CCA-building are developed and used in a building controller.

CCA operates with moderate water supply temperatures: $< 30^{\circ}C$ for heating and $> 15^{\circ}C$ for cooling. Moreover, the large thermal capacity can be used to shift CCA operation to time periods when heat and cold production is most energy (or cost) efficient. This makes CCA ideal to be combined with production systems exploiting environmental energy such as (ground coupled) heat pumps, passive cooling or night cooling.

However, the large thermal capacity of CCA hampers the communication between the production system and the building zone. Indeed, heat transfer from CCA to the building zone is determined by the temperature differences between the CCA surface and the zone. Likewise, heat and cold production systems are influenced by the CCA, since the water side heat transfer depends on the temperature difference between water supply and the CCA-core.

Analysis of measurements from an CCA-office building with a conventional control strategy (not adapted to the use of CCA), reveals a very poor energy performance, due to the switching between heating and cooling during the course of one day. This illustrates the overwhelming importance of a control

strategy that takes into account the dynamic thermal characteristics of CCA.

An analytical expression is derived that describes transient heat transfer in a CCA slab. This is used to analyse the thermal behaviour of CCA with respect to thermal power (water-to-CCA and CCA-to-zone), starting up effects, intermittent pump operation, the risk of overheating or undercooling CCA and the impact of control strategies. Neglecting the high order terms of the analytical expression results in a simplified explicit expression, which allows to calculate the time that is required to transfer heat from water to CCA or from CCA to the zone.

To analyse the interaction between water circuit, CCA and the building, integrated thermal models are required. A detailed transient thermal model of an office with CCA (in TRNSYS) is used to derive guidelines for a conventional feedback controller. Alternating zone operation is identified as an important feature to benefit from the thermal mass of CCA and reduce the installed production power. However, to apply advanced control techniques such as Model based Predictive Control (MPC), reduced thermal CCA-building models are required that are accurate (to avoid model errors), but simple (to avoid high computational effort and a large amount of engineering work). The performance of these simplified thermal models is analysed using frequency response analysis and a parameter estimation procedure.

An MPC-algorithm is formulated that determines water supply and ventilation air supply temperatures for which thermal discomfort and energy use are minimized. This results in a controller that optimally integrates the slow reacting but energy efficient CCA and the fast reacting but less energy efficient air handling unit. However, the effect of model errors, cost function errors, weather prediction uncertainties and measurement errors, are not addressed yet, and are expected to decrease the MPC performance.

Two important dynamic thermal CCA characteristics are described that should be taken into account when applying CCA: augmented thermal power required in transient operation and water flow propagation through the tubes.

A detailed study of the dynamic thermal behaviour of CCA in an office building, from component to integrated system level, highlights the relative importance of different heat transfer processes, their thermal resistances and corresponding time constants. These insights allow to develop efficient control strategies, conventional and advanced, which enable to optimally exploit the CCA thermal capacity and which avoid the CCA being overruled by fast reacting systems.

Beknopte samenvatting

Door gebruik te maken van BetonKernActivering (BKA) wordt de thermische massa van een gebouw actief gekoeld of verwarmd. Waterleidingen worden ingebed in de betonnen vloer- en plafondplaat van een kantoorgebouw en brengen die op een gewenste temperatuur.

Dit werk maakt een analyse van het dynamisch thermisch gedrag van een BKA-gebouw en stelt richtlijnen op voor het ontwerp van BKA-regelaars. De combinatie van BKA met een bijkomend snel reagerend systeem, zoals de luchtgroep, wordt onderzocht. Verder komt aan bod hoe vereenvoudigde dynamisch thermische modellen van BKA en een BKA-gebouw opgesteld moeten worden en hoe die in een gebouwregelaar geïntegreerd kunnen worden.

BKA werkt op gematigde temperaturen: $< 30^{\circ}C$ voor verwarming en $> 15^{\circ}C$ voor koeling. De grote thermische capaciteit kan gebruikt worden om BKA te laten werken op momenten dat warmte en koude productie efficiënter of tegen een lagere kost verloopt. Dit alles maakt BKA ideaal om te combineren met productiesystemen die gebruik maken van energie uit de omgeving, zoals (grondgekoppelde) warmtepompen, passieve koeling of nachtkoeling.

Maar de grote thermische capaciteit van BKA staat een goede communicatie tussen het productiesysteem en de gebouwzone in de weg. Warmteoverdracht van BKA naar het gebouw wordt gedreven door het temperatuurverschil tussen het BKA oppervlak en de gebouwzone. Maar ook het productiesysteem wordt beïnvloed door de BKA omdat de warmteoverdracht aan de kant van het water bepaald wordt door het temperatuurverschil tussen watertoevoer en BKA-kern.

Metingen, uitgevoerd in een BKA-kantoorgebouw met een conventionele regeling (niet aangepast aan BKA), duiden op een hele lage energieprestatie. Dit komt omdat de installatie schakelt tussen verwarmen en koelen in de loop

van één dag. Deze analyse toont aan hoe belangrijk een regeling is die de dynamisch thermische eigenschappen van BKA inrekent.

Een analytische uitdrukking die de transiënte warmteoverdracht in een BKA-plaat beschrijft, is afgeleid. Deze uitdrukking wordt gebruikt om het thermisch gedrag van BKA te analyseren. Als de hoge orde termen van de analytische uitdrukking verwaarloosd worden, resulteert dit in een expliciete uitdrukking die toelaat om de tijd te berekenen die nodig is om een hoeveelheid warmte van water naar BKA of van BKA naar de zone over te dragen.

Om de interactie tussen het productiesysteem, de BKA en het gebouw te beschrijven zijn geïntegreerde modellen noodzakelijk. Een gedetailleerd transiënt thermisch model van een kantoorzone met BKA (in TRNSYS) wordt gebruikt om richtlijnen voor het ontwerp van een conventionele regelaar af te leiden. Maar om meer geavanceerde regeltechnieken te gebruiken, zoals Modelgebaseerde Predictieve Regeling (Engels: MPC), zijn gereduceerde thermische BKA-gebouw modellen noodzakelijk. Deze moeten nauwkeurig zijn om modelfouten te vermijden, maar ook eenvoudig om lange rekentijd en een lange ontwerpprocedure te vermijden. De prestatie van deze modellen wordt geanalyseerd aan de hand van frequentieanalyse en parameterschatting.

Een MPC-algoritme bepaalt de optimale watertoevoer- en ventilatietoevoer-temperatuur waarvoor thermisch discomfort en energieverbruik minimaal zijn. Deze regelaar integreert op een optimale wijze de traag reagerende, maar energie efficiënte BKA en de snel reagerende, maar minder energie efficiënte luchtgroep. Het effect van modelfouten, fouten in kostenfunctie, in de weersvoorspelling en van meetfouten worden hier evenwel nog niet meegenomen, maar zullen vermoedelijk de performantie van de MPC regelaar verminderen.

Met twee dynamisch thermische eigenschappen van BKA moet rekening gehouden worden wanneer BKA wordt toegepast en geregeld: het verhoogde thermische vermogen dat nodig is in een overgangsregime en het effect van de voortplantingstijd van het water in de BKA-buizen.

Een gedetailleerde studie van het dynamisch thermisch gedrag van BKA in kantoorgebouwen, van component tot geïntegreerd systeem, toont het relatieve belang aan van de verschillende processen die de warmteoverdracht bepalen, met hun thermische weerstand en overeenkomstige tijdsconstante. Dit inzicht maakt het mogelijk om efficiënte regelstrategieën te ontwerpen, zowel conventionele als meer geavanceerde, die ten volle het dynamisch effect van de BKA benutten en de interactie met snellere backupsystemen mogelijk maken.

List of Symbols

Symbols

A (m²): heat transfer surface area

A_{CCA} (m²): CCA surface area

A_{tube} (m²): tube surface area

A_{wd} (m²): window area

A_{zone} (m²): zone area

Ad_m (W/m²): admittance for input m

c (J/kgK): specific heat capacity

$C = \rho V / Ac$ (J/Km²): specific thermal capacitance

C (J/K): thermal capacitance

C_c (J/K): thermal capacitance of the concrete core

C_{concr} (J/K): thermal capacitance of the concrete slab

C_{int} (J/K): thermal capacitance of the internal walls

C_w (J/K): thermal capacitance of the water

C_z (J/K): thermal capacitance of the zone air

d (m): CCA thickness

d (m): diameter

d_i (m): thickness of slab part i

d_x (m): tube spacing

$d_{t,o}$ (m): tube outer diameter

D (m): hydraulic diameter Δt_c (s): MPC control time step

ΔT_z (K): prediction error correction on the zone air temperature

E (kWh/m²): primary energy use

F_{1-2} (-): view from surface 1 to surface 2

F_z (-): correction factor for the thermal capacity of the zone air node

f (-): tube friction factor

- f (Hz): sample frequency
 g (-): solar factor
 $g_{solshade}$ (-): solar shading factor
 g_{wd} (-): window solar factor
 G_{day} : W/m^2 , heat gain during occupation hours
 G_{night} : W/m^2 , heat loss during non-occupation hours
 h_c or \bar{h}_c (W/m^2K): the zone convection heat transfer coefficient
 $h_{c,surface}$ (W/m^2K): the surface convection heat transfer coefficient
 $h_{c,cl}$ (W/m^2K): the surface convection heat transfer coefficient of the clothed body
 $h_{r,cl}$ (W/m^2K): the surface radiation heat transfer coefficient of the clothed body
 h_r (W/m^2K): the linearised radiative heat transfer coefficient
 h_{c+r} (W/m^2K): the convection + linearised radiative heat transfer coefficient
 h : kJ/kg_{da} , specific enthalpy
 H_p (s): MPC prediction horizon
 H_c (s): MPC control horizon
 J_{ew} (W^2): MPC CCA energy cost
 J_{ev} (W^2): MPC AHU energy cost
 J_d (K^2): MPC discomfort cost
 J_{du} (K^2): MPC discomfort cost for undercooling
 J_{do} (K^2): MPC discomfort cost for overheating
 L (m): length
 L_t (m): CCA tube length
 \dot{m}_w (kg/s): water flow rate
 \dot{m}_v (kg/s): ventilation air flow rate
 N (-): number of measurement points
 P_{tot} ($kWh/m^2/year$): combined electricity use of heat pump and chiller
 R_{cond} (K/W): conductive heat transfer resistance
 R_{concr} (K/W): thermal resistance from water to concrete slab
 R_{conv} (K/W): convective heat transfer resistance
 R_{di} (K/W or m^2K/W in Ch. 3): thermal heat transfer resistance of slab part i
 R_i (K/W): thermal resistance
 R_o (K/W): thermal resistance
 R_a (K/W): thermal resistance from tube wall to upper CCA surface
 R_b (K/W): thermal resistance from tube wall to lower CCA surface
 R_d (K/W or m^2K/W in Ch. 3): Thermal resistance to heat transfer between upper and lower CCA surface
 $R_{di} = (K/W$ or m^2K/W in Ch. 3): Upwards ($i = 1$) or downwards ($i = 2$)

- heat transfer through upper and lower CCA slab into the room at temperature $T_{zone\ i}$ (conduction and convection)
- R_x (K/W or m^2K/W in Ch. 3): Equivalent core thermal resistance
- R_t (K/W): thermal resistance of tube wall (conduction)
- R_w (K/W) or m^2K/W in Ch. 3: Thermal resistance from water to tube wall (forced convection)
- R_z (K/W or m^2K/W in Ch. 3): Thermal resistance from water supply temperature to mean water temperature
- R_{r-s} (K/W): thermal resistance between room and concrete surface
- R_{s-c2} (K/W): thermal resistance between concrete surface and lower part of the concrete slab
- R (K/W or m^2K/W in Ch. 3): thermal resistance
- \tilde{R} (K/W): thermal resistance
- R_{star} (K/W): thermal resistance between T_{ra} and T_z
- t (sec): time
- pT : state-to-state parameter of the simplified building model
- q : J/m^2 , specific heat
- \dot{q} : W/m^2 , specific heat power
- \vec{q} (W/m^2): heat flux \dot{q}_c : W/m^2 , specific convective heat flux
- Q (J): heat
- \dot{Q} : W , heat power
- \dot{Q}_{ri} : W , radiative heat flux from surface i to the zone
- \dot{q}_{CCA} (W/m^2): specific thermal power of CCA
- \dot{q}_{des} (W/m^2): design value of specific thermal production power
- $\dot{q}_{ext,sp}$ (W/m^2): specific static external heat gain
- \dot{q}_{int} (W/m^2): internal gains
- \dot{q}_{HR} (W/m^2): specific thermal power of the heat recovery unit
- \dot{q}_{lim} (W/m^2): limited specific thermal production power
- \dot{q}_{max} (W/m^2): maximum heat pump/chiller power \dot{q}_{sol} (W/m^2): solar radiation
- \dot{q}_w (W/m^2): specific water thermal power
- qT : state-to-temperature input parameter of the simplified building model
- qQ : state-to-heat flow input parameter of the simplified building model
- Tr (W/m^2): transmittance
- T ($^{\circ}C$): temperature
- T_{amb} ($^{\circ}C$): ambient temperature
- T_c ($^{\circ}C$): concrete core temperature
- T_{concr} ($^{\circ}C$): concreteslab temperature
- $T_{comf,min}$ ($^{\circ}C$): minimum allowed comfort (= operative) temperature

- $T_{comf,max}$ ($^{\circ}\text{C}$): maximum allowed comfort (= operative) temperature
 T_f ($^{\circ}\text{C}$): temperature of the fluid outside the thermal boundary layer
 T_{ia} ($^{\circ}\text{C}$): indoor air temperature
 T_{int} ($^{\circ}\text{C}$): temperature of the internal node of the simplified building model
 T_{mr} ($^{\circ}\text{C}$): mean radiant temperature
 T_m ($^{\circ}\text{C}$): mean temperature
 T_{op} ($^{\circ}\text{C}$): operative temperature
 T_{ow} ($^{\circ}\text{C}$): temperature of the outer wall
 T_{prod} ($^{\circ}\text{C}$): set point value for water supply temperature at the production level
 T_{ri} ($^{\circ}\text{C}$): radiant zone temperature for surface i
 T_{rm} ($^{\circ}\text{C}$): running mean ambient temperature defined by EN15251 [44]
 T_{rs} ($^{\circ}\text{C}$): radiant star node temperature
 T_{ra} ($^{\circ}\text{C}$): rad-air temperature
 T_{refi} ($^{\circ}\text{C}$): reference temperature for combined convection-radiation for zone i
 T_s ($^{\circ}\text{C}$): surface temperature
 $T_{set,h}$ ($^{\circ}\text{C}$): heating setpoint temperature
 $T_{set,c}$ ($^{\circ}\text{C}$): cooling setpoint temperature
 T_t ($^{\circ}\text{C}$): tube outer surface temperature
 T_{wm} ($^{\circ}\text{C}$): mean water temperature
 T_{wr} ($^{\circ}\text{C}$): water return temperature
 T_{ws} ($^{\circ}\text{C}$): water supply temperature
 T_{vs} ($^{\circ}\text{C}$): ventilation supply temperature
 T_z ($^{\circ}\text{C}$): zone temperature
 t_p (s): propagation time
 Tr_{mn} (W/m^2): transmittance for input m to input n
 v (m/s): speed
 v_w (m/s): water speed
 U ($\text{W}/\text{m}^2\text{K}$): overall heat transfer coefficient
 U_{ow} ($\text{W}/\text{m}^2\text{K}$): overall heat transfer coefficient of the outer wall
 V_z (m^3): zone volume
 x ($\text{kg}_w/\text{kg}_{da}$): humidity ratio

Abbreviations

- AHU : Air Handling Unit
 BPF : Bypass Factor (cooling coil calculations)
 CCA : Concrete Core Activation

CC: Cooling Curve
CF_h, *CF_{hsv}*: Correction Factor of the heating curve
CF_c, *CF_{csv}*: Correction Factor of the cooling curve
CLO: CLOthing factor
COP: Coefficient of Performance
DC (PPDh): thermal discomfort
DS: Data Set
EER: Energy Efficiency Ratio
FD: Finite differences
FE: Finite elements
FV: Finite volume
SEER: Seasonal Energy Efficiency Ratio
HC: Heating Curve
HCC: heating/cooling curve
HVAC: Heating, Ventilation and Air Conditioning
LMTD: Logarithmic Mean Temperature Difference
MET: METabolic rate
MPC: Model based Predictive Controller
Occ: binary, deterministic occupation profile
OCP: Optimal Control Problem
PE: Parameter Estimation
PMV: Percentage Mean Vote
PPD: Predicted Percentage of Dissatisfied
PSD (power/freq): power spectral density
RC: Resistance-Capacitance
RH (-): relative humidity
RMSE: Root-Mean-Square Error
SPF: seasonal performance factor
TMY: Typical Meteorological Year

Dimensionless numbers

Re: Reynolds number
Pr: Prandtl number
Nu: Nusselt number
 ξ : dimensionless distance
Fo: dimensionless time

Bi: Biot number

Greek symbols

α : W/m^2K , convective heat transfer coefficient

α (-): MPC weighting factor between energy and discomfort cost

$\alpha = \frac{k}{\rho c}$: m^2/s , thermal diffusivity

α (W/m^2K): forced convection heat transfer coefficient

β (-): learning factor for the prediction error correction

ϵ : -, heat exchanger efficiency

η : (-), efficiency

$\gamma = h_{boundary}/\lambda_{solid}$: $1/m$, boundary parameter in transient heat conduction solution

λ (W/mK): thermal conductivity

λ_c (W/mK): thermal conductivity of the concrete

λ_{eq} (W/mK): equivalent thermal conductivity of the air holes

λ_f (W/mK): fluid thermal conductivity

ρ (kg/m^3): density

ρ_z (kg/m^3): density of the zone air

τ (s): time constant

τ (s): heat transfer parameter (Ch. 4)

θ ($^{\circ}C$): temperature in the Laplace domain

θ (s): sample period (Ch. 5)

θ (s): measurement period (Ch. 5)

Subscripts

ah: air heating	rm: running mean (EN15251 outdoor temperature definition)
ac: air cooling	s: supply
amb: ambient	s: (concrete) surface
app: appliances	set: set point value
c: condensate	sol: solar
c: concrete core	ss: steady state
c: cooling	S: South zone
concr: concrete	t: tube
contr: control	t,o: tube outer
conv: convective	to: typical office
cond: conduction	v: ventilation
c1: upper part of the concrete slab	vs: ventilation supply
c2: lower part of the concrete slab	w: water
csv: cooling setpoint value	ws: water supply
d: slab thickness	wm: water mean
da: dry air	wr: water return
dp: dew point	x: parameters related to tube spacing
eq: equivalent	z: zone
gr, gross: refers to the gross area	zh: zone heating
h: heating	zc: zone cooling
ha: humid air	zp: zone circulation pump
hsv: heating setpoint value	
i: inner	
ia: indoor air	
int: internal	
init: initial	
l: lights	
net: refers to the net area	
mod: module	
max: maximum	
min: minimum	
N: North zone	
noprop: no propagation	
o: outer	
oa: outdoor air	
op: operative	
pred: prediction	
prop: propagation	
req: required	

Contents

Abstract	v
Beknopte samenvatting	vii
List of Symbols	ix
Contents	xvii
List of Figures	xxxi
List of Tables	xxxix
I Introduction	1
1 Introduction to Concrete Core Activation	2
1.1 Goal	3
1.2 CCA	3
1.3 CCA in a building	6
1.4 Temperatures and heat transfer in CCA and buildings	10
1.4.1 Operative temperature	10

1.4.2	Heat transfer modes	11
1.4.3	Heat exchange in a building zone	17
1.4.4	Operative temperature in the simplified building model	18
1.5	Transient heat transfer	18
1.6	Lumped capacity model or RC-model	19
1.7	CCA thermal models	21
1.7.1	EMPA CCA model	21
1.7.2	Other CCA models	24
1.8	Overview	25
2	Case study of a CCA office building	28
2.1	Introduction	28
2.2	Measurements in a CCA office building	29
2.2.1	Description of the measured building	29
2.2.2	Measurement results	32
2.2.3	Adjustment of the control parameters	33
2.3	Simulating CCA behaviour with a generic building model	33
2.3.1	Simulated cases	34
2.3.2	Room model description	35
2.3.3	Simulation period	38
2.3.4	Simulation details	39
2.4	Simulation results	39
2.4.1	Thermal comfort	39
2.4.2	Heating and cooling on-off times	41
2.4.3	Analysis of the control strategy efficiency	41

2.4.4	Analysis of the impact of the control strategy on primary energy use	44
2.5	Conclusions	46
II	Concrete Core Activation	47
3	CCA steady-state heat transfer	48
3.1	Introduction	48
3.2	Steady-state CCA heat transfer model	48
3.2.1	Thermal resistances in the CCA resistance model	51
3.2.2	Tube surface area, gross and net CCA floor area	52
3.2.3	R_d , from zone temperature to mean concrete core temperature	53
3.2.4	R_x , from mean core temperature to tube outer surface temperature	54
3.2.5	R_t , from tube outer surface to tube inner surface temperature	54
3.2.6	R_w , from tube inner surface to mean water temperature	55
3.2.7	R_z , from mean water temperature to water supply temperature	56
3.2.8	Comparison of R_x , R_t , R_w , R_z , R_d and the total thermal resistance R_{tot}	59
3.2.9	Specific heat power $\dot{q}_w = (T_{ws} - T_c)/R_c$ as a function of \dot{m}_w and T_{ws}	60
3.2.10	R_x and R_t sensitivity to material properties	62
3.3	Maximum heating and cooling power of CCA	62
3.4	Hollow core CCA	66
3.5	Conclusions	68

4	CCA transient heat transfer	69
4.1	Introduction	69
4.2	Observations from measurements	69
4.2.1	Measurement setup	70
4.2.2	Measurement results	71
4.2.3	Phenomena in transient CCA behaviour	74
4.3	Analytical expression for CCA transient heat transfer	74
4.3.1	Two operational modes	75
4.3.2	Temperature distribution $T(x, t)$ in a slab $0 < x < L$	77
4.3.3	Solution for different upper and lower temperatures	79
4.3.4	Combining the solution for the upper and lower slab part	83
4.3.5	Analysis of the CCA $T(\xi, Fo)$ equation	85
4.4	Propagation time of water flow	88
4.4.1	Water temperature as a function of time and location	91
4.4.2	Mean water temperature T_{wm} as a function of time	92
4.4.3	Heat transfer parameter τ	93
4.4.4	The influence of flow propagation on the heat transfer	94
4.4.5	Equivalent Supply Temperature	95
4.4.6	Application of Equivalent Supply Temperature approach	96
4.4.7	Impact of simplifications	96
4.5	Analysis of transient heat transfer in CCA	101
4.5.1	Case 1: Heating up CCA during 8 h	101
4.5.2	Case 2: Heating up CCA during 4 h	106
4.5.3	Case 3: Cooling down CCA	108
4.5.4	Case 4: CCA without water flow	110

4.5.5	Pump operation time	112
4.5.6	Different water supply temperature T_{ws}	114
4.5.7	Simplified $q(\text{Fo})$ expression	116
4.5.8	Avoiding overheating or undercooling	118
4.5.9	CCA controlled by room temperature feedback	120
4.5.10	Installed production power	123
4.6	Guidelines for the controller	124
4.7	Conclusions	125
5	Frequency analysis of CCA and zone disturbances	127
5.1	Introduction	127
5.2	Methodology	128
5.3	Frequency response analysis of the zone disturbances	129
5.3.1	T_{amb} , \dot{q}_{sol} and \dot{q}_{int} data set	129
5.3.2	Power spectral density	130
5.3.3	Ambient temperature T_{amb}	133
5.3.4	Solar radiation \dot{q}_{sol} on a South oriented vertical plane	133
5.3.5	Conclusion from the PDS of the zone disturbances	135
5.4	Frequency response analysis of CCA	136
5.4.1	Transfer functions Admittance and Transmittance	136
5.4.2	19 th order CCA model	137
5.4.3	Frequency response of CCA	139
5.4.4	Reducing the order of the star RC-CCA model	144
5.5	Conclusions	148

III Concrete Core Activation and building	149
6 Control of CCA buildings	150
6.1 Introduction	150
6.2 Thermal comfort criteria for CCA buildings	150
6.2.1 Thermal comfort models	151
6.2.2 Operative temperature	152
6.2.3 Thermal comfort and operative temperature ramps	153
6.2.4 Application of adaptive thermal comfort models to CCA buildings	153
6.2.5 Adaptive comfort models in moderate climates	155
6.2.6 The choice of thermal comfort model in CCA buildings	156
6.3 Model based control	156
6.4 Conventional CCA control strategies	157
6.5 Conventional CCA control by EMPA	159
6.6 Model based Predictive Control of CCA	160
6.7 Building thermal mass in MPC control	162
6.8 Conclusions	167
7 Typical office building	169
7.1 Introduction	169
7.2 2-Zone office building model	169
7.3 HVAC system layout	173
7.3.1 CCA hydraulic scheme	173
7.3.2 Production of heat and cold	175
7.3.3 Circulation pumps	176

7.3.4	Air Handling Unit	177
7.3.5	Cooling and heating coil of the air handling unit	180
7.4	Heating load and cooling load	181
7.4.1	Heating load	182
7.4.2	Cooling load	184
7.4.3	Heating curve and cooling curve	186
7.5	Parameters of the 2-zone office building model	186
7.6	Automated solar shading	187
7.7	Conclusions	188
8	CCA conventional control	189
8.1	Introduction	189
8.2	Controller performance criteria	189
8.2.1	Thermal discomfort	190
8.2.2	Energy use	190
8.2.3	Heating-cooling switching	191
8.2.4	Data sign convention	191
8.2.5	Meteorological data	191
8.2.6	Typical week	192
8.2.7	Heating and cooling production power	192
8.3	Reference cases: Zero Discomfort and Zero Energy Use	193
8.3.1	Zero Discomfort Reference: Ideal heating and cooling	193
8.3.2	Zero Energy Use Reference: no heating and cooling	193
8.3.3	Reference cases results	195
8.4	Conventional controller	196
8.5	Heating/cooling curve controller performance	199

8.5.1	Variation of all controller settings	199
8.5.2	Sensitivity to heating and cooling set points $T_{set,h}$ and $T_{set,c}$	200
8.5.3	Sensitivity to $T_{controlled}$	202
8.5.4	Heating/cooling curve correction	203
8.5.5	Illustration of the HCC correction effect	204
8.5.6	Conclusions of the controller performance evaluation	207
8.6	The best HCC controller settings	208
8.6.1	Controller performance	208
8.6.2	Heat/cold production power	208
8.7	Evaluation of the modified-HCC controller	209
8.7.1	Controller behaviour	209
8.7.2	CCA modified-HCC controller versus non-CCA reference case	211
8.8	Modified-HCC controller with limited production power	213
8.9	Alternating zone operation	217
8.10	Night set back settings	218
8.11	Modified-HCC controller without solar shading	222
8.12	Conclusions	223
9	Simplified CCA-building model	225
9.1	Introduction	225
9.2	White box building model	227
9.2.1	Simplified CCA model structure	227
9.2.2	Simplified building model structure	227
9.2.3	Solar radiation	230

9.2.4	Building model equations	231
9.2.5	Initial parameter values	232
9.3	Parameter estimation procedure	233
9.3.1	Data sets for parameter estimation	233
9.3.2	Parameter estimation tool	235
9.3.3	12 simplified building models in 3 model groups	236
9.3.4	Parameter estimation as an optimisation problem	237
9.4	Parameter estimation results	239
9.4.1	Root-Mean-Squared Error	239
9.4.2	System matrices	242
9.4.3	Thermal capacitance of the room air node	244
9.4.4	Influence of the initial parameter range	245
9.5	Conclusions	247
10	Model based Predictive Control for CCA buildings	249
10.1	Introduction	249
10.2	Implementation of MPC	250
10.2.1	MPC controller layout	251
10.3	Optimal control problem	253
10.3.1	State matrices A and B	255
10.3.2	Controller tuning parameters	255
10.3.3	Solar shading	256
10.3.4	Power limitations	256
10.3.5	Slack variables	257
10.3.6	Discomfort cost	258
10.3.7	CCA-water heating and cooling cost	261

10.3.8	Ventilation heating and cooling cost	262
10.3.9	Initialisation of the system state	264
10.4	Evaluation of the MPC controller	264
10.4.1	Evaluation period	265
10.4.2	Heating operation	265
10.4.3	Cooling operation	269
10.5	Conclusions	272
IV	Conclusions and outlook	274
11	Summary and Conclusions	275
11.1	Summary	275
11.2	Conclusions	279
12	Further research	281
V	Appendices	283
A	Adaptive versus non-adaptive thermal comfort models in moderate climates	285
A.1	Introduction	285
A.2	Thermal comfort	286
A.3	Thermal comfort theory	286
A.3.1	Basic thermal comfort theory	286
A.3.2	Operative temperature	287
A.3.3	Adaptation	288

A.3.4	Thermal comfort boundaries in terms of outdoor temperature: overview	291
A.4	Thermal comfort limits for a moderate climate	294
A.4.1	Yearly comfort band	294
A.4.2	Quantified benefit of the adaptive comfort models	294
A.4.3	Real weather data analysis for Maastricht	296
A.4.4	Weather data evaluation based on allowed operative temperatures	297
A.4.5	Analysis of the ISO7730 interpolation assumption	299
A.5	Building zone energy use as a function of the thermal comfort model applied	299
A.5.1	2 zone building section description	299
A.5.2	Simulation assumptions	300
A.5.3	Simulation results	301
A.5.4	Building zone energy use for the Maastricht year of 2003	304
A.5.5	Influence of heat gains on energy use	305
A.6	Conclusions	306
B	Ideal heating and cooling in TRNSYS	309
C	Heating and cooling coil design and control	311
C.1	Heating coil and sensible cooling coil design	312
C.2	Heating coil and sensible cooling coil control	313
C.3	Dehumidifying cooling coil design	315
C.4	Dehumidifying cooling coil control	315
D	Parameters of the 2-zone office building	319
D.1	Internal gains: heat gains from people	319

D.2	Internal gains: appliances	320
D.3	Internal gains: lighting	322
D.4	Zone capacitance value	322
D.5	Convective heat transfer values of floor and ceiling	324
D.6	Radiative heat transfer	325
D.7	Convective versus radiative heat transfer coefficients	326
D.8	Infiltration rates	327
D.9	Ventilation	328
D.10	Maximum specific heat gains and heat losses	329
D.11	Model Excitation	329
D.11.1	Water supply	330
D.11.2	Ventilation supply	330
D.11.3	Weather conditions	330
D.11.4	Files	331
D.12	Procedure for parameter estimation	331
D.13	TRNSYS related topics	332
D.13.1	Floor and ceiling boundary condition	332
D.13.2	Pre-simulation time	333
D.13.3	Batch file in TRNSYS	334
E	Automatic state space matrix construction from RC-network	335
E.1	Step 1 : drawing the RC-network	335
E.2	Step 2 : Defining states, inputs and additional outputs	336
E.3	Step 3 : State space matrices A, B, C and D	338
E.3.1	Capacitance matrix C_{ap}	338
E.3.2	Resistance matrices R_X and R_U	339

E.3.3	System matrix A	339
E.3.4	Input matrix B	340
E.3.5	Output matrix C and transmission matrix D	340
E.4	State space representation of the 2 nd order CCA building model	342
E.5	Matlab functions	343
	Bibliography	345
	Curriculum	361
	Publications	363

List of Figures

1.2	Comparison between (a) an embedded floor system and (b) CCA	5
1.3	Examples of different CCA configurations with thickness d , tube spacing d_x and tube diameter d_{to} : (1) Full concrete CCA, (2) Hollow core CCA, (3) Air box CCA	6
1.4	Schematic representation of a 2-zone office building with 3 disturbances: ambient temperature T_{amb} , solar radiation \dot{q}_{sol} and internal gains \dot{q}_{int} , 2 inputs: water supply temperature T_{ws} and ventilation supply temperature T_{vs} and 2 outputs: zone temperature T_z and concrete core temperature T_c	7
1.6	CCA time constant based on the thermal diffusivity α_c as a function of thickness d	19
1.7	1 st order lumped capacity representation of a material layer	20
1.8	EMPA CCA model [81]: Triangle-star transformation describing 2D heat flow in a 1D thermal model	23
2.3	Simplified room model for control strategy evaluation	36
2.4	Operative room temperatures for the different control strategies (\square Case 1, \triangle Case 2, \circ Case 3, $+$ Case 4)	40
2.6	On-off times of heating (H) and cooling (C) for the different control strategies; (0) means no heating and no cooling	41

2.7	24 h cumulative energy flows ($\text{Wh}/^2\text{m}$) from the load to the room and from the room to the water distribution system (via the ideal emitter for case 1 and via the CCA for case 2, 3 and 4) Case 1: threshold heating = 21°C , threshold cooling = 22.5°C ; Case 2: threshold heating = 21°C , threshold cooling = 22.5°C ; Case 3: threshold heating = 20°C , threshold cooling = 23°C ; Case 4: cooling from 0 AM until 4 AM. The room temperature profile is shown at the bottom of each figure.	43
3.1	Parameters of the investigated floor layout	49
3.2	Required concrete thickness above or below the tubes as a function of the tube step length for using the EMPA RC-model	50
3.3	EMPA's 1D RC-model of a CCA slab [81]	51
3.4	CCA-layout	53
3.5	R_x values for $L_{to} = 5\text{ m}$	54
3.6	Tube wall conduction thermal resistance R_t as a function of d_x and for $L_{to} = 5\text{ m}$, according to Eq. 3.9.	55
3.11	fig:SteadyStateMax	65
3.12	fig:SteadyStateHP	65
3.13	Hollow core RC-star network, adapted to incorporate the thermal resistance of the air holes	67
4.5	Heat power \dot{q}_w as a response to the step excitation of T_{ws}	73
4.8	$f(\beta) = \cot \beta - \frac{\beta^2 - \text{Bi}_1 \text{Bi}_2}{\beta(\text{Bi}_1 + \text{Bi}_2)}$ for different Bi-numbers. The arrow indicates the direction of increasing Bi-number.	85
4.12	The water flow propagating through the CCA tube, with t_p the propagation time, v_w the water speed and L_t the tube length.	90

4.13 Thermal resistance R_{concr} for propagation analysis as a function of d_x (5 sets of data along the linear curve), \dot{m}_w (within 1 d_x data set, decreasing R_{concr} with increasing \dot{m}_w), and d (within 1 d_x - \dot{m}_w -data set a very small influence, which is only noticeable at low \dot{m}_w -values)	94
4.14 Flow propagation	96
4.15 Dimensions of the CCA used for analysing the impact of the simplifications of the analytical expression	97
4.19 Results of the CCA transient heat transfer analysis , case 1: constant water flow	105
4.20 Results of the transient heat transfer analysis in CCA, case 2: 4h on- 4h off water flow.	107
4.21 Results of the transient heat transfer analysis in CCA, case 3: Cooling at 17°C with 8 h constant water flow. (a) The T -profile starts at 23°C and evolves towards the left. (b)-(c)-(d)-(e)-(f) Mirrored results compared to the heating up case (Fig. 4.19). The data presented are explained in Table 4.4.	109
4.22 Results of the transient heat transfer analysis in CCA, case 4: Cooling down of a CCA slab without water flow (hour 1: 1 line every 10 mins, then 1 line every hour). (a) The T -profile starts at 25°C and evolves to the right. The data presented are explained in Table 4.4.	111
4.25 Detailed (-) and approximated solution of q_{in} (*), q_{out} (×) and q_{sto} (△) for the upper half of a 0.2 m slab ($T_{ws} = 30^\circ C$ and $T_2 = 20^\circ C$). The dashed line is the steady-state solution ' $L\rho cC Fo$ ' (Eq. 4.29) indicating the slope to which both q_{in} and q_{out} evolve.	116
4.26 Detailed (-) and approximated solution of q_{down} (*), q_{up} (×) and q_{sto} (△) for a 0.2 m slab without water flow with $T_{initial} = 25^\circ C$ and $T_{room} = 20^\circ C$	118
4.29 fig:LimitT	121

4.30	CCA with room temperature feedback. Heating starts at $T_1 = 30^\circ C$ until the zone temperature $T_2 = 20^\circ C$. Assumed zone gains and stored slab energy keep T_2 increasing. Cooling at $T_1 = 15^\circ C$ starts as soon as the zone temperature reaches $T_2 = 24^\circ C$. The initial slab condition is $T_2 = 18^\circ C$. The data presented are explained in Table 4.4.	122
5.1	Relation between inputs and outputs in the CCA-office zone.	129
5.2	Hamming window for a sample vector of length 8760/4.	132
5.6	2 example transfer function representations: (left) for a variation of the water supply temperature T_3 , the admittance Ad_3 and transmittances Tr_{3-1} and Tr_{3-2} and (right) for a variation of the temperature of the zone below T_2 , the admittance Ad_2 and transmittances Tr_{2-1} and Tr_{2-3} in a CCA floor. A variation of the temperature of the zone above T_1 is similar. RC_1 and RC_2 are the lumped representations of the thermal capacitance nodes of the CCA-slab.	138
5.7	Layout of the 3 star RC-models used in the analysis of the CCA frequency response.	139
5.11	The influence of a variation in the combined heat transfer coefficient on Ad_3 and $Tr_{3-1} + Tr_{3-2}$ (Δ : h_{c+r} base model, \square : $h_{c+r} - 10\%$)	143
5.12	fig:RCtabsTransmAdmit	145
5.13	fig:RCtabsTransmAdmitPH	146
6.1	Operative temperature range as a function of the reference outdoor temperature $T_{ref,out}$ for a class B building, according to the PMV-PPD model (ISO7730 [68]). The definition of $T_{ref,out}$ is given in App. A.	157

6.2	Example of a building MPC framework: (1) zone and concrete slab temperature $y(k) = [T_z T_c](k)$ is the measured output from the office zones at time $t = k$, where, if necessary, a Kalman filter estimates unmeasured states, (2) at time k disturbance predictions, e.g. for the ambient temperature T_{amb} , solar radiation \dot{q}_{sol} and internal gains \dot{q}_{int} , and setpoint profiles, e.g. the required comfort temperature $T_{comfort}$, are generated for the prediction horizon $p = 1..H_p$, (3) using the dynamic simplified building model, the MPC determines the profile $u(k + p)$, e.g. $= [T_{ws}(k + p), \text{pump-on-off}, T_{vs}(k + p)]$, which minimizes a predefined cost and (4) the $u(k + c)$ -profile is fed to the low level building controllers for the control horizon $c = 1..H_c$	161
7.1	Schematic representation of the 2-zone office building with the disturbances ambient temperature T_{amb} , solar radiation \dot{q}_{sol} and internal gains \dot{q}_{int} , the inputs water supply temperature T_{ws} and ventilation temperature T_{vs} and the measured outputs zone temperature T_{ia} (or operative temperature T_{op}) and concrete core temperature T_c	170
7.2	Hydraulic and aeraulic scheme of the 2-zone office building section	174
7.4	Hydraulic scheme of the whole building: (1) CCA circuit, (2) horizontal piping in suspended ceiling, (3) vertical piping in shafts and (4) horizontal piping to collector.	176
7.5	Schematic presentation of the implemented air handling unit	178
7.7	Zone and AHU heat load as a function of the average outdoor air temperature	183
7.8	fig:CoolLoad	185
7.9	Available power from the air handling unit: air flow rate of 36^3m/hpers (solid line) and 54^3m/hpers (dashed line)	186
7.10	Heating (H.C.) and cooling (C.C.) curves for the office zone	186
8.1	fig:TypWeekS	192

8.9	The influence of the cooling set point $T_{c,set}$ on the temperature of the concrete core T_c : SET=0/-1 (full line) and SET=0/-2 (dashed line) Controller settings: T_s as controlled parameter, CF=3/-3 . . .	207
8.10	The controller performance for the ‘best’ controller settings . .	208
8.14	Temperature difference $T_c - T_{ws}$ at start up moments of heating (negative values) and cooling (positive values)	215
8.17	Impact of night setback settings on the controller performance for the South zone and the modified-HCC controller, for a production system sized to \dot{q}_{des} and $\dot{q}_{2 \times des}$, for a controller with night setback (\diamond), reduced night setback (\triangle) and no night setback (\blacktriangledown).	219
9.3	(left) T_{ws} (-), T_{vs} (- -), $T_{amb}(\cdot)$, (middle) \dot{q}_{sol} (- -) and \dot{q}_{int} (-), and (right) zone states T_c (-) and T_z (- -) for the identification sets DS3 (above) and DS4 (below), where DS3 is a representative of the theoretical and DS4 of the realistic input profiles. The step excitation of T_{amb} occurs at 0 h for DS3.	236
9.5	Relative difference in RMSE-values for the validation of the nx2-models with updated parameters (no active inequality constraints), compared to the original nx2-models. Positive $\Delta(\text{RMSE})$ values mean an improvement, while negative $\Delta(\text{RMSE})$ values imply a higher RMSE.	246
10.1	Simplified building representation by means of a 2 nd order building model	250
10.2	Overview of the MPC framework	253
A.1	Operative temperature range as a function of the reference outdoor temperature, according to the different thermal comfort models (boxed areas indicate the extrapolated values)	293

A.2	Comfortable operative temperature range as a function of the corresponding reference outdoor temperature for the reference year of Maastricht, the Netherlands ('90% satisfied' thermal comfort models; ISO7730: thick line; ASHRAE55: dashed line; ISSO74: dash-dotted line; EN15251: solid line)	295
A.4	Number of days the allowed lower (full line) and upper (dashed line) operative temperature is equal or smaller than the abscissa temperature, according to the different thermal comfort models (circle: ISO773; square: ASHRAE55; triangle: ISSO74; cross: EN15251)	298
A.5	2D view of the 2-zone building section	300
A.6	Required net energy for heating and cooling to keep the zone temperature within the imposed temperature range (relative to the ISO7730 energy need)	302
A.7	Cumulative net energy for heating and cooling as a function of the prescribed operative temperature by the ISSO74 comfort model for the North (N) and South (S) zone of the office building	303
C.1	Schematic presentation of the implemented air handling unit . . .	311
C.2	Cooling coil design results for the detailed ASHRAE/VDI method and the simplified procedure (the legend gives the inlet conditions)	318
D.1	Energy use values of 32 air conditioned buildings with heat recovery in the AHU and with an heating energy use less than 100 kWh/2m.y from the Swedish Energy agency survey [129] . . .	321
D.2	Natural convection coefficient for floor cooling/ceiling heating (left hand side) and for ceiling cooling/floor heating (right hand side)	326
D.3	Variation of the linearised radiative heat transfer coefficient h_r for a limited range of T_m	327

List of Tables

1.1	Comparison of typically occurring heat gains and losses in an office building with the steady-state heating and cooling power from a 20 cm CCA with a raised floor.	8
2.1	Parameters of the measured building	29
2.2	Simulated control strategies	34
2.3	Heat gain schedule used for the simulation	38
2.4	Production efficiencies and primary energy conversion factors	44
2.5	Conversion from net energy use to primary energy use of simulation cases 1 to 4	45
3.1	Parameters in the parametric study of the steady state heat transfer in CCA	49
3.2	Combinations of d_x and d fulfilling the EMPA conditions (Eqs. 3.1 and 3.2)	51
3.3	Details of the CCA parameters for the maximum heating and cooling power calculation	63
3.4	Limiting surfaces temperatures according to thermal comfort class B with an assumed room temperature of 20°C in winter and 26°C in summer. The natural convection coefficient h_c is determined by the Awbi and Hatton correlation (Sec. D.5)	64

3.5	Equivalent heat conductivity λ_{eq} , accounting for convection and radiation in the air holes of hollow core CCA ($\lambda_{air} = 0.024 \text{ W/mK}$)	68
4.1	Time constants of the heating step response of T_c , $T_{s,up}$ and $T_{s,down}$: time to reach $[T_{begin} + (1 - e^{-1})(T_{end} - T_{begin})]$	74
4.2	Data of the example TABS piece used for validating the simplifications of the analytical expression	98
4.3	Specifications of the CCA used to analyse transient heat transfer (layout see Fig. 4.6)	102
4.4	Explanation of the figures showing the transient calculation results.	102
4.5	Explanation of the figures showing the transient calculation results (continuation of 4.4).	103
4.6	Characteristic values over the 8 h period for cases 1-6	113
5.1	Conversion from frequency (1/day) to time period (hour)	129
5.2	Limit values for the TABS transfer functions: time period $\theta = \infty$ (steady state, frequency $f = 0$) and time period $\theta = 0$ (frequency $f = \infty$).	140
5.3	Overall RMSE values of the magnitude errors and of the phase shift errors between Admittances and Transmittances from the 3 rd , respectively 2 nd order CCA model and the detailed 19 th order CCA model in the 30 min and 168 h time period	147
6.1	Optimal operative temperature and operative temperature band for thermal comfort in an office environment for the different categories according to ISO7730 [68].	153
6.2	Application of adaptive model requirements to CCA buildings	155
7.1	Properties of the wall layers in the 2 zone building model (from [24])	171
7.2	Wall layouts	172
7.3	Building characteristics	172

7.4	Production efficiency (T_{ws} in °C)	176
7.5	Hydraulic and aeraulic design of the whole building	177
7.6	Properties of the Air Handling Unit	178
7.7	The effect of simulating the heating and cooling coil water circuits on the simulation time of a 1 day simulation	180
7.8	Heating and cooling load	181
7.9	Maximal permissible total heat gains in space for different room temperature amplitudes and floorings (copied from Lehmann et al. [87])	185
7.10	Parameters of the 2-zone office building model	187
7.11	Scheduled operating hours of the typical office model	187
8.1	Energy use for the reference ideal heating and cooling and discomfort for the free running 2-zone office building	195
8.2	Overview of controller settings	198
8.3	Number of days with heating and cooling in 1 day, for heating/cooling curve correction factor (CF=3/-3).	201
8.4	The best controller settings	209
8.5	Yearly energy use and maximum heating and cooling power of the South zone for the modified-HCC controller with unlimited and limited production power	217
8.6	Effect of the night setback settings on the yearly number of hours below and above the PMV-limit and the yearly thermal heating and cooling energy.	221
8.7	Modified-HCC controller performance for the South zone with unlimited heating and cooling power and with and without solar shading	223
9.1	Data sets for parameter estimation (DS1 - DS3: theoretical input profiles; set DS4 - DS5: realistic input profiles)	235

9.2	12 simplified building models in the 3 groups: Group A are models obtained from data set 1 with T_{ws} , T_{vs} and T_{amb} as inputs (no \dot{q}_{sol} and \dot{q}_{int}), Group B are models obtained from data set 2 with T_{ws} , T_{vs} , T_{amb} and \dot{q}_{int} as inputs (no \dot{q}_{sol}), and Group C are models having all inputs in the system matrix. . .	237
9.3	Initial parameter values (ini) and the assigned range for the parameter estimation problem, in units h (hour) and (kJ/h). . .	239
9.4	RMSE on zone temperature T_z (2 nd and 4 th order)	240
9.5	Input-output relation for the A and B system matrices of the 2 nd order simplified building model	242
9.6	Correction factor F_z for the thermal capacity of the zone node	244
9.7	Initial parameter range and the parameter estimation results of the nx2 models, in units h (hour) and (kJ/h). The underlined values lie on the boundaries of the parameter range.	245
10.1	Thermal discomfort, CCA and AHU primary energy use in the OCP objective function	258
10.2	Energy use (kWh/ ² m) and afternoon discomfort (Kh overheating) for the linear and quadratic thermal discomfort approach.	260
10.3	Comparison of energy use (kWh/ ² m) and thermal discomfort (Kh) between the MPC-CCA and MPC-CCA-AHU controllers from the OCP	268
10.4	Comparison of energy use (kWh/ ² m) and thermal discomfort (Kh) between the MPC-CCA and MPC-CCA-AHU controllers from the OCP	272
A.1	Categories for global thermal environment from ISO7730, Annex A. (PPD: Predicted Percentage Dissatisfied; PMV: Predicted Mean Vote)	287
A.2	Categories for local thermal environment from ISO EN 7730, Annex A. (DR: draught rate, percentage of people bothered by draught; PD: percentage dissatisfied)	287

A.3	Optimal operative temperature and operative temperature band for thermal comfort in office environment for the different categories according to ISO7730 [68]	288
A.4	Building's thermal comfort classification comparison	290
A.5	Outdoor temperature definition and operative temperature band for thermal comfort in office environment according to different comfort models (T_{op} : operative temp.; T_{rm} : running mean outdoor temp.; T_{ed-i} daily mean outdoor temp. of the i^{th} day before today; $t_{a,out}$: mean monthly outdoor air temp.; $T_{e,ref}$: running mean outdoor temp., defined differently from T_{rm} ; T_{today} : mean of maximum and minimum outdoor temp. of the specified day; T_{switch} : see footnote 4)	292
A.6	Mean outside temperature and global solar radiation on horizontal for Maastricht TMY and the years 2001 to 2008	296
A.7	Comparison of Maastricht TMY and the year 2003 'ISO7730-Exceeding' Degree Days (Kday)	297
A.8	Number of days with $T_{op,min}$ and $T_{op,max}$ in the indicated range for Maastricht TMY and the year 2003	297
A.9	Analysis of the ISO7730 interpolation assumption	299
A.10	Heating and cooling energy use for the South and North zone (with q_{heat} and q_{cool} in kWh/m ² and relative to ISO7730)	301
A.11	Heating and cooling energy use for the South and North zone (with q_{heat} and q_{cool} in kWh/m ²) for the 2003 weather data of Maastricht	305
B.1	Simulation model settings for ideal heating and cooling	310
D.1	Heat gains from people and occupation density	320
D.2	Heat gains from office appliances	321
D.3	Heat gains from lighting	322
D.4	Overview of zone thermal capacitance values from literature . .	323

D.5 Literature review of natural convection correlations	325
D.6 Ventilation parameters	328
D.7 Maximum heat gains and heat losses related to the office floor area. <i>UA</i> incorporates conduction through outside wall and window and infiltration.	329
D.8 Definition of the 7 excitation inputs signals to the TRNSYS model <i>TypicalOffice2Zone.tpf</i>	330
D.9 Impact of the erroneous radiation boundary conditions on the heating and cooling of floor and ceiling	333

Part I

Introduction

Chapter 1

Introduction to Concrete Core Activation

Knowledge of the transient behaviour of systems is of vital importance. In ‘A Heat Transfer Textbook’, by John H. Lienhard [88], the chapter on transient heat transfer starts with a story on the work of James Watt:

“James Watt, of course, did not invent the steam engine. What he did do was to eliminate a destructive transient heating and cooling process that wasted a great amount of energy. . . . Watt first recognized, and eventually eliminated, its major shortcoming. The cylinder of the engine was cold when steam entered it and nudged the piston outward. A great deal of steam was wastefully condensed on the cylinder walls until they were warm enough to accommodate it. When the cylinder was filled, the steam valve was closed and jets of water were activated inside the cylinder to cool it again and condense the steam. This created a powerful vacuum, which sucked the piston back in on its working stroke. . . . the lesson that we learn from history is that transient heat transfer can be of overwhelming importance.”

This story can be rewritten to the topic of this work: Concrete Core Activation (CCA), which is the concrete floor slab of a building having integrated water tubes. Through these tubes, heated or cooled water can circulate to heat up or cool down the slab. The heated or cooled slab exchanges heat with the room below and above, controlling the room temperature. Due to the large thermal

inertia of the concrete slab, this is a very slow process. Omitting the reference to the author, Watt's story, applied to this work on CCA in office buildings, would be:

“In this work, CCA is not invented. It is the aim of this work to eliminate the destructive transient heating and cooling process that wastes a great amount of energy. This process is recognized using a case study, understood through measurements and through the analysis of theoretical models, and eventually eliminated — or a proposal to eliminate the problem is given — by an appropriate control strategy. The office room and the CCA are cold initially. A great deal of heat is wastefully used to heat up the concrete slab until it is warm enough to heat up the room. At this point, the people working in the office room, PC's, lights and perhaps solar radiation generate heat and the room temperature rises above the set point for cooling. Cold water flows through the tubes, but, again, a great deal of cold is wastefully used to cool down the concrete slab again until it is cold enough to cool down the room.” Again, the transient behaviour is of overwhelming importance.

1.1 Goal

Originally, CCA is intended to be kept at a constant temperature. By doing so, CCA levels out temperature fluctuations in a building zone. In this work, the possibility to go one step further and actively control CCA in order to keep the zone temperatures within required limits, is investigated.

The aim of this work is to analyse the dynamic thermal behaviour of CCA integrated in a building and to derive guidelines for the design of a CCA controller. Furthermore, simplified dynamic thermal models of CCA and of a CCA-building are developed which can be used in a building system controller.

1.2 CCA

Using the building's thermal mass to obtain a comfortable indoor temperature is not new. The first concepts of combined cooking and heating are found in Northern China and Korea and date from the 11th century B.C., as shown in Fig. 1.1(a). In these regions the technique has been constantly used throughout history and developed up until now [17]. In Europe, the Greeks

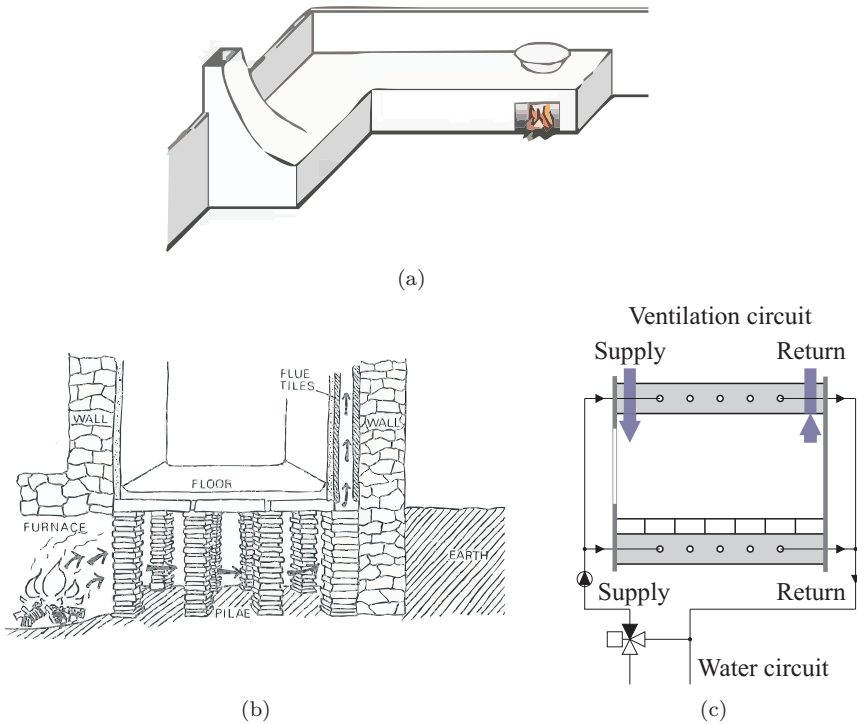


Figure 1.1: (a) Schematic view of a Korean *gudeul* (meaning heated stone) [17], (b) schematic view of a Roman hypocaust system [94] and (c) Modern equivalent of a water based CCA system with ventilation

used an underfloor heating system to heat baths, where the Romans copied and perfected the technique and applied it to their houses. The flue gasses of the fire were directed through wall channels to heat up the wall, as shown in Fig. 1.1(b). Variations on this technique are also found in the Middle East [18].

In recent years, the growing importance of energy efficiency has resulted in a search for new building heating and cooling concepts. Actively using the thermal mass of a building is an example of such a technique. The modern equivalent of this technique (Fig. 1.1(c)) was first applied in the beginning of the 20th century, “when Arthur H. Barker, a British professor, discovered that small hot water pipes embedded in plaster or concrete formed a very efficient heating system” [18].

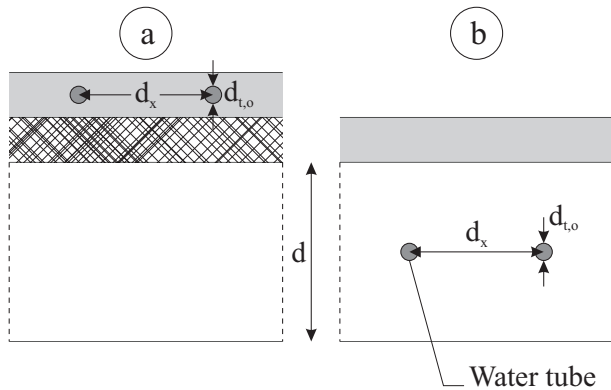


Figure 1.2: Comparison between (a) an embedded floor system and (b) CCA

The first ‘recent’ scientific paper on CCA, by Meierhans [92] in 1993, reports design considerations and measurements for an 800 m² office building in Switzerland and for an 2400 m² museum in Austria. In order to maximise night cooling of the thermal building mass, and to avoid active cooling at high outdoor temperatures, a water based radiant system was chosen, which actively conditions the core of the thermal building mass: CCA. The use in office buildings has increased ever since as described in various monitored case studies. [10, 22, 35, 26, 95, 97, 104, 130, 145, 152]. A well documented report presents the measurement analysis of the ‘Helvetia’ building in Frankfurt-Am-Main [16].

CCA and floor heating/cooling are not equal. Where in a floor heating/cooling system, the embedded pipes are separated from the building structure by a layer of insulation, with CCA the pipes are embedded in the building structure. Thereby, the whole of the thermal mass of the building, which in modern office buildings is mostly situated in the floor, is actively heated or cooled (Fig. 1.2).

Since different types of concrete slabs exist, also different types of CCA exist, of which 3 examples are shown in Fig. 1.3. CCA type (1) is a full concrete floor made at the construction site, while types (2) and (3) are examples of prefabricated floors, which are manufactured in the factory and transported to the construction site, in order to save time. To reduce weight, these types have hollow cores, air boxes, . . . , in the, regarding strength, neutral zone of the slab. In general, the term embedded water based systems is used to refer to all kinds of CCA or floor heating systems.

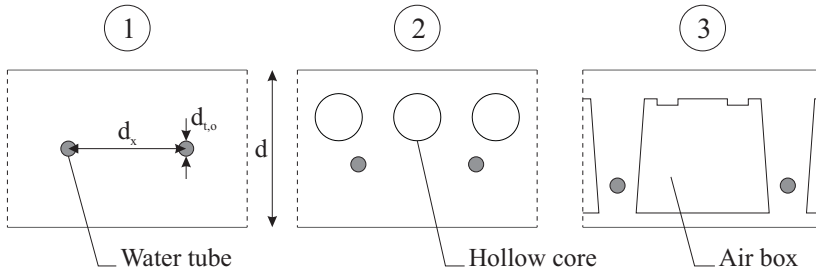


Figure 1.3: Examples of different CCA configurations with thickness d , tube spacing d_x and tube diameter $d_{t,o}$: (1) Full concrete CCA, (2) Hollow core CCA, (3) Air box CCA

Water supply temperatures in the tubes are relatively low for heating ($< 30^\circ\text{C}$), and relatively high for cooling ($> 15^\circ\text{C}$). A combination of CCA with a (ground coupled) heat pump, passive cooling or night cooling results in low exergy installations. As such this holds the promise of an efficient heating and cooling system.

Conventional HVAC systems, certainly air-based ones, are often assessed separately from the building. After all, the heat emitting side of those systems lack thermal capacity and do not influence the radiation heat exchange within the room substantially. In the case of CCA however, this does no longer hold.

Indeed, CCA represent a large thermal capacity, which is interacting with the building zone via floor and ceiling. Heat transfer from CCA to room is determined by the temperature difference between CCA surface and zone air for the convective heat transfer part and between CCA surface and the surrounding wall surface temperatures for the radiative heat transfer part. Likewise, heat and cold production and distribution systems are influenced by the CCA. The water side heat transfer depends on the state of the CCA and on the evolution of the room temperatures.

1.3 CCA in a building

An office building is typically subjected to several ‘disturbances’ (Fig. 1.4): ambient temperature T_{amb} (infiltration and conductive heat transfer), solar radiation through the windows \dot{q}_{sol} and internal gains from people, appliances and lights \dot{q}_{int} . These disturbances influence the zone temperature T_z and have

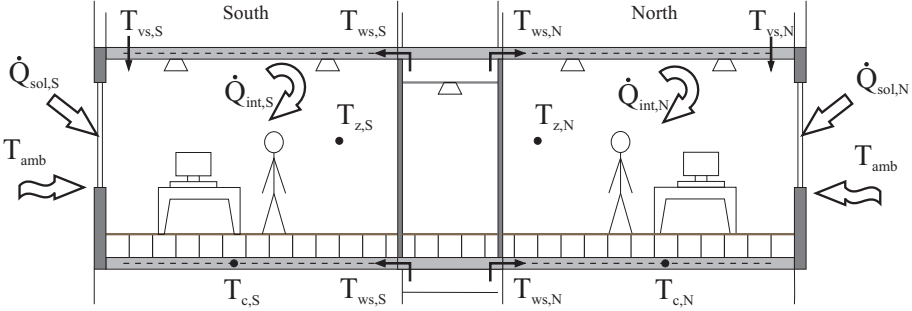


Figure 1.4: Schematic representation of a 2-zone office building with 3 disturbances: ambient temperature T_{amb} , solar radiation \dot{q}_{sol} and internal gains \dot{q}_{int} , 2 inputs: water supply temperature T_{ws} and ventilation supply temperature T_{vs} and 2 outputs: zone temperature T_z and concrete core temperature T_c

to be compensated either by the slow reacting, but high efficient CCA (T_{ws}), by the fast reacting ventilation system T_{vs} , having a lower efficiency, or possibly an additional heating/cooling system. Because CCA has more moderate heating and cooling water supply temperatures than required by the heating and cooling coil of the ventilation system, producing conditioned water for CCA can occur at a higher efficiency.

Heat transfer between CCA and room is driven by the temperature difference between the CCA surface temperature and the zone temperature: $\dot{q}_{CCA} = h_{c+r}(T_s - T_z)$, with h_{c+r} the total heat transfer coefficient combining convection and radiation (see Sec. 1.4). Since CCA is operated with low heating and high cooling supply water temperatures, $(T_s - T_z)$ is never very large. Therefore, the so-called ‘self-regulating’ effect is important: when CCA is heating the room and T_z increases, $(T_s - T_z)$ and \dot{q}_{CCA} will quickly decrease. This prevents overheating the room. This also applies for cooling. When internal or solar gains are heating up the room and T_z increases, $(T_s - T_z)$ and \dot{q}_{CCA} will quickly increase, providing extra cooling power in the zone.

Firstly, looking at the steady-state, CCA is a heating and cooling system with a low thermal power. Table 1.1 compares typically occurring heat gains and losses in an office building with the steady-state heating and cooling power from a 20 cm thick activated concrete slab: cooling is a critical issue, for which a backup system might be required. The presented values are explained further

on in this work.

Table 1.1: Comparison of typically occurring heat gains and losses in an office building with the steady-state heating and cooling power from a 20 cm CCA with a raised floor.

	Office room		CCA
Heat losses	20 – 40 W/m ²	Heating power	60 W/m ²
Heat gains	>100 W/m ²	Cooling power	30 W/m ²

Secondly, looking at the transient behaviour, the use of CCA introduces a large thermal inertia in the HVAC system of the building: a 20 cm full concrete slab has a heat capacity of $C = 403 \text{ kJ/m}^2\text{K}$ (floor area). A heating system with $\dot{q} = 60 \text{ W/m}^2$ heating power, directly transferred to the concrete slab, would need 1 h52 min to increase its temperature with 1 K. The response of the surface temperature of the same concrete slab to a step excitation of the water supply temperature has a time constant of 4 h18 min. This large thermal inertia seriously hampers the interaction between the heat and cold production system and the room: a change in room temperature does not immediately effect the water temperature in the tubes, while a change of the water supply temperature does not quickly result in a changing heating/cooling power into the room.

A simple example, using a simplified low-order CCA-building model presented in this work, clearly illustrates the transient behaviour of CCA. An office room cools down during the night, but heats up due to heat gains during the day (Fig. 1.5(a)). The CCA are cooled by the water during 4 h at night time. Knowing that the specific heat power from water to CCA \dot{q}_w is a function of the difference between mean water temperature and concrete core temperature ($T_{wm} - T_c$) and that the specific heat power from CCA to room \dot{q}_{CCA} is a function of the temperature difference between CCA surface temperature and the zone temperature ($T_s - T_z$), this example shows typical CCA behaviour. During the night, the office cools down, due to e.g. a cold ambient temperature. T_z drops faster than T_s , which means that the CCA is heating the room at that moment (Fig. 1.5(b) shows that \dot{q}_{CCA} is positive during the night). However, cold water starts cooling down the CCA at 0 AM to compensate for the heat gains of the next day (Fig. 1.5(b) shows that \dot{q}_w is negative from 0 AM-4 AM). This means that at night the CCA is heating the room, while the water is cooling the CCA. During the day, the CCA is cooling the room, while there is

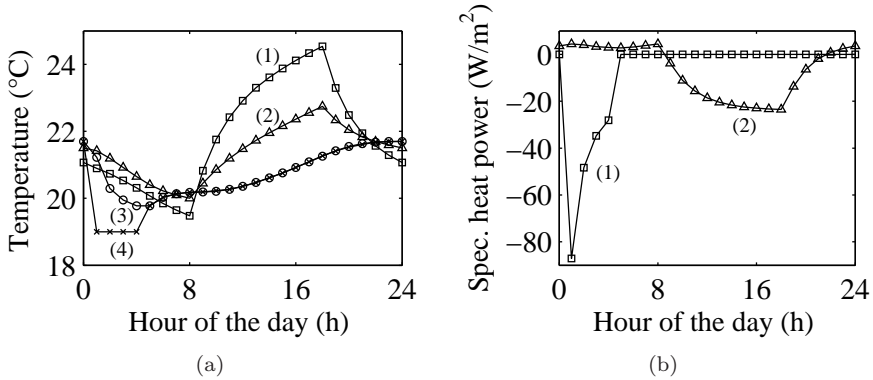


Figure 1.5: Typical CCA office building operation: (a) (1) zone temperature T_z , (2) surface temperature T_s , (3) CCA core temperature T_c , (4) water temperature T_w and (b) (1) heat power water-CCA \dot{q}_w , (2) heat power CCA-room \dot{q}_{CCA}

no water flow to cool or heat the CCA. The typical floating room temperature in a CCA building is observed in the results.

All these observations are the combined result of both the steady-state and the transient thermal properties of CCA. This example demonstrates that the control of CCA should be addressed with care. A representative transient model of CCA-and-building is required to be integrated in the building controller. Conventional water based systems, such as radiators, chilled beams or climate ceilings react faster than any of the occurring thermal loads in the building. Therefore, they can be controlled with a heating/cooling curve controller, which determines the water supply temperature based on a static model of building and system. A low level feedback loop on the zone temperature determines the on-off signal of the circulation pump. This feedback loop is no longer possible with CCA. Due to the large time constant of the CCA in relation to the occurring heat gains and heat losses, this controller will have to look forward in time, in order to define an appropriate control signal.

1.4 Temperatures and heat transfer in CCA and buildings

1.4.1 Operative temperature

A crucial temperature used to assess thermal comfort of a building occupant is the operative temperature, which is defined as:

T_{op} = the uniform temperature of an imaginary black enclosure in which an occupant would exchange the same amount of heat by radiation and convection as in the actual non-uniform environment.[68]

or otherwise stated:

T_{op} = the average of the mean radiant and ambient air temperatures, weighted by their respective heat transfer coefficients.[8]

This results in:

$$T_{op} = \frac{h_{c,cl}T_{ia} + h_{r,cl}T_{mr}}{h_{c,cl} + h_{r,cl}} \quad (1.1)$$

$$= AT_{ia} + (1 - A)T_{mr} \quad (1.2)$$

$$A = \frac{h_{c,cl}}{h_{c,cl} + h_{r,cl}} \quad (1.3)$$

with:

- A (m^2): surface area
- T_{ia} ($^{\circ}\text{C}$): the indoor air temperature
- T_{mr} ($^{\circ}\text{C}$) the mean radiant temperature from the point of view of the occupant
- $h_{c,cl}$ ($\text{W}/\text{m}^2^{\circ}\text{C}$) the surface convection heat transfer coefficient of the clothed body
- $h_{r,cl}$ ($\text{W}/\text{m}^2^{\circ}\text{C}$) surface radiation heat transfer coefficient of the clothed body

At indoor air velocities below 0.2m/s, $h_{c,cl} \approx h_{r,cl}$ and $A = 0.5$ [6] which reduces Eq.(1.2) to:

$$T_{op} = \frac{T_{ia} + T_{mr}}{2} \quad (1.4)$$

The mean radiant temperature T_{mr} is hard to determine and position dependent. It is often simplified by the area weighted mean of the surrounding surface temperatures, without taking view factors of the person present in the room into account.

1.4.2 Heat transfer modes

Conductive, convective and radiative heat transfer all play an important role in describing the thermal behaviour of CCA in buildings. The way these three modes of heat transfer are used throughout this PhD-text is described in the following subsections. It is not the aim to derive detailed heat transfer formulations or to use a numerical approach but rather to obtain simple expressions that are usable in CCA building controller models. Evidently, the relative importance of each of the three heat transfer modes has to be formulated correctly. Furthermore, this analysis is important to obtain correct definitions for the different temperatures used in the thermal models of CCA-buildings.

Steady-state conductive heat transfer

The empirical law of Fourier $\vec{q} = -\lambda\nabla T$ states that *the heat flux, \dot{q} (W/m^2), resulting from thermal conduction is proportional to the magnitude of the temperature gradient and opposite in sign to this gradient.* The proportional factor λ is the *thermal conductivity* (W/mK). This equation contains two dependent variables \dot{q} and T . When λ is a constant, or when λ is varying linearly with T and is evaluated at the average temperature, the law of Fourier in a 1D situation reduces to:

$$\dot{Q} = -\lambda A \frac{(T_{x=0} - T_{x=d})}{d} = -\frac{1}{R_{cond}}(T_{x=0} - T_{x=d}) \quad (1.5)$$

with :

- $R_{cond} \equiv \frac{d}{\lambda A}$ (K/W): the conductive heat transfer resistance
- λ (W/mK): the thermal conductivity
- d (m): slab thickness
- $T_{x=0}$ (K): temperature at boundary $x = 0$
- $T_{x=d}$ (K): temperature at boundary $x = d$

Convective heat transfer

Convective heat transfer is a difficult to determine process in building heat transfer. In this work, the focus lies on the convection from the CCA surface to the air in the building zone. In general, when convection is generating a heat flux at the surface of a body, this is described by:

$$\dot{q}_c = \underbrace{-\lambda_f \frac{\partial T}{\partial y} \Big|_{y=0}}_{\text{(conduction into the fluid)}} = h_{c,surface}(T_s - T_{fluid}) \quad (1.6)$$

with:

- λ_f (W/mK): the fluid thermal conductivity
- $h_{c,surface}$ (W/m²K): the surface convection heat transfer coefficient
- T_s (K): surface temperature
- T_{fluid} (K): temperature of the fluid outside the thermal boundary layer

Eq. 1.6 defines $h_{c,surface}$ within the fluid, which is the room air in this case. However, the temperature T_{fluid} is not equal to the indoor air temperature T_{ia} of the zone. Whereas T_{ia} is typically measured at a height of 1.1 m (for a sitting person), T_{fluid} is the air temperature just outside the thermal boundary layer at the surface. Awbi and Hatton [9] measured this T_{fluid} at a distance of 10 cm from the surface. Therefore, to be able to use measurements of T_{ia} , Eq.

1.6 should be rewritten as:

$$\begin{aligned}
 \dot{q}_c &= h_{c,surface}(T_s - T_{fluid}) \\
 &= h_{c,surface} \frac{T_s - T_{fluid}}{T_s - T_{ia}} (T_s - T_{ia}) \\
 &= h_c(T_s - T_{ia})
 \end{aligned} \tag{1.7}$$

with:

- h_c (W/m²K): the zone convection heat transfer coefficient for the specified surface

Several correlations for $h_{c,surface}$ are available for standard configurations in the literature. However, when defining a value for h_c in buildings, these correlations should be addressed with care, since a building zone forms an enclosure around the investigated surface. The contours of this enclosure induce recirculation of the air which in turn enhances heat transfer compared to the non-enclosure case. Moreover, it can be easily seen that $h_{c,surface}$ is depending on position, h_c is depending on position and temperatures of the zone, while, for the general description of the convective heat transfer from CCA-surface to zone, a global parameter \bar{h}_c is required. Reports and reviews of \bar{h}_c measurements are available in the literature. From the analysis of these correlations in App. D.5, it is concluded that the Awbi and Hatton correlation [9] for \bar{h}_c can be used in this work. Knowing \bar{h}_c , convective heat transfer from CCA-surface to zone air can be written as:

$$\dot{Q}_c = \bar{h}_c A (\bar{T}_s - T_{ia}) = \frac{1}{R_{conv}} (\bar{T}_s - T_{ia}) \tag{1.8}$$

with:

- $\bar{h}_c = \frac{c_1}{D^{c_2}} (\bar{T}_s - T_{ia})^{c_3}$ (W/m²K): the global zone convection heat transfer coefficient for the specified surface from Awbi and Hatton [9]. Values of c_1 , c_2 and c_3 are given in App. D.5. In the remainder of the PhD-text the symbols h_c and T_s will be used instead of \bar{h}_c and \bar{T}_s in the formulation of the convective heat transfer.
- D (m): hydraulic diameter
- $R_{conv} \equiv \frac{1}{\bar{h}_c A}$ (K/W): the convective heat transfer resistance

- A (m^2): CCA surface area

Radiative heat transfer

Since CCA operates at moderate temperatures, the temperature difference between CCA surface and the surrounding zone is limited. Therefore, radiative heat transfer forms (relatively seen) an important contribution to the total heat transfer from CCA to the building zone. Radiative heat exchange between two surfaces is (for long wavelengths building surfaces are grey surfaces, so $\epsilon(T) = \alpha(T)$) presented by:

$$\dot{Q}_{r,1-2} = \frac{\sigma (T_{s1}^4 - T_{s2}^4)}{\frac{1 - \epsilon_1}{\epsilon_1 A_1} + \frac{1}{A_1 F_{1-2}} + \frac{1 - \epsilon_2}{\epsilon_2 A_2}} \quad (1.9)$$

with:

- $\sigma = 5.67 \times 10^{-8}$ ($\text{W}/\text{m}^2\text{K}$): The Stefan-Boltzmann constant
- ϵ (-): The total emittance of a surface
- F_{1-2} (-): the view factor from surface 1 to surface 2

However, a building zone forms an enclosure with n different surfaces, where radiative heat exchange between each of these surfaces exists. Elaborating the general radiative heat exchange theory shows that for a surface i (e.g. in [88]):

$$C_{ij} \dot{Q}_{rj} = D_{ij} \sigma (T_{si}^4 - T_{sj}^4), \quad j=1..n \quad (1.10)$$

with:

- C_{ij} : function of emittances, areas and view factors
- D_{ij} : function of areas and view factors

Eq. 1.10 can be written explicitly as a function of the temperatures of the enclosure [88]:

$$\dot{Q}_{ri} = A_i \epsilon_i \sigma \left(T_i^4 - \sum_{j=1}^n F_{ij} \sum_{k=1}^n a_k T_k^4 \right) \quad (1.11)$$

with the coefficients a_k depending on the view factors and emittances of the enclosure.

Combined convective and radiative heat transfer

Formulating Eq. 1.11 for the radiative heat transfer emitted by surface i , is not straightforward for real building geometries. A commonly used simplification is to assume that all surrounding surface are at a ‘radiant zone temperature’ T_{r1} , which stands for the uniform temperature the surrounding surfaces should have to obtain the same radiative heat exchange as in reality. Eq. 1.9 can now be rewritten to describe \dot{Q}_r from surface 1 to the other zone surfaces:

$$\dot{Q}_{r1} = A_1 \frac{\sigma (T_{s1}^4 - T_{r1}^4)}{\frac{1}{\epsilon_1} + \frac{A_1}{\sum A_k} \frac{1 - \epsilon_k}{\epsilon_k}} \quad (1.12)$$

with:

- $\sum_{k=1}^n A_k$ (m^2): sum of the area of all surfaces surrounding surface 1
- F_{1-zone} (-): view factor is equal to 1
- ϵ_k (-): mean emittance of surrounding surfaces. Most building materials have a high emittance, from 0.8 to 0.95, for long wave radiation

Since ϵ_k is high and $\sum_{k=1}^n A_k > A_1$, the second term of the denominator of Eq. 1.12 is small compared to the first term and can be neglected. E.g. for the typical office building used in this PhD-text to evaluated CCA controller performance (see Ch. 7), the second term is less than 2% of the first term. Therefore, eq. 1.12 becomes:

$$\dot{Q}_{r1} = A_1 \epsilon_1 \sigma (T_{s1}^4 - T_{r1}^4) \quad (1.13)$$

Comparing Eq. 1.13 with Eq. 1.11 shows that the radiant zone temperature for surface 1 equals:

$$T_{r1} = \sqrt[4]{\sum_{j=1}^n F_{ij} \sum_{k=1}^n a_k T_k^4} \quad (1.14)$$

As a simplification, the radiant zone temperature for a surface is often approximated by the area weighted mean surface temperature of the surrounding surfaces, without taking view factors and emittances into account:

$$T_{r1} \approx T_{rm1} = \frac{\sum_{k=1}^n A_k T_{sk}}{\sum_{k=1}^n A_k} \quad (1.15)$$

This approach is also used to approximate the operative temperature (Sec. 1.4.1).

The difference of temperatures to the 4th power in Eq. 1.13, can be linearised [27], resulting in:

$$\dot{Q}_{r1} \approx A_1 \epsilon_1 \sigma 4T_m^3 (T_{s1} - T_{r1}) \quad (1.16)$$

$$= A_1 h_r (T_{s1} - T_{r1}) \quad (1.17)$$

$$= \frac{1}{R_{rad}} (T_{s1} - T_{r1}) \quad (1.18)$$

with:

- $T_m = (T_{s1} - T_{r1}) / 2$ (K): for the limited temperature ranges of building surfaces, this approximation yields only a limited error [60]
- $h_r = \epsilon_1 \sigma 4T_m^3$ (W/m²K): radiative heat transfer coefficient

The formulation of radiative heat exchange is now equivalent to the one of convective heat exchange, except for the fact that T_{r1} is used for radiation and T_{ia} for convection. Combining Eq. 1.8 for convection and Eq. 1.17 for radiation results in:

$$\begin{aligned} \dot{Q}_{c+r,1} &= A_1 h_c (T_{s1} - T_{ia}) + A_1 h_r (T_{s1} - T_{r1}) \\ &= A_1 (h_c + h_r) \left(T_{s1} - \frac{h_c T_{ia} + h_r T_{r1}}{h_c + h_r} \right) \\ &= A_1 h_{c+r} (T_{s1} - T_{ref1}) \end{aligned} \quad (1.19)$$

$$T_{ref1} = \frac{h_c T_{ia} + h_r T_{r1}}{h_c + h_r} \quad (1.20)$$

with T_{ref1} the reference temperature for combined convection and radiation of surface 1.

Note that, although the formulations of T_{op} (Eq. 1.1) and T_{ref1} (Eq. 1.20) are similar, they are not equal. T_{op} is formulated from the point of view of the occupant of the building zone, while T_{ref1} from the viewpoint of surface 1. Other occupants at a different location will have a different T_{op} , while other surfaces of the zone will have a different T_{ref} .

1.4.3 Heat exchange in a building zone

Convective and radiative heat flows in the building zone affect the operative temperature and consequently the thermal comfort in the zone. Convective heat exchange between the zone walls and the zone air temperature represents a star network between the wall surfaces and the zone air node. The star temperature in this case is the indoor air temperature T_{ia} (Eq. 1.8).

On the other hand, long wave radiative heat exchange is a surface-to-surface network of heat flows. For a simple geometry, it is possible to transform this surface-to-surface network into a star network, in which each surface exchanges radiative heat with a fictitious star node [121],[34][par.6.5].

Seem [121] lumped convective and radiative heat flows into one star network with the radiant-air temperature T_{ra} , having both air and radiative components, as central point. A fictitious thermal resistance R_{star} , determined by both convective and radiative heat transfer parameters, connects T_{ra} with the zone air temperature T_{ia} . Although T_{ra} is a weighted mean of the radiant and the air temperature, it is not correct to use this temperature as the operative temperature assessing thermal comfort, due to its derivation by transformations and lumping of heat transfer parameters [34]. TRNSYS, a dynamic simulation program has an integrated building model according to the approach of Seem [121]. In this rad-air building model, convective heat loads act on the T_{ia} -node, while radiative heat loads act on the T_{ra} node. This detailed thermal building model is used in this PhD-text to evaluate the dynamic thermal behaviour of CCA in buildings.

Compared to reality, even the detailed TRNSYS building model is still a simplification. However, for the controller building model as presented in Ch. 9, even a further simplification is required. Assuming that $T_{ref,k}$ ($k=1..n$) for every surface would not deviate too much from what in this text will be called

‘the zone temperature’ $T_z = \sum_{k=1}^n T_{ref,k}/n$, Eq. 1.19 becomes for all enclosure surfaces:

$$\dot{Q}_{c+r,i} = A_i h_{c+r} (T_{si} - T_z) \quad (1.21)$$

In this way a simplified but easy-to-implement star-network is created with T_z as the central temperature, equal for all surfaces.

1.4.4 Operative temperature in the simplified building model

Since thermal comfort is evaluated using the operative temperature of the office zone, the simplified building model needs to provide information regarding this temperature. The approach of the resultant zone temperature T_z , defined by Kummert [83], is used: “The temperature T_z is obtained by adding the convective and radiative heat exchange coefficients of each surface and using this global coefficient to build a star network. For the purpose of optimal control, the resultant zone temperature T_z will be used as an approximation of the operative temperature T_{op} .”

1.5 Transient heat transfer

Since the time constant of CCA is large, the system will never be in a steady-state regime when operating in a building. Regarding heat transfer, the system is continuously in a transient state, meaning that the temperature inside the concrete slab will vary with time and with position. Fourier’s law (Eq. 1.5) and the conservation of energy principle applied to a one-dimensional element, without internal heat generation, yields the heat diffusion equation. For incompressible substances ($c_v = c_p = c$), and with the thermal conductivity assumed constant, this heat diffusion equation reduces to:

$$\rho c \frac{\partial T}{\partial t} = \lambda \frac{\partial^2 T}{\partial x^2} \quad (1.22)$$

From the heat diffusion equation the thermal diffusivity $\alpha \equiv \frac{\lambda}{\rho c} [m^2/s]$ is defined, which is an important material parameter in the analysis of transient heat conduction. α is a measure for how quickly a material can drain heat from a hot source. Furthermore, the square of a characteristic length (in this

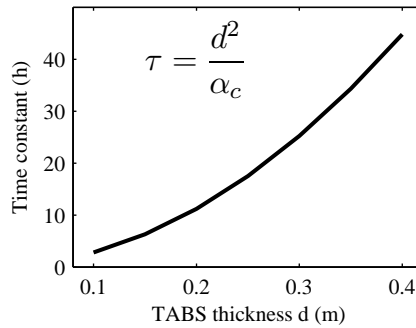


Figure 1.6: CCA time constant based on the thermal diffusivity α_c as a function of thickness d

case the CCA thickness d) divided by α represents the time constant of the conductive heat transfer (see Sec. 4.3).

The time constant $\tau = d^2/\alpha$ ranges from 2.8 h to 44.8 h for a thickness of 10 cm to 40 cm (Fig. 1.6). Since these time constants are in the range of or larger than the time constants of the heat gains and losses occurring in an office building (see Ch. 5), the heat transfer in a CCA element will always be in transient regime.

Transient effects in convective and radiative heat transfer are not taken into account in this work.

1.6 Lumped capacity model or RC-model

A commonly used method to describe transient heat transfer in a material layer is by using a thermal Resistance-Capacitance or RC-model. For an RC-model having n thermal capacitances or ‘nodes’, it is assumed that the temperature inside the material layer is characterised by the temperatures of the nodes and these temperatures can only vary with time. Such a system model approach is referred to as the lumped capacity approach. The number of nodes defines the order of the model.

In heat transfer theory, lumped capacity solutions are typically used in situations where the conduction heat transfer coefficient λ/d is much larger than the convection coefficient h at the elements surface. This is presented as

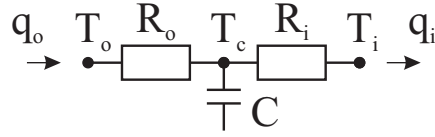


Figure 1.7: 1st order lumped capacity representation of a material layer.

the Biot number (Bi) to be very small:

$$Bi = \frac{hd}{\lambda} \ll 1 \quad (1.23)$$

with h the heat transfer coefficient from surface to surroundings (W/m²K), d the thickness (m) and λ the heat conduction coefficient of the material layer (W/mK).

Heat transfer to the surroundings from an object with a very small Biot number has a large temperature drop at the surface, while the interior is at almost constant temperature. This typically happens with metallic objects.

Fig. 1.7 shows a 1st order RC-model of a material layer with T_o and T_i the temperature of the surroundings on the outer (o) and the inner (i) surface of the layer. R_o and R_i are the thermal resistances lumping conduction in the material and convection and radiation to the surroundings. T_c is ‘the’ temperature of the material layer, which has a thermal capacitance C . The energy balance $\dot{E}_{stored} = \dot{Q}_{in} - \dot{Q}_{out}$ of this system results in:

$$C \frac{dT_c}{dt} = -\frac{1}{R_o}(T_c - T_o) - \frac{1}{R_i}(T_c - T_i) \quad (1.24)$$

with $R = d/A\lambda$ the thermal resistance (K/W) and $C = dA\rho c_p$ the thermal capacitance (J/K).

Similar the energy balance is used for all nodes of a system with more than one lumped capacitance.

In typical CCA-modeling approach (see Sec. 1.7.1), the heat transfer in CCA is divided in an upper and a lower part, which are independent from each other. Therefore, a separate Bi-number can be defined for the upper part and the lower part of the concrete slab, each having a thickness d_i . The value of d_i is defined by the position of the tubes in the CCA element. For a 20 cm thick concrete slab, with tubes in the centre of the slab, which is heating a room, the

Bi-values of upper and lower part are:

$$Bi_{lowerpart} = \frac{(h_c + h_r)(d/2)}{\lambda_{concrete}} = \frac{(0.4 + 5.6)0.1}{2} = 0.30 \quad (1.25)$$

$$Bi_{upperpart} = \frac{(h_c + h_r)(d/2)}{\lambda_{concrete}} = \frac{(3.3 + 5.6)0.1}{2} = 0.44 \quad (1.26)$$

Since these Bi-number are not very small, a certain temperature drop will appear inside the concrete slab (which will also be shown by the transient analysis in Ch. 3). Therefore, describing the heat transfer from the water in the CCA to the room air by an RC-system having 1 lumped capacity, will introduce errors. On the other hand, this approach leads to a simplified set of heat transfer equations, which are more easily solved and usable in parameter estimation problems and in model predictive control analysis. Therefore, a trade-off between simplicity and accuracy has to be found (See Ch. 5).

1.7 CCA thermal models

1.7.1 EMPA CCA model

Pioneer work on simplified modelling of CCA has been performed by EMPA, the Swiss Federal Laboratories for Materials Testing and Research. The book ‘Thermoaktive Bauteilsysteme tabs’ [81] presents a simplified RC-model for CCA. In the present work, this model will be referred to as the ‘EMPA model’. The 3D heat flow pattern inside the concrete slab is transferred into a 1D model by means of an analytic expression for the temperature in a homogeneous concrete floor with embedded tubes and by means of a triangle-star transformation on the thermal resistances network. Deriving this expression introduces the equivalent thermal resistance R_x , while the temperature T_c is the equivalent concrete core temperature. Fig. 1.8 shows the different thermal resistances in the RC-network with:

- R_a (K/W): Thermal resistance to heat transfer from tube wall to upper CCA surface
- R_b (K/W): Thermal resistance to heat transfer from tube wall to lower CCA surface

- R_d (K/W): Thermal resistance to heat transfer between upper and lower CCA surface
- $R_{di} = (K/W)$: Upwards ($i = 1$) or downwards ($i = 2$) heat transfer through upper and lower CCA slab into the room at temperature $T_{zone\ i}$ (conduction and convection)
- R_x (K/W): Equivalent core thermal resistance
- R_t (K/W): Thermal resistance of tube wall (conduction)
- R_w (K/W): Thermal resistance from water to tube wall (forced convection)
- R_z (K/W): Thermal resistance from water supply temperature to mean water temperature

If the conditions

$$\frac{d_i}{d_x} > 0.3 \quad \text{and} \quad \frac{d_{t,o}}{d_x} < 0.2 \quad (1.27)$$

are fulfilled (with d_i the thickness of the concrete layer below or above the tubes, d_x the distance between the tubes and $d_{t,o}$ the outer tube diameter), the thermal resistances R_x , R_{d1} and R_{d2} are represented by:

$$R_x \approx \frac{d_x \ln(d_x / \pi d_{t,o})}{2\pi\lambda_t} = f(d_{t,o}, d_x, \lambda_t) \quad (1.28)$$

$$R_{di} = \frac{d_i}{\lambda_c} \quad (1.29)$$

with λ_c (W/mK): thermal conductivity of concrete.

Meeting these conditions mathematically means that R_x is only a function of the parameters $d_{t,o}$, d_x and λ_c , and no longer a function of the CCA thickness d [81]. Furthermore, R_{d1} and R_{d2} represent the heat resistances to the upper and lower room and are only a function of the CCA thickness d and no longer a function of tube parameters, nor of the opposite concrete layer. Physically, meeting these conditions means that the temperature profile which exists in the core of the tabs is flattened when reaching the upper or lower boundary of the slab and the assumption of 1D heat flux to the room below or above is justified.

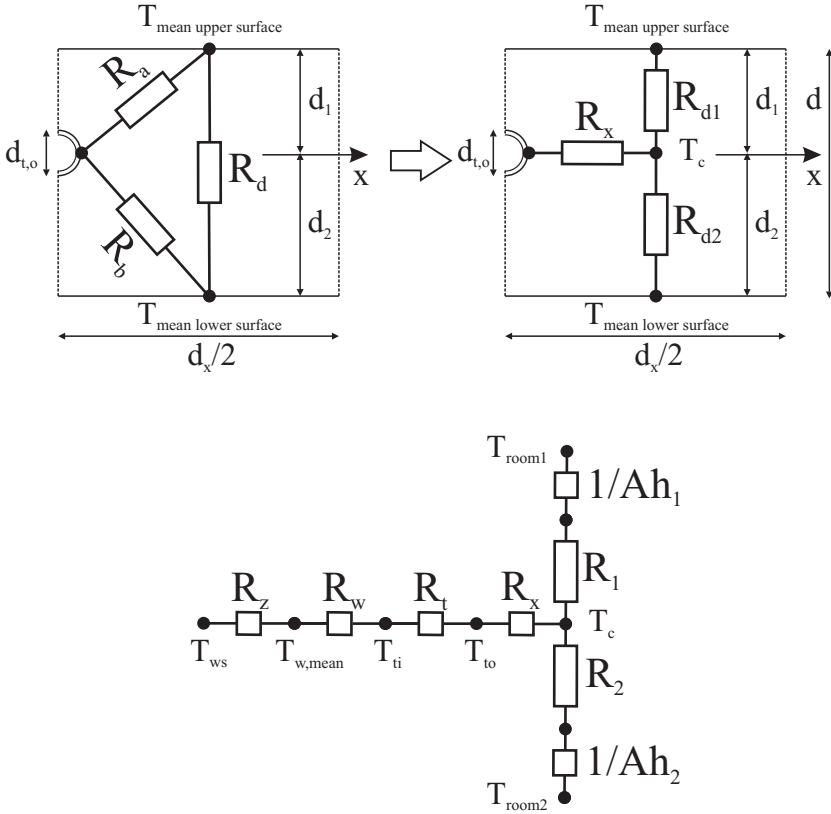


Figure 1.8: EMPA CCA model [81]: Triangle-star transformation describing 2D heat flow in a 1D thermal model

The EMPA RC-model (Fig. 1.8) is completed with thermal resistances R_t for the tube wall, R_w for the water-tube forced convection and R_z which takes into account the difference between the water supply temperature T_{ws} and the mean water temperature in the slab T_{wm} [81]. The positioning of the thermal capacitances is presented and analysed by Weber and Johannesson [144] and by Weber et al. [145]. This RC-model is integrated in the building model of the transient system simulation program TRNSYS [122].

Weber and Johannesson [144] demonstrated that it is possible to use this EMPA-RC-network to describe the two dimensional heat flow occurring in an asymmetrical CCA floor. Only when the layer on top of the pipes becomes too thin, the results will deviate significantly from reality. Also, for cycling

periods < 40 min of e.g. the water supply temperature, the heat flow from water to concrete deviates with more than 10% compared to Finite Elements (FE)-results. Weber et al. [145] report deviations < 0.2 K between a FE-model and an 11th order RC-star network model of a CCA with raised floor. Being relevant for whole building models, Weber et al. [145] demonstrated that adding an extra RC-link for the air and for the raised floor tiles, provides a good representation to obtain accurate temperatures inside the concrete floor.

The EMPA model, as validated by Weber et al. [145] and Koschenz and Lehmann [81], is used throughout this work as the starting point to model the CCA, whether the objective is to analyse the steady state behaviour, the transient behaviour or to integrate the CCA model in a high level building controller.

1.7.2 Other CCA models

Modelling of CCA has been frequently described in the literature. Very often a numerical solution is sought to calculate the 3D or 2D temperature distribution in the concrete slab. Meierhans [92] used a finite difference (FD) method to model a full concrete CCA. Antonopoulos et al. [3] compared a 3D and 2D (neglecting the z -direction along the tubes) FD-method with experimental results. Russell and Surendran [113] used a FD-model to analyse the cooling capacity and perform some parametric analysis. Olesen et al. [98] presented the FD-model which is incorporated in the European standard EN15377 on water based embedded heating and cooling systems [43]. In the transient system simulation program TRNSYS [122] a FD-model for an embedded water based system is available [49]. Hoh et al. [62] combined a Finite Volume (FV)-model and hydraulic model in the Modelica-language. Babiak et al. [11] used a FE-model to observe a depth of on average 15 cm at which a sinusoidal room temperature with a 24 h period is transmitted through the concrete slab.

RC-models or analytical expressions are sometimes used for the integration of CCA in buildings. Glück [52] presented first principle based models of various water-embedded systems. Ren and Wright [110] used a 2nd order RC-model for a ventilated hollow core CCA and integrated this in a 2nd order building model. Schmidt [120] used RC-models connected to a hydraulic model which are combined into macro elements to describe a whole building element.

Barton et al. [15] used a FD-model to analyse a hollow core CCA for which

conditioned air flows through the hollow cores. They took the bends into account by an equivalent ‘bend’ length. Weitzmann and Svendsen [147] used measurements to validate a FV-model and find a good correlation for heat flows, but temperature deviations up to 2 K.

1.8 Overview

In this introductory chapter, the literature on CCA models was summarized. In Chapter 6, the literature review of CCA control is presented. In order to achieve the goals of this work, a few gaps still have to be filled.

Firstly, every CCA controller, sophisticated or not, requires a model of CCA and building. Simple, analytical models can provide a low-cost solution, but are not available in the literature. On the other hand, for more complex models the procedure to find the correct model parameters is not straightforward, but indispensable to achieve a good controller performance. I address both topics in this work.

Secondly, regarding the control of CCA, the literature presents several pieces of the puzzle, without however deriving simple but robust guidelines for controller design. I will try to arrive at such a set of guidelines based on the different results in this work.

Thirdly, the interaction between CCA and the ventilation system has a high potential, because it combines a slow, but efficient system with a fast, but less efficient system. The way the CCA controller should deal with this interaction is a limited explored area in building system control.

This text is structured in four major parts: in the *Introduction* part, the goal of this work is presented and the problem of the transient behaviour of Concrete Core Activation (CCA) is introduced. The *CCA*-part focusses on the static and transient thermal properties of the CCA component, while the *CCA and building*-part investigates how CCA and building interact and looks at the corresponding control issues. Finally, the *Conclusion and outlook*-part summarizes the major findings and formulates points of interest for further research.

The following topics are addressed in this work:

Introduction

Chapter 1 presents CCA and models for CCA and illustrates the importance of its transient thermal behaviour by means of a simple numeric example. In **Chapter 2** a case study analysis identifies more in detail the problem of controlling the transient behaviour of CCA.

CCA

In this part, the CCA component is analysed.

Chapter 3 shows a parametric study of the thermal resistances in CCA, leading to a detailed steady-state analysis.

Subsequently, in **Chapter 4**, the transient behaviour is first analysed using lab-measurements. An analytical solution of the transient heat transfer is derived to determine the temperature and heat flows inside the CCA as a function of both location and time. The acquired formulation is used to analyse the transient behaviour of CCA and derive conclusions regarding control.

In **Chapter 5** CCA is integrated in a building. A frequency response analysis of CCA identifies the transient behaviour in relation to the occurring disturbances in a building zone: the ambient temperature T_{amb} , solar radiation \dot{q}_{sol} and internal gains \dot{q}_{int} . A detailed CCA model is used to assess the dominant time scales of the CCA.

CCA and building

In the third part, the integration of CCA in a building and its control are investigated.

Chapter 6 introduces control with CCA by analysing the literature. Moreover, a choice is made for the appropriate thermal comfort model to use in CCA buildings.

Chapter 7 presents a detailed CCA building model, which serves as a data generator for testing the CCA controller.

In **Chapter 8**, an analysis of a conventional on-off feedback controller is presented. A variation of possible controller settings learns how CCA react to controller actions. This proves the need for a predictive controller, based on a dynamic model of CCA and building.

The CCA building model of such a predictive controller is composed in **Chapter 9**. Starting from a white-box model, the parameters are identified using data from the detailed CCA building model of Chapter 7.

Finally, **Chapter 10** outlines a Model based Predictive Controller (MPC), which accounts for future disturbances and minimizes the cost for thermal comfort, for CCA operation and for operating the air handling unit, which provides the conditioned ventilation air. An analysis of the calculated optimal profiles shows the reaction of the controller to future disturbances, taking into account the CCA and building dynamics.

Conclusion and outlook

In **Chapter 11** the main conclusions are formulated, while in **Chapter 12** an outline for future work is presented.

Chapter 2

Case study of a CCA office building

2.1 Introduction

The large thermal time constant of CCA hampers the communication between the system's production and emission part. Therefore, conventional building control strategies, typically using room temperature feedback, are not appropriate to control thermal comfort efficiently. This chapter presents measurement data and simulation results that reveal the dramatic impact of a conventional feedback controller on overall energy performance. Measurements in a CCA building with room temperature feedback show the HVAC system switching between heating and cooling during the course of the day. A simplified, generic room model is used to simulate, understand and evaluate this behaviour.

Table 2.1: Parameters of the measured building

Building parameter	Value
Heated volume (m ³)	3278
Heated area (m ²)	993
Heat loss area above the ground (m ²)	1534
U-value external wall/roof/ground slab (W/m ² K)	0.35 / 0.36 / 0.44
U-value total (W/m ² K)	0.54
Glazing (U-value/g-value) (W/m ² K)/(%)	1.7 / 40
Percentage of glazing (%)	46 ¹
Installed heat pump heating power (kW)	50 ²
Installed ground cooling power (kW)	35
Overall energy use in 2006 (kWh _{el} /m ²)	94 ³

¹ Total glazed area is 706 m², of which 56% is facing South

² only 20 kW of this installed power is used in regime

³ This equals 234 kWh_{prim}/m² with an electricity conversion factor of 2.5

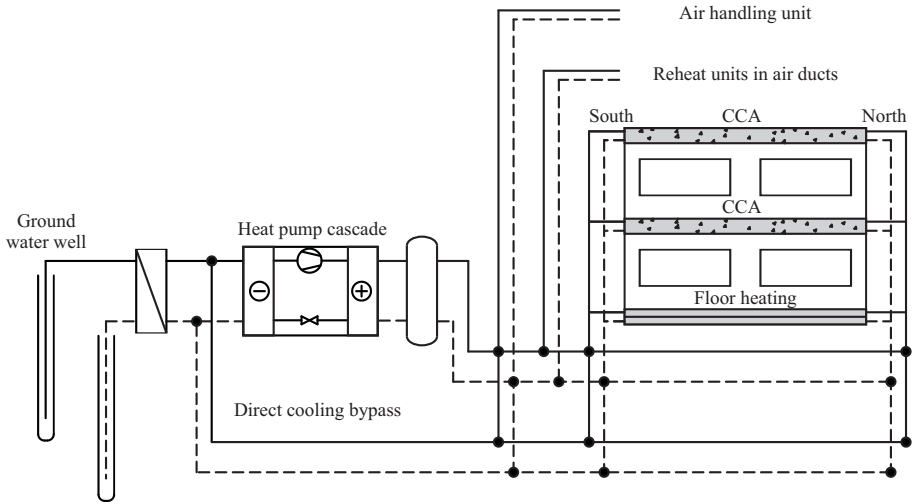
2.2 Measurements in a CCA office building

2.2.1 Description of the measured building

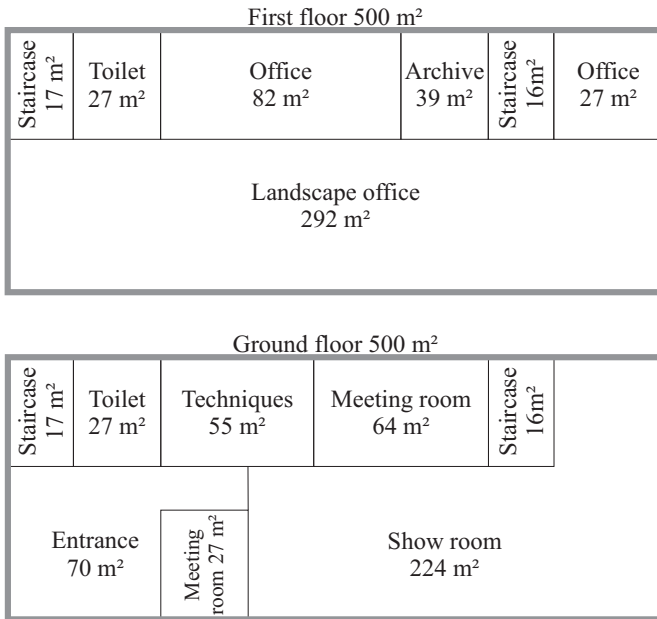
Within the framework of the IWT-TETRA-THERMAC (THERMally ACtivated buildings) research project [102] measurements were carried out on the HVAC-installation of a small scale office building equipped with CCA. A schematic view of the system is shown in Fig. 2.1(a), comprising from left to right: the supply and return ground well, the heat pump with the direct cooling by-pass and the two-floor office building with CCA. The office building is located near Arnhem (The Netherlands) and consists of 2 levels: a ground level with a reception, a meeting and a training room, and a first level with a landscape office supplemented with some rooms for filing, ICT, etc.

Table 2.1 summarizes the main building parameters. Walls and roof are constructed with 10 cm of polyurethane insulation and the ground slab with 8 cm of insulation. This leads to an overall U-value of 0.54 W/m²K, which is comparable to other newly built and energy efficient office buildings [95, 141]. The required specific heating power for the building is 70 W/m², while the required specific cooling power is 47 W/m², based on the data of the design engineers.

The electricity bill indicates that the overall energy use for this all electric



(a)



(b)

Figure 2.1: (a) Schematic view of building and installation: the supply and return ground well, the heat pump cascade with in parallel the direct cooling bypass and the two-floor building with CCA and ventilation, (b) Floor plan of the investigated office building

building was $94 \text{ kWh/m}^2\text{a}$, including electricity for heating, cooling, ventilation, lighting and appliances. With a low occupation of only 20 people ($50 \text{ m}^2/\text{pers}$), the electricity use for appliances (PC, server, copier, ...) is calculated according to the ASHRAE standards [8] to be $8 \text{ kWh/m}^2\text{a}$, which is in agreement with other measurement data [129, 145]. The remainder of the measured electricity use, $86 \text{ kWh/m}^2\text{a}$, is for HVAC and lighting and, with an electricity conversion factor of 2.5, this results in a primary energy use of $215 \text{ kWh}_{\text{prim}}/\text{m}^2\text{a}$. Given the low U-value, this is a poor result. It is more than a factor 2 higher than a German guideline for energy efficient buildings at that time (primary energy use for HVAC and lighting $< 100 \text{ kWh}_{\text{prim}}/\text{m}^2\text{a}$), which has been shown to be achievable through several case studies [95]. As demonstrated hereafter, the unadapted control strategy is a possible explanation.

The ground slab is a traditional floor heating system, whereas the first floor slab and the roof slab are CCA (Fig. 2.1(a)). Room thermal comfort is guaranteed by the CCA, together with supplementary heating or cooling by a roof top air handling unit (AHU). Terminal reheat units heat the supply air just before entering the rooms, if necessary. In heating mode, the water/water heat pump heats a buffer tank from where a collector feeds the terminal reheat units (at 45°C), the CCA and the AHU. The CCA and AHU have their own temperature control, while the terminal reheat units use directly the hot water from the buffer tank. While cooling, the heat pump is bypassed and the CCA and AHU are directly connected to the ground water well via the heat exchanger.

The building is divided into a South and North zone with a separate control (Fig. 2.1). The room air temperature is the main controlled variable of the installation. At the start of the measurements CCA cooling was activated as soon as the room temperature rises above 22.5°C , and CCA heating started for room temperatures below 21°C . This narrow dead band control is typically applied in the case of fast reacting systems, such as radiators or forced convection systems. In this case, it was applied to the slow reacting CCA.

Each terminal reheat unit is used for local control in heating regime. It has a fixed set point of 19°C which is manually adjustable by the occupant within a 3°C range. The building management system has no influence on this setting. Backup cooling is not installed.

The building management system logs several data, such as room air temperatures, water temperatures, air temperatures in the air handling unit

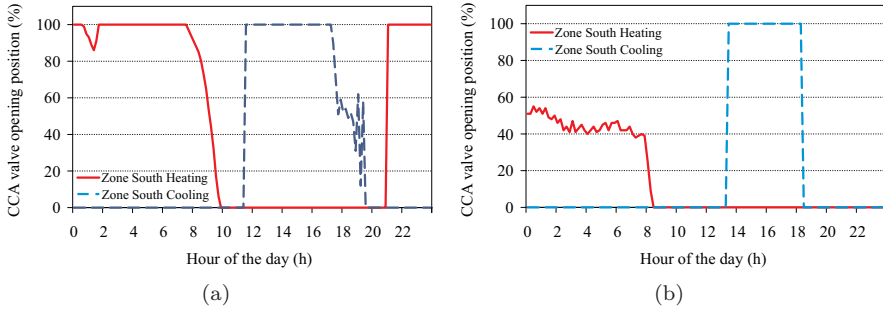


Figure 2.2: (a) CCA heating and cooling behaviour, October 16th 2006 and (b) with the adjusted controller settings, March 12th 2007

and valve positions. Water flow information is not available, so energy and performance calculations with a reasonable accuracy are not possible.

2.2.2 Measurement results

The analysis of the measurement results focuses on the evaluation of the control strategy applied. Fig. 2.2(a) shows the behaviour of the CCA circuit of the South zone landscape office on October 16th 2006. The position of the three-way valve in the CCA circuit is an indicator for the heating and cooling rate.

The implemented feedback control strategy in combination with the high thermal mass results in heating of the CCA during night time and the initial occupation period. Shortly after heating is switched off, cooling starts because internal and external heat gains increase the room temperature above the cooling set point. Cooling remains on, even some hours after occupation has ended. Heating starts again approximately 1 hour later. Subsequently, this cycle is repeated.

These measurement data indicate that the control strategy based on the room temperature is not appropriate in combination with CCA. The frequent switching between heating and cooling, caused by the narrow dead band control, suggests that there is room for improvement. However, since the room air temperature remained well within a range of 20°C to 23°C, at this stage, no comfort complaints were reported and it was assumed that the air handling unit and the terminal reheat units were responsible for this.

2.2.3 Adjustment of the control parameters

Based on the observed behaviour of the first measurement period, the dead band between the heating and cooling set point was increased mid February 2007 from 1.5°C to 3°C (heating if the room temperature drops below 20°C, cooling if the room temperature rises above 23°C). This measure was the simplest to take without having to change the system control strategy thoroughly. The adaptation led to shorter cooling and heating periods as shown by measurements of March 12th, 2007 (Fig. 2.2(b)).

The day of March 12th, 2007 was chosen because it had comparable climatic characteristics as the observed October 16th, 2006, shown in Fig. 2.2(a). October 16th is a Monday with a mean day temperature of 10.6°C and a clear sky during the whole day. The relative solar radiation time was 89% [80]. The three previous days were characterised by a little higher mean day temperature, but a relative solar radiation time of 48%, 34% and 3%. March 12th, also a Monday, had a mean day temperature of 8.6°C and also a whole day of clear sky. The relative solar radiation time was 91%. The three previous days had a slightly lower mean day temperature, and a relative solar radiation time of 7%, 68% and 45%.

2.3 Simulating CCA behaviour with a generic building model

A performance analysis was not possible with the measured building data. Therefore, in order to understand the observed system behaviour and to quantify the effect of the control strategy on the overall energy performance of the system, a simplified generic building zone model was used. This section describes four selected cases with their corresponding control strategies, the room model used, and the load profile applied. The simulation results are used to evaluate the selected cases with respect to thermal comfort, system switching between heating and cooling, the efficiency of the control strategy and the impact on the primary energy use (see Sec. 2.4).

Table 2.2: Simulated control strategies

Case	Control strategy	Setpoints
1 (Ref)	Ideal heat and cold emitters	Heating on : $T_z < 21^\circ C$ Cooling on : $T_z > 22.5^\circ C$
2	CCA with dead band control	Heating on : $T_z < 21^\circ C$ Cooling on : $T_z > 22.5^\circ C$
3	CCA with dead band control	Heating on : $T_z < 20^\circ C$ Cooling on : $T_z > 23^\circ C$
4	CCA with night time operation control	Pump on: 0 AM, Pump off: 4 AM Only cooling

2.3.1 Simulated cases

In order to evaluate the HVAC system with respect to the above mentioned criteria, three control strategies for CCA are simulated, compared with each other and compared with a reference case. Literature on feedback control strategies for CCA [87, 55, 99] report night time operation of the CCA circuit as an optimal control strategy, possibly supplemented with other specific control actions (see Chap. 6). Given the thermal inertia of the CCA, this is not an unexpected result. In the case of cooling, during night time heat is rejected from the CCA to the cold water, while during day time, the resulting lower temperature of the CCA is used to temper the room temperature. In the case of heating, heat input into the CCA from the hot water during night time coincides with the period of maximal heat loss in the room.

Table 2.2 lists the four different simulation cases used to make the comparison.

- Case 1, being the reference case, represents an idealised situation and is assumed to have a conventional HVAC system, with a gas fired boiler providing the heat and a chiller providing the cold to the system. Case 1 uses heat and cold emitters with sufficient power and no thermal capacity (which means no time delay) to keep the zone temperature within the specified thermal comfort ranges.
- Case 2, 3 and 4 represent CCA combined with a heat pump providing the heat and a direct ground cooling heat exchanger providing the cold. The dynamics of the heat pump system and ground wells are not taken into account. This corresponds to the system used in the office building monitored, excluding the ventilation system though.

- In Case 2 and Case 3 an on-off control strategy based on the zone temperature is implemented, with a dead band of 3°C in Case 3 versus 1.5°C in Case 2. Case 2 represents the initial situation of the monitoring campaign (Fig. 2.2(a)), Case 3 the situation in the second monitoring period (Fig. 2.2(b)).
- In Case 4 there is only cooling during night time at a supply temperature of 19°C. In this simulation the load is known, which makes it straightforward to determine the cooling period in order to achieve maximal energy performance and thermal comfort.

2.3.2 Room model description

The interaction between the thermal building mass and the control strategy is influenced by many parameters [67, 23]. The simulations are based on a simplified room model (Fig. 2.3), according to the theory presented in Sec. 1.4.3. Rather than attempting to simulate in detail the measured building, this approach is chosen to gain generic insight into the effect of the control strategy on the energy use. For this reason, also the parameters of the building model are not adapted in detail to the measured building parameters. In Ch. 9 a method is described to estimate the parameters of the simplified building model using simulation results from a detailed building model. As outlined there, the step from the presented approach to reality — identifying the parameters of a building model using real building measurement data — still requires further research.

The simplified room model represents one module of an open office space in the south zone of an office building. In reality, the zone boundaries are the CCA ceiling, a typical raised floor, the outside wall and window and adjacent rooms. Besides the CCA ceiling, there is little thermal capacity available. Windows are assumed to have no thermal capacity. The zone node thermal capacity C_z , comprising room air, raised floor tiles, vertical concrete pillars and wall partitions, interior walls and furniture, is assumed to be 7 times the thermal capacity of the room air. Masy [91] used 5 times this air capacity to incorporate room air and furniture only. A detailed literature review of the values used for the air capacitance can be found in App. D, while this value of 7 is derived from a parameter estimation procedure in Ch. 9.

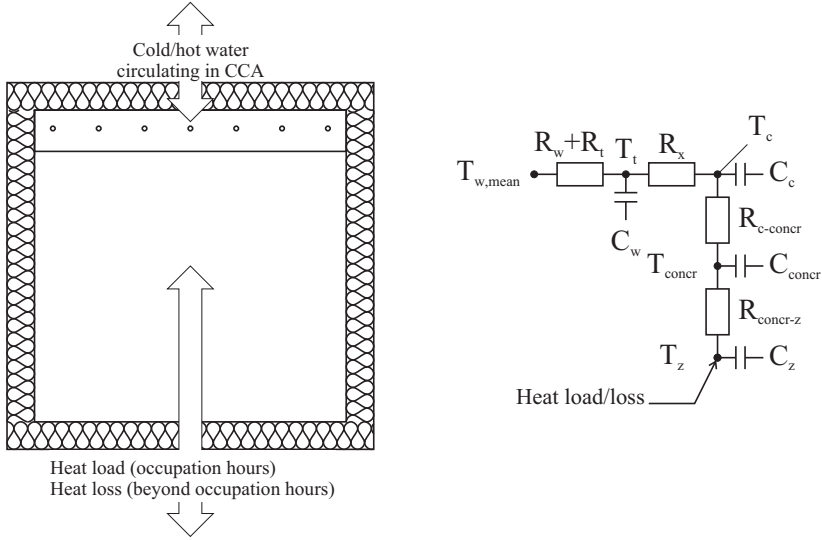


Figure 2.3: Simplified room model for control strategy evaluation

The active concrete layer with a thickness of 0.2 m is modelled using an RC-model which has 3 states: the tube outer surface temperature T_t , an equivalent concrete core temperature T_c and the concrete slab temperature T_{concr} . It is a simplified version of the EMPA-model for CCA [81], which was presented in Ch. 1.

The water flow through the CCA and the corresponding temperature drop from water supply to water return temperature (thermal resistance R_z in the EMPA-model, see Fig. 1.8) is not explicitly taken into account in this model. When water is circulating through the CCA, the temperature of the water node, T_{wm} , is assumed to be the average temperature of the inlet and outlet in the CCA circuit. Ch. 3 describes in more detail how the real water supply temperature can be incorporated. The mean water temperature used here is 23°C for heating and 19°C for cooling. These temperatures correspond to the values determined by the heating and cooling curves as used in the measured building in the observed period.

The link between T_{wm} and T_c is identical to the EMPA-model (Fig. 1.8), with the outer tube temperature T_t as a state. Its thermal capacity C_w represents the thermal mass of the water inside the tubes. This introduces a delay in the system, which is replaced in Ch. 4 by the propagation time of the water flow

through the tube, when the supply water temperature T_{ws} is used instead of $T_{w,mean}$ here.

In order to simplify the simulation model, the parallel heat flow path from the concrete core T_c to the room — one path via the floor T_{floor} and the other path via the ceiling $T_{ceiling}$ — is transformed to 1 equivalent heat flow path by assuming that the CCA interacts with only 1 room, while in reality it interacts with the room below and above. Details of this transformation are given in Ch. 9

Convective and radiative heat exchange between room air and concrete surface is modelled by a constant combined heat transfer coefficient h_{c+r} of $11 \text{ W/m}^2\text{K}$ for upwards heat flow and $6 \text{ W/m}^2\text{K}$ for downwards heat flow, according to EN15377 [45]. The same values apply for heating and cooling. More detailed values for these heat transfer coefficient is provided in App. D and will be used in the detailed and simplified CCA building models of Chs. 3, 4, 7, and 9. On the floor side of the CCA, the thermal resistance of screed and floor covering is taken into account.

The thermal capacity of the concrete slab is divided between the core node (C_c), having 1/3 of the slab thermal capacitance and the concrete node (C_{concr}), with 2/3 of the thermal capacitance. In chapter 9 it is demonstrated that this model; having its thermal capacitance divided between a core node and a concrete node, is in good agreement with more detailed models for the typical frequencies of the heat loads occurring in the room.

Heat loads and losses are supplied to the zone node of the model. Case 1 uses the same room model but without water circulating through the CCA. Instead, heating and cooling are applied directly to the zone node T_z .

Table 2.3: Heat gain schedule used for the simulation

	Heat exchange in reality	Heat gain profile
6 PM-8 AM:	no occupation, heat losses through building envelope	$G_{night} = -8 \text{ W/m}^2$
8 AM-6 PM:	occupation, heat gains from people, equipment and solar radiation	$G_{day} = 28 \text{ W/m}^2$

Based on Fig. 2.3, the energy balances for each internal temperature node give rise to the following set of equations:

$$C_w \frac{dT_t}{dt} = -\frac{1}{R_x} (T_t - T_c) - \frac{1}{R_w + R_t} (T_t - T_{w,mean}) \quad (2.1)$$

$$C_c \frac{dT_c}{dt} = -\frac{1}{R_x} (T_c - T_t) - \frac{1}{R_{c-concr}} (T_c - T_{concr}) \quad (2.2)$$

$$C_{concr} \frac{dT_{concr}}{dt} = -\frac{1}{R_{c-concr}} (T_{concr} - T_c) - \frac{1}{R_{concr-z}} (T_{concr} - T_z) \quad (2.3)$$

$$C_z \frac{dT_z}{dt} = -\frac{1}{R_{concr-z}} (T_z - T_{concr}) + G_{day} + G_{night} \quad (2.4)$$

2.3.3 Simulation period

Heat losses during night time and heat gains during occupation time are simplified to a heat gain profile (G_{day} and G_{night}) as shown in Table 2.3. This profile is based on the results of the heating and cooling load calculation for an October day in the South zone of the measured office building, comparable to the one of October 16th, 2006. The building is therefore subject to heat losses during the night, which are cooling down the building. However, the heat gains during the day are larger, and are heating up the building again. This load profile results in an energy balance over 24 h with 168 Wh/m^2 of excess heat which has to be removed from the room in order to reach a steady state situation.

2.3.4 Simulation details

The simplified room model equations (Eqs. 2.1-2.4) are implemented in Matlab using the state-space notation and solved with the ODE45 solver, based on an explicit Runge-Kutta formula, with a time step of 1 h. The algorithm defines automatically intermediate time steps based on the system dynamics. The simulation was run with the same load profile $G_{day} + G_{night}$ during consecutive days until a steady state situation was reached, defined by:

$$T_{z,day(i)} - T_{z,day(i-1)} < 0.0001^{\circ}C \quad (2.5)$$

This simulation constraint eliminates the influence of initial conditions in the simulation results.

2.4 Simulation results

The energy balance over a 24 h period is reached with a maximum error of 0.4% for each node over the 4 different simulation cases. It should be noted that reaching steady state took up to a period of 19 days, dependent on the control strategy applied. Given the fact that weather conditions and building behaviour change more rapidly, this means that history is important in determining the thermal behaviour of the room.

2.4.1 Thermal comfort

As elaborated in Sec. 1.4.4, the zone temperature T_z is used to evaluate the thermal comfort in the room and shown in Fig. 2.4. None of the CCA control strategies (cases 2, 3 and 4) are able to keep the zone temperature within the range as outlined in ISO7730 [68] for a class B building, $20^{\circ}C < T_{op} < 24^{\circ}C$. However, the exceeding is limited.

In case 4, precooling during the night causes the zone temperature to drop below $20^{\circ}C$ in the early office hours. However, because the temperature of the concrete ceiling is approximately the same as the room temperature in that first hour, the zone temperature rises quickly above $20^{\circ}C$, due to the heat gains occurring. It is only in the next hours, when a temperature difference is established between room and ceiling, that the CCA can dissipate cooling power

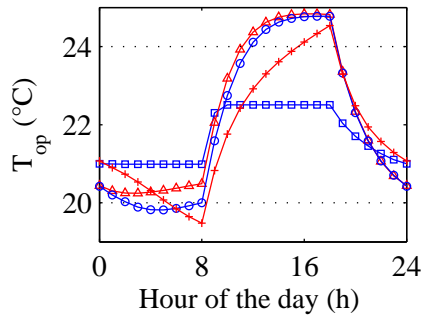


Figure 2.4: Operative room temperatures for the different control strategies (\square Case 1, \triangle Case 2, \circ Case 3, $+$ Case 4)

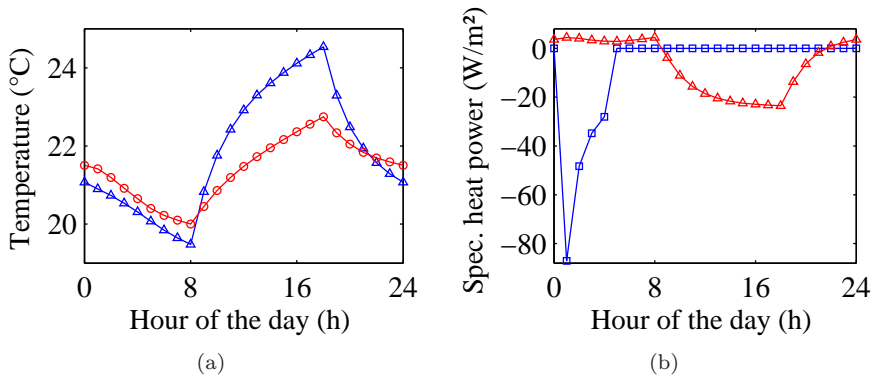


Figure 2.5: Case 4 simulation results: (a) Air, operative and concrete surface temperatures ($\triangle T_{room}$, $+$ T_{op} , $\circ T_{surf}$), (b) heat flow from CCA to room (\triangle) and from water to CCA (\square)

to temper the zone temperature rise, caused by the heat gains. This behaviour, as shown in Fig. 2.5(a), agrees with typical CCA temperature profiles [87, 43]. Also, the T_z result from an optimal controller as presented in Ch. 10, shows a similar pattern. Fig. 2.5(b) shows the corresponding thermal power from water to CCA and from CCA to room.

Hour		2	4	6	8	10	12	14	16	18	20	22	24												
Case 1	(Ref)	H	H	H	H	H	H	H	H	0	C	C	C	C	C	C	C	C	C	C	0	0	0	0	H
Case 2	(21-22.5°C)	H	H	H	H	H	H	H	H	0	C	C	C	C	C	C	C	C	C	C	0	0	H	H	
Case 3	(20-23°C)	0	0	H	H	H	H	H	H	0	0	C	C	C	C	C	C	C	C	C	0	0	0	0	0
Case 4 (Cooling only)		C	C	C	C	0	0	0	0	0	0	0	0	0	0	0	0	0	0	0	0	0	0	0	0

Figure 2.6: On-off times of heating (H) and cooling (C) for the different control strategies; (0) means no heating and no cooling

2.4.2 Heating and cooling on-off times

The simulation results indicate substantial differences in heating and cooling system behaviour for the four control strategies examined. Fig. 2.6 shows the on-off times for heating and cooling for the different control strategies. Case 2 represents the situation as it was initially measured in the office building.

The simulation confirms the on/off behaviour as monitored and presented in Fig. 2.2: the narrow dead band in case 2 results in a maximum of 2 h between switching from heating to cooling or vice-versa. Changing the dead band to 3°C in case 3 improves the situation slightly: 2 h between the heating and cooling period and 7 h between cooling and heating. Case 4, with the 4 h of cooling during the night, is a major improvement in eliminating the alternation between heating and cooling, compared to case 2 and 3, however with a small loss in thermal comfort.

2.4.3 Analysis of the control strategy efficiency

From the measurements in Sec. 2.2.2 and the simulation results from the previous section, it can be concluded that the applied feedback control results in inefficient CCA behaviour with respect to the exchange of thermal power to the room. The simulation results enable an in-depth analysis of the energy flows from the CCA into the room and from the water circuit into the CCA. To quantify the effect of the control strategies, the ratio between these energy flows over a 24 h period is assessed. This ratio gives an indication of the control

strategy efficiency, for heating and for cooling, as represented by Eq. 2.6.

$$\begin{aligned} \text{Control efficiency, heating: } \eta_{contr,h} &= \frac{\int_0^{24} (\dot{q}_{CCA-room} > 0) dt}{\int_0^{24} (\dot{q}_{water-CCA} > 0) dt} \\ \text{Control efficiency, cooling: } \eta_{contr,c} &= \frac{\int_0^{24} (\dot{q}_{CCA-room} < 0) dt}{\int_0^{24} (\dot{q}_{water-CCA} < 0) dt} \end{aligned} \quad (2.6)$$

The integral energy flows cumulated over one day are shown in Fig. 2.7. In case 1, the sum of the heat and cold put into the room add up to 168 Wh/m² net cooling. This equals exactly the amount of excess heat supplied to the room by means of the assumed load profile. Fig. 2.7 shows the low efficiency of the control strategies based on a dead band: in the case of heating 26% (70/268) for a dead band of 1.5°C (case 2) and 32% (60/187) for a larger dead band of 3°C (case 3). In the case of cooling, the control efficiency is 56% (239/429) and 64% (229/356) respectively. The remainder of the energy which was put into the CCA, is simply exchanged between the heating and cooling systems. For case 2, 260 Wh/m² of heat is extracted again by cooling. For case 3 this is reduced to 187 Wh/m². Enlarging the dead band (case 3) improves the control efficiency only slightly (6% increase for $\eta_{contr,h}$ and 8% for $\eta_{contr,c}$) compared to the initial situation (case 2).

In the office building studied, this means that during the night the heat pump extracts heat from the ground water, converts it into heat at a higher temperature level by using electricity and injects it into the building. With the heat gains increasing during office hours, room temperature rises and cooling starts. Heat, supplied to the CCA during night time, is removed again from the building to the ground water via the heat exchanger. The possibility of a closed loop in the ground water system is not taken into account in these simplified simulations.

The night time operation control of the circulation pump (case 4) yields a high efficiency. $\eta_{contr,c}$, defined in Eq. 2.6, is even above 100% (205/169 = 120%). The specific heat flow of case 4, as presented in Fig. 2.5(b), shows that $\dot{q}_{CCA-room} > 0$ during night time: the room is cooling down the CCA. In Fig. 2.7 this can be seen as 36 Wh/m² of heat entering the room although there is no heat supplied by the water. On the other hand, the load injects netto 168 Wh/m² into the room over 24 h. This adds up to the total value of 205 Wh/m² (cfr. 0.4% error on the energy balance), which is extracted from

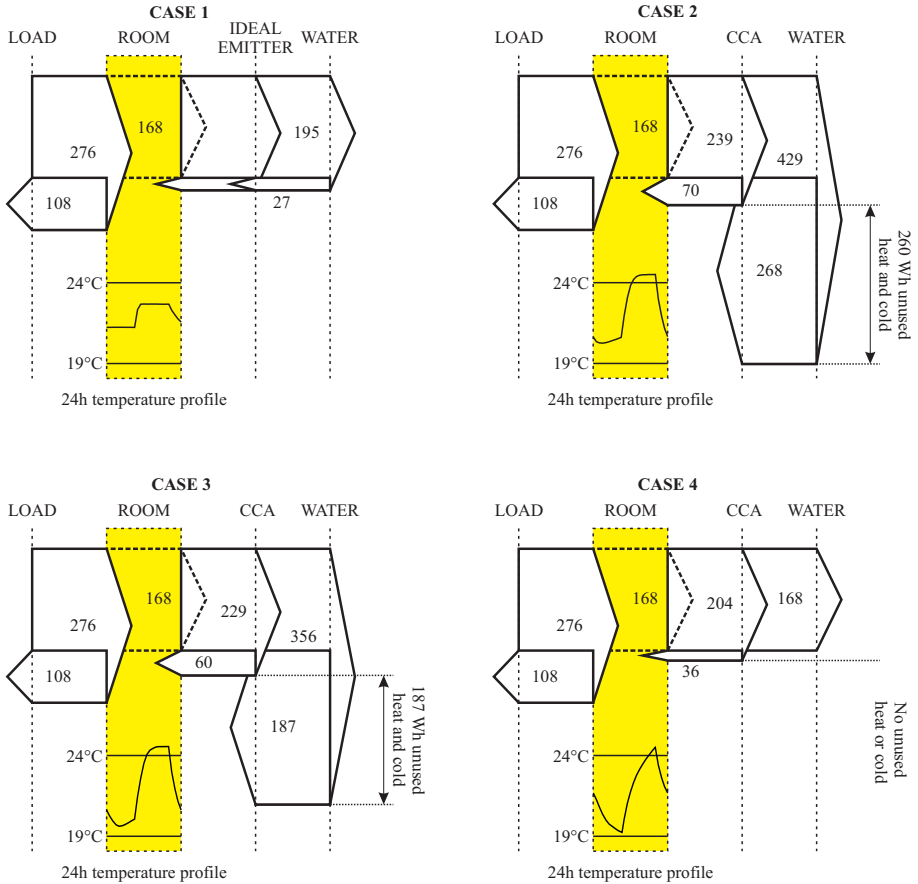


Figure 2.7: 24h cumulative energy flows (Wh/m²) from the load to the room and from the room to the water distribution system (via the ideal emitter for case 1 and via the CCA for case 2, 3 and 4)

Case 1: threshold heating = 21°C, threshold cooling = 22.5°C;

Case 2: threshold heating = 21°C, threshold cooling = 22.5°C;

Case 3: threshold heating = 20°C, threshold cooling = 23°C;

Case 4: cooling from 0 AM until 4 AM.

The room temperature profile is shown at the bottom of each figure.

Table 2.4: Production efficiencies and primary energy conversion factors

Case	Type of production unit	η , SPF, EER
Case 1 heat production	gas fired boiler	0.95 (η)
Case 1 cold production	chiller	3 (EER)
Case 2, 3, 4 heat production	water/water heat pump	4.25 (SPF)
Case 2, 3, 4 cold production	direct ground cooling	12 (SEER)
Primary energy conversion factor for natural gas		1.0 [1]
Primary energy conversion factor for electricity		2.5 [1]

the room by the CCA on a 24 h basis. The water extracts the same amount of heat that netto has entered the room by the heat load/loss.

2.4.4 Analysis of the impact of the control strategy on primary energy use

Sec. 2.2.1 mentioned the rather high energy bill of the measured office building. Analysing the energy use of the system with the 4 control strategies shows that this high energy consumption can be attributed to the poor performing control strategy.

To calculate the (primary) energy use corresponding to the different simulation cases, the system efficiencies as presented in Table 2.4 are used. The step towards primary energy use is made in order to compare the CCA-cases 2, 3 and 4 with the reference case 1. Since it is the aim to obtain a indicative assessment comparing case 1 with case 2, 3 and 4, the simplified approach of constant primary energy conversion factors is used. For the reference case 1, a conventional gas boiler and air cooled chiller is used (see Sec. 7.3.2 for reference on these values), while for the CCA cases 2, 3 and 4 a heat pump with the estimated SPF = 4.25 is used. For cooling, SEER = 12, which is a reasonable estimate given the large water extraction and injection pumps required to operate the ground system.

With these system efficiencies and primary energy conversion factors, Table 2.5 shows the primary energy use for the four simulated cases. The first column, *Net*, presents the values shown in Fig. 2.7. The second column are the *Net* energy values, multiplied with the production efficiencies. In the third column, these system energy values are multiplied with the primary energy conversion

factors, while the fourth column shows the sum of heating and cooling primary energy.

Table 2.5: Conversion from net energy use to primary energy use of simulation cases 1 to 4

Case	Net (Wh/m ²)	System (Wh/m ²)	Primary (Wh/m ² _{prim})	Primary total (kWh/m ² _{prim})
1 (heating) ^(a)	27	28	28	191
1 (cooling) ^(b)	195	65	163	
2 (heating) ^(c)	268	63	158	247
2 (cooling) ^(d)	429	36	89	
3 (heating) ^(c)	187	44	110	184
3 (cooling) ^(d)	356	30	74	
4 (heating) ^(c)	0	0	0	35
4 (cooling) ^(d)	168	14	35	

^(a) Gas fired boiler
^(b) Chiller
^(c) Heat pump
^(d) Direct ground cooling

Case 1 results in a primary energy use which is 23% (1-191/247) lower than case 2 and almost equal to case 3. Although the system components used in case 2 and case 3 are energy efficient, unadapted control strategies result in higher primary energy consumptions compared to conventional HVAC systems. Despite the fact that case 3 uses a far from ideal control strategy, the very simple measure of enlarging the dead band from 1.5°C to 3°C results in a primary energy use reduction of 26%, without violating the thermal comfort requirements (see also Fig. 2.4).

The control strategy of case 4 results in a very low primary energy use: 86% (1-35/247) and 81% (1-35/247) reduction compared to case 2 and case 3, respectively. On the other hand, due to the large time constant of the CCA, the thermal response is not adequate enough to guarantee the desired thermal comfort in all circumstances. Therefore, a combination with a fast reacting system seems appropriate. The simulation results indicate that the night time operation control strategy and its combination with supplementary fast reacting systems should be subjected to further optimisation, both with respect to the control strategy and with respect to implementation in real

buildings. The control strategy problem can be tackled by an optimal controller as presented in Ch. 10.

2.5 Conclusions

Although the CCA are heated and cooled in an efficient way — the heat pump SPF was estimated to be 4.25 and the direct ground cooling SEER to be 12 — a significant part of the produced heat and cold is not used to guarantee thermal comfort in the building. The CCA, which present a large thermal storage capacity between the installation and the office room, prevent the thermal energy from entering the room. Heat that has been put into the CCA by warm water during the night and early morning is extracted again from the CCA by cold water shortly afterwards when cooling starts up. At this short time-scale very little of the thermal energy entering the CCA can flow into the room.

This inappropriate control of the CCA-heat pump-direct ground cooling system has a dramatic impact on the energy performance of the overall system. On the other hand, night time operation control suffers from not achieving thermal comfort requirements. Real systems will certainly encounter these problems, because, in contrast to the simulations presented in this chapter, the real running time of the circulation pump has to be estimated based on the measured system behaviour of previous days. A supplementary, fast reacting system, such as conditioned ventilation air, seems inevitable in this case.

The insight in the behaviour of CCA as observed in this case study, is used as a starting point for the remainder of this work. Ch. 4 presents an analytical solution, which is used to quantify in detail the ratio between heat storage and heat transfer to the room and allows to predict the required operation time for the circulation pump. Simulations with an accurate building model (Ch. 8) show the detailed behaviour of the CCA throughout the year, subject to different settings of an on-off feedback controller as used here. Finally, in Ch. 10 a Model based Predictive Controller (MPC) is presented, which takes into account future heat loads and heat gains to determine the optimal control profile.

Part II

Concrete Core Activation

Chapter 3

CCA steady-state heat transfer

3.1 Introduction

Designing an appropriate control strategy for CCA starts with a thorough design of the CCA. CCA design requires knowledge of both steady-state and transient behaviour. In this chapter, the steady-state heat transfer in a CCA floor is analysed. In order to obtain general results, an uncovered concrete floor is considered, for which the parameters are varied. Using the EMPA star RC-network approach as a starting point, a parametric study is set up to reveal the influence of the different thermal resistances on the overall heat transfer. Using these results, conclusions are drawn regarding the maximum attainable heating and cooling power of CCA.

3.2 Steady-state CCA heat transfer model

As discussed in Ch. 1, Koschenz and Lehmann [81] presented the EMPA-model in which the 3D heat flow pattern inside the concrete slab is transformed into a 1D RC-model. A parametric study of the steady-state EMPA-model, reveals the importance of the different thermal resistances in this model. To restrict

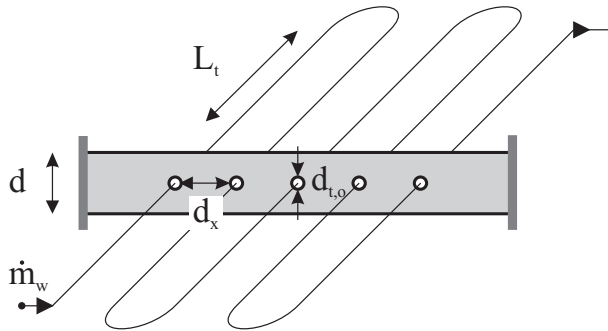


Figure 3.1: Parameters of the investigated floor layout

Table 3.1: Parameters in the parametric study of the steady state heat transfer in CCA

Parameter	Units	Values	Description
\dot{m}_w	(kg/h)	0-500	water flow rate in the tubes
d	(m)	0.1-0.4	concrete total thickness (see Fig. 1.8)
d_x	(m)	0.1-0.3	tube spacing (see Fig. 1.8)
$d_{t,o}$	(m)	0.02	only 1 tube size is considered, corresponding inner diameter $d_{t,i} = 0.0154$ m, smallest bending radius equals $5 \times d_{t,o} = 0.1$ m
L_t	(m)	66.7	only 1 tube length is considered, corresponding to a gross office floor area of 12 m^2 with a tube spacing $d_x = 0.15$ m, cfr. the 2-zone office building model of Ch. 7

the number of parameters, this parametric study does not incorporate the size of the tubes, which is fixed to the most current size (outer diameter of 0.02 m). Also, the tube length L_t is restricted to 66.7 m, which is the tube length of the typical office zone used in Ch. 7 and which corresponds to a gross office floor area of 12 m^2 with a tube spacing $d_x = 0.15$ m. Fig. 3.1 shows the investigated slab layout. The parameters which are considered, are summarised in Table 3.1. The tubes are located in the centre of the concrete slab for the presented results.

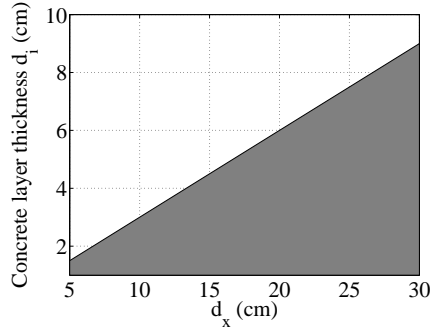


Figure 3.2: Required concrete thickness above or below the tubes as a function of the tube step length for using the EMPA RC-model

As stated in Ch. 1, the EMPA RC-model is only valid for the conditions:

$$\frac{d_i}{d_x} > 0.3 \quad (3.1)$$

$$\frac{d_{t,o}}{d_x} < 0.2 \quad (3.2)$$

with d_i (m) the thickness of the concrete layer below or above the tubes (Fig. 1.8).

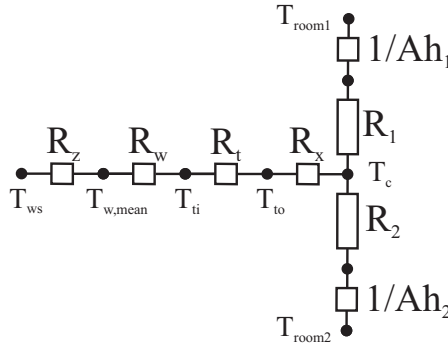
The constraint for the tube diameter $d_{t,o}$ (Eq. 3.2) causes no problems in real CCA configurations. With the assumption that the smallest tube spacing d_x is 0.1 m, a maximal tube diameter of 20 mm can be modelled for this smallest tube spacing. For smaller d_x , the 20 mm tube can not be bended anymore. For d_x -values above 0.15 m, the maximal tube diameter is 30 mm, which is already larger than the diameters currently used in CCA ($d_{t,o}$ between 14 mm and 25 mm typically). For the parameter values in this study (Table 3.1) all combinations fulfil condition (3.2), except for $d_x = 0.1$ for which $\frac{d_{t,o}}{d_x} = 0.2$, which is still acceptable (Table 3.2).

However, the constraint for the required concrete thickness above or below the tubes (Eq. (3.1)) should be kept in mind when modelling the CCA with the EMPA RC-model. Figure 3.2 shows that for a tube spacing of e.g. 0.2 m the minimal thickness of concrete above and below the tubes should be 6 cm. Weber and Johannesson [144] have shown that a model for which condition (3.1) is not fulfilled, does not accurately calculates temperatures and heat flows

Table 3.2: Combinations of d_x and d fulfilling the EMPA conditions (Eqs. 3.1 and 3.2)

$d_x(\text{m})/d(\text{m})$	0.1	0.15	0.2	0.25	0.3	0.35	0.4
0.10 ⁽¹⁾	(X)	(X)	(X)	(X)	(X)	(X)	(X)
0.15	X	X	X	X	X	X	X
0.20	0	X	X	X	X	X	X
0.25	0	X	X	X	X	X	X
0.30	0	0	X	X	X	X	X

⁽¹⁾ $d_{t,o}/d_x = 0.2$ instead of $d_{t,o}/d_x < 0.2$

**Figure 3.3:** EMPA's 1D RC-model of a CCA slab [81]

in the slab.

For the parameter values in this study, constraint (3.1) is not fulfilled for a slab thickness $d = 0.1$ m in combination with tube spacing values $d_x = 0.2 - 0.25 - 0.3$ m and for $d = 0.15$ m in combination with $d_x = 0.3$ m. These combinations will be omitted from the results (Table 3.2).

3.2.1 Thermal resistances in the CCA resistance model

In this section, the thermal resistance network for the heat flow from the water in the CCA tube to the room is elaborated in terms of the gross floor area of the room. The total thermal resistance R_{tot} from the water supply temperature T_{ws} over the mean core temperature T_c to the zone temperature T_z consists of 5 contributions, according to the EMPA model as presented in Ch. 1, Sec. 1.7.1 (see Fig. 3.3):

1. $R_{di} = (\text{K/W})$: Upwards ($i = 1$) or downwards ($i = 2$) heat transfer through upper and lower CCA slab into the room at temperature $T_{zone\ i}$ (conduction and convection)
2. R_x (K/W): Equivalent core thermal resistance
3. R_t (K/W): Thermal resistance of tube wall (conduction)
4. R_w (K/W): Thermal resistance from water to tube wall (forced convection)
5. R_z (K/W): Thermal resistance from water supply temperature to mean water temperature

The thermal resistance R_z , relating the mean water temperature to the water supply temperature, is a function of the tube length and the water flow rate in the tubes (Sec. 3.2.7).

3.2.2 Tube surface area, gross and net CCA floor area

In order to design the CCA, its heating and cooling power has to be associated with the surface area of the office zone. However, the EMPA-formulation is written in terms of the net CCA area $d_x \cdot L_t$, with d_x the tube spacing and L_t the total tube length of 1 CCA circuit. In this work, a conversion between net and gross CCA area is made, based on the dimensions presented in Fig. 3.4(a). $A_{CCA,net}$ relates to $A_{CCA,gross}$ with a factor ranging from 80% to 85% (Fig. 3.4(b)). This is however a simplification of reality, where the heat transfer effects at the tube bends will enhance conduction to the non activated part of the slab. The different areas related to the CCA module are defined by:

$$A_{CCA,gross} = d_x L_{to} \quad (3.3)$$

$$A_{CCA,net} = d_x L_t \quad (3.4)$$

$$A_{tube} = \pi d_{t,i} L_t \quad (3.5)$$

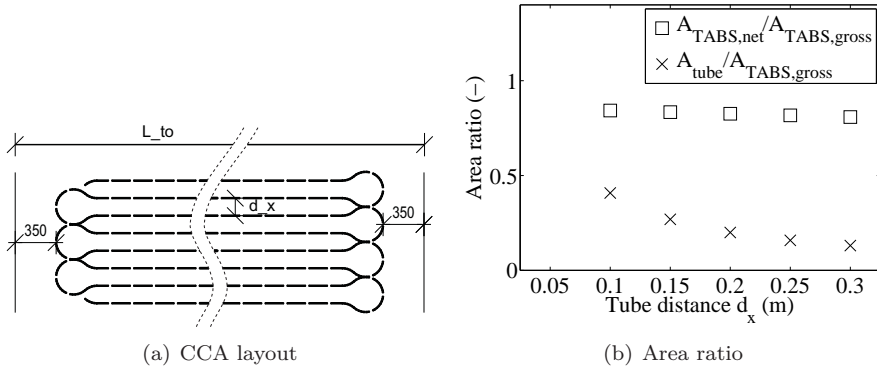


Figure 3.4: (a) Dimensions and tube layout of CCA module, and (b) CCA area ratios for $L_{to} = 5$ m.

3.2.3 R_d , from zone temperature to mean concrete core temperature

In the most simple representation of the static thermal CCA model, the zone temperature T_z above and below the slab is assumed to be equal, resulting in the thermal resistance R_d , describing the two parallel heat flows through the upper and lower surface into the room, given by Eq. (3.6). R_d combines conduction through the concrete and convection and radiation to T_z .

$$R_d = \frac{1}{1/R_{d1} + 1/R_{d2}} \quad (3.6)$$

with :

- $R_{di} = \frac{d_i}{\lambda_c} + \frac{1}{h_{tot,i}}$ (m^2K/W), $i = 1,2$
- h_{c+r} : convective and linearised radiative heat transfer at the CCA surface (W/m^2K) (see Sec. 1.4.3, App. D.5 and D.6)

Related to the CCA net area, R_d ranges between $0.08 m^2K/W$ and $0.12 m^2K/W$ for the considered thicknesses $d = 0.1 - 0.4$.

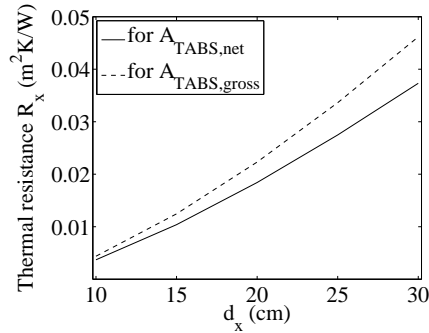


Figure 3.5: R_x values for $L_{to} = 5$ m

3.2.4 R_x , from mean core temperature to tube outer surface temperature

The thermal resistance R_x defines the temperature difference between the tube outer surface temperature and the equivalent concrete core temperature T_c . The simplified equation for R_x is given by Eq. (3.7). Fig. 3.5 shows the values of R_x as a function of d_x .

$$R_x = \frac{d_x \ln \left(\frac{d_x}{\pi d_{t,o}} \right)}{2\pi \lambda_t} \quad (3.7)$$

3.2.5 R_t , from tube outer surface to tube inner surface temperature

The standard equation describing heat conduction through a cylinder of length L_t with internal diameter $d_{t,i}$ and external diameter $d_{t,o}$ is used (Eq. 3.8). \tilde{R}_t stands for the thermal resistance (units K/W), while R_t is the specific thermal resistance related to the floor area (units Km²/W). The resulting thermal resistance has values (see Fig. 3.6) of the same order of magnitude compared to the equivalent core resistance R_x (Fig. 3.5). This is an important observation since R_t is often neglected due to the small thickness of the tubes. These values

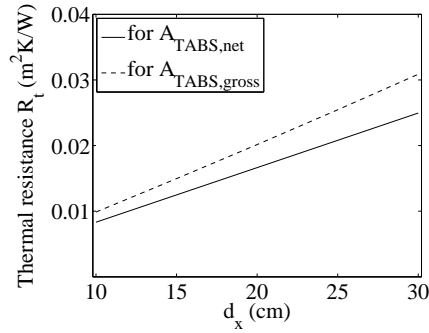


Figure 3.6: Tube wall conduction thermal resistance R_t as a function of d_x and for $L_{to} = 5$ m, according to Eq. 3.9.

show that this is not acceptable.

$$\tilde{R}_t = \frac{\ln(d_{t,o}/d_{t,i})}{2\pi L_t \lambda_t} \quad (\text{K/W}) \quad (3.8)$$

or, related to $A_{CCA,net}$

$$R_t = \frac{\ln(d_{t,o}/d_{t,i}) d_x}{2\pi \lambda_t} \quad (\text{m}^2\text{K/W}) \quad (3.9)$$

with:

- L_t (m): tube length
- $\lambda_t = 0.5$ (W/mK): tube thermal conductivity

3.2.6 R_w , from tube inner surface to mean water temperature

The forced convection between the tube wall and the water inside the tube is modelled using the correlation suggested by EMPA [81], since this correlation is used in the active layer wall model of TRNSYS. This active layer wall model is an important component of the whole building simulation model in Chapter 7. For reference, Fig. 3.7(a) compares the EMPA correlation, presented by Eq. 3.10 [81] with the well known Gnielinski correlation, presented by Eq. 3.11 [88].

$$\alpha_w = 2040 (1 + 0.015T_w) \frac{v_w^{0.87}}{d_{t,i}^{0.13}} \quad [81] \quad (3.10)$$

$$\text{Nu}_d = \frac{(f/8) (\text{Re}_d - 1000) \text{Pr}}{1 + 12.7\sqrt{f/8} (\text{Pr}^{2/3} - 1)} \quad (3.11)$$

With:

- α_w (W/m²K): forced convection heat transfer coefficient ¹
- T_w (°C): water temperature in the tube
- v_w (m/sec): water velocity
- friction factor f for smooth pipes : $f = \frac{1}{(1.82 \log_{10} \text{Re}_d - 1.64)^2}$
- the Gnielinski correlation (Eq. 3.11) is valid for $2300 < \text{Re}_d < 5 \times 10^6$ and $0.5 < \text{Pr} < 200$.

The heat transfer coefficient for forced convection can be written in terms of $A_{\text{CCA,net}}$ as a function of d_x and \dot{m}_w . The results are presented in Figs. 3.7(b) and 3.7(c). Fig. 3.7(b) presents the convection coefficient for $d_x = 0.1$ m and $d_x = 0.3$ m. The results for the other tube distances lie in between. The dotted line in Fig. 3.7(b) is the solution of Eq. 3.10. Fig. 3.7(c) presents the same data as in Fig. 3.7(b) but as a function of d_x in order to compare with the other thermal resistances in the CCA model.

$$R_w = \frac{d_x L_t}{\alpha_w \pi d_{t,i} L_t} = \frac{d_x d_{t,i}^{0.87}}{2040 (1 + 0.015T_w) \pi \left(\frac{4\dot{m}_w}{\rho_w \pi} \right)^{0.87}} \quad (3.12)$$

R_w values are at least an order of magnitude lower than R_x and R_t values.

3.2.7 R_z , from mean water temperature to water supply temperature

The EMPA CCA model is derived for a 2D section of a CCA concrete slab, where a constant water temperature $T_{w,\text{mean}}$ is assumed for the water in the

¹Koschenz and Lehmann [81] use a value of 8W/m²K to approximate $2040 (1 + 0.015T_w) v_w^{0.87}$, which makes a 20% error on the value of R_w

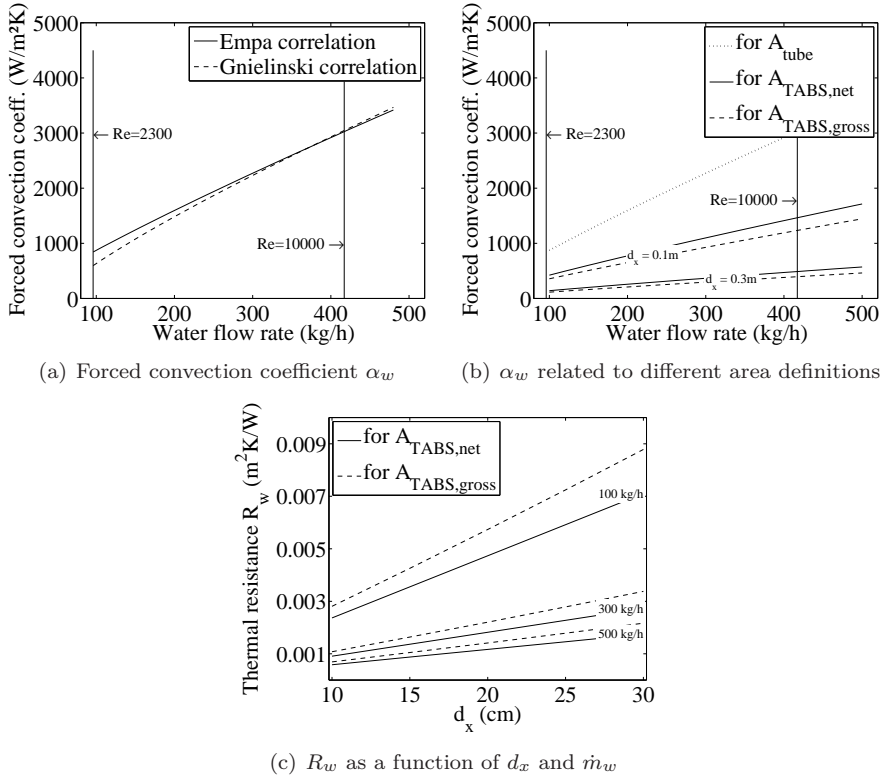


Figure 3.7: (a) Comparison of the EMPA and Gnielinski correlation, (b) α_w related to tube, net and gross CCA area for $L_{to} = 5$ m, and (c) the thermal resistance R_w related to the forced convection in the tubes as a function of d_x and \dot{m}_w

tube. To integrate this model in a building simulation model, the varying water temperature along the length of the tube has to be accounted for. Using the energy balance of a CCA piece with an infinitesimal length dz leads, by applying the LMTD heat exchanger approach, to the formulation of R_z as presented in Eq. 3.13. This approach is also used by Koschenz and Lehmann [81] and integrated into the TRNSYS CCA model.

$$-\dot{m}_w c_p dT_w(z) = \frac{1}{R_1} d_x dz (T_w(z) - T_z)$$

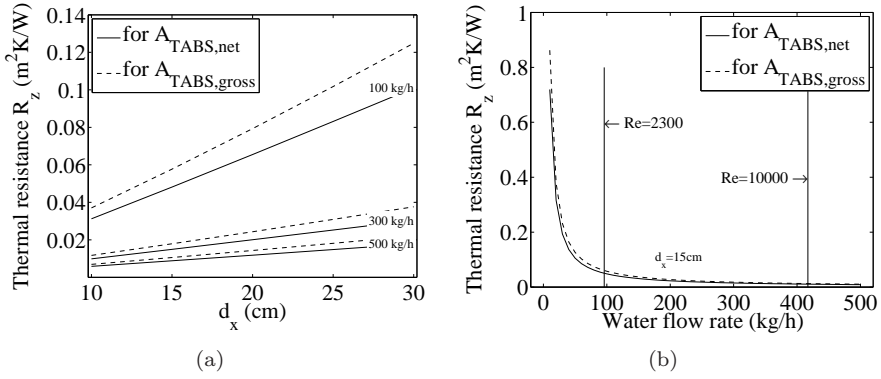


Figure 3.8: For a total tube length $L_t = 66.7\text{ m}$, (a) presents R_z as function of d_x and \dot{m}_w , (b) presents R_z as a function of \dot{m}_w for $d_x = 0.15\text{ m}$, $L_{to} = 5\text{ m}$ and a CCA tickness $d = 0.2\text{ m}$

results in:

$$R_z = \frac{d_x L_t}{\dot{m}_w c_p \left(1 - \exp\left(-\frac{d_x L_t}{R_k \dot{m}_w c_p}\right)\right)} - R_k \quad (3.13)$$

with :

- L_t : tube length of the total CCA slab
- $R_k = R_w + R_t + R_x + \frac{1}{U_1 + U_2}$
- $U_i = \frac{\lambda_c}{d_i} + h_{c+r}$, $i = 1, 2$
- h_{c+r} : convective and linearised radiative heat transfer coefficient (see Ch. 1 and Secs. D.5 and D.6)

While the previous thermal resistances were only dependent on d_x and/or \dot{m}_w , R_z is, evidently, also a function of the total tube length L_t present in the CCA office floor (see Table 3.2).

The dependency of R_z on the CCA thickness d , or in general on R_d is rather weak : for d ranging from 10 cm tot 40 cm, the maximum difference in R_z is $0.0031\text{ m}^2\text{K/W}$, which is about 10% of the R_z value.

Fig. 3.8(a) presents the thermal resistance R_z caused by the temperature variation along the tube length as a function of d_x . Fig. 3.8(b) clearly

demonstrates the impact of the water flow rate on the value of R_z , decreasing towards zero for the higher water flow rates. R_z tends to become very high for small water flow rates, but since this occurs in the laminar flow regime, this will not happen in realistic situations.

This thermal resistance R_z is not negligible compared to the values of other resistances (R_x , R_t , R_w).

3.2.8 Comparison of R_x , R_t , R_w , R_z , R_d and the total thermal resistance R_{tot}

In order to compare the importance of the different thermal resistances R_x , R_t , R_w , R_z from water supply temperature T_{ws} to the mean core temperature T_c , Fig. 3.9(a) presents all the thermal resistances related to $A_{CCA,net}$ for all parameter combinations fulfilling the EMPA-conditions (see Sec. 3.2). Where R_w is of minor importance, R_x , R_t and R_z all contribute comparably to the total thermal resistance between T_{ws} and T_c . The total thermal resistance R_{tot} ranges from 0.11 – 0.24 m²K/W related to $A_{CCA,net}$.

Fig. 3.9(b) presents data for $d_x = 0.15$ m, $L_{to} = 5$ m, $\dot{m}_w = 150$ kg/h and $d = 0.2$ m, which are the design values of the typical office zone used in Ch. 7. This detail of Fig. 3.9(a) shows that R_z will clearly cause the largest temperature drop (after R_c), while the values for R_t and R_x are of equal magnitude. As mentioned before, this is an important observation, because the thermal resistance R_t of the tube is often neglected, given that its wall thickness is small. The plastics of the tube material as used in practice, have a significant contribution to the thermal resistance. E.g., Jin et al. [72] obtained a 0.74°C floor surface temperature difference when neglecting the tube's thermal resistance.

R_c represents the sum of R_x , R_t , R_w and R_z and counts for 38% of the total thermal resistance. The conduction through the concrete mass remains the main thermal resistance (R_d). However, the contribution of R_c , representing 38% of the total thermal resistance, can not be neglected.

In order to design CCA for a building, it should be stressed to use the correct area definition (net versus gross area, see Sec. 3.2.2) when using area related values for thermal resistance or heat flow. Erroneous use of area values leads to deviations up to 20%.

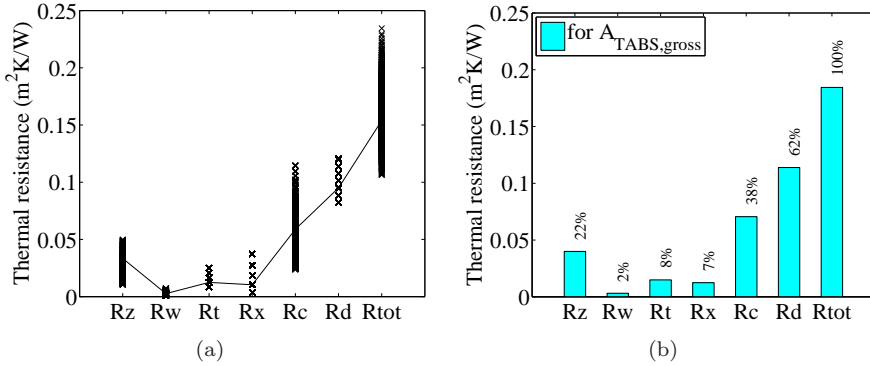


Figure 3.9: (a) Comparison of the thermal resistances $R_c = R_x + R_t + R_w + R_z$ and R_d related to $A_{CCA, net}$ for all parameter combinations fulfilling the EMPA-conditions (see Sec. 3.2) and (b) for the design values of $d_x = 0.15$ m, $L_{to} = 5$ m, $\dot{m}_w = 150$ kg/h and $d = 0.2$ m. The full line in (a) connects the values of (b).

3.2.9 Specific heat power $\dot{q}_w = (T_{ws} - T_c)/R_c$ as a function of \dot{m}_w and T_{ws}

The values of the thermal resistance R_c between T_{ws} and T_c as a function of \dot{m}_w and T_{ws} provide information on whether to change water flow or water supply temperature in order to control heat transfer from water to CCA. Fig. 3.10(a) shows the specific heat power \dot{q}_w for T_{ws} between 24 and 40°C and for \dot{m}_w between 100 and 400 kg/s for a constant concrete core temperature $T_c = 22^\circ\text{C}$. Analysis of these values shows the effect of changing T_{ws} or \dot{m}_w :

- a 1 K increment of T_{ws} increases \dot{q}_w with 12 – 29 W/m^2 (/K)
- a 1 K increment of T_{ws} decreases the COP with 0.03 for the heat pump used in Ch. 7, which means that heat pump efficiency decreases with 0.7%
- a 1 kg/h increment of \dot{m}_w increases \dot{q}_w with 0.5 – 19 W/m^2 (/kg/h)
- a 1 kg/h increment of \dot{m}_w increases the circulation pump consumption with 2% (simplified calculation based on the values used in Ch. 7)

For all points in Fig. 3.10(a), the corresponding specific electric power can be calculated with the presented increment values for COP and pump

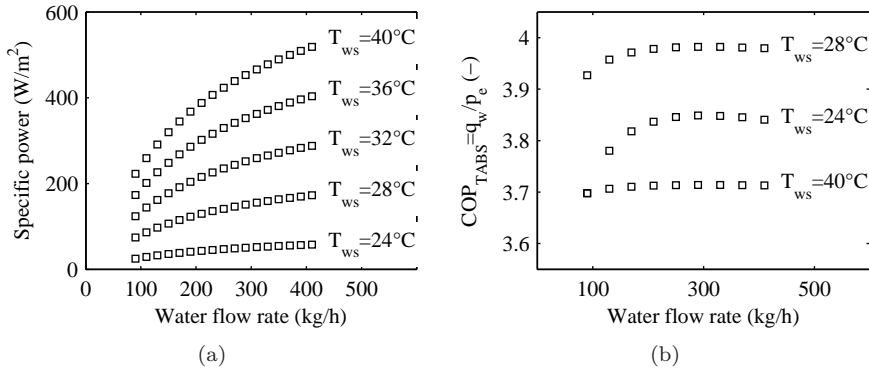


Figure 3.10: (a) Specific heat power $\dot{q}_w = (T_{ws} - T_c)/R_c$ as a function of \dot{m}_w and T_{ws} in W/m^2 net CCA floor area, (b) Specific electric power $\dot{p}_e = \dot{p}_{HP} + \dot{p}_{pump}$ related to the specific heat power $\dot{q}_w = (T_{ws} - T_c)/R_c$ as a function of \dot{m}_w and T_{ws} and $T_c = 22^\circ\text{C}$.

consumption. This yields a COP_{CCA} value for the heat transfer from water to CCA, as presented in Eqs. (3.14-3.15).

$$\dot{p}_e = \dot{p}_{HP} + \dot{p}_{pump} = \dot{q}_w / \text{COP}(T_{ws}) + \dot{p}_{pump}(\dot{m}_w) \quad (3.14)$$

$$\text{COP}_{CCA} = \frac{\dot{q}_w}{\dot{p}_e} \quad (3.15)$$

Fig. 3.10(b) shows the maximum COP_{CCA} -values for $T_{ws} = 28^\circ\text{C}$: heat is transferred the most efficiently at this temperature. Lower and higher T_{ws} -values decrease COP_{CCA} , due to the higher thermal resistance R_z for low T_{ws} -values and the lower COP_{HP} -values for high T_{ws} -values. Moreover, COP_{CCA} increases up to $\dot{m}_w = 300 \text{ kg/h}$. However, care should be taken while evaluating the results regarding the water flow rate, since for increasing \dot{m}_w -values, the initial investment increases: larger pumps and larger pipe diameters are needed in the system. The conclusions regarding \dot{m}_w are therefore a rough estimate only. Changing T_{ws} does not require a different heat pump, as long as its nominal power is sufficient.

From this, the following conclusions can be drawn:

1. It is more efficient to change the water supply temperature T_{ws} than to change the water flow rate \dot{m}_w in order to control the heat transfer from

water to CCA.

2. The best COP of the CCA system for this specific geometry is at $T_{ws} = 28^\circ\text{C}$

3.2.10 R_x and R_t sensitivity to material properties

In general, all thermal resistances are sensitive to parameters or round-off errors. R_x and R_t , in particular are a function of the thermal conductivities λ_c and λ_t , for which the values have to be chosen carefully. In the literature λ_c values are ranging from 1.8 to 2.5 W/mK, while for λ_t values of 0.35 to 0.5 W/mK can be found [102, 81]. This means that for both λ_c and λ_t deviations up to 30% compared to the mean value can occur. Since both R_x and R_t are inversely proportional to the thermal conductivity (Eqs. (3.7) and (3.9)), this results in differences ranging from +43% to -23% compared to the mean value as shown by Eqs. (3.16-3.18). To conclude, since $R_x + R_t$ make up a considerable part of the total thermal resistance, defining the correct material parameters is crucial.

$$R_{i,\Delta} = \frac{1}{1+a} R_i \text{ with } i = x, t \text{ and } a = \pm 0.3 \quad (3.16)$$

$$\Delta R_i = R_{i,\Delta} - R_i = \frac{-a}{1+a} R_i \quad (3.17)$$

and

$$\frac{-a}{1+a} \in [0.43, -0.23] \text{ for } -0.3 < a < 0.3 \quad (3.18)$$

3.3 Maximum heating and cooling power of CCA

Knowledge of the steady-state heat transfer parameters in the CCA allows to determine the maximum thermal capacity of CCA. While in the previous section results were presented for an uncovered concrete slab, in this section, an example is presented for a real implementation of CCA in an office building: a thermally activated concrete slab with a raised floor and a stucco finishing of the ceiling is considered. This is the floor construction which is used in the standard office building model, as presented in Ch. 7 and has the parameters

Table 3.3: Details of the CCA parameters for the maximum heating and cooling power calculation

CCA parameter	Unit	Value	Remark
\dot{m}_w	(kg/h)	144	mass flow rate
d_x	(m)	0.15	tube spacing
d	(m)	0.2	slab thickness
The tubes are located in the centre of the slab			
$h_{c,c}$ (ceiling)	(W/m ² K)	3.36	convection heat transfer coefficient for a cooled ceiling ⁽¹⁾
$h_{c,h}$ (ceiling)	(W/m ² K)	0.48	convection heat transfer coefficient for a heated ceiling ⁽¹⁾
$h_{c,c}$ (floor)	(W/m ² K)	0.44	convection heat transfer coefficient for a cooled floor ⁽¹⁾
$h_{c,h}$ (floor)	(W/m ² K)	3.62	convection heat transfer coefficient for a heated floor ⁽¹⁾
h_r	(W/m ² K)	5.6	linearised radiative heat transfer coefficient ⁽¹⁾
$R_{raised\ floor}$	(m ² K/W)	0.3044	thermal resistance of the raised floor covering the concrete slab at the floor side ⁽¹⁾
$R_{ceiling\ plaster}$	(m ² K/W)	0.025	thermal resistance of the plaster covering the concrete slab at the ceiling side ⁽¹⁾

⁽¹⁾ Details of this floor design are presented in Ch. 7

as presented in Table 3.3. The maximum available thermal power of this CCA is limited by thermal comfort and condensation considerations.

Firstly, ISO7730 [68] provides data to determine the maximum and minimum surface temperatures by limiting the radiant asymmetry between floor and ceiling and for the floor side by limiting its surface temperature to prevent local discomfort (cold feet). Choosing the ISO7730 thermal comfort class B (10% dissatisfied people, see Ch. 6), the limiting temperatures are given in Table 3.4 for floor and ceiling. Secondly, the maximum ceiling surface temperature is determined by thermal radiation received by a person's head. Based on radiant asymmetry limitations from ISO7730 [68], Hens [60] suggests a value for a person sitting in the middle of the office room (view factor to ceiling = 0.14 [65], correlation C-121). And lastly, the minimal ceiling surface temperature is determined by the risk for condensation instead of thermal comfort considerations: e.g. a dry bulb temperature of 27°C and a relative humidity of 60% results in a dew point temperature of 18.6°C. In Table 3.4 a value of 19°C is chosen as the minimal ceiling surface temperature, which is

Table 3.4: Limiting surfaces temperatures according to thermal comfort class B with an assumed room temperature of 20°C in winter and 26°C in summer. The natural convection coefficient h_c is determined by the Awbi and Hatton correlation (Sec. D.5)

	Floor	Ceiling
Minimum surf. temp (°C)	19	19
Max. cooling power (W/m ² , T _{ia} = 26°C)	42	65
Maximum surf. temp (°C)	29	33 *
Max. heating power (W/m ² , T _{ia} = 20°C)	86	79

* 28 for standing person, based on the requirements of radiant asymmetry

identical to the floor temperature limited by local discomfort.

The limiting surface temperatures determine the maximum attainable heating and cooling power of ceiling and floor surface. The maximum flux is calculated with Eq. 3.19. The reference zone temperature T_{zone} is the optimal comfort temperature determined by ISO7730: 22°C for winter and 24.5°C for summer situation.

$$\dot{q}_{max} = (h_c + h_r) \|T_z - T_s\| \quad (3.19)$$

For the investigated floor construction, these surface temperature limits determine the supply water temperature and the maximum attainable heating and cooling power. Fig. 3.11 shows the results with $R_c = R_x + R_t + R_w + R_z$, $R_1 = R_{d1} + R_{raised\ floor}$, $R_2 = R_{d2} + R_{plaster}$ and $R_{conv} = 1/(h_c + h_r)$ for floor and ceiling (see Table 3.3).

Due to the uncovered ceiling and the low resulting thermal resistance R_2 , the highest flux occurs at the ceiling. However, due to the typical configuration with the raised floor, the screed surface below the floor tiles, is the limiting factor for cooling. Suppose the screed surface temperature can not drop below 19°C to avoid condensation, the maximum cooling power is given in Fig. 3.11(a). For heating, the ceiling surface is the limiting factor, as shown in Fig. 3.11(b). As a result, in order to limit the surface temperatures as required by thermal comfort and condensation considerations (see Table 3.4), the supply water temperatures can not be lower than 13°C for cooling and not higher than 47.5°C for heating.

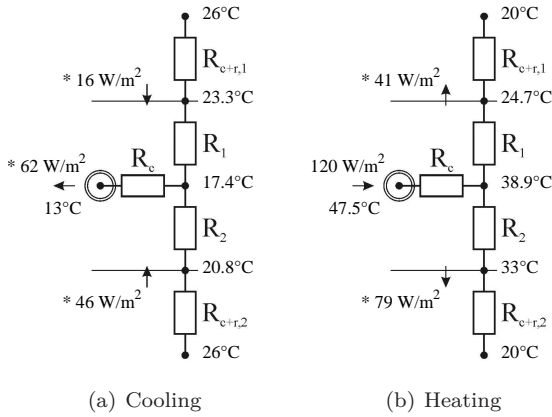


Figure 3.11: Steady state temperatures and heat flows limited by thermal comfort and condensation considerations for the CCA with raised floor. (*) Multiply heat flows by approximately 0.8 for values related to the gross floor area

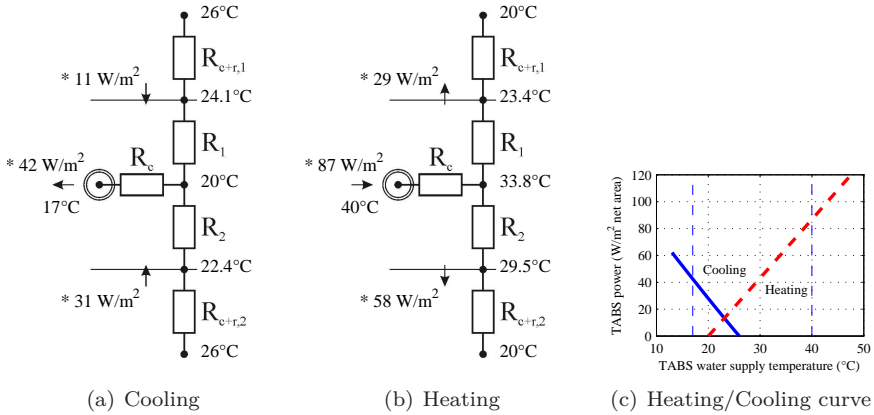


Figure 3.12: (a) and (b) Steady state temperatures and heat flows for the CCA with raised floor, limited by minimal and maximal supply water temperatures for a heat pump/direct cooling system. ((*) Multiply heat flows by approximately 0.8 for values related to the gross floor area), (c) heating and cooling power related to the gross floor area as a function of the water supply temperature.

For floor configuration without raised floor, the total maximum cooling power can go up to 80 kW/m^2 .

In case the temperature of the supply water T_{ws} is limited to realistic values using a heat pump/direct cooling production system, the maximum heating and cooling power is lower than the values determined by thermal comfort and condensation restrictions. Figure 3.12 shows that, for $T_{ws,cooling} = 17^\circ\text{C}$ and $T_{ws,heating} = 40^\circ\text{C}$, the specific cooling and heating power of the ‘CCA-with-raised-floor’ is limited to respectively 42 W/m^2 and 87 W/m^2 .

3.4 Hollow core CCA

Hollow core CCA is constructed at the factory and transported as a whole to the construction site. In order to save material and thus reduce mass, hollow cores are integrated in the structural neutral zone of the slab. Due to the presence of the hollow cores (see Fig. 1.3), the assumption of a homogeneous concrete floor is no longer correct and the analytical expression which served as a basis for the EMPA model is no longer valid (see Sec. 1.7.1 and [81]). The solution to this problem has been addressed during this PhD-research. However, since the focus shifted towards control, the results will be presented only briefly. More details can be found in [126, 76, 134]. Based on a FE-model and measurement results, an extended RC-star network for hollow core CCA is proposed (Fig. 3.13). The FE results indicate that the physical interpretation of the EMPA model boundary condition - the constant temperature at the upper and lower boundary of the concrete slab - is still valid in the case of a 20 cm slab.

In the extended RC-model (Fig. 3.13), the thermal resistance R_1 is replaced by a series of three thermal conduction resistances: the concrete layer between tubes and hollow cores (d_{1a}), a parallel connection of concrete and air with thickness d_{1b} and the upper concrete layer (d_{1c}). In layer 1b, the air gaps are approximated by squares with the length equal to the air gap diameter. The results of this RC-model are compared with the FE-results. Since the difference between the FE- and the RC-model is only weakly dependent on the value d_{1a} , it can be concluded that the deviation is mainly caused by the simplified RC-equivalent of layer d_{1b} . After all, for $d_{1a} > 45 \text{ mm}$, the simplification condition (Eq. 1.27) is satisfied for the observed hollow core case, which means that the temperature at the upper boundary of layer d_{1a} is reasonably constant.

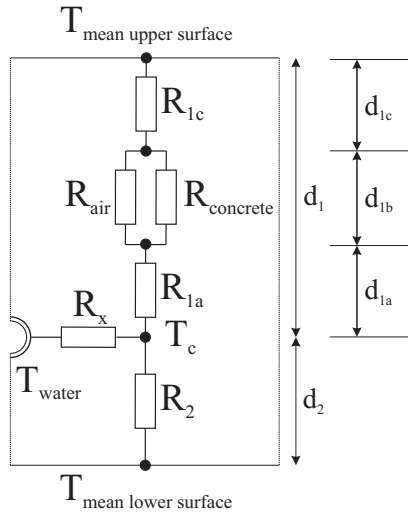


Figure 3.13: Hollow core RC-star network, adapted to incorporate the thermal resistance of the air holes

The effect of radiation and convection inside the air holes was analysed to improve the simplified RC-equivalent of the layer d_{1b} , containing the hollow cores. firstly, the air was approximated by a solid with $\lambda = 0.024 \text{ W/mK}$, thereby neglecting the effects of radiation and convection in the air holes. Due to the different surface temperature at the bottom and the top of the air holes, radiative and convective heat exchange occurs inside the air hole. The FE-results identify thermal radiation as an important parameter: including thermal radiation increases heat transfer with 10%, while convection enhances heat transfer with only 2%. As a next step, these effects are incorporated in the extended RC-model by introducing an equivalent heat conductivity λ_{eq} for the air holes, as proposed by Çengel [29]. The thermal resistance of layer $1b$ is calculated by:

$$\frac{1}{R_{1b}} = \frac{1}{R_{air}} + \frac{1}{R_{concrete}} = \frac{\lambda_c}{d_{1b}} + \frac{\lambda_{eq}}{d_{1b}} \quad (3.20)$$

The adapted RC-model results are fitted to the FE-results including radiation and convection in order to find λ_{eq} . Table 3.5 shows that λ_{eq} is a function of the heating/cooling regime and the thickness (and corresponding geometry of the air holes) of the concrete slab. Due to the heat flow direction, radiation and convection in the air holes is especially working in the heating regime.

Table 3.5: Equivalent heat conductivity λ_{eq} , accounting for convection and radiation in the air holes of hollow core CCA ($\lambda_{air} = 0.024 \text{ W/mK}$)

Slab thickness (m)	Heating/cooling (-)	λ_{eq} (W/mK)
0.2	Heating	0.065
	Cooling	0.030
0.28	Heating	0.120
	Cooling	0.030
0.4	Heating	0.124
	Cooling	0.030

3.5 Conclusions

This chapter presents a thorough analysis of the thermal resistances making up the CCA steady-state thermal model. Although the conduction through the concrete is the most important thermal resistance, the resistance representing the temperature drop between water supply temperature T_{ws} and the mean water temperature T_{wm} should not be neglected. Furthermore, the thermal resistance of the tube wall material should be taken into account, even with the typically small tube thickness. The results also indicate that controlling the CCA power should be done by varying the water supply temperature, rather than varying the water flow rate through the tubes.

The knowledge of the steady-state values of the CCA floor is used to obtain design values for a typical CCA floor construction. As already mentioned in Ch. 1, heating power is sufficient compared to typical heating loads of an office building. This is not the case for cooling, though.

In the next chapter, the transient behaviour of CCA is analysed in detail to determine the impact of the large thermal inertia on the heat transfer between CCA and room.

Chapter 4

CCA transient heat transfer

4.1 Introduction

In this chapter, the transient heat transfer in a CCA floor is analysed. As in Ch. 3, in order to obtain general results, an uncovered concrete floor is considered, for which the water flow rate, thickness and tube spacing are varied. First, lab measurements on CCA are used to highlight important properties of the transient heat transfer from water in the CCA tubes to the room below and above. In order to analyse the transient heat transfer in a concrete slab, an analytical solution of the heat diffusion equation is adapted to the appropriate boundary conditions. This analytical solution is used to investigate the time and space dependent temperature distribution in the slab. Moreover, the power and the cumulated heat transfer distribution are derived. These expressions allow an analysis of the effect of start-stop pump operation, the self-regulating effect of CCA and the heat storage potential under different circumstances.

4.2 Observations from measurements

In this section, experimental data from a CCA-test setup are used to demonstrate transient heat transfer effects for water flowing through the CCA.

4.2.1 Measurement setup

The results are generated with a $4 \times 4 \times 3 \text{ m}^3$ heat transfer test room, constructed according to EN244-2 [42], in which a prefabricated hollow core CCA slab was tested (see Fig. 4.1(a) and Sec. 3.4).

The test room (Fig. 4.1(b)) has a $4 \times 4 \text{ m}^2$ internal floor area and an internal height of 3 m. Water in the ‘Test setup circuit’ and the ‘Test room circuit’ can be heated (max. 90°C) or cooled (min. 6°C) by means of a condensing gas boiler and an air-cooled chiller. The walls, floor and ceiling are water-filled metal panels, externally insulated with 10 cm PU-foam, through which warm or cold water of the ‘Test room circuit’ flows. A high flow rate of 156 l/min ensures a constant internal surface temperature of the metal panels.

A fully programmable controller (Siemens) is used in combination with Matlab for controlling the measurements and for data acquisition. The water flow rate in both ‘Test setup’ and ‘Test room’ circuits are measured by an electromagnetic flow meter with an error of respectively 0.5% and 0.2%. The systematic error on the flow rate reading has been corrected for. The temperatures in both ‘Test setup’ and ‘Test room’ circuits can be controlled by three-way valves. Temperatures in the circuits and on the room internal surfaces are measured with LG-Ni1000-sensor having an error of $\pm 0.5 \text{ K}$ at 0°C and $\pm 1 \text{ K}$ at 85°C . Temperatures in the CCA test element are measured with T-type thermocouples.

Measurement data for a $2.4 \times 2.4 \text{ m}^2$ floor of these hollow core CCA elements (Fig. 4.1(b)) show some important features which should be predicted by the transient CCA model. A step change from 20°C to 30°C in the water supply temperature T_{ws} is induced and the response of the slab is registered using the temperature sensors indicated with the numbers 1–13 on Fig. 4.1(a). These sensors are located in the middle of the slab. Fig. 4.2(a) shows the evolution of the supply and return water temperatures, T_{ws} and T_{wr} respectively. Initially the step excitation is not perfectly followed, the overshoot to 38°C is caused by the setting of the PID controller of the three-way valve used to control T_{ws} .

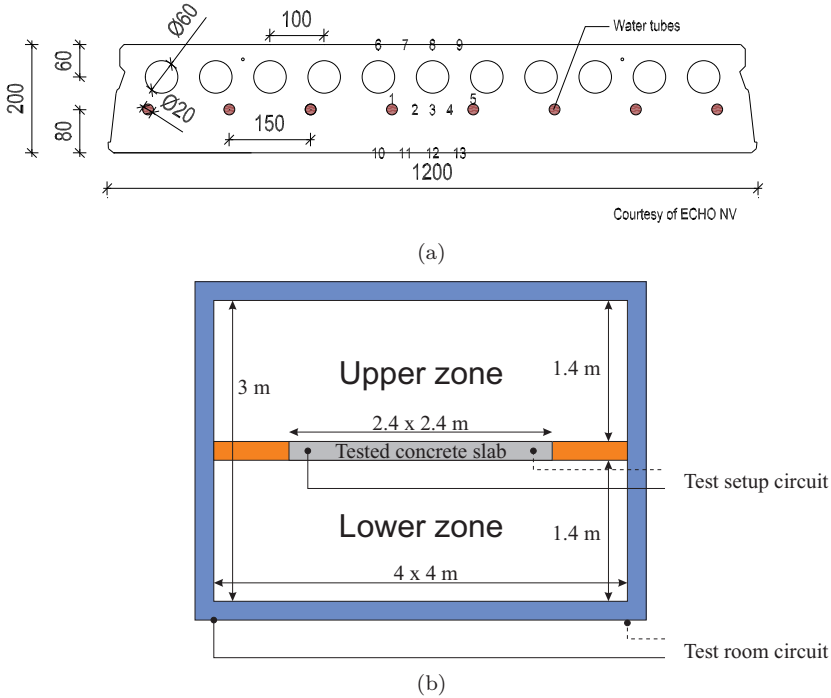


Figure 4.1: (a) Hollow core CCA used for measurements. Numbers 1-13 indicate the location of the temperature sensors, (b) placement of hollow core CCA test element in the $4 \times 4 \times 3 \text{ m}^3$ heat transfer test room

4.2.2 Measurement results

Zooming into the first minutes of this graph, Fig. 4.2(b), shows the effect of flow propagation, which is the time delay corresponding to the water flow from tube inlet T_{ws} to tube outlet T_{wr} . A small drop in temperature is monitored when the valves are opened to activate the step excitation. Fig. 4.2(b) shows that this drop is seen in T_{wr} approximately 3 min later with a certain attenuation. This flow propagation effect is further elaborated in Sec. 4.4.

Fig. 4.3 shows the response of the mean core temperature T_c , which is calculated as the mean of the sensor 1–5 values and corresponds to the equivalent mean core temperature as used in the star network presented previously. After 4 h a value of 25°C is reached, while the steady state value is 26.5°C . Also here a time delay is measurable: after around 1.5 min, the drop

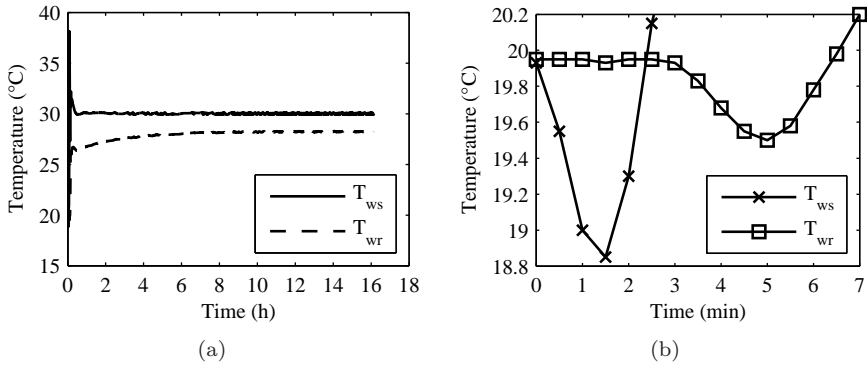


Figure 4.2: Response of the water return temperature T_{wr} to a step excitation of the water supply temperature T_{ws} for (a) the full measurement period and (b) a detail showing the effect of flow propagation

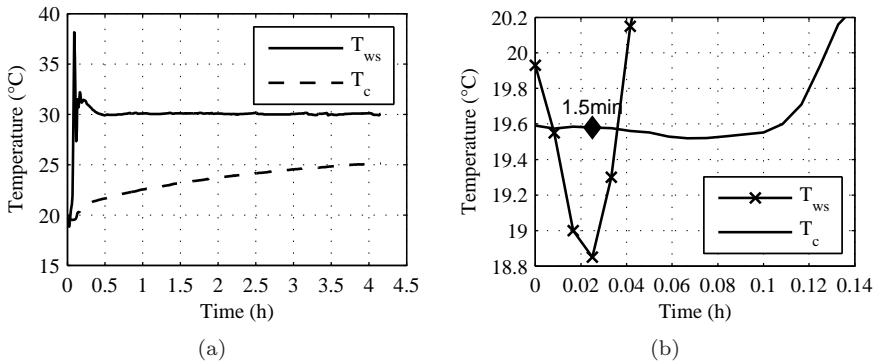


Figure 4.3: Response of T_c to a step excitation of T_{ws} for (a) the full measurement period and (b) a detail showing the combined effect of flow propagation and thermal capacity

in temperature is measured in T_c , while the attenuation is much stronger than for the T_{wr} -result. However, here, it is a combined effect of flow propagation and thermal capacity of the concrete. This delay time is evidently dependent on the positions where the concrete temperatures are measured.

For the surface temperatures (Fig. 4.4), evaluated as the mean of the sensor 6–9 values for $T_{s,up}$ and the sensor 10–13 values for $T_{s,down}$, the delay time is respectively 14 min and 9 min. Fig. 4.1(a) shows the positions of the

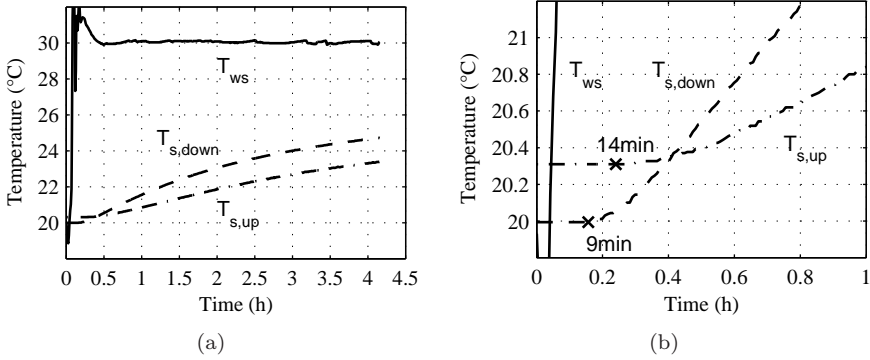


Figure 4.4: Reponse of the surface temperature T_s to a step excitation of T_{ws} for (a) the full measurement period and (b) a detail showing the combined effect of flow propagation and thermal capacity

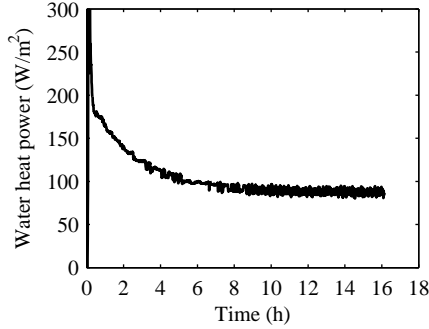


Figure 4.5: Heat power \dot{q}_w as a response to the step excitation of T_{ws}

temperature sensors. Although, due to the thermal resistance of the air holes, $T_{s,up}$ is reacting slower than $T_{s,down}$, it eventually ends up at a lower steady state temperature (24.8°C against 26.1°C) because of the higher heat transfer coefficient at the surface (in the case of heating which is considered here).

The heat power \dot{q}_w transferred from water to concrete — $\dot{m}c_p(T_{ws} - T_{wr})$ — shows a very high initial value compared to the steady state situation (Fig. 4.5). After the first peak, which is caused by the initial overshoot of T_{ws} going up to 38°C, $\dot{q}_w \approx 190 \text{ W/m}^2$ and drops down to a steady state value of $\bar{\dot{q}}_w = 86 \text{ W/m}^2$. Initially, the temperature difference between water and concrete is maximal, which explains the high initial power.

Table 4.1: Time constants of the heating step response of T_c , $T_{s,up}$ and $T_{s,down}$: time to reach $[T_{begin} + (1 - e^{-1})(T_{end} - T_{begin})]$

Heating step response of temperature	τ (h-min)
T_c	2 h19 min
$T_{s,up}$	3 h40 min
$T_{s,down}$	2 h46 min

The time constants of the response of T_c , $T_{s,up}$ and $T_{s,down}$ to the step excitation of T_{ws} are presented in Table 4.1. Due to the thermal resistance of the air holes, $T_{s,up}$ reacts the slowest to the step excitation, although the heat transfer coefficient at the upper surface is larger (in the case of heating). For a ‘full’ concrete floor, this will differ.

4.2.3 Phenomena in transient CCA behaviour

The measurements reveal important phenomena, that a transient CCA model should be able to reproduce:

- Flow propagation
- Delayed input signal when measuring T_c and $T_{surface}$
- Damped input signal when measuring T_{wr} , T_c or $T_{surface}$
- High power peaks at the start of an excitation
- Time constant for surface temperature reaction of 3 – 4 h

4.3 Analytical expression for CCA transient heat transfer

This section derives analytical expressions for the transient behaviour of CCA in order to grasp the effects that were measured during the experiment presented in the previous section. The choice to derive an analytical expression was made

in order to obtain a result which would be easily implementable in a building controller, without relying on specific software or skills.

Analysing these analytical expressions will help to clarify these transient phenomena and are used to explain and quantify control behaviour of CCA. In order to obtain general results, the analytical expressions are generated for an uncovered full concrete slab (without air holes). This is the configuration used in Sec. 3.2 to analyse the steady-state heat transfer in CCA. Parameters are varied using the same values as presented in Sec. 3.2.

Analytical solutions of the transient heat diffusion equation (Eq. 1.22) for slabs are presented by Carslaw and Jaeger [27] for various boundary conditions. The difference with the CCA case is the fact that water flows through the tubes at discrete points instead of the continuous boundary assumed in the analytical solutions. However, knowledge of the thermal resistances in the CCA component can be used to transform the location dependent temperature profile at the CCA core to a uniform temperature T_c (Section 3.2). In this way, the existing analytical solutions for transient heat conduction in materials can be used to investigate the time dependent behaviour.

4.3.1 Two operational modes

CCA operate in two modes: with and without water flow. Both modes can be derived from the same analytical expression, since they require identical boundary conditions. Fig. 4.6 presents the nomenclature for the two operational modes. In the first mode, the so-called *free running mode*, without water flow, the slab is treated as a whole, with different convective heat transfer coefficients $h_{2,1}$ and $h_{2,2}$ above and below, and, in order to generalise the solution, with different temperatures $T_{2,1}$ and $T_{2,2}$ above and below the slab. In the second mode, the *water flow mode*, the upper and lower part of the slab are treated separately. At the water side, the equivalent concrete core temperature T_c is the surface temperature. The inverse of the equivalent thermal resistance $R_c = R_z + R_w + R_t + R_x$ from the star network (see Section 3.2) determines the heat transfer coefficient h_1 from supply water T_{ws} to T_c . It is important to notice that no thermal inertia is assumed between T_{ws} and T_c . At the room side, the temperature is respectively $T_{2,1}$ and $T_{2,2}$ for the upper and the lower part of the slab. The corresponding heat transfer coefficients are again $h_{2,1}$ and $h_{2,2}$.

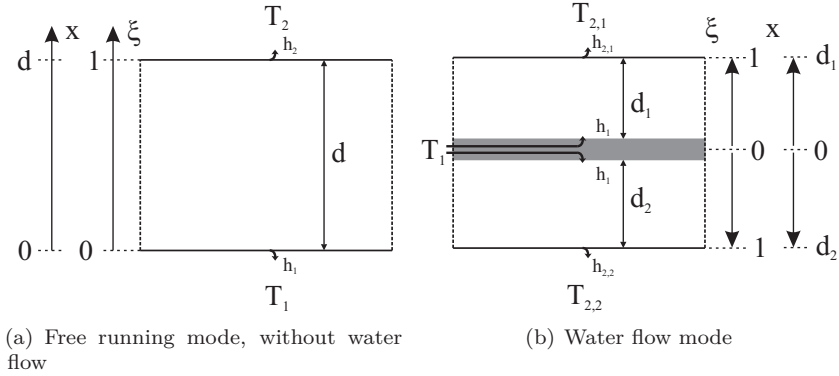


Figure 4.6: Nomenclature for the two operational modes in transient heat conduction

The boundary conditions at the slab surfaces represent a linear dependency of the heat flow on the temperature difference. In the two operational modes, the conventions used for the heat diffusion equation are:

1. Free running CCA (Fig. 4.6(a)):

- $T_1 = T_{zone,below}$; $T_2 = T_{zone,above}$,
- Slab thickness $L = d$,
- $x = 0$ at the ceiling surface (lower surface), $T(0, t) = T_{ceiling-surface}$,
- $x = d$ at the floor surface (upper surface), $T(1, t) = T_{floor-surface}$,
- h_1 : global heat transfer coefficient for radiation and convection at the ceiling,
- h_2 : global heat transfer coefficient for radiation and convection at the floor.

2. CCA with water flow (Fig. 4.6(b)):

- The upper and lower part of the slab are treated separately,
- $T_1 = T_{ws}$,
- $T_{2,1} = T_{room,above}$; $T_{2,2} = T_{room,below}$,
- Slab thickness $L = d_i$ ($i = 1, 2$),
- $x = 0$ at the tube level, $T(0, t) = T_c$, the mean core temperature,

- $x = d_i$ at the upper *or* lower CCA surface, $T(1, t) = T_{surface\ i}$,
- $h_1 = (R_z + R_w + R_t + R_x)^{-1} / 2$ is the equivalent heat transfer coefficient between T_{ws} and T_c , as in Section 3.2 ⁽¹⁾
- $h_{2,1}$ and $h_{2,2}$: global heat transfer coefficient for radiation and convection to the adjacent zone.

4.3.2 Temperature distribution $T(x, t)$ in a slab $0 < x < L$

Solving the CCA $T(x, t)$ problem with a semi-infinite approach, where only the water side boundary is taken into account and the concrete has a infinite thickness, shows that this is only suitable to analyse CCA transient heat transfer in a short time frame: the time at which the heat flow, induced by the hot water flowing through the tubes in the CCA, causes a temperature increase at a depth equal to d_i ranges from 4 min for a 0.1 m slab to 50 min for a 0.4 m slab. The water flow rate \dot{m}_w and the tube distance d_x only have a minor influence on these results.

Therefore, in order to analyse temperature variations in a CCA floor within time frames equal to its time constant, it is necessary to incorporate the CCA upper and lower boundary into the analytical solution.

Carslaw and Jaeger [27, par. 3.11] present an equation $T(x, t)$ for a slab $0 < x < L$, subjected to different boundary conditions (h_1 and $h_{2,i}$) at upper and lower surface. First, in order to generalise the results, x and t are replaced by their dimensionless counterparts ξ and Fo, together with the dimensionless material parameter Bi. Typical Bi values for CCA systems are between 0.1 and 1. The equation expresses the 1-dimensional temperature distribution in a slab of general thickness L as a function of time and space for a temperature $T_{2,i} = 0$ ($i = 1, 2$), thus the same upper and lower room air temperatures.

$$\xi = \frac{x}{L} \quad (4.1)$$

$$Fo = \frac{t}{L^2/\alpha_c} \quad : \text{ the Fourier number} \quad (4.2)$$

$$Bi_i = \frac{h_i L}{\lambda} \quad (i=1,2) \quad : \text{ the Biot number at surface 1 or 2} \quad (4.3)$$

¹See Sec. 4.3.4 for details on the exact value of h_1

The dimensionless counterparts of the boundary conditions for which Carslaw and Jaeger [27] derived their analytical expression, are:

$$\frac{\partial T}{\partial t} = \alpha \frac{\partial^2 T}{\partial x^2} \Leftrightarrow \frac{\partial T}{\partial \text{Fo}} = \frac{\partial^2 T}{\partial \xi^2} \quad (4.4)$$

$$\lambda_c \frac{\partial T}{\partial x} - h_1 T = 0, x = 0 \Leftrightarrow \frac{1}{\text{Bi}_1} \frac{\partial T}{\partial \xi} - T = 0, \xi = 0 \quad (4.5)$$

$$\lambda_c \frac{\partial T}{\partial x} + h_2 T = 0, x = L \Leftrightarrow \frac{1}{\text{Bi}_2} \frac{\partial T}{\partial \xi} + T = 0, \xi = 1 \quad (4.6)$$

$$T = f(x), t = 0 \Leftrightarrow T = f(\xi), t = 0 \quad (4.7)$$

The dimensionless formulation of the analytical solution given by Carslaw and Jaeger [27, par. 3.11], is then:

$$T(\xi, \text{Fo}, \text{Bi}_i) = \sum_{n=1}^{\infty} A_n Z_n(\xi) e^{(-\beta_n^2 \text{Fo})} Z_{n,init} \quad (4.8)$$

with:

$$A_n(\text{Bi}_i) = \left(\frac{2 \left(\left(\frac{\beta_n}{\text{Bi}_2} \right)^2 + 1 \right)}{\frac{1}{\text{Bi}_2} \left(\left(\frac{\beta_n}{\text{Bi}_1} \right)^2 + 1 \right) \left(\text{Bi}_2 \left(\left(\frac{\beta_n}{\text{Bi}_2} \right)^2 + 1 \right) + 1 \right) + \frac{1}{\text{Bi}_1} \left(\left(\frac{\beta_n}{\text{Bi}_2} \right)^2 + 1 \right)} \right)^{(1/2)} \quad (4.9)$$

$$Z_n(\xi, \text{Bi}_i) = \frac{\beta_n}{\text{Bi}_2} \cos(\beta_n \xi) + \sin(\beta_n \xi) \quad (4.10)$$

$$Z_{n,init}(\text{Bi}_i, T_{init}) = \int_0^1 A_n Z_n(\xi') f(\xi') d\xi' \quad (4.11)$$

and $\beta_n(\text{Bi}_i)$, ($n=1,2$),... the positive roots of :

$$\cot \beta = \frac{\beta^2 - \text{Bi}_1 \text{Bi}_2}{\beta (\text{Bi}_1 + \text{Bi}_2)} \quad (4.12)$$

4.3.3 Solution for different upper and lower temperatures

Temperature distribution $T(\xi, Fo)$

For the free running CCA, it is required that the temperature distribution can be determined for non-zero room temperatures, which differ above and below the slab. For the CCA with water flow, the upper and lower part of the slab are treated separately: in the $0 < x < L$ concrete slab part, $x = 0$ at the tube level, where the water supply temperature acts and $x = L$ is respectively the upper and lower slab surface, where the room temperatures acts.

For both operational modes, the analytical expression Eq. 4.8 is extended in this work to non-zero and different temperatures below and above the slab. This is implemented by separating the temperature variable $T(\xi, Fo)$ into $u(\xi)$ and $w(\xi, Fo)$. The problem description with boundary conditions (Eqs. 4.4 - 4.7) changes into:²

$$\frac{\partial T}{\partial Fo} = \frac{\partial^2 T}{\partial \xi^2} \quad (4.13)$$

$$\frac{1}{Bi_1} \frac{\partial T}{\partial \xi} - (T - T_1) = 0, \xi = 0 \quad (4.14)$$

$$\frac{1}{Bi_2} \frac{\partial T}{\partial \xi} + (T - T_2) = 0, \xi = 1 \quad (4.15)$$

$$T = f(\xi), t = 0 \quad (4.16)$$

²For the free running CCA, T_1 must be replaced by $T_{2,2}$ and T_2 by $T_{2,1}$ as shown in Fig. 4.6(a)

by substituting $T = u + w$ in these equations the following set of equations is obtained:

$$\frac{\partial^2 u}{\partial \xi^2} = 0 \text{ or } u = (C\xi + D) \quad (4.17)$$

$$\frac{1}{\text{Bi}_1} \frac{\partial u}{\partial \xi} - (u - T_1) = 0, \xi = 0 \quad (4.18)$$

$$\frac{1}{\text{Bi}_2} \frac{\partial u}{\partial \xi} + (u - T_2) = 0, \xi = 1 \quad (4.19)$$

and

$$\frac{\partial w}{\partial \text{Fo}} = \frac{\partial^2 w}{\partial \xi^2} \quad (4.20)$$

$$\frac{1}{\text{Bi}_1} \frac{\partial w}{\partial \xi} - w = 0, \xi = 0 \quad (4.21)$$

$$\frac{1}{\text{Bi}_2} \frac{\partial w}{\partial \xi} + w = 0, \xi = 1 \quad (4.22)$$

$$w = \tilde{f}(\xi) = f(\xi) - u, t = 0 \quad (4.23)$$

Parameters C and D in Eq. 4.17 can be found by using the appropriate boundary conditions (Eqs. 4.18, 4.19):

$$\frac{1}{\text{Bi}_1} C - (C\xi + D - T_1) = 0, \xi = 0$$

$$\frac{1}{\text{Bi}_2} C + (C\xi + D - T_2) = 0, \xi = 1$$

resulting in

$$C = \frac{(T_2 - T_1)}{\frac{1}{\text{Bi}_1} + \frac{1}{\text{Bi}_2} + 1} \quad (4.24)$$

$$D = \frac{T_2 + \text{Bi}_1 \left(\frac{1}{\text{Bi}_2} + 1 \right) T_1}{1 + \text{Bi}_1 \left(\frac{1}{\text{Bi}_2} + 1 \right)} \quad (4.25)$$

The solution for $w(\xi, \text{Fo})$ is equal to Eq. 4.8 with the only difference that the

initial temperature distribution $\tilde{f}(\xi) = f(\xi) - u$. $f(\xi)$ is the initial temperature profile at time $t = 0$. In order to avoid solving the integral in Eq. 4.11 each time for different initial temperature distributions, a general applicable approach is proposed: this initial temperature distribution is approximated by discretising the resulting T_{init} -profile into K parts and interpolating linearly between its values: $\tilde{f}(\xi)_{k \rightarrow k+1} = (M(\xi - O) + N) - (C\xi + D) = M'\xi + N'$, where the values of M , N and O are determined by $T_{init}(k)$ and $T_{init}(k + 1)$, $k \in [0, K - 1]$. Integrating this initial temperature distribution into the integrand part of Eq. 4.11 results in:

$$Z_{n,init} = \int_0^1 A_n Z_n(\xi) \tilde{f}(\xi) d\xi = \sum_{k=0}^{K-1} \int_{\xi_k}^{\xi_{k+1}} A_n Z_n(\xi) (M'\xi + N') d\xi \quad (4.26)$$

Heat power $\dot{q}(\xi, Fo)$

With the known temperature distribution in the slab, the heat flux (W/m^2) in the slab can be derived using:

$$\begin{aligned} \dot{q}(\xi, Fo) &= -\frac{\lambda_c}{L} \frac{\partial T}{\partial \xi} \\ &= -\frac{\lambda_c}{L} \left[C + \sum_{n=1}^{\infty} A_n \frac{\partial Z_n(\xi)}{\partial \xi} e^{(-\beta_n^2 Fo)} Z_{n,init} \right] \end{aligned}$$

which results in:

$$\dot{q}(\xi, Fo) = -\frac{\lambda_c}{L} \left[C + \sum_{n=1}^{\infty} A_n \beta_n \left(\cos(\beta_n \xi) - \frac{\beta_n}{Bi_1} \sin(\beta_n \xi) \right) e^{(-\beta_n^2 Fo)} Z_{n,init} \right] \quad (4.27)$$

with λ_c/L the heat flux per degree K (W/m^2K).

From Eq. 4.27 it follows that after a certain time, the specific power reaches a steady-state value, determined by the parameter C , which is the steady-state heat flux $\dot{q} = \Delta T/R$:

$$\dot{q}_{Fo \gg 1} = -\frac{\lambda_c}{L} C = -\frac{1}{\frac{1}{h_1} + \frac{L}{\lambda_c} + \frac{1}{h_2}} (T_2 - T_1) \quad (4.28)$$

Cumulated specific heat $q(\xi, Fo)$

The cumulated specific heat (J/m^2) is deduced from Eq. 4.27:

$$\begin{aligned}
 q(\xi, Fo) &= \int_0^t \dot{q} dt = \int_0^{Fo} -\frac{\lambda_c}{L} \frac{\partial T}{\partial \xi} \frac{L^2}{\alpha} dFo \\
 &= \int_0^{Fo} -L\rho c \frac{\partial T}{\partial \xi} dFo \\
 &= -L\rho c \left[\int_0^{Fo} C dFo + \int_0^{Fo} \sum_{n=1}^{\infty} A_n \frac{\partial Z_n(\xi)}{\partial \xi} e^{(-\beta_n^2 Fo)} Z_{n,init} dFo \right] \\
 &= -L\rho c \left[C Fo + \sum_{n=1}^{\infty} A_n \frac{\partial Z_n(\xi)}{\partial \xi} \frac{1 - e^{(-\beta_n^2 Fo)}}{\beta_n^2} Z_{n,init} \right] \quad (4.29)
 \end{aligned}$$

with $L\rho c$: cumulated specific heat per degree K (J/m^2K).

Again, for large $Fo \gg 1$, the specific heat reaches a steady-state value $L\rho c C Fo$, which is linearly dependent on Fo . Moreover, since β_n increases rapidly ($\beta_1 \leq \pi/2$, $\beta_{n>2} = (n-1)\pi$), this relation can be simplified by using only the first term of the infinite sum. This analysis is elaborated in Sec. 4.3.5.

$$q_{Fo \gg 1} = -L\rho c \left[C Fo + \left(A_1 \frac{\partial Z_1(\xi)}{\partial \xi} \frac{1}{\beta_1^2} Z_{1,init} \right) \right] \quad (4.30)$$

Summary

In summary, it can be concluded that the temperature and flux profiles can be found from:

$$T(\xi, Fo) = C\xi + D + \sum_{n=1}^{\infty} A_n Z_n(\xi) e^{(-\beta_n^2 Fo)} Z_{n,init} \quad (4.31)$$

$$\dot{q}(\xi, Fo) = -\frac{\lambda_c}{L} \left[C + \sum_{n=1}^{\infty} A_n \beta_n \left(\cos(\beta_n \xi) - \frac{\beta_n}{Bi_1} \sin(\beta_n \xi) \right) e^{(-\beta_n^2 Fo)} Z_{n,init} \right] \quad (4.32)$$

$$q(\xi, Fo) = -L\rho c \left[C Fo + \sum_{n=1}^{\infty} A_n \beta_n \left(\cos(\beta_n \xi) - \frac{\beta_n}{Bi_1} \sin(\beta_n \xi) \right) \frac{1 - e^{(-\beta_n^2 Fo)}}{\beta_n^2} Z_{n,init} \right] \quad (4.33)$$

In free running mode, for a situation with equal temperatures T_{zone} below and above the slab, the C parameter equals zero and $D = T_{zone}$. In the case where $T_{zone} = 0$ below and above the slab, the above expression for T reduces to the expression formulated by Carslaw and Jaeger [27] (for which Eq. 4.8 gives the dimensionless form).

4.3.4 Combining the solution for the upper and lower slab part

The approach that calculates the upper and lower slab part separately asks for a correction when combining the two results. Since $Bi_{2,1} \neq Bi_{2,2}$, due to a different heat transfer coefficient at the slab surfaces or a difference in slab thickness, the amount of heat transferred to the upper and lower part will also differ. If, as assumed up to now, the value of h_1 is equal for upper and lower slab part ($= (R_z + R_w + R_t + R_x)^{-1} / 2$), the $T(\xi, Fo)$ -solution will result in a different T_c -value for upper and lower part. This is, considering the physical meaning of the equivalent core temperature T_c , not feasible.

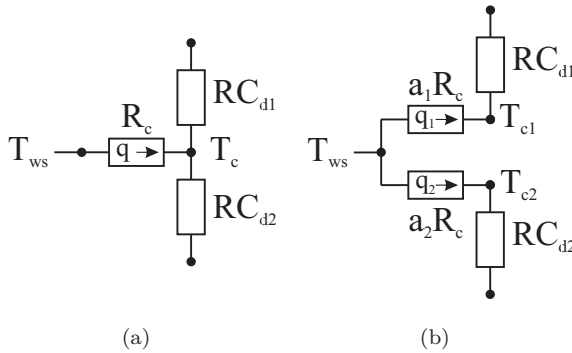


Figure 4.7: (a) Real heat flow pattern in a CCA star network, (b) Heat flow pattern resulting from the separate calculation of upper and lower slab part

Fig. 4.7 shows the difference between the real heat flow pattern in the star network (b), and the resulting heat flow pattern by combining the solution for the upper and lower slab part (a). The correction factors a_1 and a_2 are

introduced to make sure that $T_c = T_{c1} = T_{c2}$, and are calculated from:

$$\frac{q_1}{q} = \frac{\frac{1}{a_1 R_c} (T_{ws} - T_{c1})}{\frac{1}{R_c} (T_{ws} - T_c)} = \frac{1}{a_1} \quad (4.34)$$

$$\frac{q_2}{q} = \frac{\frac{1}{a_2 R_c} (T_{ws} - T_{c2})}{\frac{1}{R_c} (T_{ws} - T_c)} = \frac{1}{a_2} \quad (4.35)$$

The correction factors a_1 and a_2 relate as $\frac{1}{a_1} + \frac{1}{a_2} = 1$. While finding the temperature distribution in the concrete slab, defined by Eq. (4.31), an iteration is performed to find the values of a_1 and a_2 for which $T_c = T_{c1} = T_{c2}$. For reference, after circulating 30 water during 4 h through a CCA slab of 0.2 m thickness with a room temperature of 20 above and below the slab, the correction values for the equivalent core thermal resistance R_c are $1/a_1 = 1 - 1/a_2 = 0.49$. Since a symmetrical slab is considered, with equal room temperatures above and below, this difference is induced by the different h -values above and below. The a_1 -value can be understood as follows:

- For the uncovered slab in heating regime, the heat transfer coefficient at the ceiling is lower (thermal resistance larger) than at the floor surface ($R_{d1} > R_{d2}$).
- With equal room temperatures T_2 below and above the slab, $q_1 < q_2$.
- If $a_1 = a_2$, then $T_{c1} > T_{c2}$ (heating regime, so $T_{ws} > T_2$), which is contradictory to the physical meaning of T_c in the CCA-RC-model.
- In order to have $T_{c1} = T_{c2}$ with $q_1 < q_2$, a_1 should be larger than a_2 . An iteration is required to find the values of a_1 and a_2 , because $a_i R_c$ is an integral part of the total resistance between T_{ws} and T_2 , which determines \dot{q}_i .

To conclude, the approach of using the correction factors a_1 and a_2 can be seen as adapting the size of the ‘tunnel’ through which the heat flows. A larger tunnel upwards and a smaller tunnel downwards makes sure that more heat flows upwards while still having equal ΔT upwards and downwards.

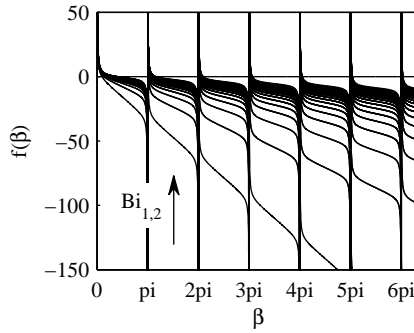


Figure 4.8: $f(\beta) = \cot \beta - \frac{\beta^2 - Bi_1 Bi_2}{\beta(Bi_1 + Bi_2)}$ for different Bi-numbers. The arrow indicates the direction of increasing Bi-number.

4.3.5 Analysis of the CCA $T(\xi, Fo)$ equation

In order to assess the impact of the different terms and factors in Eqs. 4.31, 4.32 and 4.33, their numerical values are presented for Bi_i -values varying from 0 to 1 with a 0.1-step. These are typical values for concrete slabs.

The values β_n are the roots of Eq. 4.12, which represents a cotangent-function subtracted by a linear increasing function. Except for the first root, its roots lie close to π as can be deduced from Fig. 4.8.

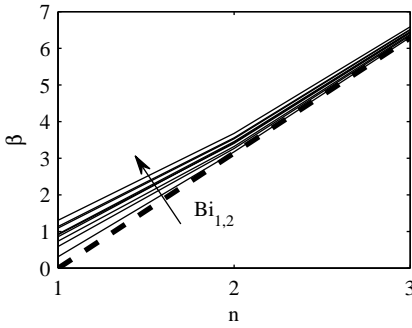
Fig. 4.9(a) shows that, except for the first root, the roots of the β -function approach $(n - 1)\pi$, which is indicated by the thick dashed line on the figure. The arrow indicates the impact of increasing values of Bi_1 or Bi_2 .

The value of A_n decreases for larger n -values. It is affected by Bi_1 and to a minor extend and only for the first n -values, by Bi_2 . This indicates the dominance of the first terms in the infinite sum.

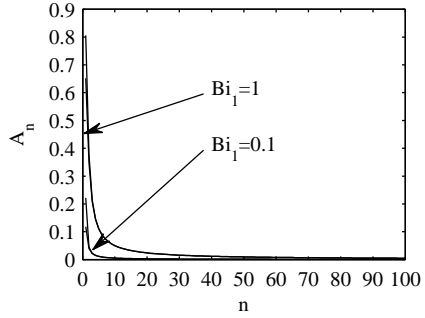
The space dependent Z_n -term is presented in Fig. 4.9(c) for two values of Bi_1 , which affects the amplitude of the solution. The higher the Bi-number, the lower the space dependent term in the infinite sum. The frequency of the Z_n -oscillation as a function of n , is determined by ξ : the graph presents solutions for $\xi = 0$ (constant), $\xi = 0.1$ and $\xi = 1$ (highest frequency).

The initial condition factor $Z_{n,init}$ appears to decrease to zero for approximately $n > 10$ and will therefore have a large impact on the solution of the transient temperature profile.

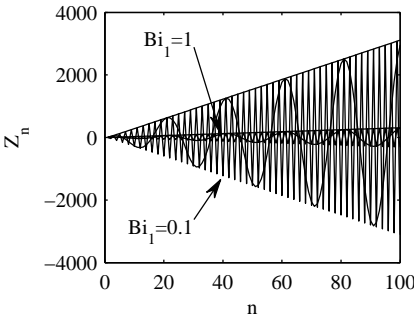
The two time dependent factors, the decay factor in the solution for T and \dot{q} ,



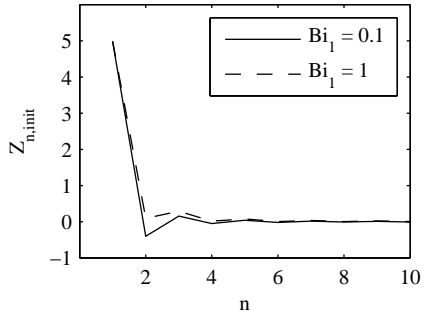
(a) Roots of β -equation (dashed line represents $(n - 1)\pi$)



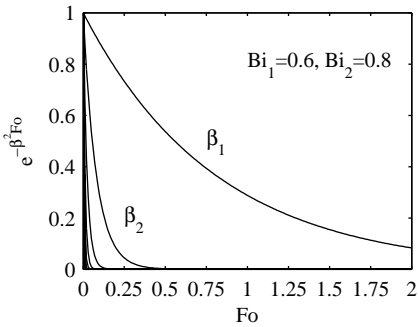
(b) A_n for two values of Bi_1



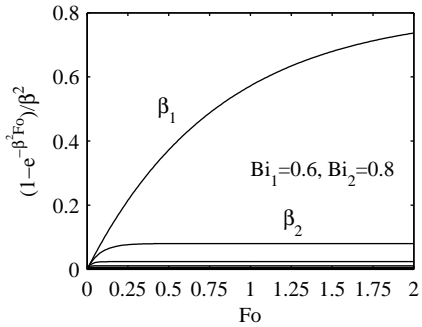
(c) Z_n for $Bi_1 = 0.1, 1$ and $\xi = 0, 0.1, 1$



(d) $Z_{n,init}$ for $Bi_1 = 0.1, 1$ and $T_{init} = 5$



(e) Time dependent decay factor for T and \dot{q}



(f) Time dependent factor for q

Figure 4.9: Parameter analysis of the different terms in the transient temperature, heat power and cumulated heat equations for a concrete slab

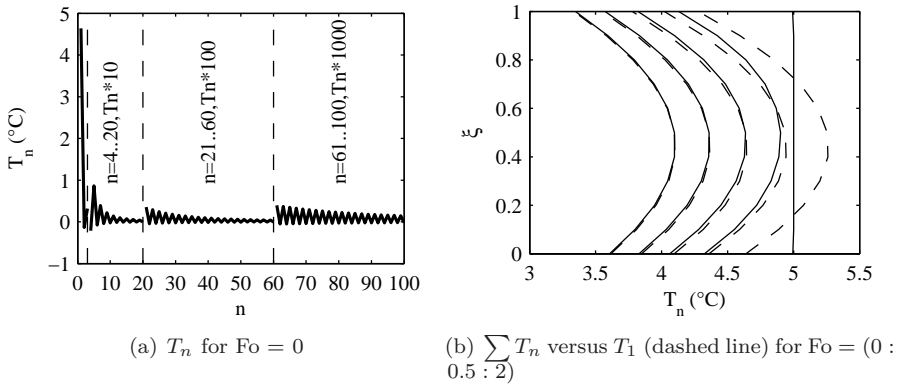


Figure 4.10: The different terms of the temperature equation (a) and the difference between $T(n = 1)$ and $T(n = 1..100)$ (b) for $Bi_{2,1} = 0.6, Bi_{2,2} = 0.8$

and in the solution for q (Figs. 4.9(e) and 4.9(f) respectively) show that after a certain time, the influence of the initial condition will extinct. For higher β_n -values this already occurs at a time which is only a fraction of the system's time constant. Since β_n ($n \geq 2$) is only weakly dependent on the Bi-numbers (Fig. 4.9(a)), these decay times are almost independent of the specific situation. Supposing the n^{th} term is negligible when it's value reaches 1% of it's initial value, it follows that

$$e^{(-\beta_n^2 Fo)} = 0.01 \Rightarrow Fo = -\frac{\ln 0.01}{\beta_n^2} \tag{4.36}$$

E.g., for uncovered concrete slabs with a thickness ranging from 10 cm to 40 cm, for $n = 2$, this time ranges from $Fo = 0.4$ ($t = 1.1$ h) to $Fo = 0.3$ ($t = 13.9$ h), so around 1/3 of the slab's time constant. For $n = 3$ and $n = 4$ this is approximately 10% and 5% of the time constant.

Analogously, the same reasoning applied to the first term ($n = 1$) leads to the time at which the temperature has almost reached steady state. For the same concrete slabs, this appears to be after, respectively, $Fo = 6.8$ ($t = 19$ h) to $Fo = 2.0$ ($t = 90$ h). Therefore, this steady state time is a function of the Bi-number.

Fig. 4.10(a) shows the individual values of the terms of the sum in the temperature equation for $Fo = 0$ and $\xi = 0$. It shows that the solution is dominated by the first term. However, as presented in Fig. 4.10(b), for small

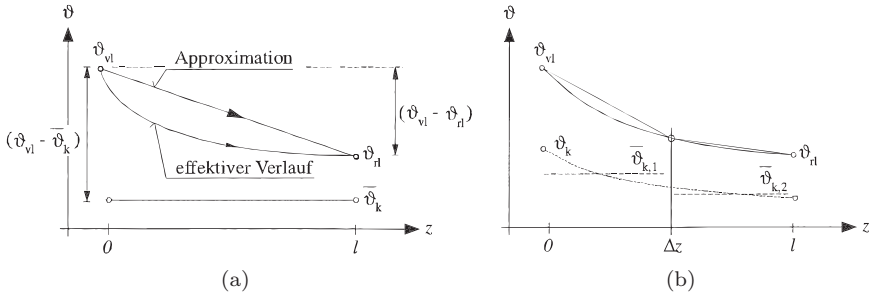


Figure 4.11: (a) Linear approximation of water temperature progress along the CCA tube (adapted from [81]), (b) Division of the CCA tube in two parts (taken from [81]). θ : temperature, vl : ‘Vorlauf’ = water supply, rl : ‘Rücklauf’ = water return, k : ‘Kern’ = concrete core.

values of Fo , it is crucial to include more than the first term of the temperature equation, in order to obtain a correct result. For $Fo > 1$, it is reasonable to approximate the temperature distribution by only taking into account the first term ($n = 1$). To conclude, although the $n = 2$ -decay term is very small for $Fo > 0.4$, the joint effect of the T_n -sum seems to affect the solution up to $Fo = 1$. This is certainly true for larger Bi-numbers, as in the case of the free running CCA. For CCA with water flow, since upper and lower part are treated separately, the Bi-numbers are in the range of $0.3 - 0.4$, for which the $n \geq 2$ decay more rapidly. However, as a general rule, using $Fo = 1$ as a threshold to neglect $n \geq 2$ -terms seems appropriate.

4.4 Propagation time of water flow

In the previous sections, CCA were always treated as a 1-dimensional system. However, a CCA floor is evidently a 3-dimensional system which means that the concrete temperature T_c is a distributed variable, so a function of both time and location. In the EMPA-model, the difference between T_{ws} and T_{wm} is incorporated in the model by the thermal resistance R_z (see [81] and Sec. 3.2.7). Koschenz and Lehmann [81] derived that $T_{wm} = (T_{ws} + T_{wr})/2$, meaning that the effective temperature of the water along the tube length is approximated by a linear curve, as shown in Fig. 4.11(a).

The approach to model the concrete core temperature T_c as a constant might overestimate the heat transfer from water to concrete, which might result in T_{ws} being lower than T_c . However, $(T_{ws} - T_{wr})$ can not be larger than $(T_{ws} - T_c)$, as shown in Fig. 4.11(a). From the energy balance, Koschenz and Lehmann [81] deduce the condition:

$$\frac{1}{R_c} (T_{ws} - T_c) = \frac{\dot{m}_w}{d_x L_t} c_p (T_{ws} - T_{wr})$$

$$\Downarrow$$

$$\frac{\dot{m}_w c_p R_c}{d_x L_t} \geq 1 \quad (4.37)$$

If Eq. 4.37 is not fulfilled, Koschenz and Lehmann [81] propose the solution to divide the tube length in n parts, as in Fig. 4.11(b), which changes Eq. 4.37 into:

$$\frac{n \dot{m}_w c_p R_c}{d_x L_t} \geq 1 \quad (4.38)$$

However, due to the nature of R_z , there is no thermal capacity between T_{ws} and T_{wm} in the EMPA-model, which makes $T_{wm} = (T_{ws} + T_{wr})/2$, immediately after the pump is switched on and water at temperature T_{ws} enters the CCA.

This still neglects the effect of water flow propagating through the CCA tube, as shown in Fig. 4.12. The effect of propagation time was already demonstrated while analysing the measurement results in Sec 4.2. Next to the concrete core temperature T_c , this means that the mean water temperature T_{wm} is also a distributed variable. In order to determine the short term flow switching behaviour of the CCA, it is important to assess the effect of propagation time on the transferred energy from water to concrete. Furthermore, this propagation time might be the reason why Weber et al. [144] reported model errors for pump cycling times lower than 40 min.

In heat exchanger applications this problem is often resolved numerically. However, to account for propagation time in a controller, Cool et al. [71] proposed an analytical solution for a condensing fluid (constant temperature) around the tubes of a heat exchanger, while the fluid in the tubes is subjected to a step change. This approach is adapted to the CCA case in this section.

Assume that water conditioned at set point temperature is immediately

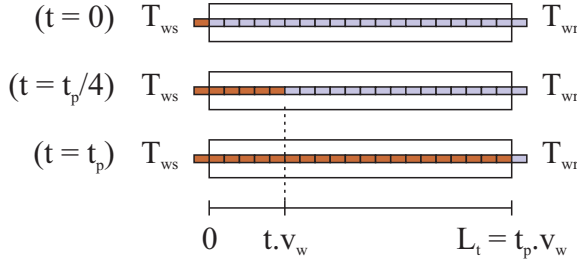


Figure 4.12: The water flow propagating through the CCA tube, with t_p the propagation time, v_w the water speed and L_t the tube length.

available at the CCA tube entrance. When water flow is switched on, it takes a certain time before the change in water temperature is propagated through the whole CCA floor. The propagation time t_p is evidently a function of the water velocity and the length of a single loop.

$$t_p = \frac{L_t}{v_w} \quad (4.39)$$

with $v_w = 4\dot{m}_w / \rho_w \pi d_{t,i}^2$ (m/s) the water velocity in the tube. Without taking into account the propagation of the water flow, a step in the supply temperature T_{ws} will immediately result in a step change of the mean water temperature $T_{wm} = (T_{ws} + T_{wr})/2$ in the CCA floor. For this case, from the steady state energy balance, T_{wm} can be derived, leading to Eq. 4.40. This approach is used in the current EMPA-model.

$$\dot{q} = \frac{1}{R_c} (T_{ws} - T_c) = \frac{1}{R_z} (T_{ws} - T_{wm})$$

⇓

$$T_{wm} = T_{ws} - \frac{R_z}{R_c} (T_{ws} - T_c) \quad (4.40)$$

with T_c the concrete core temperature from the equivalent star network (Sec. 3.2).

4.4.1 Water temperature as a function of time and location

With the propagation time taken into account, the energy balance between a water temperature T_w at some point in the slab and a constant, for the time being not specified, concrete temperature T_{concr} on a CCA-piece dz along the length of the tube is:

$$c_w \rho_w \frac{\pi d_{t,i}^2}{4} dz \frac{\delta T_w}{\delta t} = \dot{m}_w c_w (T_w(z) - T_w(z + dz)) - \frac{d_x dz}{R_{concr}} (T_w - T_{concr}) \quad (4.41)$$

With $T_w(z + dz) = T_w(z) + \frac{\partial T_w(z)}{\partial z} dz$ Eq. 4.41 becomes:

$$T_{concr} - T_w = \frac{c_w \rho_w \pi d_{t,i}^2}{4 d_x} R_{concr} \frac{\partial T_w}{\partial t} + \frac{\dot{m}_w c_w R_{concr}}{d_x} \frac{\partial T_w}{\partial z} \quad (4.42)$$

With

$$\tau = R_{concr} c_w \rho_w \pi d_{t,i}^2 / 4 d_x \quad [\text{s}] \quad (4.43)$$

and v_w the water velocity, the Laplace transform is an ordinary differential equation in z :

$$\theta_{concr} = \tau v_w \frac{\partial \theta_w}{\partial z} + (\tau s + 1) \theta_w \quad (4.44)$$

With the assumption that T_{concr} is constant during the propagation time t_p , $\theta_{concr} = 0$ and $T_w(z, t)$ is the solution of the homogeneous part of Eq. 4.44:

$$\theta_w(z, s) = A e^{-\frac{\tau s + 1}{\tau v_w} z} \quad (4.45)$$

The constant A can be found by putting $\theta_w = \theta_w(0, s)$ for $z = 0$, which results in the final transfer function:

$$\frac{\theta_w(z, s)}{\theta_w(0, s)} = e^{-\frac{z}{\tau v_w}} e^{-s \frac{z}{v_w}} \quad (4.46)$$

↓

$$T_w(z, t) = T_w(0, t) e^{-\frac{z}{\tau v_w}} u\left(t - \frac{z}{v_w}\right) \quad (4.47)$$

From Eq. 4.47 it follows that the response to a change of the water temperature at the entrance of the CCA module is delayed by a time z/v_w and damped by a

factor $e^{-z/\tau v_w}$, which is a function of the heat transfer characteristics through the factor τ .

4.4.2 Mean water temperature T_{wm} as a function of time

The effect of the propagation time on the mean water temperature T_{wm} can be found by averaging $T_w(z, t)$ over the total length L_t of the tube.

$$T_{wm}(t) = \frac{1}{L_t} \int_0^{L_t} T_w(z, t) dz = \frac{T_w(0, t)}{L_t} \int_0^{L_t} e^{-\frac{z}{\tau v_w}} u\left(t - \frac{z}{v_w}\right) dz \quad (4.48)$$

Two regions can be distinguished for which this integral is solved: $t < L_t/v_w$ and $t > L_t/v_w$, where $L_t/v_w = t_p$ is the propagation time of the concrete slab. The integral is solved with the assumption that the initial water temperature $T_w(z, 0) = 0$. When this is not the case, a simple transformation justifies this assumption.

$t < t_p$: before the end of the flow propagation

The delay factor $u\left(t - \frac{z}{v_w}\right)$ divides the z -interval $[0, L_t]$ in two parts (see Fig. 4.12):

1. $z < tv_w \Leftrightarrow t > z/v_w : u\left(t - \frac{z}{v_w}\right) = 1$
2. $z > tv_w \Leftrightarrow t < z/v_w : u\left(t - \frac{z}{v_w}\right) = 0$

Therefore, the mean water temperature is calculated by

$$\begin{aligned} T_{wm}(t) &= \frac{T_w(0, t)}{L_t} \left[\int_0^{tv_w} e^{-\frac{z}{\tau v_w}} u\left(t - \frac{z}{v_w}\right) dz + \int_{tv_w}^{L_t} e^{-\frac{z}{\tau v_w}} u\left(t - \frac{z}{v_w}\right) dz \right] \\ &= \frac{T_w(0, t)}{L_t} \int_0^{tv_w} e^{-\frac{z}{\tau v_w}} dz \\ &= -\frac{T_w(0, t)}{L_t} \tau v_w e^{-\frac{z}{\tau v_w}} \Big|_0^{tv_w} \\ &= T_w(0, t) \frac{\tau}{t_p} \left(1 - e^{-\frac{t}{\tau}} \right) \end{aligned} \quad (4.49)$$

$t \geq t_p$: **after the end of the flow propagation**

The delay factor $u(t - \frac{z}{v_w})$ always equals 1, resulting in a mean water temperature given by

$$\begin{aligned} T_{wm}(t) &= \frac{T_w(0, t)}{L_t} \int_0^{L_t} e^{-\frac{z}{\tau v_w}} dz \\ &= -\frac{T_w(0, t)}{L_t} \tau v_w e^{-\frac{z}{\tau v_w}} \Big|_0^{L_t} \\ &= T_w(0, t) \frac{\tau}{t_p} \left(1 - e^{-\frac{t_p}{\tau}}\right) \end{aligned} \quad (4.50)$$

A summation of Eqs. 4.49 and 4.50 results in a global formulation (see Eq. 4.51) of the mean water temperature T_{wm} as a function of time t , the propagation time t_p , the inlet condition $T_w(0, t)$ and the heat transfer to the CCA, incorporated in the parameter τ :

$$T_{wm}(t) = T_w(0, t) \frac{\tau}{t_p} \left[\left(1 - e^{-\frac{t}{\tau}}\right) - \left(1 - e^{-\frac{-t+t_p}{\tau}}\right) e^{-\frac{t_p}{\tau}} u(t - t_p) \right] \quad (4.51)$$

4.4.3 Heat transfer parameter τ

In the derivation of the T_{wm} -equation (Sec. 4.4.2), the concrete temperature T_{concr} and the heat transfer resistance R_{concr} are not specified. They can be determined by stating that for $t = t_p$, the T_{wm} -value from the steady state energy balance (Eq. 4.40) is equal to T_{wm} from the propagation energy balance (Eq. 4.50). Because T_{concr} , and therefore also T_c is assumed to be constant, this variable can be put equal to zero in the energy balance.

$$T_{ws} - \frac{R_z}{R_c} (T_{ws} - T_c) = \left(1 - \frac{R_z}{R_c}\right) T_w(0, t) = T_w(0, t) \frac{\tau}{t_p} \left(1 - e^{-\frac{t_p}{\tau}}\right)$$

which results in:

$$\frac{\tau}{t_p} \left(1 - e^{-\frac{t_p}{\tau}}\right) - \left(1 - \frac{R_z}{R_c}\right) = 0 \quad (4.52)$$

Since $\tau = f(R_{concr})$ (Eq. 4.43), it follows from Eq. 4.52 that R_{concr} is a function of the propagation time t_p and the ratio R_z/R_c , or, in terms of the

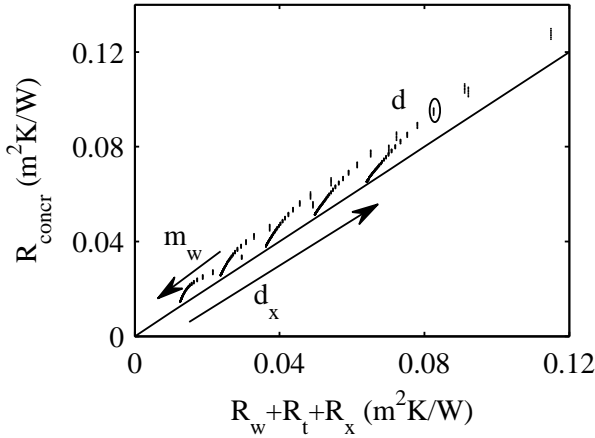


Figure 4.13: Thermal resistance R_{concr} for propagation analysis as a function of d_x (5 sets of data along the linear curve), \dot{m}_w (within 1 d_x data set, decreasing R_{concr} with increasing \dot{m}_w), and d (within 1 d_x - \dot{m}_w -data set a very small influence, which is only noticeable at low \dot{m}_w -values)

CCA dimensions, a function of the water velocity $v_w = f(\dot{m}_w, d_{t,i})$, the tube length L_t , the tube spacing d_x and the CCA thickness d .

Fig. 4.13 shows a parameter analysis of the thermal resistance R_{concr} (1) as a function of d_x , which give the 5 sets of data along the linear curve, (2) within 1 d_x -data set, as a function of \dot{m}_w (decreasing R_{concr} with increasing \dot{m}_w), and (3) within 1 d_x - \dot{m}_w -data set, as a function of d (a very small influence, which is only noticeable at low \dot{m}_w -values).

With Eq. 4.52 solved for R_{concr} , Fig. 4.13 shows that d_x has the largest influence on the value of R_{concr} , followed by \dot{m}_w and finally d . The figure shows that the thermal resistance $R_w + R_t + R_x$ between mean water temperature T_{wm} and the equivalent mean concrete core temperature T_c is a valuable first approximation for R_{concr} : the error is over 40% for the smallest value of d_x and drops to 17% for the largest.

4.4.4 The influence of flow propagation on the heat transfer

Using the star network (Fig. 1.8) to calculate heat transfer in the CCA floor, flow propagation has an influence on the transferred heat from water to concrete.

Starting from Eq. 4.51, the heat power and the transferred energy during the propagation time for a step change of the water supply temperature can be expressed as

$$\begin{aligned} \dot{q}_{prop} &= \frac{1}{R_{concr}} (T_{wm} - 0) \\ q_{prop} &= \int_0^{t_p} \dot{q}_{prop} dt \\ &= \frac{T_w(0, t)}{R_{concr}} \frac{\tau}{t_p} \left[\tau \left(e^{-\frac{t_p}{\tau}} - 1 \right) + t_p \right] \end{aligned} \quad (4.53)$$

Without taking into account the propagation time, this would have been

$$\begin{aligned} \dot{q}_{noprop} &= \frac{1}{R_{concr}} (T_{wm}(t > t_p) - 0) \\ q_{noprop} &= \frac{T_w(0, t)}{R_{concr}} \frac{\tau}{t_p} \left(1 - e^{-\frac{t_p}{\tau}} \right) t_p \end{aligned} \quad (4.54)$$

Therefore, the impact on the heat transfer by taking into account the propagation time can be expressed by the ratio of q_{prop} to q_{noprop} :

$$\frac{q_{prop}}{q_{noprop}} = \frac{1}{\left(1 - e^{-\frac{t_p}{\tau}} \right)} - \frac{\tau}{t_p} \quad (4.55)$$

4.4.5 Equivalent Supply Temperature

The ratio of q_{prop} to q_{noprop} (Eq. 4.55) allows to define an equivalent mean water temperature for which the energy transferred in the period $[0 - t_p]$ equals q_{prop} . However, since $T_{wm} = f(T_{ws})$, it is equally valid to define a constant equivalent water supply temperature $T_{ws,eq}$ for the period $[0 - t_p]$, according to Eq. 4.56.

$$T_{ws,eq} = \left(\frac{1}{\left(1 - e^{-\frac{t_p}{\tau}} \right)} - \frac{\tau}{t_p} \right) T_{ws} \quad (4.56)$$

As a result, using the star network approach to calculate CCA heat transfer (Fig. 1.8) and because flow propagation causes a delayed increase of the mean water

temperature in the slab, the effect on the heat transfer from water to concrete can be calculated by using the constant equivalent water supply temperature $T_{ws,eq}$ during the flow propagation time t_p .

4.4.6 Application of Equivalent Supply Temperature approach

The $T_{ws,eq}$ -approach is applied for a 10 step change of the water supply temperature in an uncovered concrete slab of thickness $d = 0.2\text{m}$ having a total area of 12m^2 . For a mass flow rate $\dot{m}_w = 150\text{kg/h}$ the propagation time $t_p = 319\text{s}$. Fig. 4.14(a) shows the effect of the propagation time on the mean water temperature in the slab, while Fig. 4.14(b) demonstrates the use of $T_{ws,eq}$ to calculate the cumulated heat transfer: at the end of the propagation time, the energy transferred is equal to the case where propagation is taken into account in detail. The ratio q_{prop}/q_{noprop} is 65.6% in this case.

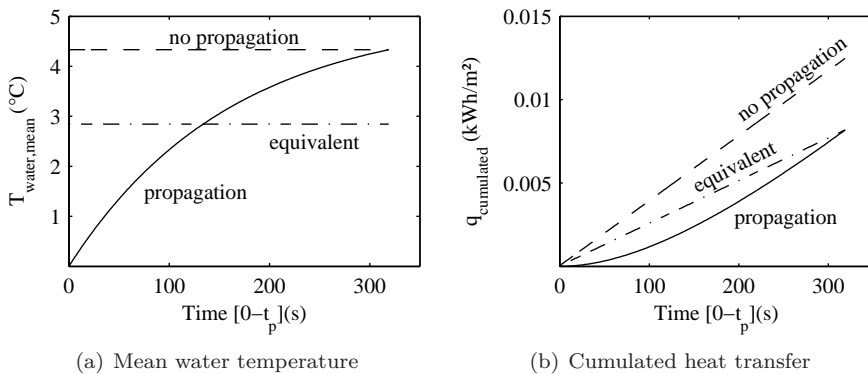


Figure 4.14: The effect of flow propagation on the mean water temperature (a) and the heat transfer (b), and the effect of using the constant equivalent water supply temperature for a 10°C step change of the water supply temperature

4.4.7 Impact of simplifications

While setting up the analytical solution of the transient heat transfer in CCA, two important simplifications are made. Firstly, a simplification originating from the EMPA-model is that the mean water temperature T_{wm} is the mean of the water supply and return temperature, T_{ws} and T_{wr} . In reality this is

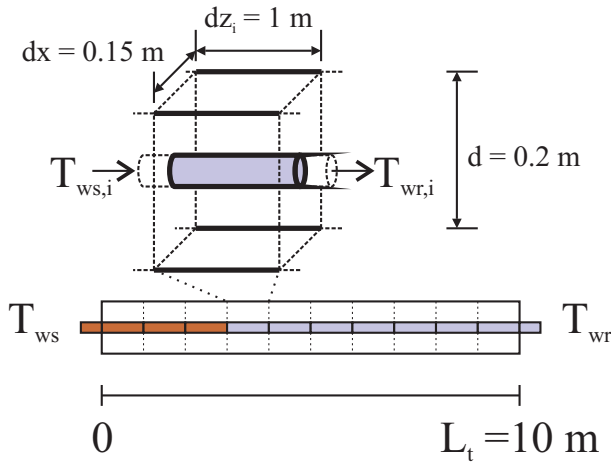


Figure 4.15: Dimensions of the CCA used for analysing the impact of the simplifications of the analytical expression

an exponential-shaped curve, as shown in Fig. 4.11. Secondly, by deriving the Equivalent Mean Temperature to account for the propagation time, the assumption was made that during this propagation time, the temperature of the concrete is constant. Both assumptions tend to overestimate the heat transfer from water to CCA, which is proportional to $(T_{wm} - T_c)$.

To analyse the impact of these assumptions on the calculated temperatures and heat transfer rates in the CCA, a comparative calculation is set up between 3 cases:

- Case 1: the ‘finite difference’-approach, the analytical solution for a slab divided into n parts, to have a good approximation of the real water temperature profile and heat transfer from water to CCA.
- Case 2: the ‘no-propagation’-approach, the analytical solution for a slab without propagation time and
- Case 3: the ‘propagation’-approach, the analytical solution for a slab with propagation time (see Sec. 4.4.5).

The CCA is initially at 20°C and the water temperature experiences a step to 30°C .

Table 4.2: Data of the example TABS piece used for validating the simplifications of the analytical expression

Parameter	Value	Units
L_t	10	(m)
d	0.20	(m)
The tubes are located in the center of the slab		
$d_{t,o}^{(1)}$	20	(mm)
d_x	0.15	(m)
d_z	1.00	(m)
v_w	0.20	(m/s)
\dot{m}_w	0.04	(kg/s)
$\frac{d/2}{d_x} > 0.3$	0.67	(-)
$\frac{d_{t,o}}{d_x} < 0.2$	0.13	(-)
$R_c(L_t)$ (calculated)	0.031	(m ² K/W)
$\frac{\dot{m}_w c_p R_c}{d_x L_t} \geq 1$	3.2	(-)
$R_c(dz)$ (calculated)	0.026	(m ² K/W)
$\frac{\dot{m}_w c_p R_c}{d_x dz} \geq 1$	27.1	(-)

⁽¹⁾: $d_{t,o}$ = outer tube diameter

The dimensions of the example CCA piece, as shown in Fig. 4.15, are chosen such that they fulfill the EMPA steady state conditions (Eqs. 3.1 and 3.2) and the EMPA energy balance condition (Eq. 4.37). This means that the EMPA star-RC-network can be applied to this CCA. The CCA is divided into 10 parts and the calculation time step dt is chosen to be 5 s. The water velocity v_w is such that the water flows through 1 CCA part in 1 time step dt . This means that the effect of water propagation in 1 CCA part is not present from t to $t + dt$. The EMPA energy balance condition is fulfilled for both the whole CCA piece as well as for 1 dz -CCA part. The propagation time of the CCA is $t_p = 50 \text{ s} = 10 \times dt$. Table 4.2 shows the data of the example CCA piece.

The energy balance condition of the dz -part $\frac{\dot{m}_w c_p R_c}{d_x dz}$, which has to be larger than 1, is equal to 27.1. This shows that the division of the 10 m CCA into 10 parts is sufficient: this value means that the water temperature drop ($T_{ws} - T_{wr}$) will only be 4% ($1/27.1$) of the difference between water and concrete ($T_{ws} - T_c$). The linear interpolation over dz to obtain T_{wm} will therefore be sufficient to approximate the real T_{wm} .

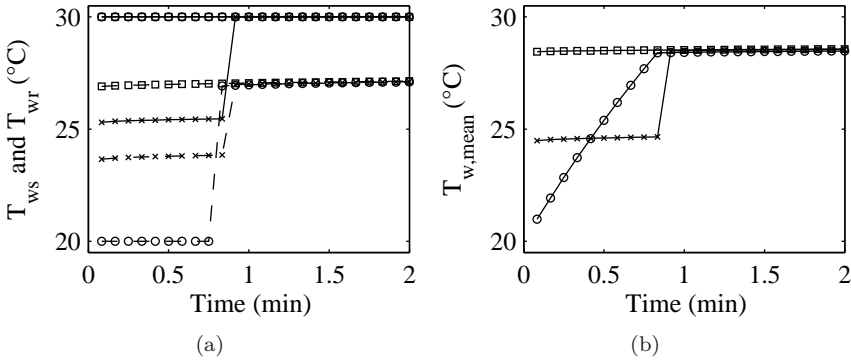


Figure 4.16: (a) T_{ws} (-), T_{wr} (- -) and (b) T_{wm} for the ‘no-propagation’- (\square), the ‘propagation’- (\times) and the ‘finite difference’- (\circ) approach to calculate the CCA transient heat transfer.

To show the effect of the three approaches, Fig. 4.16 presents the water supply, water return, and mean water temperatures, T_{ws} , T_{wr} and T_{wm} . Remember that the heat transfer from water to concrete is proportional to $(T_{wm} - T_c)$, with T_c the concrete core temperature (cfr. the EMPA-star-RC network in Fig. 1.8). Without propagation (\square -line), the lumped analytical solution immediately results in a high T_{wr} and T_{wm} . With the ‘finite difference’-approach (\circ -line), T_{wr} remains at 20°C until the propagation time $t_p = 50$ s. With propagation (\times -line), the impact of the increasing T_{wm} in the CCA is compensated by using a lower water supply temperature T_{ws} during the propagation time t_p . The mean water temperature T_{wm} in Fig. 4.16(b) corresponds well to the results from the analytical solution in Fig. 4.14(a), where \dot{T}_{wm} was calculated with Eq. 4.51 for the ‘propagation’-approach.

Fig. 4.17(a) shows the impact of taking into account flow propagation in the calculation of the heat transfer q . In the ‘propagation’-approach, q matches the ‘finite difference’-approach much closer, which is also shown by looking at the ratio q_{noprop}/q_{FD} and q_{prop}/q_{FD} in Fig. 4.17(b). Where both ratios are in the first seconds very high — but the absolute value of q very low — q_{prop}/q_{FD} quickly drops towards a very small value: 0.07% after 4 min and increasing slightly to 0.6% after 10 min. For the ‘no-propagation’-approach, q_{noprop}/q_{FD} is 10% after 4 min and over 4% after 10 min.

These figures show that the two simplifications made in the analytical expression — linear interpolation of the water temperature and the constant

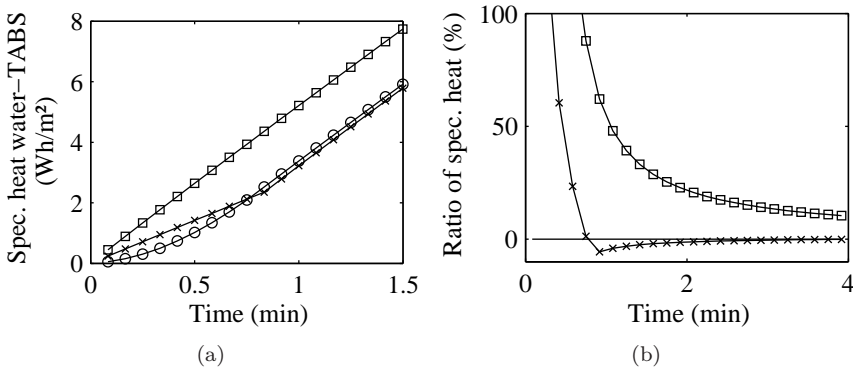


Figure 4.17: (a) Specific heat transferred from the water flow to the CCA, as calculated by the ‘no-propagation’- (\square), the ‘propagation’- (\times) and the ‘finite difference’- (\circ) approach, (b) the ratio q_{noprop}/q_{FD} (\square) and q_{prop}/q_{FD} (\times)

concrete temperature — do not lead to significant errors. After the propagation time, T_{wm} is almost equal for the three approaches, as can be seen in Fig. 4.16(b), showing the small effect of the linear interpolation. The ‘finite difference’-approach (\circ -line in Fig. 4.18(a)) indeed shows that the concrete core temperature T_c is not constant during the propagation time. So the constant T_c which was needed to derive the expression for the Equivalent Supply Temperature, is not valid. However, the cumulated heat transfer q in Fig. 4.17 shows that this error does not counteracts the benefits of taking into account the propagation time using the ‘propagation’-approach (Mean Supply Temperature).

Fig. 4.18(b) shows that the ‘finite difference’-approach leads to slightly higher surface temperatures than calculated by both simplified expressions. Also for T_c , the ‘finite difference’-approach leads to higher temperatures: ‘finite difference’:21.92°C, ‘no-propagation’:21.91°C and ‘propagation’:21.88°C after 10 min. However, the difference is very small, and therefore the impact on the heat transfer is negligible.

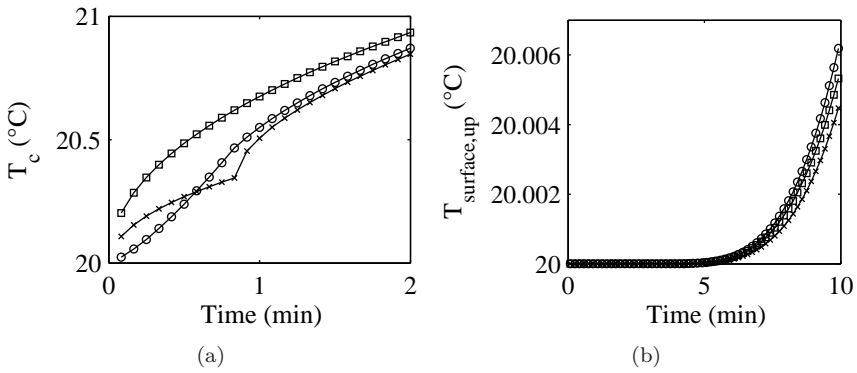


Figure 4.18: (a) Mean concrete core temperature T_c and (b) mean upper surface temperature $T_{s,up}$ for the ‘no-propagation’- (\square), the ‘propagation’- (\times) and the ‘finite difference’- (\circ) approach.

4.5 Analysis of transient heat transfer in CCA

4.5.1 Case 1: Heating up CCA during 8 h

As a first application, in order to demonstrate the analytical solution, the results of CCA being heated for 80 h are shown for an uncovered concrete slab with specifications as presented in Table 4.3. In this case, the temperatures of the zones below and above are kept constant at 20°C. Heat transfer is considered in both directions, upwards and downwards, so into both zones. The energy balance condition Eq. 4.37, as formulated for the EMPA model, is fulfilled, with $\frac{\dot{m}_w c_p R_c}{d_x L t} = 1.03$.

In this case, the CCA are heated during 8 hours with water at 30°C, while in the next case, the pump stops running after 4 hours and the CCA are free running during the last 4 hours. The time is presented by the dimensionless Fourier number, with $Fo = 1 \Leftrightarrow t = 11.2\text{h}$.

The calculation is performed with a time step of 10 min to incorporate the effect of water propagation, while Fig. 4.19 shows the hourly results. The results are presented in 6 figures (a)-(f), as explained in Table 4.4.

From Fig. 4.19 different aspects of the transient heat transfer occurring in the concrete slab can be analysed. The meaning of the different subfigures is:

Table 4.3: Specifications of the CCA used to analyse transient heat transfer (layout see Fig. 4.6)

	Value	Unit
Uncovered CCA		
Thickness d	0.2	m
Tubes spacing d_x	0.15	m
Area A_{gross}	12	m ²
Area A_{net}	10	m ²
Tube length L_t	66.7	m
Flow rate m_w	0.042	kg/s
	150	kg/h
Calculated R_z	0.0564	m ² K/W

Table 4.4: Explanation of the figures showing the transient calculation results.

Fig. nr. showing	x-axis units	y-axis Linetype	Explanation
(a) Temperature	$T(\xi, Fo)$	ξ (—)	The thick dashed line (- -) shows the upper and lower CCA surface Each line represents the temperature distribution of 1 h later. E.g. when heating, $T(\xi, Fo)$ is evolving from left to right.
(b) Spec. heat power	$\dot{q}(\xi, Fo)$	ξ (—)	the sign is determined by the direction of the heat flow; positive in the positive ξ -direction and negative in the negative ξ -direction. E.g. in a heating situation, \dot{q} is positive for the upper part and negative for the lower part. With water flow, the \dot{q} -profile has the largest difference between the centre and the surfaces at small Fo , and evolves to a constant value (see Eq. 4.28) for large values of Fo (after a long time). Without water flow, the \dot{q} -profile has no discontinuity at $\xi = 0.5$.
(c) Spec. cumulated heat	q kWh/m ²	ξ (—)	equal sign convention as for \dot{q} . The q -profile starts from 0 at $Fo = 0$. In the centre ($\xi = 0.5$), q increases more rapidly when the water flow (heating or cooling) is on.

Table 4.5: Explanation of the figures showing the transient calculation results (continuation of 4.4).

Fig. nr. showing	x-axis units	y-axis Linetype	Explanation
(d)	Fo	E_{elec}	For an air-water heat pump with a COP = 3.9, a chiller with an COP = 3.5 and a circulation pump consuming 0.84 W/m ² or 252 W/l/s.
$E_{elec,heatpump/chiller}$	kWh/m ²	(—)	Cumulative electricity use for production: heat pump (in heating mode) or chiller (in cooling mode).
$E_{elec,total}$	kWh/m ²	(—)	Cumulative electricity use for production and circulation pump.
(e)	Fo	\dot{q}	Specific heat power
$\dot{q}_{water-CCA}$	W/m ²	(×)	Sum of heat power to upper and lower slab part
$\dot{q}_{CCA-room}$	W/m ²	(—)	Sum of heat power to the room below and above
(f)	Fo	q	Specific cumulated heat
$q_{water-CCA}$	kWh/m ²	(o)	Sum of heat to upper and lower slab part
$q_{CCA-room}$	kWh/m ²	(—)	Sum of heat to the room below and above

- Fig. 4.19 (a) T starts at 20°C and evolves from left to right,
- Fig. 4.19 (b) \dot{q} evolving towards a constant value,
- Fig. 4.19 (c) q evolving from 0 to an over ξ constantly increasing value.
- Fig. 4.19 (d) Production energy (heating+cooling) is given by the solid line (—), while production+pump consumption is presented by the plus-sign (+).
- Fig. 4.19 (e) Summed upper and lower \dot{q} , $\dot{q}(\xi = 0.5)$ indicated with ×, $\dot{q}(\xi = 0 + \xi = 1)$ indicated with the solid line (—).
- Fig. 4.19 (f) Summed upper and lower cumulated heat q , $q(\xi = 0)$ indicated with o, $q(\xi = 0 + \xi = 1)$ indicated with the solid line (—).

General conclusions that can be drawn for this case are:

1. Initially, the temperature increases more in the middle than at the edges (a), gradually evolving towards the steady state situation given by $C\xi + D$ (see Eq. 4.31).

2. The specific heat power profile (b)-(e) follows this trend with initially a large difference between power from the water and power to the room, while evolving very slow to the steady state heat power $-\lambda_c C/L$ (see Eq. 4.32), which is 65 W/m^2 in this case.
3. The heat power the heat pump has to supply is larger than the steady state power for which the unit would normally be designed. In both cases a maximum of 153 W/m^2 is attained (reached in the first hour of operation, between the first two \times -markers in Fig. 4.19, which is a factor 2.4 higher compared to the steady state design power.
4. The centre of the CCA is loaded with heat prior to heat transfer starting up at the edges (c)-(f). This results in a large amount of heat stored in the slab after 8 h run time: 0.53 kWh/m^2 , as can be seen from the difference between the two curves in Fig. 4.19 (f).
5. The electricity use (solid line (—) in Fig. 4.19 (d)) is directly related to the cumulated heat (Fig. 4.19 (f)) at $\xi = 0.5$, the tube level of the slab. The electricity consumption of the circulation pump is only a minor fraction of the heat pump electricity use.

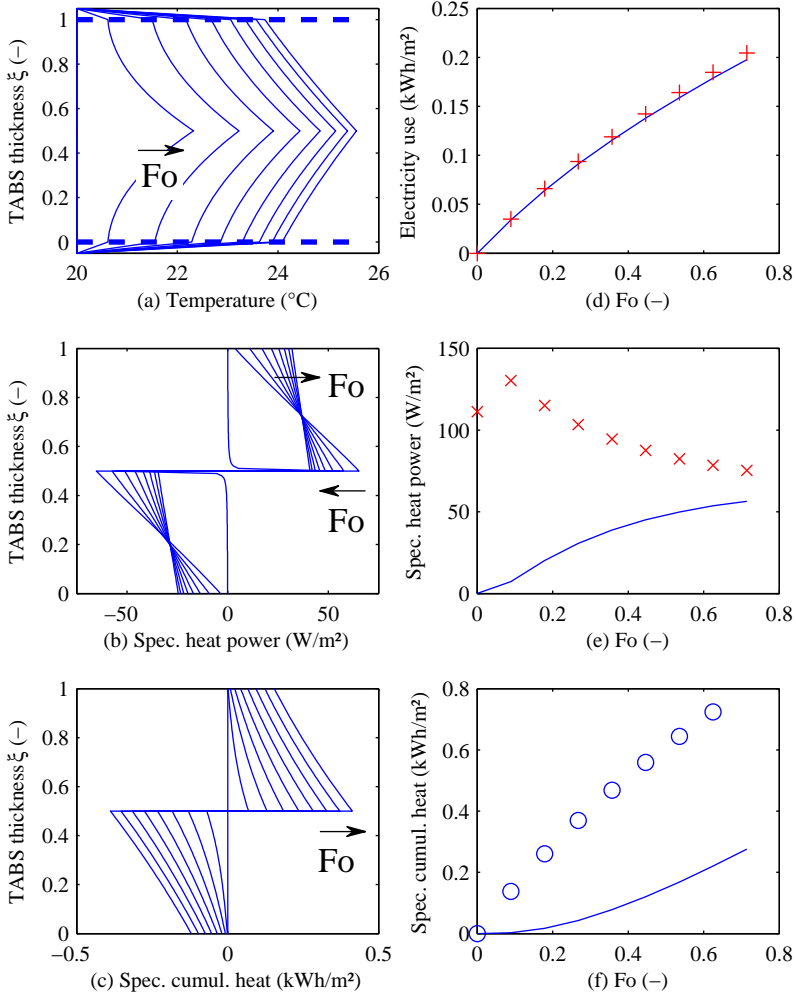


Figure 4.19: Results of the CCA transient heat transfer analysis , case 1: constant water flow

4.5.2 Case 2: Heating up CCA during 4 h

Compared to case 1, the water flow is now switched off during the last 4 hs. Fig. 4.20 shows the following parameters:

- Fig. 4.20 (a) $T(\xi, Fo)$ starts at 20°C and evolves to the right for the first 4 h and back to the left when the slab is cooling down for the next 4 h.
- Fig. 4.20 (b)-(e) show that $\dot{q} = 0$ at the tube level ($\xi = 0.5$) for the last 4 h, while heat transfer remains at the surface due to the heat stored in the slab, which is released gradually.
- Fig. 4.20 (c)-(f) show the same effect where q stops increasing at $\xi = 0.5$.
- Fig. 4.20 (d) shows that the electricity use remains constant when the circulation shuts down.

The first 4 lines in Fig. 4.20 (a) are equal to case 1, but then a cosine-like T -profile arises in the concrete slab [27], when it is cooling down towards the room temperature (next 4 lines). In the last 4 hour, the \dot{q} -distribution in Fig. 4.20 (b) shows that no more power is added to the slab by the water: $\dot{q} = 0$ at $\xi = 0.5$. The q -distribution in Fig. 4.20 (c) shows clearly that for the zero-water flow situation, no extra heat is added to the slab (for $\xi = 0.5$). The heat loaded in the slab during the first 4 h, is gradually released into the room: $q(\xi = 0)$ and $q(\xi = 1)$ keeps increasing after the pump has shut down. This is also visible in Figs. 4.20 (d)-(e)-(f). No more heat is added to the slab after the 4th hour, therefore the electricity use also stops increasing (d). However, heat transfer in the rooms below and above remains, though gradually decreasing (e)-(f).

Again, the centre of the CCA is loaded with heat prior to heat transfer starting up at the edges (c)-(f). Due to the water flow stop after 4 h, the amount of heat stored in the slab after 8 h run time is lower than in case 1: 0.25 kWh/m² in this case (Fig. 4.20 (f)), while this was 0.53 kWh/m² in case 1. However, the difference in heat transfer to the zone is smaller: 0.22 kWh/m² in this case (full line in Fig. 4.20 (f)), while this was 0.28 kWh/m² in case 1. So, it can be concluded that the longer pump run time in case 1 especially increased the amount of heat stored in the slab, and does not have an equal effect on the heat transfer to the zone.

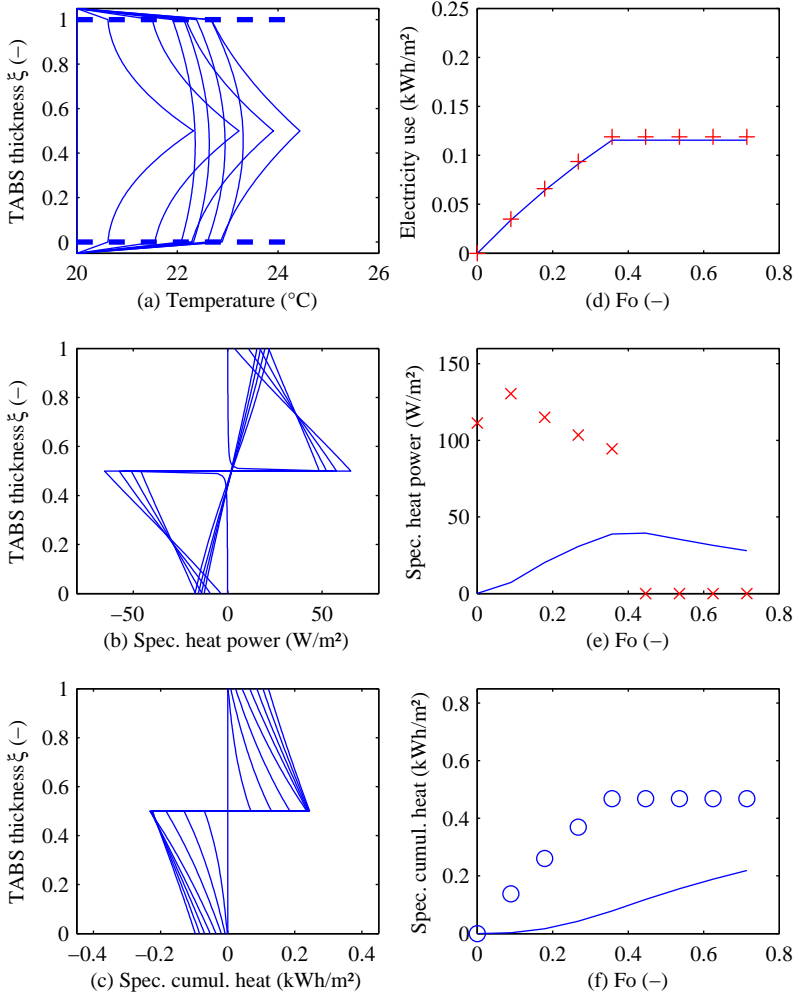


Figure 4.20: Results of the transient heat transfer analysis in CCA, case 2: 4 h on-4 h off water flow.

4.5.3 Case 3: Cooling down CCA

In the case of cooling the general conclusions drawn for the ‘heating up’ case maintain. The results of CCA, starting at 23°C and being cooled for 8 hours with water at 17 are presented in Fig. 4.21. The profiles are mirrored compared to the heating up case (Case 1, Fig. 4.19). Therefore, the conclusions drawn for the heating case, apply also to the cooling case.

In order to shorten the simulation time, the next results are calculated with $n = 1..20$ instead of $n = 1..100$ in Eq. 4.31. This will only effect the initial values: for $Fo = 0$ this approximation results in a fluctuating temperature distribution, which is visible in the fluctuating pattern of the specific heat power at $Fo = 0$ in Fig. 4.21 (b). Since for $Fo > 0$ the first 20 terms of the sum are sufficient, this fluctuation disappears for these results. The solution is calculated with a 10 min time step, but presented with a 1 h time step.

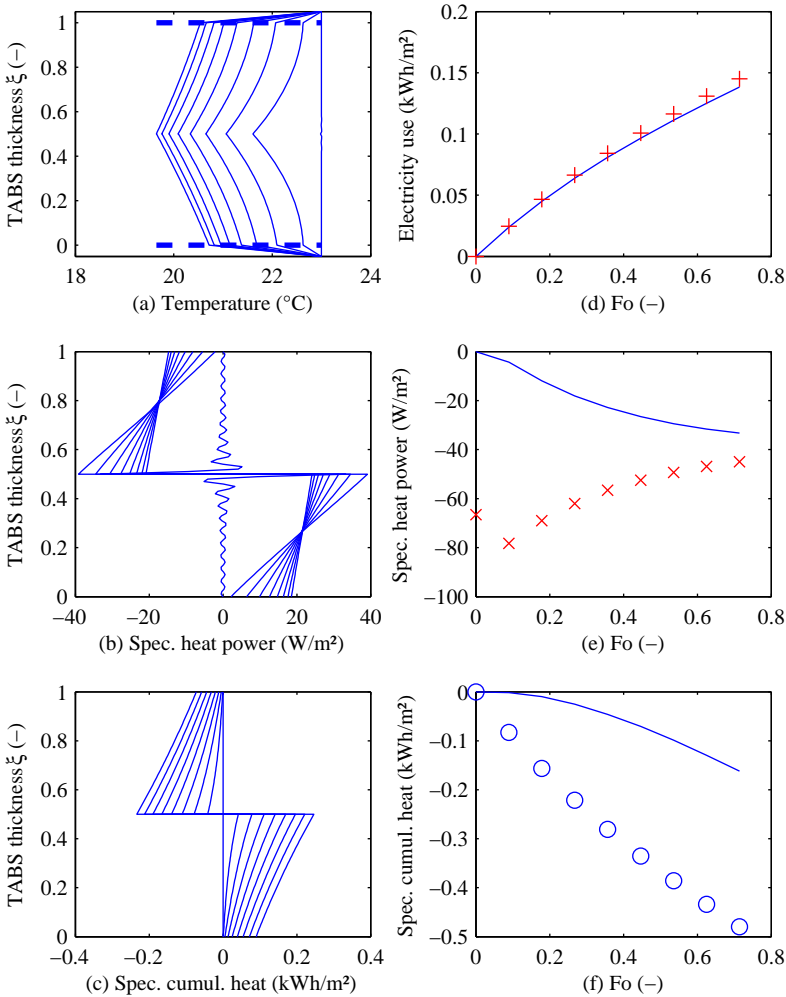


Figure 4.21: Results of the transient heat transfer analysis in CCA, case 3: Cooling at 17°C with 8 h constant water flow. (a) The T -profile starts at 23°C and evolves towards the left. (b)-(c)-(d)-(e)-(f) Mirrored results compared to the heating up case (Fig. 4.19). The data presented are explained in Table 4.4.

4.5.4 Case 4: CCA without water flow

In the case of a free running CCA, the cooling down to eventually room temperature is visualised in Fig. 4.22. The CCA starts initially at a constant temperature of 25°C , while the rooms below and above remain at 20°C throughout the whole period. As in Case 2 (Fig. 4.20) a cosine-like temperature distribution arises in the slab. \dot{q} gradually evolves towards zero. However, after 8 h, the CCA is still heating the rooms with more than 20 W/m^2 . q , in Fig. 4.22(f), will eventually stop increasing, but again here, this is certainly not the case after 8 h.

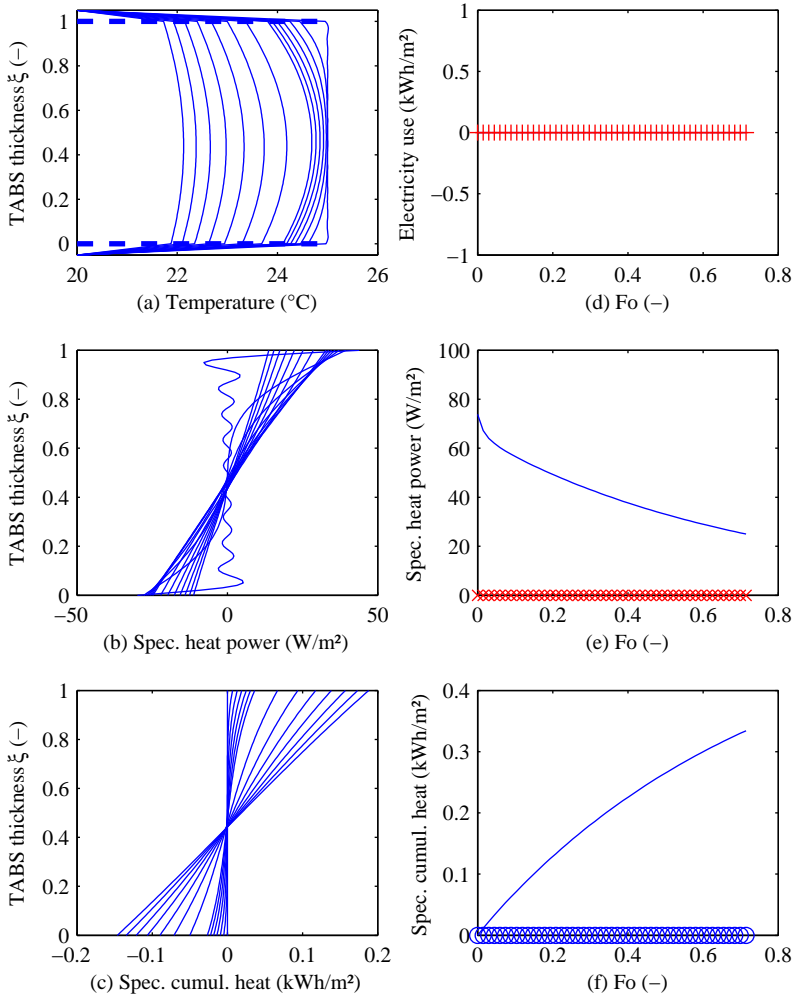


Figure 4.22: Results of the transient heat transfer analysis in CCA, case 4: Cooling down of a CCA slab without water flow (hour 1: 1 line every 10 mins, then 1 line every hour). (a) The T -profile starts at 25°C and evolves to the right. The data presented are explained in Table 4.4.

4.5.5 Pump operation time

Since the resistance to heat transfer associated with heat conduction through the concrete slab is about double as large as the resistance to heat transfer between the supply water and the concrete (see Fig. 3.9), it is possible to save on circulation pump operation time, and therefore save on electricity cost. After all, shutting down the pump for a period allows the heat to diffuse through the concrete. To analyse this effect, 6 different cases are investigated:

1. pump-case 1: 8 h period, sequence of 8 h pump operation
2. pump-case 2: 8 h period, sequence of 4 h pump operation, 4 h free running
3. pump-case 3: 8 h period, sequence of 2 h pump operation, 2 h free running
4. pump-case 4: 8 h period, sequence of 1 h pump operation, 1 h free running
5. pump-case 5: 8 h period, sequence of 30 min pump operation, 30 min free running
6. pump-case 6: 8 h period, sequence of 10 min pump operation, 10 min free running

For all cases, $T_{ws} = 30^{\circ}\text{C}$ and $T_{room} = 20^{\circ}\text{C}$, which means the CCA is heated by the water flow.

Fig. 4.23 shows the following trends for the different pump operation modes. For pump-cases 2 to 6, the pump run time is equal over the 8 h period, and half of the run time of pump-case 1. The heat input from the water to the concrete slab appears to be almost equal for pump-cases 2-5 (Fig. 4.23(a)). Only pump-case 6 has a lower cumulated heat amount, due to the effect of the propagation time: from every 10 min pump operation, 5.3 min are at the lower equivalent water supply temperature (see Sec. 4.4 and Sec. 4.4.7 for the validation of this approach).

However, the cumulated heat output to the rooms below and above differ from case to case (Fig. 4.23(b)). For a longer continuous operation time of the pump (e.g. pump-case 2), the surface temperatures of the CCA reach higher values, resulting in a higher specific power output to the rooms. Numerical values supporting this observation are given in Table 4.6, which presents in the first row the mean specific heat power to the room over the 8 h period for the different pump-operation cases.

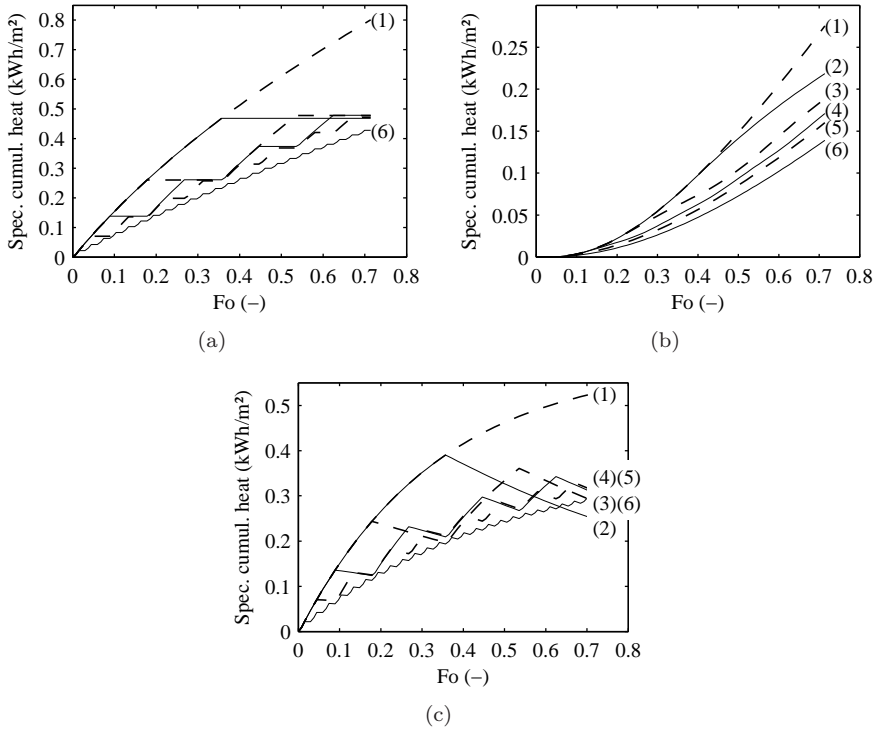


Figure 4.23: The effect of different pump operating time on inputted, stored and transferred heat from CCA to room, with
 (a) q_{input} , specific cumulated heat from water to CCA,
 (b) q_{output} , specific cumulated heat from CCA to both rooms below and above and
 (c) q_{stored} stored heat

Table 4.6: Characteristic values over the 8 h period for cases 1-6

Case	1	2	3	4	5	6
\bar{q}_{output} (W/m ²)	34.4	27.3	23.6	21.4	20.0	17.4
q_{input} (kWh/m ²)	0.80	0.47	0.48	0.48	0.47	0.43
q_{output} (kWh/m ²)	0.28	0.22	0.19	0.17	0.16	0.14
q_{stored} (kWh/m ²)	0.53	0.25	0.29	0.31	0.31	0.29
q_{stored}/q_{input} (%)	66	53	61	64	66	67

Since the CCA have a large thermal capacity, operating the system implies that the CCA are 'loaded' with heat. Table 4.6 shows that operating the CCA with longer pump operation times (as in pump-case 2) also leads to the lowest q_{stored} . Pump-cases 3-6 are comparable, while pump-case 1 has the largest amount of energy stored in the concrete slab (which is mainly due to the larger amount of heat added by the water (see Fig. 4.24(a)). Comparing pump-case 1 and pump-case 2 shows that, although pump-case 1 has 26% more heat output to the room, 71% more heat input was needed to reach this situation. The remainder of the heat is stored in the CCA. To conclude, in pump-case 2 an amount of heat, almost equal to pump-case 3-5, is transferred to the CCA, but more heat is transferred to the room, due to the higher surface temperatures. As a consequence, less heat is stored.

Due to the effect of the propagation time, in pump-case 6, the system has the lowest performance, for heat input, for heat output and for the amount of stored heat.

These observations indicate that, in order to use the CCA as heating or cooling device, the pump operation time should be as continuous as possible for a certain operation time (case 2 has an operation duty load of 50%) in order to reach high surface temperatures. On the other hand, if the CCA are used to store energy, rather than transferring heat to the office zones, it is beneficial to operate the pump intermittently. Because of the propagation time an operation time period of less than 30 min should be avoided.

4.5.6 Different water supply temperature T_{ws}

For other water supply temperatures, whether the CCA are heating or cooling, the conclusions of the previous section remain the same. For a period of 8 h, the pump-case 2 setting uses the heat input in the most efficient way. However, when the CCA have to transfer a certain amount of heat into the room, by varying the water supply temperature and pump operation settings a different result is obtained.

Fig. 4.24 presents the simulation results for a 0.2 m thick slab to reach $q_{req} = \pm 0.1 \text{ kWh/m}^2$ cumulated heat transfer to the room. In the case of heating, the supply temperature is varied between 25, 30 or 40, and in the case of cooling, 8 or 17. The COP and EER of the production unit are temperature dependent (see Fig. 7.3) The vertical axis presents heat pump and

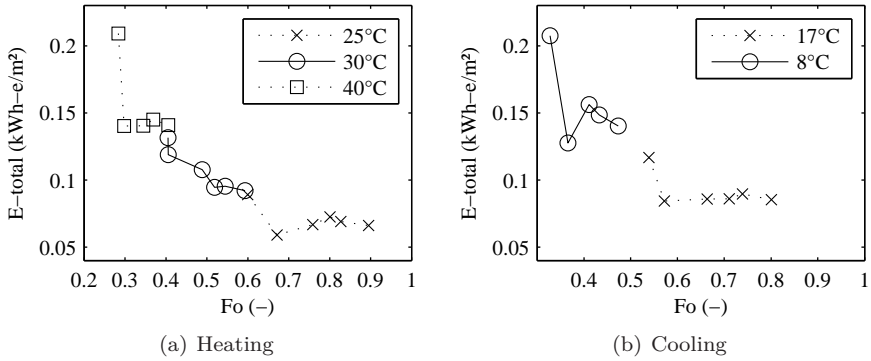


Figure 4.24: Heat pump (a) and chiller, (b) electricity consumption (circulation pump consumption included) for different supply temperatures as a function of the dimensionless time to reach $q_{zone} = \pm 0.1 \text{ kWh/m}^2$ cumulated heat transfer to the zone. Cases 1-6 are represented by the $\square - o - x$ -markers for each temperature, where case 1 is the most left hand marker and case 6 the most right hand marker.

chiller electricity consumption, together with the electricity needed to drive the circulation pump, as a function of the dimensionless time Fo needed to reach q_{req} .

A trade-off is visible between time and amount of electricity needed to reach the required heat output. For $T_{ws} = 40^\circ C$, the required 0.1 kWh/m^2 is already reached within the first 4h period, making the result for case 1 and case 2 identical: the ‘first’ \square -marker in Fig. 4.24(a) at $Fo = 0.28, E = 0.21$ represents the results of case 1 and case 2. Remember from Figs. 4.19 and 4.20 that the difference between case 1 and 2 only starts after 4h. This is equally true for $T_{ws} = 8^\circ C$ in the cooling regime (Fig. 4.24(b)). For these extreme temperatures, case 1 and case 2 both load too much energy into the slab to achieve the goal of $q_{req} = \pm 0.1 \text{ kWh/m}^2$. Only for the more restricted temperatures $25^\circ C$ for heating and $17^\circ C$ for cooling, the case 2 pump settings achieve q_{req} in the shortest time frame and at a comparable energy cost compared to cases 3-6, where case 1 always has the highest energy cost.

In general, since pump-case 2 remains the best solution for all observed cases, it can be concluded that the pump cycle time should be around half of the time to reach q_{req} .

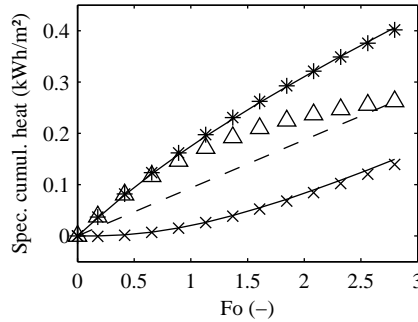


Figure 4.25: Detailed (—) and approximated solution of q_{in} (*), q_{out} (×) and q_{sto} (△) for the upper half of a 0.2 m slab ($T_{ws} = 30^\circ\text{C}$ and $T_2 = 20^\circ\text{C}$). The dashed line is the steady-state solution ‘ $L\rho cC Fo$ ’ (Eq. 4.29) indicating the slope to which both q_{in} and q_{out} evolve.

4.5.7 Simplified $q(\text{Fo})$ expression

The previous conclusion suggests that a simplified expression that determines the time needed to reach q_{req} , would provide essential control information towards start up time and pump cycle time. In Section 4.3.5 (Fig. 4.10), it was demonstrated that calculating the temperature profile with only the first term of the infinite sum, only yields acceptable results for $\text{Fo} > 1$. However, this appears not to be true for the cumulated heat q .

Fig. 4.25 shows the small deviation between the detailed solution in solid line (—) (Eq. 4.33) and the solution where only the first term of the sum is taken into account (markers × and *). The dashed line is the steady-state solution ‘ $L\rho cC Fo$ ’ (Eq. 4.29) indicating the slope to which both q_{in} and q_{out} evolve. The △ presents the stored energy q_{sto} , which is the difference between q_{in} and q_{out} . For small Fo -numbers, there is a difference between the exact and the approximated solution, which however does not result in large absolute errors. Therefore, the q -solution with the first term can be used as an approximation of the cumulated heat. Starting from Eq. 4.33, the cumulated heat at the room side and at the water side can be approximated as presented in Eq. 4.57.

$$q_{room} = q(1, \text{Fo}) = -L\rho c \left[C \text{Fo} + A_1 \beta_1 \left(\cos(\beta_1) - \frac{\beta_1}{\text{Bi}_1} \sin(\beta_1) \right) \frac{1 - e^{-\frac{(-\beta_1^2 \text{Fo})}{\beta_1^2}}}{\beta_1^2} Z_{1,init} \right] \quad (4.57)$$

$$q_{water} = q(0, Fo) = -L\rho c \left[C Fo + A_1 \beta_1 \frac{1 - e^{(-\beta_1^2 Fo)}}{\beta_1^2} Z_{1,init} \right] \quad (4.58)$$

With $K_1 = \frac{A_1}{\beta_1} \left(\cos(\beta_1) - \frac{\beta_1}{Bi_1} \sin(\beta_1) \right) Z_{1,init}$ and $K_2 = \frac{A_1}{\beta_1} Z_{1,init}$ these expressions can be rearranged to Fo, leading to:

$$Fo - \frac{K_1}{C} e^{(-\beta_1^2 Fo)} = -\frac{1}{C} \left(\frac{q_{room}}{L\rho c} + K_1 \right) \quad (4.59)$$

$$Fo - \frac{K_2}{C} e^{(-\beta_1^2 Fo)} = -\frac{1}{C} \left(\frac{q_{water}}{L\rho c} + K_2 \right) \quad (4.60)$$

Furthermore, the heat stored in the slab is found by putting $q_{sto}(Fo) = q(0, Fo) - q(1, Fo)$. The term $C Fo$ is cancelled out, resulting in:

$$q_{sto}(Fo) = -L\rho c (K_2 - K_1) \left(1 - e^{(-\beta_1^2 Fo)} \right) \quad (4.61)$$

Eqs. 4.59 and 4.60 are written in the form $1/e^x = x$, which is the exponential variant of the golden section equation $1/x = x - 1$ [59]. The solution of this exponential variant is the ‘omega constant’ and is found by evaluating the Lambert W function in $1 : W(1) = 0.567$. Mathematica uses this Lambert W function to suggest a solution for Fo for both heat transfers and the heat stored:

$$Fo = \frac{W \left(e^{[\beta_1^2 \frac{1}{C} (\frac{q_{room}}{L\rho c} + K_1)]} \frac{K_1}{C} \beta_1^2 \right) - \beta_1^2 \frac{1}{C} \left(\frac{q_{room}}{L\rho c} + K_1 \right)}{\beta_1^2} \quad (4.62)$$

$$Fo = \frac{W \left(e^{[\beta_1^2 \frac{1}{C} (\frac{q_{water}}{L\rho c} + K_2)]} \frac{K_2}{C} \beta_1^2 \right) - \beta_1^2 \frac{1}{C} \left(\frac{q_{water}}{L\rho c} + K_2 \right)}{\beta_1^2} \quad (4.63)$$

$$Fo = -\frac{1}{\beta_1^2} \ln \left(1 + \frac{q_{sto}}{L\rho c (K_2 - K_1)} \right) \quad (4.64)$$

The above expressions are extremely useful for control purposes. They provide an analytical solution to find the time required to either transfer a certain amount of heat to the room q_{room} (Eq. 4.62) or to put an amount of heat into the slab q_{water} (Eq. 4.63) or to store an amount of heat in the slab q_{sto} (Eq. 4.64). Moreover, this is achieved by taking into account the initial state of the slab (through $Z_{1,init}$), the heat transfer rate at both sides of the slab (through Bi_1 and Bi_2) and the water and room temperatures T_1 and T_2 (through the

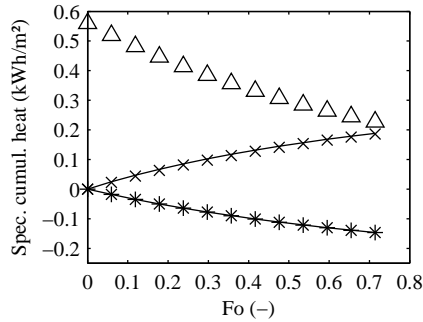


Figure 4.26: Detailed (-) and approximated solution of q_{down} (*), q_{up} (\times) and q_{sto} (\triangle) for a 0.2m slab without water flow with $T_{initial} = 25^{\circ}C$ and $T_{room} = 20^{\circ}C$.

parameter C).

The Fo-expressions are valid for both the case with water flow, where every slab part is treated separately, and for the case without water flow. Fig. 4.26 shows the three different heat flows for a slab without water flow, initially at a temperature of $25^{\circ}C$ and cooling down towards the room temperature of $20^{\circ}C$.

The error caused by taking only the first term of the infinite sum was already addressed in Fig. 4.10 showing the large deviation of the temperature profiles for $Fo < 1$. Fig. 4.27 shows the relative error on the cumulated heat transfer q for both a situation with water flow (a) and a slab cooling down by convection to the rooms below and above (b). The free running case does not seem to cause too much problems, with errors decreasing rapidly in time and below 15% for the full period observed. In the waterflow case however, the error on q_{water} — the dashed line in Fig. 4.27(a) — increases to almost 50% in the beginning. The relative error on q_{room} — the solid line in Fig. 4.27(a) — shows an extremely high value at the start of the water flow, up to $3.10^7\%$, after the first 10 min. However, since q_{room} is very small in the beginning, the relative error is blown up. The absolute error is very small (see Fig. 4.25).

4.5.8 Avoiding overheating or undercooling

In real office applications, the CCA will not be subject to a constant room temperature as in the two previous examples. On the contrary, CCA office

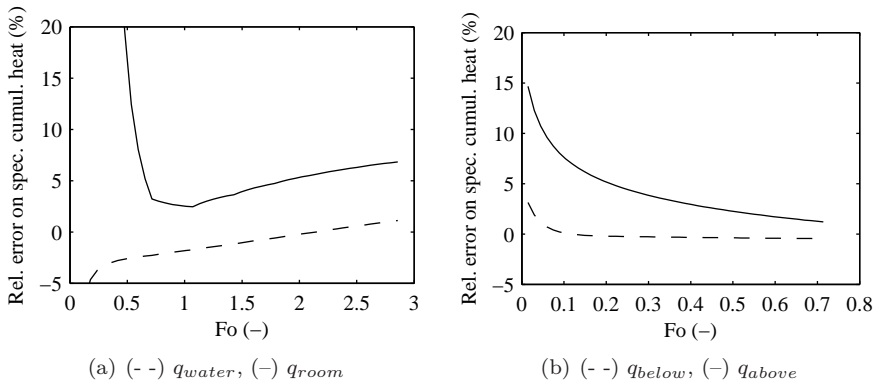


Figure 4.27: Relative error of simplified q -calculation (a) for the upper slab part with water flow and (b) for a slab in free running mode

buildings are known to experience a floating room temperature during the course of the day. The moderate temperatures at which the CCA operate are of high importance in this respect.

In the case of heating, a rise in room temperature will make the room temperature T_2 become equal or larger than the surface temperature of the slab. This means that heat transfer to the room will stop and, when T_2 rises above the slab surface temperature (e.g. by solar or internal gains), the slab will start absorbing heat, and therefore cools the room air.

In the case of cooling, a rise in room temperature will increase the heat transfer rate from the room to the slab due to the increasing temperature difference.

Fig. 4.28 shows that, in case the room temperature rises, the heat transfer to the room is blocked by the rising room temperature (e), and is even reversed when T_2 rises above the surface temperature of the slab.

In order to actively create this damping effect, the surface temperature of the CCA should be limited to a value within the thermal comfort band. The steady state surface temperature is given by the expression $u(1, \infty) = C + D$ (Eq. 4.17). In order to limit the surface temperature to a chosen value T_{lim} , this can be rearranged to T_1 :

$$T_{1,lim} = Bi_2 \left(T_{lim} \left(\frac{1}{Bi_1} + \frac{1}{Bi_2} + 1 \right) - T_2 \left(1 + \frac{1}{Bi_1} \right) \right) \tag{4.65}$$

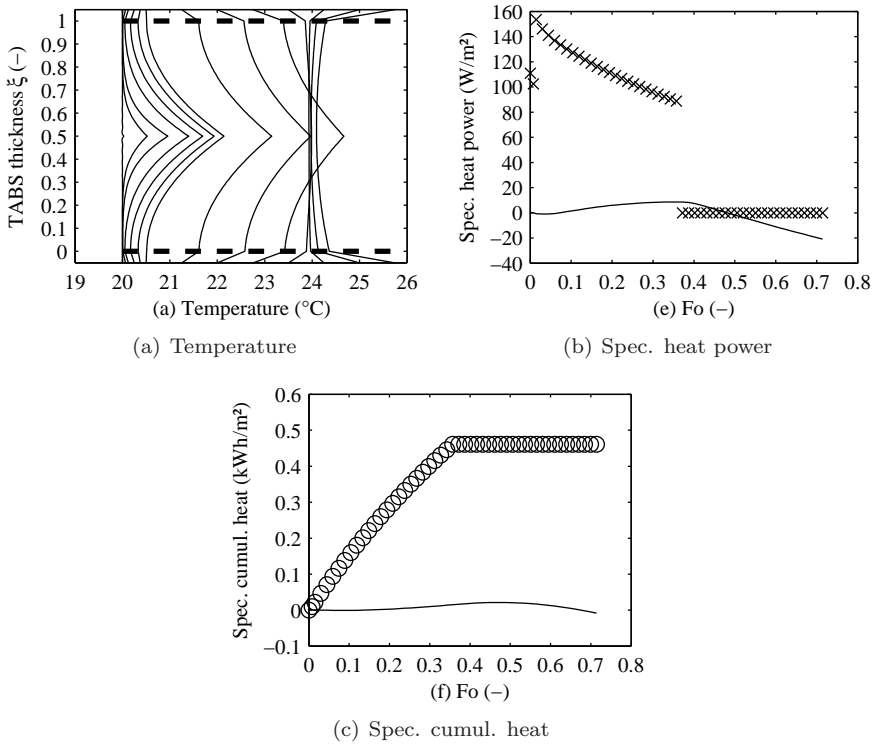


Figure 4.28: Self regulating effect of a 0.2 m slab, $T_{ws} = 30$ and T_2 increasing from 20 to 26 (hour 1: 1 line every 10 min, then 1 line every hour). The data presented are explained in Table 4.4.

Fig. 4.29 shows the tolerated water supply temperatures $T_1 = T_{ws}$ as a function of the room temperature in order to limit the surface temperature to 24°C in the case of heating (a) and to 20°C in the case of cooling (b).

4.5.9 CCA controlled by room temperature feedback

As observed in the case study of Ch. 2, controlling the CCA by a feedback on the room temperature, holds the risk of a switching CCA behaviour: in the morning heating is needed, while due to the temperature rise caused by internal and solar gains, in the afternoon the cooling is switched on. In Fig. 4.30 a situation is presented in which the room is initially at 18 in the morning.

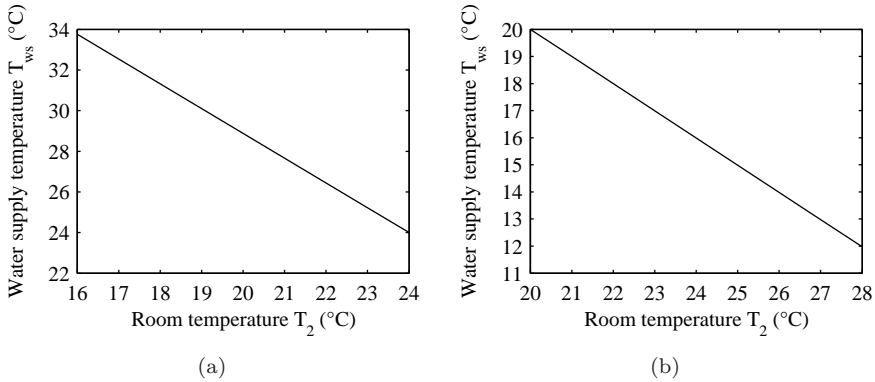


Figure 4.29: Tolerated water supply temperatures T_{ws} as a function of the room temperature, in order to limit the slab surface temperature to (a) 24°C in heating regime and (b) 20°C in cooling regime

However, due to heat gains, the temperature increases in the room with 1/h. Heating is on until the room reaches 20. Cooling starts at 24°C.

Fig. 4.30 (f) shows the heat put into and extracted from the slab by the water and the heat exchanged between the slab and the room (solid line). While a large amount of heat is exchanged between the water and the slab, this only has a minor effect on the heat exchange with the room. Only for the 2 h cooling period, the cooling is able to keep the surface temperature constant instead of having it increased by the increasing room temperature. Apparently, the CCA is not heating the room, although heating is on during the first 2 h, as is clearly visible in 4.30(f), by the flat horizontal solid line for low Fo-values.

Fig. 4.31 presents the cumulated heat q for two cases. Case (a) is identical to the situation presented in Fig. 4.30. With these settings, the first 2 h of heating injects 0.31 kWh/m² in the slab without causing a noticeable heat transfer into the room (0 kWh/m²). During the next 4 h without water flow, the room temperature increases above the CCA surface temperature: the CCA start cooling due to the self-regulating effect and extract 0.05 kWh/m² from the room. q_{water} remains at 0.31 kWh/m². In the next period cooling starts up: the slab extracts another 0.10 kWh/m² (0.15-0.05) from the room. To obtain this, the water has extracted 0.17 kWh/m² (0.14-0.31) from the slab.

In case (b), the heating is switched off, and only the cooling period is identical to the previous situation: cooling starts at hour 6. Before the cooling is switched

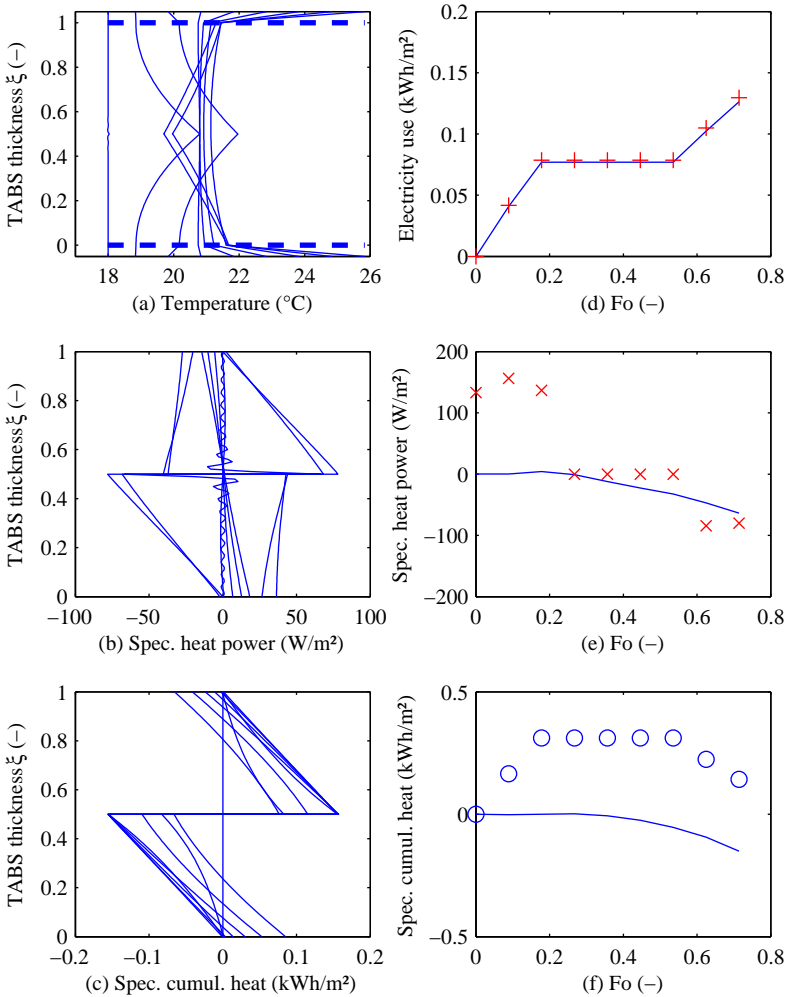


Figure 4.30: CCA with room temperature feedback. Heating starts at $T_1 = 30^{\circ}C$ until the zone temperature $T_2 = 20^{\circ}C$. Assumed zone gains and stored slab energy keep T_2 increasing. Cooling at $T_1 = 15^{\circ}C$ starts as soon as the zone temperature reaches $T_2 = 24^{\circ}C$. The initial slab condition is $T_2 = 18^{\circ}C$. The data presented are explained in Table 4.4.

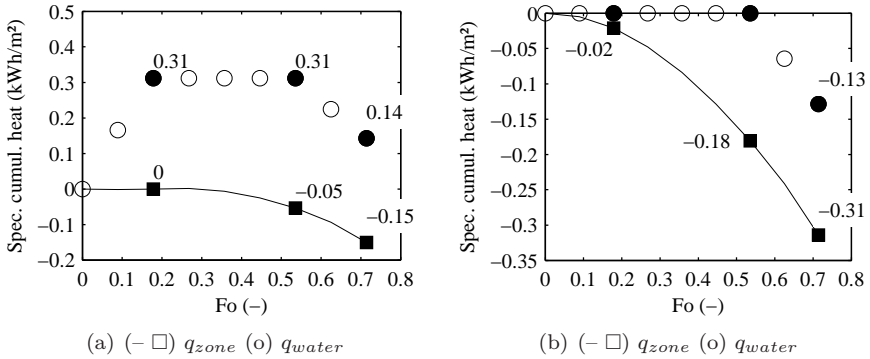


Figure 4.31: Heat transfer from CCA to zone (- □) and from water to CCA (o) for CCA subjected to an increasing room temperature: (a) 2 h heating - 4 h free - 2 h cooling and (b) 6 h free - 2 h cooling. The black markers show the hour 2, hour 4 and hour 6 moments

on, the CCA already extracts 0.18 kWh/m² from the room by the self-regulating effect. With the cooling on, another 0.13 kWh/m² is extracted from the room, which is equal to the heat extracted by the water flow. The actively produced cold is therefore perfectly used in this case and the self-regulating effect is maximised.

For case (a), in total 0.13 kWh/m² electric energy was used to extract 0.15 kWh/m² of heat from the room (see Fig. 4.30(d)). In case (b) however, only 0.04 kWh/m² electric energy was used to extract in total 0.31 kWh/m² of heat from the room. This example clearly illustrates the drawback of applying a conventional, room temperature feedback control to CCA. It can be concluded that there is a strong need for a dedicated control strategy for CCA.

4.5.10 Installed production power

Designing the production power to be installed by using the nominal steady state power \dot{q}_{SS} of the CCA (see Sec. 3.3) will result in a too low installed power. In Figs. 4.19-4.21(e), the difference between the heat power by the water (marked with ×) and the steady state power (for $Fo \Rightarrow \infty$) is clearly visible. Since CCA are constantly operating in a transient regime, the temperature difference $T_{ws} - T_c$, which is the driving factor of the water-to-CCA heat transfer, will often be higher than the steady state value. Together with the

thermal resistance R_c from water to concrete core, this temperature difference determines the desired heat power \dot{q}_{des} of the production units. Suppose the concrete slab is initially at room conditions: $T_{c,initial} = T_2$. With the steady state core temperature $T_{c,ss} = D$ (derived from Eq. 4.31 with $\xi = 0$ and $Fo = 0$ and D is given by Eq. 4.25), the required installed production power is derived as follows:

$$\begin{aligned} \frac{\dot{q}_{des}}{\dot{q}_{ss}} &= \frac{(T_{ws} - T_{c,initial})/R_c}{(T_{ws} - T_{c,ss})/R_c} \\ &= \frac{T_1 - T_2}{T_1 - \left[\frac{T_2 + Bi_1 (1/Bi_2 + 1) T_1}{1 + Bi_1 (1/Bi_2 + 1)} \right]} \\ &= 1 + Bi_1 \left(\frac{1}{Bi_2} + 1 \right) \end{aligned} \quad (4.66)$$

For the different cases and temperature levels as presented in the previous sections, using average Bi-numbers, this ratio is approximately 2.6-2.7. This means that, for an intermittently operated CCA-system, in order to guarantee the temperature levels required by the controller, the installed power should be almost 3 times higher than the value obtained by the steady state calculations.

4.6 Guidelines for the controller

Analysis of the transient behaviour of CCA with different pump operation times and temperature levels, delivers the required operation time which can be used to determine the settings of the CCA controller. Whether the objective is to transfer a certain amount of thermal energy to the room, or to store an amount of thermal energy in the slab, the value of Fo obtained from Eqs. 4.62-4.64 is an indication for the start up time of the system.

From the indicative results of Sec. 4.5.6, where different switching behaviour of the circulation pump was compared, a rule of thumb can be derived. If heat transfer to the room is required, the circulation pump should run approximately for the first half of the period Fo obtained from Eqs. 4.62-4.64, in order not to overload the system.

The water supply temperature T_{ws} should be chosen according to Eq. 4.65

in order to not overheat or undercool the room in case of a bad heat load prediction.

Of course, the issue of installed production power (Eq. 4.66) should be addressed in combination with the controller design.

4.7 Conclusions

An analytical solution is presented to calculate the transient heat transfer as a function of location in the slab x and of time t . This results in an (x, t) -expression for temperature, heat power and cumulated heat. The propagation time of the water flow through the tubes is incorporated in this formulation. The expressions have been used to analyse the transient behaviour of CCA in a heating, cooling or free running situation:

1. The operation time required to reach a certain heat/cold output or stored thermal energy can be determined analytically, taking into account initial conditions, heat transfer rates and temperature levels.
2. With the operation time known, the start time of the system is known.
3. In order not to overheat or undercool the slab, it is beneficial to have the circulation pump running intermittently, with periods not exceeding half of the required operation time.
4. Intermittently operating CCA always requires a thermal power of the production unit which is higher than the steady state power for which units are conventionally designed. A whole building solution might be to operate different zones consecutively, since the circulation pump for 1 zone can run intermittently. Therefore, the operation of different zones can be alternated, and the thermal power to be installed may be smaller.
5. Operating CCA results in a large amount of thermal energy being stored in the concrete slab: examples given in this chapter show that more than 50% of the thermal energy input is not used within the time frame assumed.
6. In order to avoid overheating or undercooling, the CCA surface temperature must not be too high or too low. The heat transfer rates (and

the corresponding Bi-numbers) determine an indicative maximum or minimum water supply temperature.

A simplified expression can be derived from the detailed analytical expression relating time with the cumulated heat $q_{CCA \rightarrow room}$, $q_{water \rightarrow CCA}$ and q_{stored} . The simplified expression can be used to determine the time that is required to obtain a certain amount of heat transfer, taking into account heat transfer parameters and the initial condition of the slab, whether the objective is heat transfer from CCA to room, from water to CCA or to store thermal energy in the CCA. The simplified expression is valid both for heating and cooling. This expression can be used to determine start up times of CCA, which is an extremely important control parameters in a CCA installation.

Chapter 5

Frequency analysis of CCA and zone disturbances

5.1 Introduction

While in the previous two chapters the CCA-element was analysed as such, this chapter makes the step towards an integrated approach of CCA and building. The case study in Ch. 2 illustrates that CCA hold the promise of obtaining an energy efficient heating and cooling system for an office building. However, in contrast to conventional, fast reacting systems, advanced control algorithms are required to take into account the large time constant of CCA in relation to the different time constants of the building. Therefore, these time constants of CCA and building are important parameters, which are analysed in this chapter using a frequency domain approach.

Heat exchange between the CCA and the building zone is determined by the overall heat transfer coefficient h_{c+r} , including both natural convection and radiation contributions, and the temperature difference ΔT between CCA surface and air. Since $h_{c+r}\Delta T$ is small compared to load peaks in the building zone, these peaks will result in a rise of the zone air temperature, before they are absorbed by the CCA. The CCA surface temperature can be controlled by changing the water temperature in the tubes. However, the large thermal capacity which is present between the office zone and the water flow, hampers

a fast communication between them. Analysing the CCA frequency response reveals the large thermal energy storage capacity of CCA and provides an indication for the required model order of a simplified CCA model, suitable for integration in a building controller.

On the other hand, the frequency response analysis reveals the range of dominant frequencies of the different disturbances which are influencing thermal comfort of a building: ambient temperature T_{amb} , solar radiation \dot{q}_{sol} and internal gains \dot{q}_{int} . This range is then compared to the frequency response of a CCA floor.

5.2 Methodology

The office zone thermal comfort is subjected to three disturbances, which are the outdoor temperature T_{amb} , the solar radiation \dot{q}_{sol} and the internal gains \dot{q}_{int} , as shown in Fig. 5.1. The controlled variable is the zone temperature T_z and the control variable is the CCA water supply temperature T_{ws} . After all, the results of the CCA steady state analysis in Ch. 3 show that controlling the water supply temperature T_{ws} is preferred over the water flow rate. Therefore, this section will focus on T_{ws} as input to the CCA. Ventilation is not considered at this stage, so T_{vs} is not taken into account as control variable.

The zone temperature is affected when the disturbances set in faster than the thermal power of the CCA can be changed by changing T_{ws} . In the frequency domain, this means that the disturbances have a higher bandwidth than the CCA. An analogue approach has been used by Weber et al. [145] to couple CCA system behaviour to measurement data of a case study.

In Sec. 5.3, the Power Density Spectrum is used to determine the dominant frequencies of the disturbances T_{amb} , \dot{q}_{sol} and \dot{q}_{int} . Next, in Sec. 5.4, these are compared with the frequency response of CCA, obtained by solving Fourier's heat conduction equation in the frequency domain.

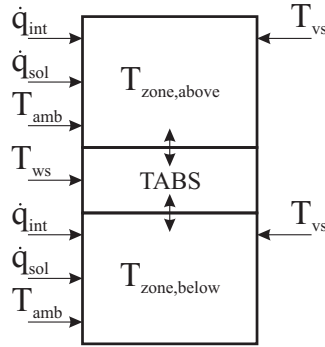


Figure 5.1: Relation between inputs and outputs in the CCA-office zone.

5.3 Frequency response analysis of the zone disturbances

In order to make a comparison with the CCA time constant, the dominant frequencies related to the three disturbances to the building zone are identified using an analysis of the Power Density Spectrum (PDS), which is introduced in Sec. 5.3.2. Both Weber et al. [145] and Keller [75] propose a similar approach to link the building characteristics to the input signal characteristics, but do not use the PDS approach.

The results from the PDS analysis in Secs. 5.3.3 and 5.3.4 are presented as a function of the time period (in unit *hour*), as well as the frequency response results of the CCA. The relation between the time period θ and the frequency $f = 1/day$ is presented in Table 5.1.

Table 5.1: Conversion from frequency (1/day) to time period (hour)

Frequency (1/day)	0	1	2	3	4	5	6	7	8	9	10	11	12
Time period (hour)	∞	24.0	12.0	8.0	6.0	4.8	4.0	3.4	3.0	2.7	2.4	2.2	2.0

5.3.1 T_{amb} , \dot{q}_{sol} and \dot{q}_{int} data set

For the weather data analysis (T_{amb} and \dot{q}_{sol}) the typical meteorological file for Ukkel, Belgium, as provided by TRNSYS [122], is used. The time step of the data file is 1 h and the length of the data file is 8760 h which immediately

determines the frequency resolution and the lowest and the highest detectable frequency.

The frequency resolution is:

$$f_{resol} = \frac{f_s}{N} = \frac{1}{\theta_s N} \approx \frac{1}{\theta_m} = 3.2 \times 10^{-8} \text{ (Hz)} \quad (5.1)$$

$$f_{NYQ} = \frac{1}{2\theta_s} = 1.4 \times 10^{-4} \text{ (Hz)} \quad (5.2)$$

with:

- $f_s = 2.8 \times 10^{-4}$ Hz: sample frequency
- $\theta_s = 1/f_s = 3600$ s: sample period
- $N = 8760$: number of points
- $\theta_m = 3.15 \times 10^7$ s: measurement period

The lowest detectable frequency is limited by the measurement period θ , which corresponds to the highest detectable period of 8760 h, while the highest detectable frequency is determined by the Nyquist frequency (Eq. 5.2), which corresponds to a lowest detectable period of $2\theta_s = 2$ h.

The internal gains \dot{q}_{int} are derived from the stochastic user behaviour model as defined by Parys et al. [101], from which a data set of 8760 samples is constructed.

5.3.2 Power spectral density

Since weather phenomena such as outdoor temperature and solar radiation are partly characterized by random fluctuations, it is better to adopt a statistical viewpoint in analysing the spectral characteristics. As stated by Proakis and Manolakis [106][Ch.12]: ‘In particular, the autocorrelation function of a random process is the appropriate statistical average to be used for characterizing random signals in the time domain, and the Fourier transform of the autocorrelation function, which yields the power density spectrum, provides the transformation from the time domain to the frequency domain.’

To analyse the signal’s dominant frequencies, the power spectral density (PSD) is calculated. The PSD tells how the average power of the signal is distributed as a function of frequency. The PSD is the average Fourier transform squared, taken over a long time interval [106]:

$$P_{xx}(f) = \frac{1}{N} \left| \sum_{n=0}^{N-1} x(n)e^{-j2\pi fn} \right|^2 = \frac{1}{N} |X(f)|^2 \tag{5.3}$$

where $X(f)$ is the Fourier transform of the sample sequence $x(n)$. This form of the power density spectrum estimate is called the *periodogram*. Proakis and Manolakis [106] showed that the mean of the estimated power density spectrum is a smoothed version of the true spectrum and suffers from spectral leakage problems, due to the finite number of data points. However, the limit for $N \rightarrow \infty$ of the variance of P_{xx} does not converge to the true power density spectrum, so it is not a consistent estimate.

Nonparametric methods for power spectrum estimation try to obtain a consistent estimate for the power density spectrum through averaging and smoothing operations performed on the periodogram or the autocorrelation. These operations aim to reduce frequency resolution, while decreasing the variance of the estimate (should be zero to provide a fully consistent estimate of the spectrum). Nonparametric methods make no assumption on how the data are collected, which means that they are not based on a model of how the data were generated. The Barlett method and the Welch method are two nonparametric methods.

The Barlett method divides the N points sequence into K non-overlapping segments with length $M = N/K$. Instead of a spectral width of N , a spectral width of $M = N/K$ is obtained, or the frequency resolution is reduced by a factor K (larger steps between analysed frequencies). On the other hand, the variance is reduced by the same factor K , giving a more consistent estimate of the power density spectrum.

The Welch method makes two modifications to the Barlett method: (1) data segments can overlap and (2) the segments are windowed prior to computing the periodogram to avoid spectral bias due to sharp truncation of the data set. These modifications result in a further leakage reduction, and a sharper determination of the power density peaks. The Matlab-function *pwelch* is based on this approach and is used hereafter to compute the PDS of the different data sets. In the *pwelch*-function, the data segments are windowed using a

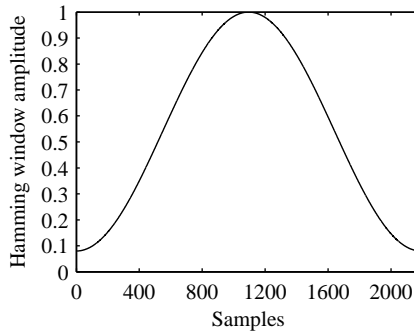


Figure 5.2: Hamming window for a sample vector of length 8760/4.

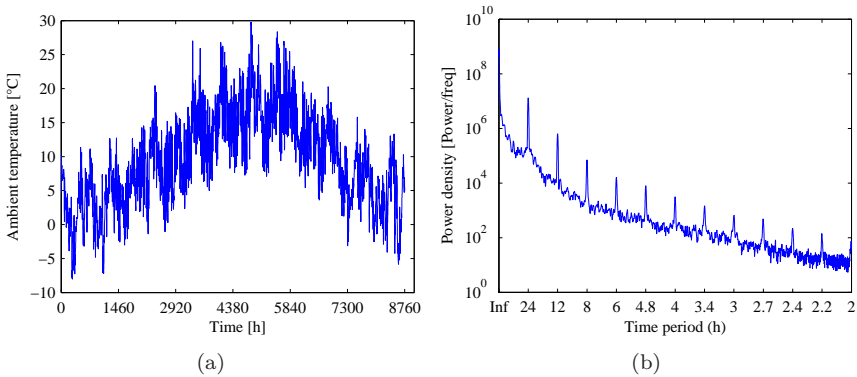


Figure 5.3: (a) Ambient temperature profile of Ukkel (Belgium) and (b) the Power Density Spectrum.

Hamming-window (see Fig. 5.2).

The PDS of the different data sets of T_{amb} , \dot{q}_{sol} and \dot{q}_{int} is estimated using Matlab's *pwelch*-function, where the 8760 samples of the data sets are divided into 8 segments, which overlap for 50%. This means that the data sets are divided in $K = 8$ segments of length $M = 8760/8 \times (1 + 2 \times 0.5)$ with overlap = 0.5. The corresponding Hamming window is shown in Fig. 5.2.

5.3.3 Ambient temperature T_{amb}

The first data set for which the PDS is calculated is the ambient temperature T_{amb} of Ukkel, as shown in Fig. 5.3(a). Analysing the PDS provides the dominant frequencies as shown in Fig. 5.3(b). The average ambient temperature is 9.73°C. Peaks in the average power of the ambient temperature clearly occur at distinct time periods $24\text{ h}/n$, with $n = 1..11$. The first peak, which is not clearly visible on Fig. 5.3(b), occurs at a time period of 1 year, which is the base time period of the T_{amb} -signal. The mean of the signal's amplitude at this time period equals 9.73°C. Longer time periods can not be detected because of the limited samples in the data set. However, those longer time periods are not relevant while analysing the dynamic behaviour of a building.

Although the time period peaks occur at $24\text{ h}/n$, with $n = 1..11$, the logarithmic scale of the y-axis in Fig. 5.3(b) implies that the peak at $\theta = 24\text{ h}/1$, the daily variation of the ambient temperature, is dominant with respect to the others, as expected.

5.3.4 Solar radiation \dot{q}_{sol} on a South oriented vertical plane

Without the influence of atmospheric phenomena, such as clouds, mist or turbid air, solar radiation is no more than a cut-off cosine curve [75]. The height of the cut-off is determined by the geographical location and the time of the year. In reality, solar radiation is evidently highly influenced by these atmospheric conditions. Particularly in unstable weather conditions, cloudiness will cause higher frequencies to appear in the frequency spectrum of solar radiation.

Fig. 5.4 shows that for solar radiation on a South oriented vertical plane, the average power is clearly concentrated in three peaks at $\theta = 24\text{ h}/1$, $\theta = 24\text{ h}/2$ and $\theta = 24\text{ h}/3$. Lower time periods do not show distinct peaks anymore. Analysing meteo-data of other climate types than Ukkel showed identical results. Therefore, from this simple analysis, it is not possible to clearly identify more unstable from more stable climate types.

The dominant time period again equals $\theta = 24\text{ h}/1$, but the PDS at higher frequencies does not drop to low values, as was the case for the PDS of T_{amb} . This means that \dot{q}_{sol} contains a considerable amount of short term variations.

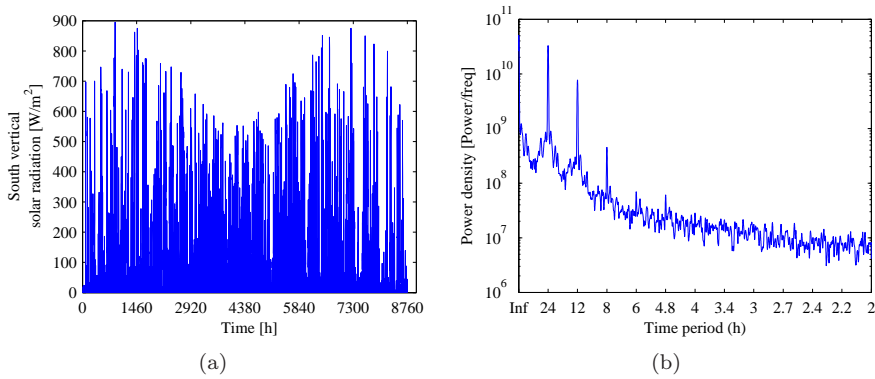


Figure 5.4: (a) Solar radiation on a South facing vertical plane and (b) its Power Density Spectrum for Ukkel (Belgium)

Internal gains \dot{q}_{int}

Internal gains are caused by heat emitted by people working in the zone, by appliances such as computers, printers or other office equipment and by lighting in the zone. Stochastic models, such as presented by Parys et al. [101], try to incorporate the occupant behaviour in order to obtain a real occupancy profile instead of the typical fixed-scheduled profiles used in building simulation models. One week of these stochastic internal gains, comprising gain from people, lighting and appliances, is shown in Fig. 5.5(a). The PDS of such a stochastic profile shows a distribution of peaks, yet concentrated around the time periods of $24\text{ h}/n$.

Two power peaks occur at a time period higher than $\theta = 24\text{ h}/1$ (more to the left of the $24\text{ h}/1$ -peak on Fig. 5.5(b)), which was not the case for the PDS of T_{amb} and \dot{q}_{sol} . They correspond to signals with a time period of 7 days (168h) and 3.5 days (84 h). This is evidently due to the weekly pattern of the office occupation.

As with \dot{q}_{sol} , also this PDS has a rather flat course which shows that \dot{q}_{int} contains a considerable amount of short term variations. Moreover, the peaks at $24\text{ h}/2$, $24\text{ h}/3$ and $24\text{ h}/4$ are almost equal in magnitude.

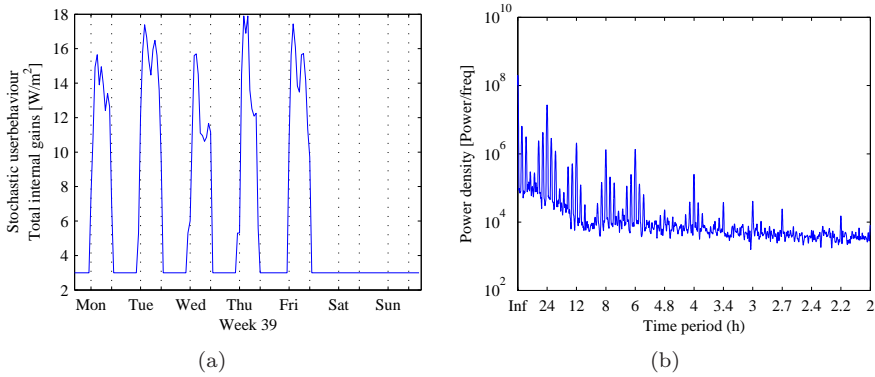


Figure 5.5: (a) Stochastic occupant internal gains in an office environment and (b) its Power Density Spectrum

5.3.5 Conclusion from the PDS of the zone disturbances

From the results presented above, conclusions can be drawn regarding the frequency range which the building controller has to take into account. The base frequency in the signals, corresponding to a time period of 1 year, is typically tackled by a heating/cooling curve controller, in which the water supply temperature to the CCA is determined as a function of the static heat transfer characteristics of CCA and building, and as a function of the ‘running mean’ ambient temperature. This concept is presented in detail in Ch. 6.2.

The largest time period associated with inputs to the office building is 168 h (1 week). Due to the Nyquist-frequency, Time periods lower than 2 h can not be detected. However, with the pump operation control, which is often proposed in the literature (see Ch. 8), the CCA water flow can be controlled within time intervals down to 30 min. The pump runtime example (Sec. 4.5.5 of Ch. 4 showed that operating CCA on a 30 min basis is beneficial for storing thermal energy. Therefore, the frequency response analysis of the CCA floor should focus on time periods in the range between 30 min and 168 h. This is the range in which the CCA have to operate.

5.4 Frequency response analysis of CCA

The frequency range of the disturbances can now be compared with the frequency response of CCA. As shown in Fig. 5.1, T_{amb} , \dot{q}_{sol} and \dot{q}_{int} disturb the zone temperature T_z . The water flow in the CCA, which should be controlled in such a way, that heat can be exchanged between the zone air and the concrete slab to counter the effect of the disturbances on T_z .

The CCA heat exchange \dot{q}_{CCA} between zone and concrete slab is determined by the overall heat transfer coefficient h_{c+r} , including both natural convection and radiation contributions, and the temperature difference ΔT between CCA surface and the zone air together with the temperature of the surrounding surfaces. \dot{q}_{CCA} changes in two ways: (1) by varying conditions of the water flow, which adapts the CCA surface temperature and (2) by varying conditions of the zone.

The convective and radiative heat transfer are lumped into 1 global heat transfer coefficient h_{c+r} (see Sec. 1.4.3). By doing so, the indoor air temperature T_{ia} and the temperature of the surrounding surfaces, are also lumped into the zone temperature T_z (Ch. 1), which is used here. Therefore, the zone temperature T_z above and below the CCA are the 1st and 2nd input to the CCA. On the other hand, the water supply temperature T_{ws} is the 3rd input to the CCA. The output is the heat exchanged by the CCA, either to the water or to the zone below or above the CCA. The frequency dependency of the transfer function relating CCA input and output is to be compared with the frequency range of the disturbances T_{amb} , \dot{q}_{sol} and \dot{q}_{int} . A lumped capacity model of the CCA consisting of thermal resistances R and thermal capacitances C , is used to define these transfer functions.

5.4.1 Transfer functions Admittance and Transmittance

In this section, the thermal behaviour of CCA is characterised using the admittance Ad_m and the transmittance Tr_{mn} , which are transfer functions

relating the heat flow output q_n to a temperature input T_m :

$$\text{Ad}_m = \frac{\tilde{q}_n}{\tilde{T}_m} \quad (n = m) \tag{5.4}$$

$$\text{Tr}_{mn} = \frac{\tilde{q}_n}{\tilde{T}_m} \quad (n \neq m) \tag{5.5}$$

with \tilde{q} the sinusoidal boundary heat flux (W/m²) and \tilde{T} the oscillating boundary temperature (K). A sinusoidal input (\tilde{T}_m) results in a sinusoidal output (\tilde{q}_n) with the same frequency but with different amplitude and phase. A symbol with a ‘~’ refers to its sinusoidal course.

Using the concept of Admittance and Transmittance, a 3 × 3 transfer function matrix is constructed based on the EMPA CCA-model (see Sec. 1.7.1). The transfer function matrix relates a variation in water supply temperature T_{ws} or in room temperatures $T_{z,above}$ or $T_{z,below}$ to the heat flows from water to concrete and from concrete to the zone below and to the zone above. In order to have a shortened notation, in this section, $T_{z,above}$, $T_{z,below}$ and T_{ws} are presented as respectively T_1 , T_2 and T_3 , as shown in Fig.5.6. The transfer function matrix is given by:

$$\begin{bmatrix} \tilde{q}_1 \\ \tilde{q}_2 \\ \tilde{q}_3 \end{bmatrix} = \begin{bmatrix} \text{Ad}_1 & \text{Tr}_{1-2} & \text{Tr}_{1-3} \\ \text{Tr}_{2-1} & \text{Ad}_2 & \text{Tr}_{2-3} \\ \text{Tr}_{3-1} & \text{Tr}_{3-2} & \text{Ad}_3 \end{bmatrix} \begin{bmatrix} \tilde{T}_1 \\ \tilde{T}_2 \\ \tilde{T}_3 \end{bmatrix} \tag{5.6}$$

5.4.2 19th order CCA model

A CCA-slab is usually modelled as a star-RC-network (see Sec. 1.7.1). Weber and Johannesson [144] describe an analysis of a 11th order star RC-network for CCA, which has been validated by Weber et al. [145] against FEM-results. Admittance at the water tube in the CCA yields very good results down to periods of 40 min. Transmittance from the water tube to the floor shows a deviation of 4% in steady state and a deviation of more than 10% at periods lower than 3.5 h [145]. The amplitude of the transmittance is low for these small periods, indicating the uselessness of controlling CCA at high frequency. Using the star-network model also in this work to simulate CCA, these reported deviations should be taken into account when interpreting the response of the CCA to inputs with frequencies in that range.

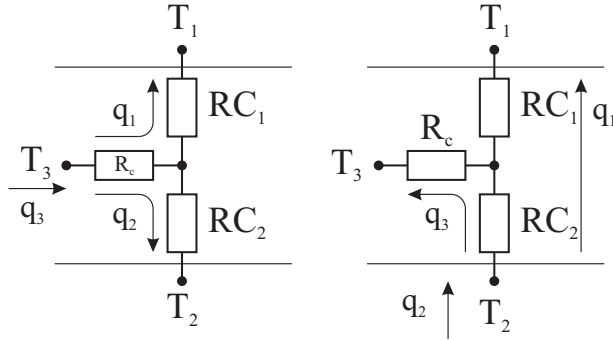


Figure 5.6: 2 example transfer function representations: (left) for a variation of the water supply temperature T_3 , the admittance Ad_3 and transmittances Tr_{3-1} and Tr_{3-2} and (right) for a variation of the temperature of the zone below T_2 , the admittance Ad_2 and transmittances Tr_{2-1} and Tr_{2-3} in a CCA floor. A variation of the temperature of the zone above T_1 is similar. RC_1 and RC_2 are the lumped representations of the thermal capacitance nodes of the CCA-slab.

In order to have a model that describes accurately the temperature profile through the slab, a 19th-order star RC-network is chosen to model the CCA in this section. According to the procedure described in App. E, a state-space model of the 19th order RC-network, as shown in Fig. 5.7, is constructed and transfer functions are generated using Matlab's *ss*-function. This high order model will ensure enough detail to represent the temperature gradient in the slab in transient regime. The base CCA model used for the frequency response analysis of this Section is a 0.2 m thick uncovered concrete floor, with a water flow rate of 140 kg/h and a tube spacing of 0.15 m. The tubes are located in the centre of the slab. The chosen CCA thickness is the minimum that is required for constructional reasons.

However, in order to use a simplified building model in an advanced controller algorithm, a low model order of the overall building model is beneficial [90]. Therefore, firstly, this section presents the analysis of the frequency response of the detailed 19th order model, while secondly, a comparison is made between the frequency response of this base model with a 3rd and a 2nd order CCA model in order to assess their performance regarding the energy flow due to changing temperature boundary conditions. The layout of the three models is shown in Fig. 5.7.

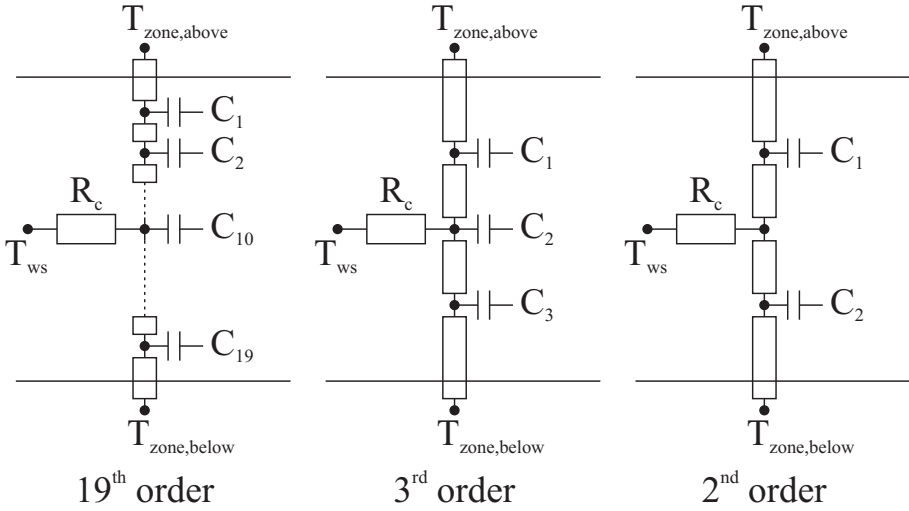


Figure 5.7: Layout of the 3 star RC-models used in the analysis of the CCA frequency response.

5.4.3 Frequency response of CCA

The thermal capacity of CCA blocks at least partially the heat flow from the zone to the water tubes or vice versa for a high frequency input. The capacitance C acts as a filter for the inputs entering the CCA. The difference between admittance at position i and transmittance from i to j will be used as a measure for the buffering action of the CCA:

$$\dot{q}_{stored,i} = Ad_i - \sum_j Tr_{i-j} \tag{5.7}$$

In steady state (time period $\theta = \infty$ or frequency $f = 0$) the capacitance C of the CCA does no longer act as a filter and the energy balance $Ad_m = Tr_{m-n1} + Tr_{m-n2}$ must be fulfilled, with Ad_m equal to the sum of the thermal resistances. On the other hand, for $\theta = 0$ ($f = \infty$) the capacitance C completely filters the input and $Tr_{m-n1} = Tr_{m-n2} = 0$. In this case, Ad_m is equal to the convective resistance from T_m to the respective surface. These limit values, for the 3 temperature inputs, are presented in Table 5.2.

Fig. 5.8 shows the admittance and the transmittance for the base CCA model as a response to \tilde{T}_1 , a temperature variation of the zone above, which is induced

Table 5.2: Limit values for the TABS transfer functions: time period $\theta = \infty$ (steady state, frequency $f = 0$) and time period $\theta = 0$ (frequency $f = \infty$).

	$Ad_{\theta=0}$ (W/m ² K)	$Ad_{\theta=\infty}$ steady state (W/m ² K)
Ad_1	8.1	4.6
Ad_2	5.8	3.8
Ad_3	17.0	6.5

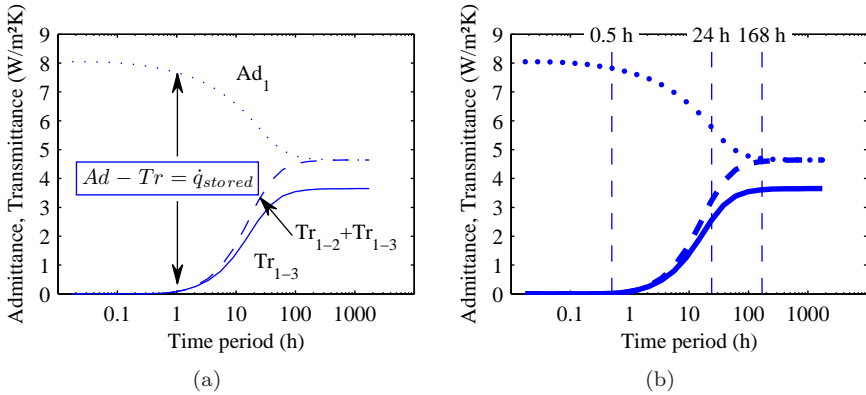


Figure 5.8: (a) Admittance Ad_1 at the CCA lower surface, transmittance Tr_{1-3} to the water tubes and the total transmittance $Tr_{1-2} + Tr_{1-3}$ in response to a temperature variation at the upper surface. (b) shows the relation with the time period range of the disturbances.

by one of the zone inputs T_{amb} , \dot{q}_{sol} or \dot{q}_{int} . The limit values correspond to the values presented in Table 5.2. Although of course not applied to the same CCA configuration, the trends presented in Fig. 5.8 are similar to the ones presented by Weber et al. [144]. The zone inputs will induce heat transfer to the water tubes in the CCA, but at small time periods thermal energy is buffered to a large extent. Only for $\theta = 168$ h, admittance equals the total transmittance, $Ad_1 = Tr_{1-2} + Tr_{1-3}$, and the signal is fully transmitted.

The difference between the transmittance curve and the admittance curve is proportional to the amount of energy that is stored in the CCA but not transmitted to the water tubes and thus not ‘sensed’ by the HVAC system (Fig. 5.8(a)). This difference (\dot{q}_{stored}) is the amplitude of the heat storage and

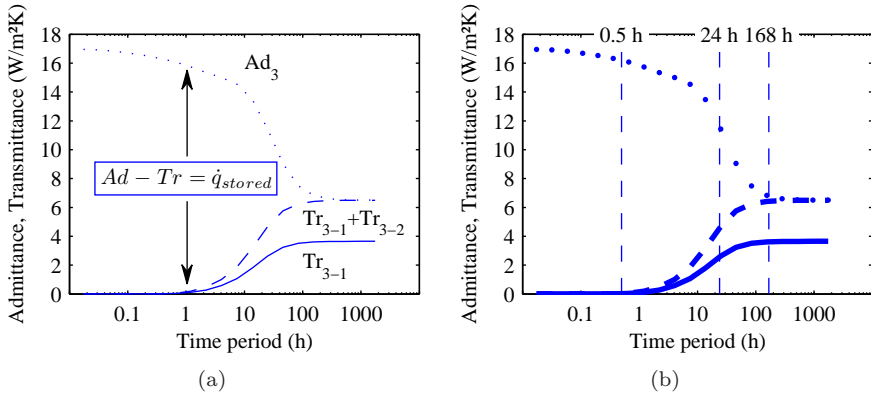


Figure 5.9: (a) Admittance Ad_3 at the tubes level, transmittance Tr_{3-1} to the CCA upper surface and the total transmittance $Tr_{3-1} + Tr_{3-2}$ in response to a varying water supply temperature. (b) shows the relation with the time period range of the disturbances.

heat release caused by the sinusoidal temperature change at the CCA surface. In time domain, the integral of this heat storage sine is the thermal energy storage/release as a function of time per unit area and per degree temperature difference.

Moreover, in Fig. 5.9, \dot{q}_{stored} quantifies the controllability of the CCA. Also here, the limit values of the admittance Ad_3 can be found in Table 5.2. Varying the water temperature in the tubes with frequencies at which the transmittance tends towards zero induces virtually no effect. Changing between heating and cooling with frequencies at which the difference between admittance and transmittance is large, means that energy is exchanged between the heating and the cooling system without a useful effect on the zone temperature. This phenomenon was observed in the case study of Ch. 2.

Judging by the difference $Ad - Tr = 11.7 - 4.5 = 7.2 \text{ W/m}^2\text{K}$ at $\theta = 24 \text{ h}$, even switching from heating to cooling from one day to the next, induces a substantial storage loss in the CCA. This observation was also quantified in the transient heat transfer analysis of Chapter 4 (Sec. 4.5.5).

The low controllability of CCA at high frequencies indicates that, in order to guarantee thermal comfort under all circumstances, a faster reacting additional heating and cooling system, such as air-conditioning, may be needed.

Influence of the thermal capacitance

The frequency response of the CCA model is influenced by physical parameters, such as the CCA thermal capacitance and the combined (natural convection and radiation) heat transfer coefficient h at the CCA surface.

First, the influence of the thermal capacitance of CCA on the frequency response of the model is investigated. To this end, the CCA thickness is varied from 20 cm to 30 cm and 40 cm. To illustrate this effect on the controllability of CCA by varying the water supply temperature, Fig. 5.10 shows the admittance and transmittance from this water supply temperature T_3 . The admittance is only limited affected by the change in thickness, with a maximum difference of 17% between $Ad_{20\text{ cm}}$ and $Ad_{40\text{ cm}}$ at a time period of 55.2 h. The transmittance is more largely influenced. Fig. 5.10(b) zooms in on the smallest periods of the input signals and shows that the total transmittance for the 40 cm CCA is reduced with 94% compared to the 20 cm CCA. For a time period $\theta = 24$ h, the total transmittance to the office zone is reduced by 50%. Within the normal CCA operating range, the storage effect increases even further for a thicker slab, while it was already large for the 0.2 m base CCA model. Therefore, it can be concluded that increasing the CCA thickness above what is required for constructional reasons, is useless from a control point of view.

Influence of the heat transfer coefficient h_{c+r}

The combined heat transfer coefficient h_{c+r} consists of a convective part h_c and a radiative part h_r . Correct determination of h_c has been the subject of many scientific contributions. App. D compares several correlations which can be found in the literature. Furthermore, in a real office environment, the heat transfer from CCA to room depends on the covering and the furniture in the zone. Fig. 5.11 shows the frequency response for a variation in again the water supply temperature T_3 . The values marked with a \square are calculated for h being 10% lower than in the base model, which is marked by a \triangle . While the admittance Ad_3 hardly changes below time periods of 24 h, the transmittances do. The change in total transmittance goes from 10% to 20%, which is up to twice the difference in h which was imposed.

This means that, if the value of h_{c+r} is wrongly estimated in the building zone model, the error on the transmittance is even larger than the error on the h_{c+r} -parameter. Consequently, the calculated energy flows in the time domain will

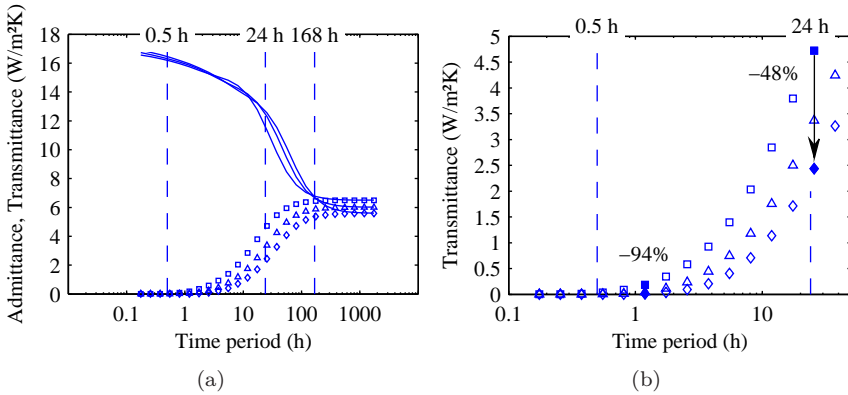


Figure 5.10: Impact of the CCA thickness (\diamond : 40 cm, \triangle : 30 cm and \square : 20 cm thickness) on the total transmittance $Tr_{3-1} + Tr_{3-2}$ from the water tubes to the office zone. (a) shows both total transmittance and admittance Ad_3 , and the relation with the time period range of the disturbances, while (b) zooms in on the total transmittance of the smallest time periods.

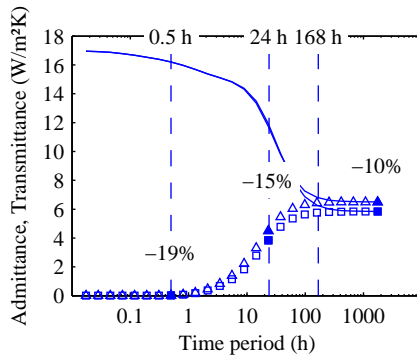


Figure 5.11: The influence of a variation in the combined heat transfer coefficient on Ad_3 and $Tr_{3-1} + Tr_{3-2}$ (\triangle : h_{c+r} base model, \square : $h_{c+r} - 10\%$)

show a significant deviation from reality. It should be concluded that the CCA RC-model used is very sensitive to the choice of the heat transfer coefficient. Control algorithms which are incorporating a CCA-model, should be robust regarding changes of this h -parameter.

5.4.4 Reducing the order of the star RC-CCA model

As already stated, in order to use a simplified building model in an advanced controller algorithm, a low model order of the overall building model is beneficial [90]. Using the 19th order model would increase the computational effort substantially. Therefore, the magnitude and phase shift of the 19th, 3rd and 2nd order model (Fig. 5.7) as a function of the time period θ are compared to assess the error made by lumping the thermal capacitance of the CCA-slab.

Magnitude

Fig. 5.12 shows the amplitude of the different admittances and transmittances for the 19th, 3rd and 2nd order CCA model. Like in the previous paragraph, the indices 1-2-3 refer to respectively the upper room, the lower room and the water in the tubes. For the large time periods (low frequencies, with the steady state as a limit), the magnitude of all heat flows are modelled correctly. Because the steady state value is equal for all models, this is an evident conclusion. The transmittance is modelled with a good accuracy by the 3rd and 2nd order model compared to the detailed 19th order model, but admittances show a considerable deviation towards the smaller time periods. The difference in limit values — thermal resistance between a temperature input and its nearest temperature node — are evidently causing this deviation, as can be seen from Fig. 5.7. By placing an extra node in the concrete core, the 3rd order RC-model is able to model the admittance q_3/T_3 rather well for the small time periods up to 30 min. As this is important to implement intermittent flow control, a 3rd order CCA model is required for model based control strategies.

Phase shifts

The phase shift, in Fig. 5.13 shows the delay on the heat flow output signal \dot{q} compared to the temperature input signal T . The phase shift for the admittances is rather small and comparable for the three models. The transmittance phase shifts are considerably deviating, caused by the lower order of the simplified models. Therefore, since the admittance and transmittance are complex values, their will be a considerable deviation in the thermal behaviour of the low order models compared to reality.

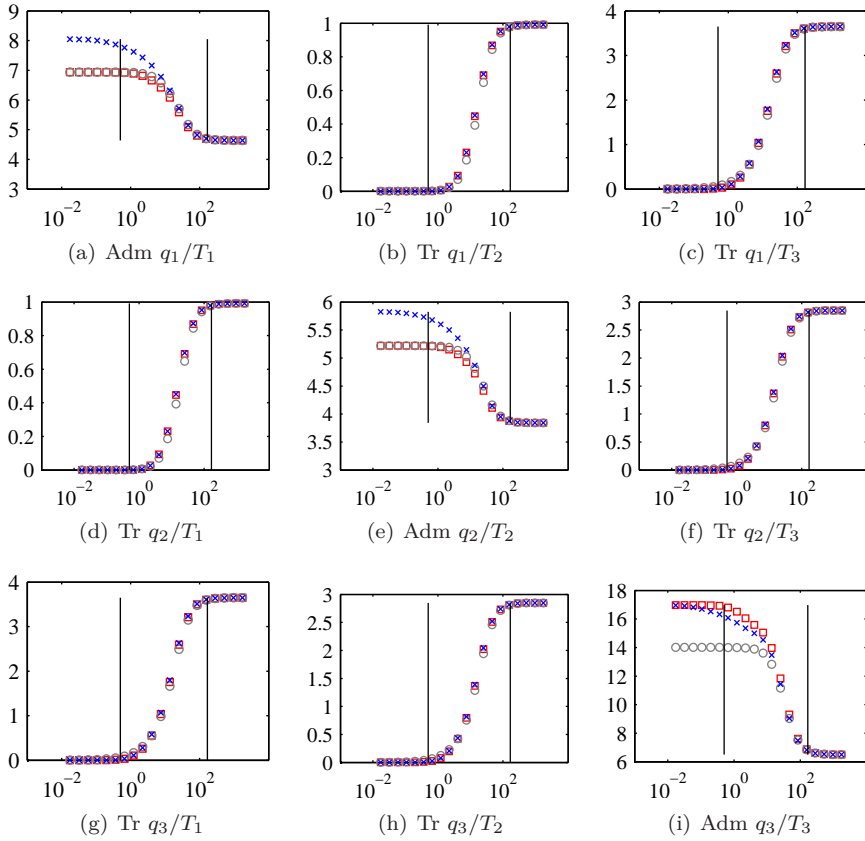


Figure 5.12: Magnitudes of the transmittances and admittances for the 19th (marker : x), 3rd (marker : □) and 2nd (marker : o) order CCA model. The x-axis has the units of time (h) and the y-axis thermal power (W/m^2). The vertical lines indicate the 30 min and 168 h time period.

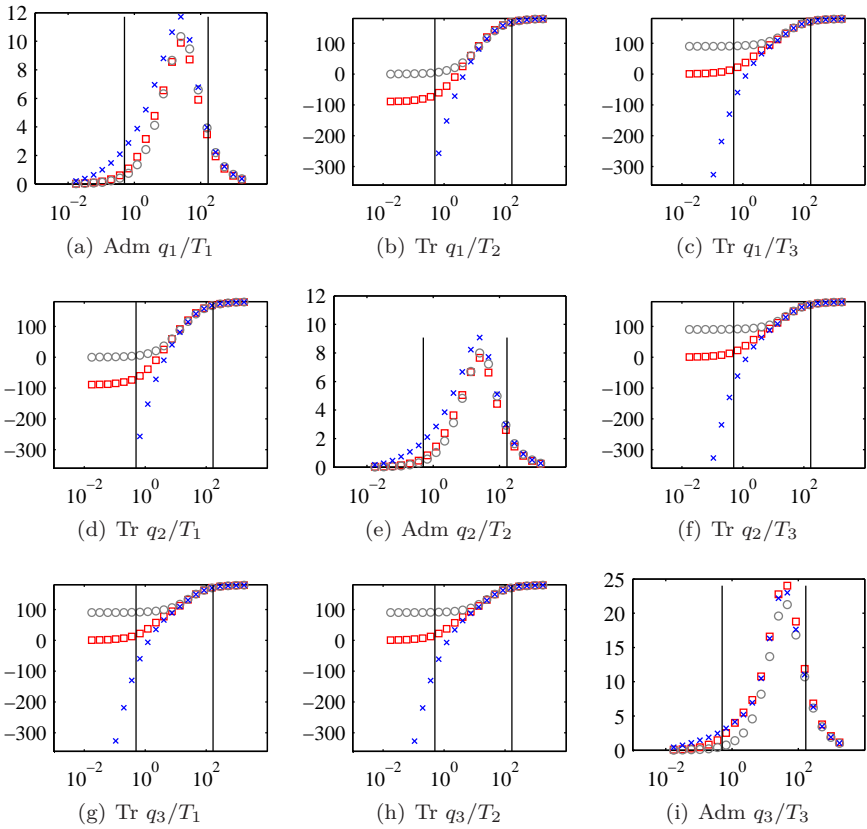


Figure 5.13: Phase shifts of the transmittances and admittances for the 19th (marker : \times), 3rd (marker : \square) and 2nd (marker : \circ) order CCA model (in $^\circ$). The x-axis has the units of time (h) and the y-axis of degrees. The vertical lines indicate the 30 min and 168 h time period.

Table 5.3: Overall RMSE values of the magnitude errors and of the phase shift errors between Admittances and Transmittances from the 3rd, respectively 2nd order CCA model and the detailed 19th order CCA model in the 30 min and 168 h time period

	Magnitude RMSE (W/m ²)	Phase shift RMSE (degree)
3 rd order CCA model	0.21	34.7
2 nd order CCA model	0.34	54.0

In Table 5.3 the error between the simplified 3rd, respectively 2nd order model and the detailed 19th order model is quantified. The values shown are the root-mean-squared errors (RMSE) of the magnitudes and phase shifts of all Ad_i and Tr_{ij} transfer functions. The RMSE values of both 3rd and 2nd order model are shown. It can be concluded that the transfer function magnitude is good for the simplified models. The error is mostly caused by the Ad_i -magnitude values, which can be seen on Fig. 5.12. The individual magnitude errors are in general equal for the 3rd and 2nd order model, except for Ad_3 , the admittance at the water level, where the 3rd- Ad_3 -RMSE = 0.44, while the 2nd- Ad_3 -RMSE = 0.92, so the error more than doubles. This was also addressed in the analysis of Fig. 5.12.

For the phase shift errors, the overall values of Table 5.3 are a good representation of the individual errors: the 3rd order model performs better than the 2nd order model.

5.5 Conclusions

This chapter shows that CCA hampers to a considerable extent the communication between the water flow and the office zone. For the dominant frequencies in the zone disturbances T_{amb} , \dot{q}_{sol} and \dot{q}_{int} , the difference between the admittance and transmittance of the CCA is large, both for the zone temperature, as well as for the water supply temperature. Therefore, while operating a CCA system, a large thermal energy storage effect will always take place (as already shown in Ch. 4). This can be turned into a benefit, if the CCA controller is able to account for stored energy which can be used later during the day.

The frequency response of the CCA determines the CCA behaviour as a controlled thermal storage in the building zone. Due to the large thermal inertia, the response at the water tube level to changes in the office zone, is very low. As a consequence, cooling and heating installations characterized by smaller time constants (such as air-based systems) may be needed in combination with CCA to guarantee thermal comfort in the building zone at all times.

Increasing the CCA thickness deteriorates the ratio Tr/Ad even more and therefore decreases the controllability of CCA even more. This will increase the need for an additional, faster reacting system even more. Also, while modelling an office zone with CCA, care should be taken to choose the correct heat transfer value h_{c+r} between CCA surface and the office zone. After all, an error in estimating h_{c+r} results in an even larger error on the transmittance. The control algorithm should therefore be robust enough to deal with this uncertainty.

Reducing the order of the CCA RC-model to 3 compared to 19 leads to an acceptable performance, since the steady state values remain comparable. However, this is no longer true for a 2nd order model. This leads to the conclusion that a minimum order of 3 is required for a thermal CCA model. This 3rd order model was used in the case study presented in Ch. 2.

However, when identifying a model suitable for an optimal CCA controller (Ch. 9), the 2nd order model is chosen, because measurements of all the 3rd order model states are not available and to reduce the computation time of the optimisation routines used in Ch. 9 and Ch. 10. Simplicity is chosen over accuracy in that case, but the results of this chapter are indicative for the error that is made.

Part III

Concrete Core Activation and building

Chapter 6

Control of CCA buildings

6.1 Introduction

The control of CCA has been the subject of several studies over the last decade, which will be presented in this chapter. Due to the active integration of the building mass in the HVAC system, the choice of control strategy and controller settings play a decisive role in reaching both thermal comfort and low energy use. Indeed, CCA, with its high thermal inertia, is the connection between the heating and cooling production system and the building where thermal comfort has to be guaranteed. It is inevitable to take CCA dynamic behaviour into account. In the next section, the choice of thermal comfort model is covered. CCA buildings typically operate with a floating indoor temperature, which should be addressed while evaluating thermal comfort. Subsequently, an overview of existing literature on control of CCA is presented. Finally, building models are covered, since they are an important and integral part of a CCA controller. The topics presented in this chapter will be used in the subsequent chapters to introduce and evaluate CCA control strategies.

6.2 Thermal comfort criteria for CCA buildings

In general, creating a comfortable environment in buildings requires achieving thermal comfort, visual comfort, acoustic comfort and a good air quality.

Visual and acoustic comfort are not addressed in this work, although acoustic comfort is an important issue in CCA buildings. After all, maximizing heat transfer between CCA and room, requires an uncovered ceiling. This means that conventional acoustic measures such as an acoustic ceiling are not possible anymore and should be compensated by ‘ceiling islands’ or wall panels. Weitzmann et al. [146] conclude that a 50% covering does not affect the cooling capacity, while improving acoustic comfort. They do not report on heating capacity though, for which the heat exchange is dominated by radiation.

For the design and operation assessment of CCA buildings, for which it is known that indoor temperatures float during the course of the day [87, 81], it is important to define suitable thermal comfort criteria, in order to evaluate the performance of the building correctly. When choosing between the standard comfort models with the fixed temperature limits at one hand, and the adaptive comfort models with the temperature limits changing with the outdoor temperature on the other hand, it seems obvious to choose the latter for CCA buildings. After all, CCA buildings typically encounter floating indoor air temperatures during the course of the day. When indoor climate expectations are less stringent, the occupants will be more tolerant towards a wider range of temperatures [36]. However, the question still remains whether adaptive models may be applied to CCA buildings? How is thermal comfort in CCA buildings evaluated when using the static or adaptive thermal comfort models as guideline? An answer will be looked for in the next sections.

6.2.1 Thermal comfort models

CCA, with their limited cooling power, are considered as top-cooling systems rather than as full air-conditioning systems. Since it is known that indoor temperatures vary during the course of the day [87, 81], it is important to define suitable thermal comfort criteria. Two main categories exist.

Firstly, the standard thermal comfort models apply to air-conditioned buildings and assume that the building is kept within fixed temperature limits. Within the standard comfort models, Fanger’s thermal comfort model [68] is widely applied. The model calculates a heat balance between the human body and its surroundings and uses the parameters PMV (Predicted Mean Vote) and PPD (Percentage of People Dissatisfied) to assess thermal discomfort. $PMV = 0$ means that the occupants judge the thermal sensation as neutral, for $PMV < 0$ as too cold and for $PMV > 0$ as too warm.

Secondly, adaptive thermal comfort models, as e.g. described in ASHRAE-55 [6] or EN15251 [44], assume that building occupants adapt their behaviour towards thermal comfort: e.g. in summer, clothing is adapted and windows are opened or people are getting used to higher temperatures after a certain period. Furthermore, when expectations towards thermal comfort are not too strict, people are more tolerant to temperature swings. Compared to the PMV-PPD model, adaptive thermal comfort models are expected to lower the cooling requirement of a building, since they allow higher indoor temperatures.

6.2.2 Operative temperature

Conventional, heat balance based, thermal comfort models, e.g. the PMV-PPD model, are all based on environmental parameters from the direct surroundings of the occupants. Furthermore, it is required to estimate the occupants' clothing insulation (CLO-factor) and metabolic rates (MET-factor). Input parameters needed to calculate thermal comfort are, amongst others, air temperature, mean radiant temperature, relative air velocity, water vapour partial pressure and local discomfort assessment. As it is difficult, certainly taking into consideration the accuracy levels of measuring equipment, to verify thermal conditions point by point, usually the operative temperature is used as defining parameter ([68], Annex A). Nicol and Humphreys [96] identified the operative temperature as a simple but well performing thermal comfort index, while more complex indices show a lower correlation with the thermal comfort votes of the respondents.

Depending on the activity (MET) and the clothing level of the occupants (CLO), an optimal operative temperature $T_{op,opt}$ exists, corresponding to $PMV = 0$. Each comfort category has the same $T_{op,opt}$, but has a different permissible range around this optimal point. Table 6.1 summarizes $T_{op,opt}$ -values and the allowed temperature range for the different categories, as prescribed by the PMV-PPD thermal comfort model. The thermal comfort models define categories which describe the quality of the thermal comfort. A lower quality corresponds to a lower thermal comfort. Table 6.1 presents the classification of the PMV-PPD thermal comfort model, expressed in % PPD.

Table 6.1: Optimal operative temperature and operative temperature band for thermal comfort in an office environment for the different categories according to ISO7730 [68].

Category	PPD (PMV)	Operative temperature (°C)	
		Winter	Summer
A	6% (± 0.2)	$22.0 \pm 1.0^{\circ}C$	$24.5 \pm 1.0^{\circ}C$
B	10% (± 0.5)	$22.0 \pm 2.0^{\circ}C$	$24.5 \pm 1.5^{\circ}C$
C	15% (± 0.7)	$22.0 \pm 3.0^{\circ}C$	$24.5 \pm 2.5^{\circ}C$

6.2.3 Thermal comfort and operative temperature ramps

Although the PMV-PPD model is intended for use under mostly steady state conditions, it has been suggested by Knudsen et al. (cited by [78] and in [46]) that this PMV-PPD model can be used to predict thermal sensation during temperature ramps up to ± 5 K/h. Kolarik et al. [78] concluded that for temperature ramps up to 2.4 K/h, the PMV/PPD model was well suited to predict thermal comfort. For a 4.8 K/h temperature ramp, the percentage of dissatisfied increased faster than predicted. This is a considerably higher value than the 2.2 K/h suggested by ASHRAE [6]. In the Thermco project report on thermal comfort in transient environments [46], literature findings are summarised in a general guideline, stating that the PMV/PPD model is usable for temperature drifts lower than 4 K/h. This is already a high value, even for CCA buildings, indicating that the transient CCA behaviour does not pose a problem in applying the PMV-PPD model.

6.2.4 Application of adaptive thermal comfort models to CCA buildings

According to the different standards and guidelines on adaptive thermal comfort, these models can only be applied to :

1. buildings with no mechanical cooling systems (air conditioning),
2. buildings used mainly for sedentary activity,
3. buildings in which occupants have easy access to operable windows or some other occupants intervening possibility on ventilation,

4. buildings in which occupants must be allowed to adapt their clothing or work schedule to the indoor or outdoor thermal conditions,
5. buildings in which occupants are correctly informed about the thermal comfort to be expected.

Neither of these restrictions is necessarily satisfied by CCA buildings, except for the second requirement, since the buildings evaluated in this PhD-text are all office buildings.

While in heating regime heat loss and heat input are almost equal, the cooling case is more problematic: the available cooling power from the CCA can be 2 to 3 times lower than the occurring heat gains. Consequently, when CCA buildings do not have an additional HVAC system to substantially cover the peak load, a CCA system cannot be regarded as a full air conditioning system, capable of keeping the temperature at a specified set point. On the other hand CCA buildings can not necessarily be classified as naturally ventilated buildings (Sec. A.3.3), neither as mixed-mode buildings with a hybrid ventilation system. Often they are classified as passively cooled buildings, in which the heat load during the day is stored and removed by means of ground cooling, night ventilation or a cooling tower [103].

Regarding the requirement that the occupants also have some control on the ventilation (e.g. by opening or closing windows), Pfafferott et al. [103] described in their large survey of low-energy office buildings (including a number of CCA buildings) that the occupants perceive their impact to control or change the working environment by manual operation of windows in summer as limited : “Since the temperature difference in summer between inside and outside is smaller, the manual control of windows changes the room temperature not as significant as in winter and, hence, the occupant cannot perceive his interaction directly”. This is also confirmed by Wagner et al. [142]. They therefore concluded that the adaptive comfort criteria are applicable to both naturally ventilated as well as to, what they call, mixed-mode buildings. Buildings with CCA fall under the latter category in their view.

Oseland [100] extensively compared predicted and reported thermal sensation in a Great Britain climate. He concluded that “the PMV-PPD thermal comfort model is better in predicting optimum temperatures in climate controlled offices, when activity and clothing are constant, than in other environments”. Moreover, if no restrictions are imposed on activity level or clothing level, the occupants appear to be satisfied with a wide range of temperatures, possibly because

Table 6.2: Application of adaptive model requirements to CCA buildings

Adaptive requirement	CCA buildings	but...
No mechanical cooling system	not necessarily	CCA \neq full airco
Mainly sedentary activity	OK	
Operable windows/ventilation	not necessarily	limited effect in summer
Allowance to adapt clothing/behaviour/work schedule	possible	has to be allowed
Correct thermal expectation	possible	inform occupants

they adapt their clothing, activity or other behaviour. On the other hand, regarding the 4th requirement, work schedule adaptation is perhaps not possible in every economical context, as Barlow and Fiala [14] suggested. Their research also demonstrated that only 4% of the occupants changed clothing during the day, proving the importance of office overheads' policy in the adaptive thermal comfort model story.

deDear, Brager and Cooper [37] stated that thermal satisfaction is achieved by a correct matching between the actual thermal conditions and the occupant's thermal expectations of what the indoor climate should be. One of the factors determining the expectations is the level of thermal comfort occupants expect to receive from the building and its HVAC system. This means that, if user's expectations of the building comfort are not high, or in other words realistic, room temperature can be less strict.

For CCA buildings, with their changing room temperatures during the day, this all means that adaptive thermal comfort models are applicable if occupants are allowed to change their clothing and/or activity level freely and if they are well aware of the characteristic features of their HVAC system with respect to thermal comfort. Table 6.2 summarizes the applicability of adaptive thermal models to CCA buildings.

6.2.5 Adaptive comfort models in moderate climates

App. A evaluates both a standard and an adaptive thermal comfort model in a moderate climate. It is concluded that the high outdoor temperatures for which adaptive models allow higher indoor temperatures than the PMV-PPD model, hardly occur in our moderate climate. Therefore, the benefit of

the adaptive models is lost for the most part, as also stated by Vanhoof and Hensen [137]. Furthermore, due to the adaptation idea, adaptive models allow lower temperatures in a winter situation, which should result in a lower heating energy use. However, looking at modern, high quality buildings, even in winter a considerable cooling load is existing. The lower temperature limits from the adaptive models therefore make the cooling switch on earlier. This results in a higher annual cooling energy use, instead of lowering the heating energy use.

6.2.6 The choice of thermal comfort model in CCA buildings

Analysis of the adaptive thermal comfort models and their evaluation by several authors show that these models, although by definition not applicable to CCA buildings, can be applied. The details of this analysis are as elaborated in App. A. However, in a moderate climate as in the most part of Western Europe, the potential of the adaptive models to reduce energy use is low. Moreover, the standard PMV-PPD thermal comfort model predicts thermal comfort well, even under the floating indoor temperature conditions which typically occur in CCA buildings. Therefore, it can be concluded that the widely used PMV-PPD thermal comfort model is the best to be applied in moderate climates, not only in the case of CCA buildings, but also in general.

In this work, the PMV-PPD class B thermal comfort model is used, which means that the operative temperature should be kept within the range $20 < T_{op} < 24$ in winter and $23 < T_{op} < 26$ in summer, in order to guarantee thermal comfort, as presented in Fig. 6.1.

6.3 Model based control

The controller of an HVAC system is faced with a multi-objective problem: maximizing thermal and air quality comfort while minimizing energy use. To satisfy these objectives, the building controller has to direct the (1) CCA circuit, (2) air handling unit (AHU), (3) solar shading, (4) lighting, and (5) possibly auxiliary heating or cooling systems. All subsystems influence thermal and air quality comfort to some extent, and require energy to achieve this. Moreover, mutual interaction creates a complex system, which has to be accounted for when setting up the control strategy.

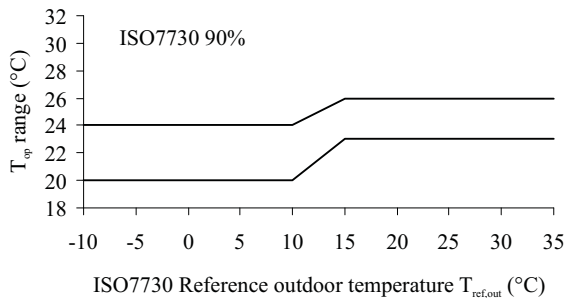


Figure 6.1: Operative temperature range as a function of the reference outdoor temperature $T_{ref,out}$ for a class B building, according to the PMV-PPD model (ISO7730 [68]). The definition of $T_{ref,out}$ is given in App. A.

The presented building controllers are listed in two categories:

- Conventional control: any type of on-off feedback controller, usually with a dead band to avoid oscillation. This type of controller is often combined with a feedforward, outdoor temperature dependent heating/cooling curve, which incorporates a static building model and CCA model in the controller
- A specific category of optimal control is Model based Predictive control (MPC): this terminology is used for a controller which incorporates a dynamic building model and takes into account disturbances such as outdoor temperature, solar radiation or internal gains, to predict the future dynamic behaviour of the building. This predictive controller defines an optimal trajectory of the system input parameters, such as the water or ventilation supply temperatures, in order to minimise a pre-defined cost function: minimal energy use or cost and maximal thermal comfort, avoiding power peaks, . . . , or a combination of these objectives.

6.4 Conventional CCA control strategies

A simple on-off feedback controller with a dead band will be used in Ch. 8 to obtain important information of the behaviour of CCA under different conditions. Apart from the heating and cooling curve, which are based on a

steady-state CCA building model, no detailed building model is required for this type of controller.

Several authors report conventional control strategies for CCA or radiant floor systems in general. It is shown that an appropriate selection of available controller settings, can result in well-controlled systems, without the use of time consuming optimal control strategies. However, they always start from an analysis of the response of the building to different controller settings in order to obtain a good combination. With optimal control strategies on the contrary, it is the aim to start from the occurring dynamics of building and disturbances, to arrive at a controller which takes all constraints into account and operates the building in a way that energy use is minimized while thermal comfort is maximized.

Güntensperger et al. [55] defined one supply temperature curve, depending on the outdoor temperature, in combination with a pump operation time control. Moreover, they added the concrete core temperature as an extra corrective variable in their building controller simulation. This concrete core temperature together with the room air temperature was used to correct the calculated supply temperature.

Olesen [97] proposed to keep the concrete core temperature at a constant temperature of 22°C as a very simple control strategy for buildings with a low heating and cooling load. The self-regulating effect was acting when the room temperature drops above or below this value.

Olesen et al. [99] studied the effect of pump operation time, intermittent pump control and supply water temperature on the energy use for a CCA office building in summer period. Night time operation was beneficial from the energy point of view, but with a slightly higher thermal discomfort. Intermittent pump control could dramatically lower energy use, while maintaining a comparable level of thermal comfort. For the supply temperature, a slightly inclined, outdoor temperature dependent cooling curve appeared to be the best in balancing energy use and thermal comfort.

Tian and Love [131] investigated measurements in a real office building. A slab cooling system was circulating constant flow, high temperature chilled water. This system was combined with a Variable Air Volume (VAV) system with terminal reheat coils and with radiant heating panels. They observed conflicting behaviour between CCA and the ventilation system, for which the controller had to be corrected by applying time schedules for both CCA and

ventilation system and by adapting heating and cooling set points.

Zaheer-uddin et al. [150] compared conventional on-off control with an adapted multi-stage on-off control and an improved proportional controller. They demonstrated that the improved proportional control of a radiant floor heating system, which used an initial constant gain on top of the proportional gain, resulted in a robust controller, yielding a stable control of the room temperature.

Rijksen et al. [111] presented a combined measurement and simulation study of an office building in the Netherlands. They controlled the cooling of the CCA during the night and in the weekend starting from 15 h. CCA cooling operated for a room temperature above 22.5 and stopped below 22.0, with a supply water temperature of 15. During office hours only conditioned ventilation was active. For higher cooling loads, the CCA were also activated during the day. The results pointed at a reduction of required cooling power of up to 50%, compared to the peak heat load value. Results of the acquired thermal comfort were not mentioned, though.

Kolarik et al. [79] presented a simulation study of a two zone office building separated by a corridor. Comparing a VAV-system and a CCA system combined with a Constant-Air-Volume (CAV)-system, the results showed a 20% primary energy reduction for the CCA system. Discomfort increased with the CCA, although an adapted control strategy limited the number of hours violating the PPD=10%-limit to 2% of the year. The adapted control strategy consisted of a changed pump operation and a lower water supply temperature.

6.5 Conventional CCA control by EMPA

Extensive work on modelling and control of CCA has been performed by EMPA, the Swiss Federal Laboratories for Materials Testing and Research, together with Siemens Building Technologies, Switzerland. Tödtli et al. [132] presented an integrated system and control design procedure, because both are bounded, due to the integration of the thermal mass in the heating and cooling system. This work defines a combination of a compulsory outdoor temperature dependent heating and cooling curve, an optional room air temperature feedback and an optional intermittent pump control, based on the thermal resistances of the CCA. The feedback module allows a correction

of the calculated set points from the heating and cooling curve, while the intermittent pump control tries to benefit from the different rates of the heat transfer processes from water to concrete and from concrete to room air.

A fully integrated design approach is obtained for CCA buildings using the ‘unknown-but-bounded’ method, which eliminates the use of intensive simulation work. Due to the CCA thermal inertia, the time-varying profile of heat gains and losses can be replaced by an estimation of constant upper and lower boundaries for the heat gains (internal and external heat loads). These values are integrated in the static heating and cooling curve formulation, relating outdoor temperature with the water supply temperature. If the heating and cooling curve overlap, a backup system is required, otherwise a range of outdoor temperatures exists, for which simultaneous heating and cooling appears.

Different hydraulic configurations are considered to define their impact on multi-zone control of CCA. Several extensively elaborated examples with different combinations of controlled variables, controller settings and hydraulic configurations clearly illustrate that control of CCA influences the design of CCA.

6.6 Model based Predictive Control of CCA

Careful tuning of the parameters of rule based control strategies enables to satisfy thermal comfort requirements within the physical constraints imposed by the system [124]. However, they can not explicitly exploit the dynamics of CCA and building in order to optimize the operation with respect to energy and discomfort cost. An alternative to the conventional controller is to formulate the control task as an optimal control problem (OCP) [30, 74, 115].

With an optimal control strategy, system operation is determined by solving at each control time step an optimal control problem, as shown in Fig. 6.2. This yields a control input profile, e.g. for the water supply temperature, which minimizes a given cost function, using a dynamic system model, updated system information and disturbances predictions (e.g. weather forecast and occupancy prediction). The cost function is typically a weighted sum of the conflicting objectives of minimizing the energy cost and the thermal discomfort. At each MPC time step, e.g. at ($k = 0$ AM), the MPC is called to provide

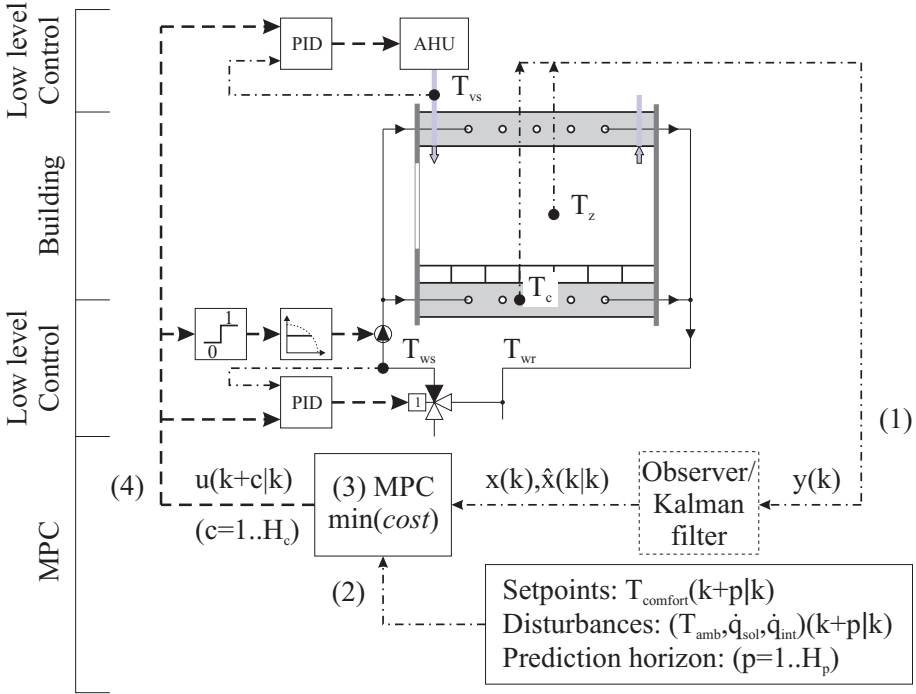


Figure 6.2: Example of a building MPC framework: (1) zone and concrete slab temperature $y(k) = [T_z T_c](k)$ is the measured output from the office zones at time $t = k$, where, if necessary, a Kalman filter estimates unmeasured states, (2) at time k disturbance predictions, e.g. for the ambient temperature T_{amb} , solar radiation \dot{q}_{sol} and internal gains \dot{q}_{int} , and setpoint profiles, e.g. the required comfort temperature $T_{comfort}$, are generated for the prediction horizon $p = 1..H_p$, (3) using the dynamic simplified building model, the MPC determines the profile $u(k+p)$, e.g. $= [T_{ws}(k+p), \text{pump-on-off}, T_{vs}(k+p)]$, which minimizes a predefined cost and (4) the $u(k+c)$ -profile is fed to the low level building controllers for the control horizon $c = 1..H_c$.

the control signals for low level controllers of the heat and cold production and distribution system. The procedure contains following steps: (1) feedback of the measured office zone data to the MPC to determine the state of the zone, (2) setpoints and prediction of the disturbances for the entire prediction horizon H_p , (3) solving the optimal control problem, (4) returning the calculated output (control action) to the low level building controllers for the control horizon H_c .

This approach requires the selection of a model structure which is as simple as

possible but still catches the control relevant processes. Thanks to their simple structure, those models can be identified or fine-tuned online, as stressed by Kummert [84], Bianchi [21] or Maciejowski [90]. Moreover, the computational power to run the optimization can be significantly reduced. The standard MPC framework, with a receding horizon procedure, incorporates a feedback mechanism which allows - to a great extent - to compensate for model and prediction errors (see [90]). Additionally, low-level local proportional-integral controllers can compensate for small modelling and prediction errors to ensure stable and robust zone temperature control [149].

6.7 Building thermal mass in MPC control

The building thermal mass can be actively or passively used in the control strategy of an HVAC system. Braun [23] correctly stated that the benefits of using building mass — reduction of power peaks, shift to off-peak electricity demand, more efficient part-load system operation — should be held against an increase of total cooling requirement that occurs with precooling. However, with CCA, there is no other option than to actively use the building mass.

Augmenting the building control level, whether the objective is peak-shifting, precooling, fault detection or diagnosis, adaptive control, predictive control, . . . , all require a dynamic building model which can be identified by a general and reliable identification procedure.

Modelling the dynamics of a real building is of major importance in the design phase of a building. When the controller needs information about those dynamics too, an appropriate building model is again required in the operation phase. This explains the large research effort in the field of system identification of building controller models. Although efforts have been made to re-use design phase detailed models of the building (e.g. [32, 128]) and the installation (e.g. [51]) and incorporate them in the controller, this seems infeasible due to the complexity of both the building model and of the resulting optimal control problem.

The alternative is to use simplified building controller models, which can be derived using a white-box, grey-box or a black-box approach. In the white-box approach, an RC-model based on the physical properties of the building materials and based on the known heat transfer phenomena [2, 33, 50, 66, 73,

[91, 110, 149] is constructed to represent the building dynamics. With the grey-box approach, these white-box model parameters are used as the initial estimate in an identification procedure using measurement data. On the other hand, by using a black-box approach, the model order and architecture are not defined beforehand, but identified together with the parameters of the model by using measurement data [47, 31]. The model order refers to the number of time constants of the model, or in terms of an RC-model, to the number of thermal capacitances C in the model.

White-box models have been widely used to analyse building dynamic behaviour, not only in a control environment. Davies [34] gives an elaborate overview of all aspects of a first principles building model, which serves as the starting point for the simplified building models in Ch. 9. Methods to optimise the model parameters based on frequency domain analysis have been proposed by Akander [2], Masy [91] and Fraisse et al.[50]. For the EMPA CCA-model, a similar procedure was used by Weber and Johannesson [144].

Bianchi [21] used a 3rd and 2nd order model to optimally control a residential floor heating system, and presents an overview of different on-line recursive and off-line parameter identification methods. In a comparable study Wimmer [148] used a 2nd order building model — air temperature and temperature of the embedded floor.

Braun [23] presented results for an optimal use of building thermal mass with a conventional air-conditioning system. Although the system differs from CCA, the conclusions can also be valid for CCA. Conventional on-off control with night setback was subjected to high peak loads, due to the start-up in early morning. On the other hand, the optimal control trajectory tried to make optimal use of the thermal comfort band. The building was cooled during the night in order to be at $T_{comf,min}$ at the beginning of the office hours. The system started cooling again during the day to prevent an overshoot above $T_{comf,max}$ within office hours. The same behaviour should be looked for when operating CCA.

Ren and Wright [109, 108, 110] applied the approach of Braun [23] to a building with a hollow core ventilated CCA, using the ventilation air to condition the CCA temperature. The building was represented by a first order model, while the activated floor and ceiling slab are added as 2nd order models. The plant was represented by a static model. The air supply temperature and flow rate was optimized, together with the on-off control of the heat recovery in order to

obtain free cooling. Different time stages with high or low cooling or heating load were implemented. In the period of low cooling and heating load, only the heat recovery was active. Outdoor temperature and solar radiation were predicted. The 24 h optimal profile was applied without feedback. In winter operation, the MPC made optimal use of the building mass to operate the AHU, to determine the optimal start up time, in order to reach the desired set point at the beginning of the office period. In summer operation, night operation was used to maximize the effect of free cooling with the cold outdoor air.

Hudson and Underwood [66] used measurements to validate the model before applying it as a building analysis tool. Lee and Braun [86, 85] trained an inverse building model with measurement data and used this model to reduce peak cooling loads of an HVAC system.

Bălan et al. [13] used a 2nd order building model, for which the parameters are identified using a ‘bank of models’, from which at each time step, the best model is chosen, while an updated set of models was generated for the next time step. Gouda et al. [53] minimized the error of step responses of a detailed and of a low-order building model to optimize the parameters of the latter.

Gruber et al. [54] presented an MPC on a 2nd order building model, with an idealised heating system. They proved the applicability of MPC by replacing a heating curve control in a real multi-zone office building with a predictive controller. A recursive parameter estimation scheme was applied, in which new measurements are used to update the parameter vector, while the room air temperature data was used for state initialisation. The prediction horizon was split up in different time periods, being smaller for the periods close to the actual time. Application of this MPC to two real case studies learned that one cause of errors is that the real system is not always able to supply the set point required by the MPC. Energy reduction results could not be presented, but they managed to have MPC working in a real building, satisfying comfort for the occupants, while being easily implementable by the building manager.

Armstrong et al. [4] identified the relevance of physically derived constraints on heat transfer rates and time constants, in order to achieve a physically feasible 2nd and 3rd order transfer function model. Parameters were defined by a Least Squares approach. The 2nd order model predicted the time constants better than the 3rd order model. Accurate solar gains measurements were required to obtain a valid 3rd order model. The method was used to avoid peak cooling peaks by passively activating the thermal building mass of a

real office building [5]. They defined optimal start- and precooling-control of a conventional air-conditioning system. System efficiencies were predicted using system measurements. The controller obtained a seasonal cooling load reduction of 30-60%.

Gwerder and Tödli [56] applied a moving horizon MPC to a building having cooling through CCA. The building dynamics were modelled using a white-box 7th order model. The MPC minimized the deviation from the required room temperature and managed to optimize low cost heating (opening solar shading when solar radiation is present) and cooling (natural ventilation) at the expense of active heating and cooling. It prepared the building for warmer days by lowering the temperature of thermal mass during the previous day.

Zaheer-uddin et al. [149] proposed a 4th order white box state space model representing a house with a floor heating system and a boiler. Moreover, they demonstrated the effect of a low level PI-controller to compensate for prediction errors.

Zaheer-uddin and Zheng [151] presented an interesting approach of an MPC application on an HVAC system of a 2 zone office building. Although not applied to CCA, the combination of the fast air-system with the slow building response was tackled, together with 3 operation modes (night, start up and day). Different system equations were used for the slow and the fast reacting system, as well as for the three operating stages. The slow system comprises the 2 zones, each represented by 1 state, complemented with an extra state for the water circuit. A varying electricity price profile made the HVAC system work at full load during low price periods. Cooling energy was stored in the building mass to be used at periods of high electricity price.

Cho and Zaheer-uddin [30] referred to a radiant floor heating controlled by changing the total operating hours during the day and the distribution of these on-hours during the day, based on the predicted outdoor temperature for the next day. Also in their MPC variant of the controller, they tried to find the number of operating hours and the distribution throughout the day. The experience based settings achieve thermal comfort, but were conservative. Certainly the length of the on-times of the system was a parameter which could be optimised. The building load was determined as a function of the outdoor temperature (residential applications are investigated, so solar radiation and internal gains are no dominant heat loads) and let the MPC calculate the on-times of the system. This resulted in an energy use reduction of 15-

35% compared to the fixed operation schedule. Temperature levels were not mentioned in their paper.

Ihm and Krarti [67] compared conventional proportional control of a radiant floor heating system with an MPC, which was minimizing both energy and thermal comfort using the PMV value. Energy use and thermal comfort were clearly identified as conflicting objectives. They identified a simplex direct search method as more suitable than a scatter search method. Savings up to 30% were achieved using the optimal control.

Prívará et al. [105] presented an implementation of MPC in a CCA building in heating regime, with a tuned heating curve controller as reference controller. Both controllers had an outdoor temperature forecast incorporated. Two identical building blocks, one with MPC and one with the reference controller, were compared. The MPC achieved a measured energy reduction of 30%, with lower power peaks, while thermal comfort sensation remained unchanged. Identification of their black-box building model was identified as a crucial step for the implementation of MPC. They concluded that the excitation signals should trigger the dominant modes of the building in order to obtain an accurate controller model.

Ferkl and Siroky [47] proposed a black box, deterministic subspace identification (ID) method in order to obtain a building model which is suitable for control purposes. This method first estimated the future state sequence, from which the system matrices were defined. In a classical approach, the order is reversed [31]. This method is able to deal with MIMO systems, is robust and incorporates model order reduction in the algorithms. The most important advantage was that the identification process was tuned by only 1 parameter, which made the method suitable for inexperienced users. However, incorporating prior knowledge into the system was not straightforward. A comparison with ARMAX models was made, concluding that, for systems subject to white noise the subspace identification outperforms the ARMAX model approach. For example, identifying the ceiling temperature of a CCA building for which disturbance inputs were damped due to the high thermal mass of the concrete slab, yielded the best results with the subspace ID method. However, modelling the zone air temperature, having a direct impact from disturbances such as solar radiation, door openings, people's actions, . . . , performed best with the ARMAX model approach.

Whereas the concept of Model Predictive Control (MPC) for energy and

comfort management has proven to have clear advantages over other control strategies, it also has drawbacks which currently hamper its widespread implementation. Dounis and Caraiscos [38] identified different problems, amongst which (1) the need for an adequate dynamic controller model, (2) the need for online estimation of the corresponding parameters which is robust in the presence of noise, (3) the fact that the adopted thermal comfort models do not reflect the complex, nonlinear features which characterize thermal comfort and (4) the lack of user friendliness, user interaction and learning methods. Also Morari and Lee [93] referred to bottlenecks as (1) system identification, which has to go from a SISO to MIMO approach, also non-linear system identification (2) the integration of performance monitoring and diagnosis in the MPC formulation, in order to maintain control quality over time (3) state estimation in the non-linear case and (4) the integration of integer variables in the OCP formulation.

6.8 Conclusions

The literature on conventional CCA controllers is often based on a trial-and-error approach, where a limited set of controller settings is evaluated on a CCA building. Also, these references only observe the global results of varying controller settings, without looking into the dynamic response of the CCA on the applied controller actions. In Ch. 8 an in-depth analysis of a conventional on-off feedback controller will be presented, for which a parameter analysis of the controller settings reveals a trade-off between energy use and thermal comfort. A detailed analysis of controller setting combinations reveals valuable information on CCA behaviour and on the properties an optimal controller should have.

The literature references show that an MPC with a low-order building model is suitable to actively control the thermal mass of a building. However, a simplified but accurate CCA building model is required. Concerning the parameter estimation procedure in the field of building control, little information can be found on the impact of the measured data set used. To what extent should the solar gains and the internal gains be present in the data set? Moreover, what is the impact of the structure of the controller model and the model order? It is indisputable that for low-cost implementation of MPC, minimizing the amount of data required for either system identification as well as on-line optimization is highly desirable. It is the goal of Ch. 9, which

presents a grey-box approach to obtain the controller building model, to assess the impact of controller model structure and data set for model parameter estimation.

The cost function of the MPC should closely represent the real energy and discomfort cost of the building. If not, the mathematical minimum found by the optimization routine, will not be the real operational minimum. This will give rise to cost function errors. Literature on the control of a combined slow (CCA) and fast (AHU) system is scant. When both subsystems are taken into account, a realistic assessment of either energy cost is crucial in order to find an optimal system operation. With the simplified building model composed, an MPC formulation is presented in Ch. 10, which determines an optimal water and ventilation supply temperature T_{ws} and T_{vs} in order to minimize energy use and thermal discomfort. The implementation of this MPC in a building, dealing with the disturbance prediction errors and model errors, falls outside the scope of this text.

Chapter 7

Typical office building

7.1 Introduction

In Chs. 3, 4 and 5, the CCA has been investigated as an independent system, interacting with a predefined room air temperature to determine the heat transfer from CCA to the — for the rest undefined — environment.

However, a whole building analysis of CCA buildings has to be executed with a simulation model that is capable to grasp both room-side and water-side phenomena. This chapter describes a 2-zone office building with production system, elaborated in the transient system simulation software TRNSYS [122], which is used to analyse the building and HVAC system from a global system perspective. The following topics are addressed successively: the office zone layout and building physics, the HVAC system layout with the heat/cold production system and the air-handling unit, and the heating and cooling load calculation.

7.2 2-Zone office building model

The building considered in this study is a 2-zone office building with CCA floor and ceiling and a constant air volume (CAV) ventilation system. A schematic view is given in Fig. 7.1.

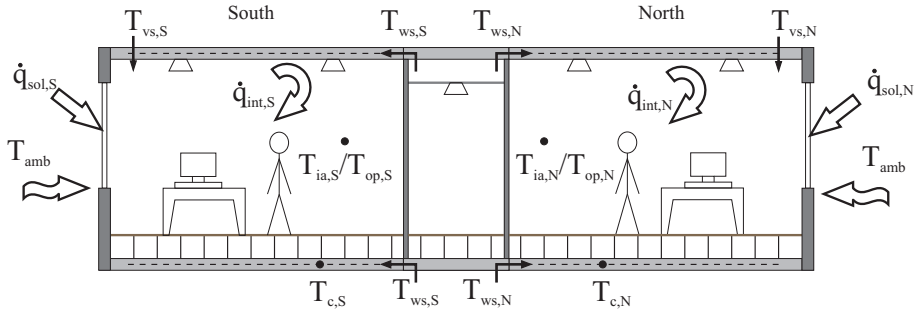


Figure 7.1: Schematic representation of the 2-zone office building with the disturbances ambient temperature T_{amb} , solar radiation \dot{q}_{sol} and internal gains \dot{q}_{int} , the inputs water supply temperature T_{ws} and ventilation temperature T_{vs} and the measured outputs zone temperature T_{ia} (or operative temperature T_{op}) and concrete core temperature T_c .

In Sec. 3.3 it has been shown that the maximal heating and cooling power, limited by thermal comfort, equals $\dot{q}_{h,max} = 120 \text{ W/m}^2$ and $\dot{q}_{c,max} = 62 \text{ W/m}^2$, related to the gross floor area. If typical heat pump and direct cooling supply temperatures are taken into account, these values even decrease to respectively 87 W/m^2 and 42 W/m^2 . Moreover, the transient behaviour analysis showed that the steady state heat power is almost never reached. Therefore, the heating/cooling production power has to be in the same range, otherwise the effect of control actions will be completely lost due to shortage of power. A high quality building with high levels of insulation and with solar shading is considered.

The 2-zone office building should be representative for a modern, high quality office building (raised floor, lighting level, ...) and it should be adapted to CCA (good insulation, solar shading, ...).

The 2-zone building section is a cut-out of a typical office building with South and North oriented offices, both separated from the corridor by a light gypsum wall. The offices have a raised floor in order to provide the necessary flexibility to the work environment [116]. This is an important design condition for CCA — or by extension for any HVAC system which uses the thermal mass of the building [117] — since the heat transfer from CCA to the room is hampered. Lehmann et al. [87] conclude that using a raised floor compared to carpet, decreases the permissible total heat gains with 15-20% to $27 - 45 \text{ W/m}^2$ depending on the allowed temperature drift in the room. The

Table 7.1: Properties of the wall layers in the 2 zone building model (from [24])

Layer name	λ (W/mK)	c (kJ/kgK)	ρ (kg/m ³)	R (m ² K/W)
Brick	0.75	1.00	1000	
Concrete block	1.27	1.00	1200	
Reinforced Concrete	2.50	1.00	2400	
Plaster	0.40	1.00	800	
Gypsum board	0.25	1.00	800	
Mineral wool	0.05	1.03	100	
Polyurethane	0.035	1.40	30	
Linoleum	0.17	1.40	1200	
Floor tiles	0.44	0.73	1500	
Non ventilated air layer > 50mm	(average of value for upward and for downward heat flow)			0.175
Screed	1.30	1.00	1600	
Ceiling tiles	0.06	0.59	370	

thermal properties of the floor tiles are taken from Spitler and Rees [127] and are in between the values used by Schiavon et al. [116] for tiles with and without carpet.

Only in the corridor a suspended ceiling is placed, which is used to put the horizontal distribution of hot and cold water supply, air ducts, electricity and ICT.

The outer wall has 0.1 m mineral wool insulation and high quality windows¹. This is a high level of insulation compared to standard building practice in Belgium [95]. With the solar shading having a g-value of 25% and with the window, which has a g-value of 0.36%, the overall g-value is $0.36 \times 0.25 = 0.09$.

There are no walls to the adjacent building modules, which implies a landscape office is assumed. The only difference with a building having internal walls would be their thermal capacity, since the adjacent zone is assumed to be at the same temperature as the zone investigated. Tables 7.1 and 7.2 summarize the properties of the office zone walls as they are implemented in the TRNSYS simulation model.

Table 7.3 summarizes the typical building parameters. In order to estimate the circulation pump and the fan pressure drop (see Table 7.5), it is assumed that the building has a total office floor area of 3024 m², which is an equivalent of

¹The overall window properties are the U- and g-value calculated by TRNSYS, based on the glass and frame properties. This overall U-value corresponds to the value provided by the Belgian U-value standard [24]

Table 7.2: Wall layouts

Wall	d (m)	U (W/m^2K)
Outer wall	Plaster-Concrete block-Mineral wool-Brick 0.01 - 0.14 - 0.1 - 0.09	0.41
Internal wall	Gypsum board-Mineral wool-Gypsum board 0.012 - 0.05 - 0.012	0.79
Floor/Ceiling	Floor tiles-Air layer-Screed-Reinforced concrete with CCA-Plaster 0.04 - 0.41 - 0.05 - 0.2 - 0.01	1.38
Suspended ceiling	Ceiling tiles-Air layer-Reinforced concrete-Screed-Air layer-Floor tiles 0.01 - 0.2 - 0.2 - 0.05 - 0.41 - 0.04	1.11
Window	U (W/m^2K)	g-value
Window glass	1.10	0.40
Window frame (15%)	2.00	-
Window total	1.29	0.36
Solar shading	-	0.25

Table 7.3: Building characteristics

2 zone building parameters		
Area of the South or North zone	(m^2)	12
Area of the corridor	(m^2)	4.32
Heated volume	(m^3)	96.3
Heated area	(m^2)	28.3
Transmission area	(m^2)	8.6
U-value external wall	($W/m^2 K$)	0.41
U-value total façade	($W/m^2 K$)	0.85
Percentage of glazing	(%)	50
Whole building parameters		
Number of 2-zone modules		126
Number of floors		3
Heated volume	(m^3)	10886
Heated area	(m^2)	3024

126 modules of the above 2-zone office or a 3-floor building with 42 modules per floor.

7.3 HVAC system layout

The HVAC system as simulated in the TRNSYS model consists of four major parts. Each building zone has a CCA ceiling and a CCA floor, which are used to distribute and emit the heat and cold from the production units into the office zone. By using CCA, the tubes through which the heated or cooled water flows, are integrated in the concrete floor and ceiling. The supplied heat is first transported (and therefore stored) in the concrete, before it is transferred to the office zone. Together with the air inlet and exhaust from the Air Handling Unit (AHU), those parts make up the emitting side of the HVAC system.

7.3.1 CCA hydraulic scheme

The CCA supply collector has two circuits supplying water to the ceiling and floor CCA (at the same temperature), one for the South zone and one for the North zone (see Fig. 7.2). Two secondary pumps circulate the water from the collectors to the zone and back to the collectors. In order to set up a general case, the hydraulic scheme enables the heating of one zone, while the other zone is being cooled.

Both South and North circuits have a modulating 3-way valve controlled by the instantaneous $T_{ws,set}$ -value in the associated zone circuit. In case of a difference in $T_{ws,set}$ between the two zones, the production units are forced to supply the most extreme value (T_{prod}). In the TRNSYS simulation model, this 3-way valve is modelled ideally using energy and mass balances, as presented

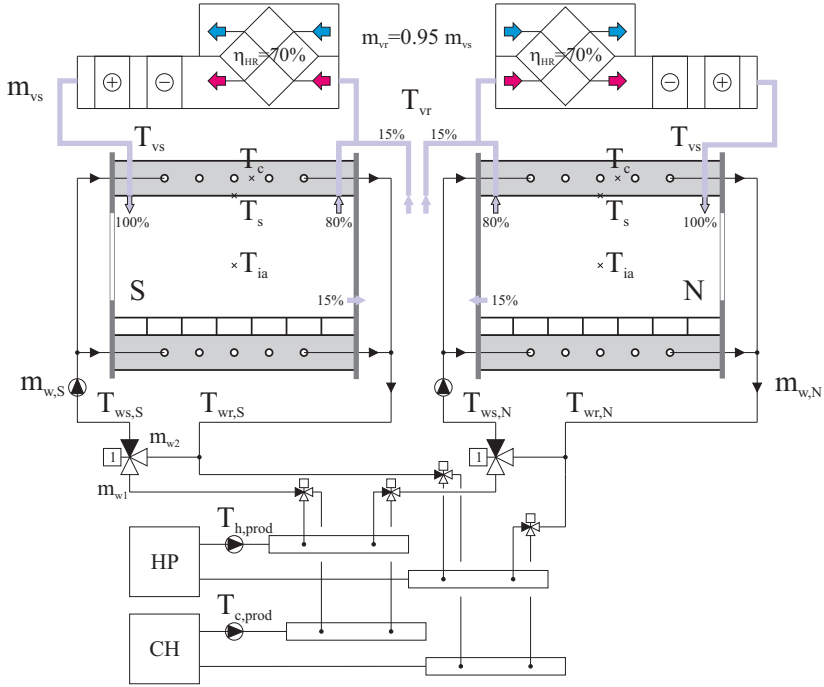


Figure 7.2: Hydraulic and aeraulic scheme of the 2-zone office building section

by Eq. 7.1.

$$m_w T_{ws,set} = m_{w1} T_{prod} + m_{w2} T_{wr}$$

$$m_w = m_{w1} + m_{w2}$$

↓

$$\frac{m_{w2}}{m_{w1}} = \frac{T_{prod} - T_{ws,set}}{T_{ws,set} - T_{wr}}$$

$$m_{w1} = \frac{m_w}{1 + m_{w2}/m_{w1}}$$

(7.1)

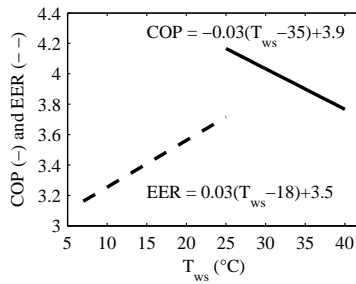


Figure 7.3: COP (solid line) and EER (dashed line) as a function of T_{ws} for the typical reversible air-cooled heat pump used in the simulation model (based on IEA-ECBCS Annex 48 data [19])

7.3.2 Production of heat and cold

The heat and cold production units are highly simplified in the simulation model. Since CCA are well suited to operate at low-exergy temperature levels, the production units must be able to benefit from this. Therefore, gas-fired boilers are excluded, while heat pumps are suitable as heating units. However, since the focus of this study does not lie on the analysis of the production system, it is more convenient to choose a heat pump and chiller for which the heat source/heat sink is independent from the system operation. Therefore, the heat and cold production is modelled as an air-cooled heat pump and as a high temperature air cooled chiller respectively. The heating and cooling energy delivered to the AHU is assumed to be supplied by an additional boiler and low temperature chiller system, given the required temperature levels of the heating and cooling coil.

In TRNSYS, the heat pump and chiller are implemented as ideal boiler (TYPE 6) and chiller (TYPE 92). This means that, given a limited power, no dynamics are modelled. The units are modulating perfectly in the range of 0%-100% and the production efficiencies are taken from the analysis of Eurovent data (units > 50 kW) as presented in the IEA-ECBCS Annex 48 final report [19][Fig. 6-7]: for all units, tested under cooling/heating floor standard conditions, the upper range of the standard deviation reveals a nominal COP = 3.9 and EER = 3.5. Together with a typical efficiency dependency on outdoor air and water temperatures, this leads to a COP and EER as a function of the supply water temperature as presented in Fig. 7.3.

Table 7.4: Production efficiency (T_{ws} in °C)

	Production efficiency
Condensing gas boiler	$\eta = 0.95$
Low temperature air-cooled chiller	$EER = 3$
Low temperature heat pump	$COP = -0.03(T_{ws} - 35) + 3.9$
High temperature air-cooled chiller	$EER = 0.03(T_{ws} - 18) + 3.5$

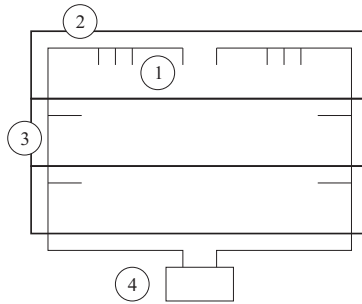


Figure 7.4: Hydraulic scheme of the whole building: (1) CCA circuit, (2) horizontal piping in suspended ceiling, (3) vertical piping in shafts and (4) horizontal piping to collector.

7.3.3 Circulation pumps

For the calculation of the pump energy use, a whole building design is assumed as shown in Fig. 7.4 and Table 7.5. The pipe pressure loss is determined by the friction factor f , based on the Churchill relationship between Reynolds number, relative roughness and friction factor ([8]). The pipe pressure loss is multiplied by an arbitrary factor 3 to take into account the fitting losses. For this building the pipe pressure loss is 26 m for a flow of $36 \text{ m}^3/\text{h}$, which is equal to a power of $0.84 \text{ W}/\text{m}^2$. With an assumed yearly pump runtime of 2400 h, this leads to a nominal pump electricity use of 6114 kWh for the whole building or $2 \text{ kWh}/\text{m}^2$ (Table 7.5).

The design of the AHU, for which the design parameters are already given in Table 7.5, is elaborated in the following section.

Table 7.5: Hydraulic and aeraulic design of the whole building

Hydraulic design						
Per section (Fig. 7.4)						
Section	Floor area (m ²)	Flow (m ³ /h) (12 kg/h.m ²)	Pipe size (DN)	Velocity (m/s)	Δp (Pa/m)	length (m)
1	12	0.14	20	0.22	69	67
2	504	6.1	50	0.97	232	101
3	1512	18.2	80	1.1	166	222
4	3024	36.4	100	1.4	193	100
Whole building						
	Δp (kPa)	Pipe head (m)	P_{pump} (W)	$P_{pump,sp}$ (W/m ²)	E_{pump} (kWh@2400h)	$E_{pump,sp}$ (kWh/m ²)
	252	26	2547	0.84	6114	2
Aeraulic design						
Fan						
Flow rate (m ³ /h)	SFP_{fan} kW/(m ³ /s)	$SFP_{Building}$ kW/(m ³ /s)	SFP category (EN13779)	$P_{SupplyFan}$ (kW)	$P_{ReturnFan}$ (kW)	$P_{FanTotal,sp}$ (W/m ²)
10886	0.75	1.5	3	2.04	1.94	1.32
Heating and cooling coil						
	\dot{Q} (kW)	Rows (-)	$T_{w,supply}$ (°C)	$T_{w,return}$ (°C)	Δp (Pa)	
Heating coil	24.4	1	37	32	55	
Cooling coil	32.4	2	8	13	110	

7.3.4 Air Handling Unit

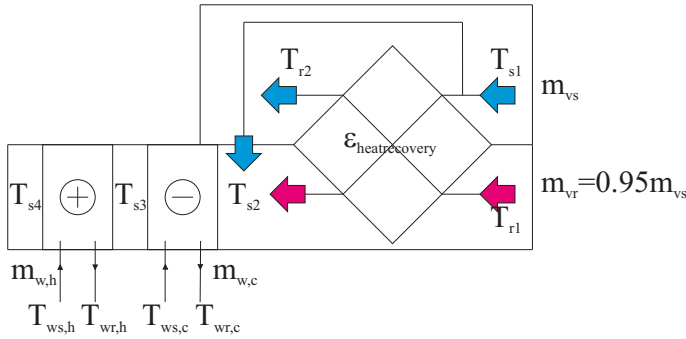
The air conditioning part of the system has 2 AHU's supplying each zone with fresh air. Since a CAV system with only hygienic air flow rate is chosen, recirculation is not provided in the AHU. The AHU consists of a heat recovery cross flow heat exchanger, a heating coil and a cooling coil, characterized by the parameters, presented in Table 7.6.

The heat recovery unit of the AHU is bypassed in those cases where the heat recovery would make the exiting air temperature trespass the limit defined by the set point (Fig. 7.5). The bypass is made modulating so that, when the bypass is on, the bypass flow rate results in a heat recovery exit temperature $T_{s2} = T_{v,set}$. Using this bypass model can also be seen as applying a rotary wheel system with angular velocity control.

The bypass factor (BPF) is calculated using the energy balance at the mixing point behind the heat recovery. A correction of 0.5°C is taken into account to

Table 7.6: Properties of the Air Handling Unit

Parameter	Value
100% supply air flow	$\dot{m}_{vs} = 36 \text{ m}^3/\text{h pers}$
95% return air flow	$\dot{m}_{vr} = 0.95\dot{m}_{vs}$
	15% flows to the corridor: 10.8 m^3 from the South and North zone
	80% is extracted in the room: 28.8 m^3 per zone
Heat recovery	70%
Specific Fan Power	$\text{SFP}_{\text{building}} = 1500 \text{ W}/\text{m}^3/\text{s} = 1.25 \text{ W}/\text{m}^2 \text{ floor area}$
Supply temperature	equal to the lower boundary of the thermal comfort band: $T_{vs} = 20^\circ\text{C}$ in winter and $T_{vs} = 23^\circ\text{C}$ in summer as basic control strategy

**Figure 7.5:** Schematic presentation of the implemented air handling unit

compensate for the temperature rise caused by the fan.

Bypass on (heating) : $T_{s2} > T_{vs,set} - 0.5$ with $T_{s1} < T_{r1}$ and $T_{s1} < T_{vs,set} - 0.5$

Bypass on (cooling) : $T_{s2} < T_{vs,set} - 0.5$ with $T_{s1} > T_{r1}$ and $T_{s1} > T_{vs,set} - 0.5$

$$\begin{aligned}
 \dot{m}_v (T_{vs,set} - 0.5) &= \dot{m}_{HR} T_{s2} + \dot{m}_{BP} T_{s1} \\
 &= (1 - \text{BPF}) \dot{m}_v T_{s2} + \text{BPF} \dot{m}_v T_{s1} \\
 &\Downarrow \\
 \text{BPF} &= \frac{(T_{vs,set} - 0.5) - T_{s2}}{T_{s1} - T_{s2}}
 \end{aligned}$$

(7.2)

Humidity control has not been integrated in the AHU.

The heat recovery efficiency ϵ_{HR} (temperature difference based definition) is a difficult value to determine since real ϵ_{SHR} (Seasonal Heat Recovery efficiency) can drop dramatically compared to design values. The literature mentions several reasons for this drop in efficiency. One reason is the air leakage in the building, the duct system and the air handling unit itself, making the actual air flow through the heat recovery unit less than designed. Roulet [112] measured 13 AHU's with an average $\epsilon_{HR} = 70\%$ and $\epsilon_{SHR} = 43\%$. The smallest drop in efficiency was 11%. Schild [119] refers to frost protection cancelling out the heat recovery in cold weather circumstances. He gives ϵ_{SHR} -values of 60% for a cross-flow plate heat exchanger and 70% for a rotary system. The Belgian Energy Performance Directive for offices prescribes an efficiency reduction factor of 0.85 for AHU without inside air flow measurements, which is considered in this case. This leads to the conclusion that $\epsilon_{SHR} = 70\%$ is a reasonable value for a well-designed and well-controlled AHU. Eqs. 7.3-7.10 present the derivation of the temperature of the air exiting the heat recovery.

$$\dot{q}_{HR} = \epsilon_{HR} C_{min} (T_{r1} - T_{s1}) \quad (7.3)$$

$$= C_{min} (T_{r1} - T_{r2}) \quad (7.4)$$

$$= C_{max} (T_{s2} - T_{s1}) \quad (7.5)$$

$$C_{min} = \dot{m}_{vr} c_{air} = 0.95 \dot{m}_{vs} c_{air} \quad (7.6)$$

$$C_{max} = \dot{m}_{vs} c_{air} \quad (7.7)$$

$$\Downarrow \quad (7.8)$$

$$\epsilon_{HR} = \frac{T_{r1} - T_{r2}}{T_{r1} - T_{s1}} \quad (7.9)$$

$$T_{s2} = T_{s1} + 0.95\epsilon (T_{r1} - T_{s1}) \quad (7.10)$$

$$(7.11)$$

For the fan electrical power use the minimum value of EN13779 category SFP3 ($SFP_{fan} = 750 \text{ W/m}^3/\text{s}$) is used, resulting in $SFP_{building} = 1500 \text{ W/m}^3/\text{s}$. For reference, the standard design guideline proposed by the Air Infiltration and Ventilation Centre AIVC [118], results in $SFP_{building} = 2000 \text{ W/m}^3/\text{s}$, which

Table 7.7: The effect of simulating the heating and cooling coil water circuits on the simulation time of a 1 day simulation

	Simulation time	
	without water circuits (Trnsys types 754,752)	with water circuits (Trnsys types 753,508)
Friday of week 29	14.36 s	23.03 s
AHU in standard operation		(= +60%)
Air set point $T_{vs} = 23^{\circ}\text{C}$		
Ideal heating/cooling		

is the average value of category 3. The latest UK regulations stipulate an $\text{SFP}_{\text{building}} = 1000 \text{ W/m}^3/\text{s}$ for a balanced ventilation with heat recovery. However, this value seems difficult to obtain. The Belgian Energy Performance Directive prescribes SFP3 or lower. Therefore, the AHU and the duct system are assumed to be designed with care. The supply fan electricity use enters the supply air as an additional heat load, giving a temperature rise of approximately 0.5°C . The characteristics of the fan are given in Table 7.5.

7.3.5 Cooling and heating coil of the air handling unit

The heating and cooling coils of the AHU model are dry bulb temperature controlled and are modelled using the bypass factor approach: the air flow is divided into a bypass fraction and a conditioned fraction, where the latter is assumed to reach the average temperature of the liquid filled heating or cooling coil. In cooling situations this fraction exits the coil at saturated conditions. The coil temperature is determined iteratively in order to obtain the desired outlet temperature of the remixed air flow. By using this approach, the latent cooling energy is also included in the result of the cooling coil.

In order to speed up simulation time, the water circuits of the coils are not taken into account in the simulation model: Table 7.7 shows a 60% increase in computational time when the water circuits are modelled. This avoids an iteration during the simulation run to match the air and water side heat transfer rates.

Simulating the heating and cooling coil with this simplified bypass method speeds up the simulation, but does not bound the performance of the coils to any physical constraint. In reality, however, the coil design with its fin

Table 7.8: Heating and cooling load

Heating power w/o reheat capacity	(W/m ²)	24
Heating power w reheat capacity	(W/m ²)	26
Cooling power North zone (peak at 17h)	(W/m ²)	30
Cooling power South zone (peak at 17h)	(W/m ²)	31
Cooling power South zone (8h-18h average)	(W/m ²)	23
Cooling power South zone (24h average)	(W/m ²)	13

configuration and its number of rows limits the achievable temperature rise or drop by the coil. To take this into account, a limit ventilation supply set point $T_{vs,lim}$ is determined from a simplified method based on the ByPass Factor (BPF) approach which was originally defined by Carrier. Using this method, the coil leaving air conditions (e.g. T_{s3} for the cooling coil) are calculated by mixing a saturated air stream, flowing through the coil, with an unconditioned air stream, which is bypassed. The details of design and control of both sensible and dehumidifying coils are explained in Appendix C.

This simplified method is incorporated in the building controller to determine $T_{vs,min}$. If $T_{vs,min}$ is higher than $T_{vs,set}$ requested by the controller, the simplified coil model is limited to this $T_{vs,min}$ set point. In this way, a simulation method is obtained using a simplified coil model and speeding up simulation time, while taking into account physical limitations of the coils.

7.4 Heating load and cooling load

In this section the heating and cooling load calculations of the 2-zone office building are elaborated. Although it is known from the analysis of the CCA transient behaviour (Chap. 4) and from Lehmann et al. [87] and Schiavon et al. [116] that the heat transfer at the water side and at the room side are decoupled, the steady-state heating and cooling load calculation still provides a relevant starting point for the design of the system. The results of these calculations are summarized in Table 7.8.

The heating load is calculated according to EN12831 [41] and the cooling load according to VDI2078 [139]. Since both methods are based on look-up tables, the parameters and boundary conditions used might deviate from the values applied in the detailed simulation model of the office zone. Nevertheless, the

results serve as reference values characterizing the building.

Following the EN12831 procedure, the infiltration rate for the typical office building is 0.2 ACH/h. In the simulation model it is assumed that this value reduces to 0.05 if the ventilation system, with a surplus of supply air, is working. An extra reheating capacity is also provided in EN12831, and is set to the minimal value of 2 W/m^2 . This is actually a building-and-system dependent parameter, which has been proven to be very high for CCA (see Chap. 4, Sec. 4.5.10).

The cooling load calculation according to VDI2078 is performed to resemble as much as possible the standard working conditions of the typical office zone. The following deviations, however, remain:

- Occupation time is from 7 AM-12 PM and 2 PM-5 PM, while from 8 AM-12 PM and 1 PM-6 PM in the simulation model to correspond more to modern office occupation.
- Convective heat from appliances is 40% (84% in the simulation model, details are presented in App. D).
- Infiltration rate is 0.05 ACH/h. VDI2078 refers to low summer wind speed and the high air tightness of modern building façades to limit the influence of infiltration on the cooling load. Therefore, in contrast with the heating load calculation, the infiltration rate with the ventilation system on is used here.

Part I from VDI2078, concerning the cooling load calculations of buildings with cooled walls and ceilings was not used in this calculation.

7.4.1 Heating load

Figure 7.6(a) shows the heating load energy balance for the reference office building ($d_{insul} = 0.1 \text{ m}$; $U_{glass} = 1.1 \text{ W/m}^2\text{K}$; $U_{frame} = 2.2 \text{ W/m}^2\text{K}$; $T_{amb} = -10^\circ\text{C}$) where the window is responsible for the major part of the heat loss. Improving the U-value of the window glass and frame — $U_{glass} = 0.8 \text{ W/m}^2\text{K}$; $U_{frame} = 1.8 \text{ W/m}^2\text{K}$ — lowers the overall heat loss with approximately 10%. This is shown by the markers in Fig. 7.6(b). The effect of doubling the insulation thickness to 0.2 m is similar (10%).

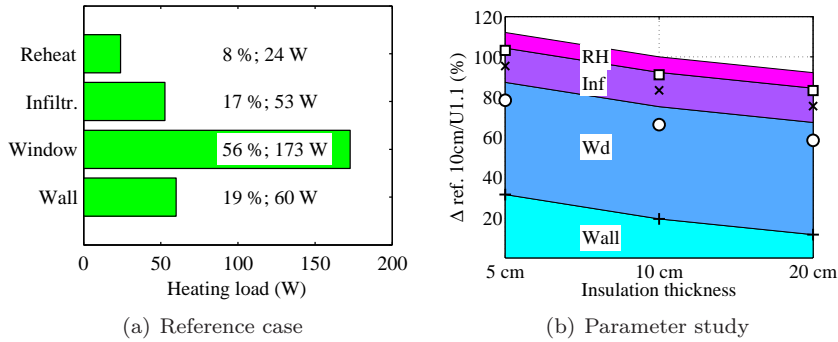


Figure 7.6: Heating load analysis for the South zone of (a) the reference case with $d_{insul} = 0.1\text{ m}$; $U_{glass} = 1.1\text{ W/m}^2\text{K}$; $\dot{Q}_{heat,tot} = 315\text{ W}$, $\dot{q}_{heat,tot} = 26\text{ W/m}^2$ and (b) a parameter study as a function of the insulation thickness and the glass type ($U_{glass} 1.1, U_{frame} 2.2$: area; $U_{glass} 0.8, U_{frame} 1.8$: markers)

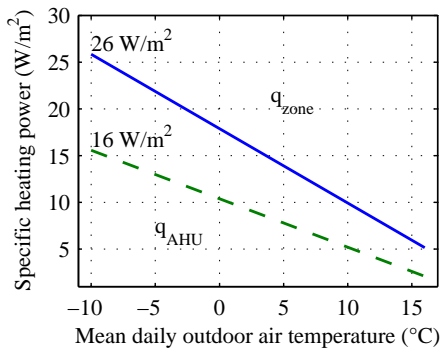


Figure 7.7: Zone and AHU heat load as a function of the average outdoor air temperature

The heating coil in the AHU needs to heat the air from the temperature at the outlet of the heat recovery (7.1°C) to the supply temperature T_{vs} of 20°C . For the reference case this requires 16 W/m^2 . Figure 7.7 shows the required heating load both for the zone and for the AHU as a function of the average outdoor temperature \tilde{T}_{amb} . The maximum CCA value of 26 W/m^2 is below the maximum attainable heating power of 63 W/m^2 as mentioned at the start of this chapter.

7.4.2 Cooling load

The cooling load analysis is presented in Figure 7.8. The reference case assumes a building with the standard building parameters (Tables 7.2 and 7.3) and scheduled user behaviour corresponding to the values presented in Sec. 7.5. This is the situation typically used for sizing the HVAC system. The ‘no solar shading’ case is equal to the reference case except for the absence of solar shading. The ‘stochastic user behaviour’ case represents the real working conditions of the office building by assuming a mix of stochastically behaving users [101].

In the reference case (Fig. 7.8(a)), the cooling load is dominated by the internal gains (more than 80%). App. D provides detailed information on how the internal gains are defined. Solar gains are small due to the well performing solar shading of the building. Without solar shading (Fig. 7.8(b)), the solar gains part becomes equal to the gains from people and lighting. With the average stochastic user values (Fig. 7.8(c)), the cooling load lowers with 30% compared to the reference case, which is mainly due to the reduction of lighting gains and gains from people. The radiative gains are higher than in the reference case, meaning that the solar shading is blocking less solar radiation when controlled by the users compared to the automated case.

Fig. 7.8(c) summarizes the results of the 3 cases, the reference case, the case without solar shading and the user behaviour case, relative to the reference case.

Since these results agree with the permissible heat gains for CCA buildings as presented by Lehmann et al. [87], it can be concluded that the proposed design of the office building is suitable for CCA. For reference, the table from Lehmann et al. [87], is copied in Table 7.9. It shows the maximal permissible heat gains (solar + internal) for a carpet and a raised floor, as a function of the allowed daily temperature drift.

Should extra cooling power be required to compensate for occurring peaks, the air handling unit could assist. However, this depends on the design of the cooling coil as elaborated in App. C. Fig. 7.9 presents the achievable extra cooling power as a function of the ventilation supply temperature ($\dot{q}_{AHU} = \dot{m}_{vs} c_{p,a} (T_{vs} - T_{ia})$) and for two typical air flow rates (class 1 and class 2 according to EN15251 [44]). The 36 m³/h pers case is the default value of the 2-zone office building.

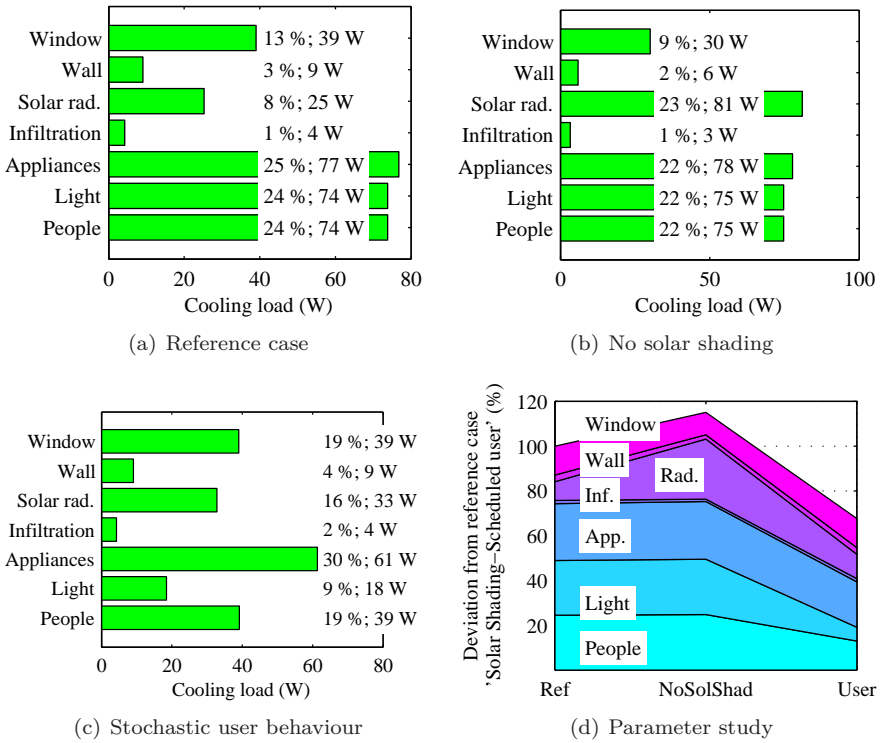


Figure 7.8: Cooling load analysis for
 (a) the reference case: Automated solar shading; scheduled user behaviour, $\dot{Q}_{c,tot} = 302 \text{ W} - \dot{q}_{c,tot} = 25 \text{ W/m}^2$,
 (b) the ‘no solar shading’ case: $\dot{q}_{c,tot} = 29 \text{ W/m}^2$,
 (c) the ‘stochastic user behaviour’ case: $\dot{q}_{c,tot} = 17 \text{ W/m}^2$ and
 (d) a comparison of the 3 cases: solar shading (Ref) - no solar shading (NoSolShad)- userbehaviour (User).

Table 7.9: Maximal permissible total heat gains in space for different room temperature amplitudes and floorings (copied from Lehmann et al. [87])

Room temperature amplitude (°C)	Maximum permissible total heat gain (W/m ²)	
	Carpet	Raised access floor
3	33-34	27
4	41-44	36-37
5	50-53	42-45

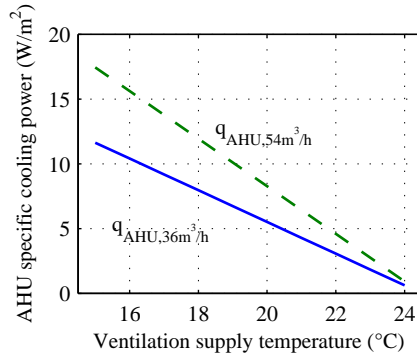


Figure 7.9: Available power from the air handling unit: air flow rate of 36 m³/hpers (solid line) and 54 m³/hpers (dashed line)

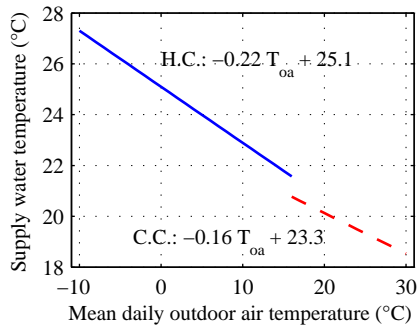


Figure 7.10: Heating (H.C.) and cooling (C.C.) curves for the office zone

7.4.3 Heating curve and cooling curve

Knowing the required heating and cooling loads of the office zone, and knowing the thermal resistance of the CCA, the heating and cooling curve for the CCA can be derived. The result is presented in Fig. 7.10.

7.5 Parameters of the 2-zone office building model

For the other parameters of the 2-zone office building model, a detailed overview and background of these data are presented in App. D. A short overview of those parameters is given in Table 7.10.

Table 7.10: Parameters of the 2-zone office building model

Parameter	Value
Occupancy rate	1 person per 10 m ²
Sensible heat gains from people	7.5 W/m ²
Latent heat gains from people	5.5 W/m ²
Appliances heat gains	7.8 W/m ²
Lighting heat gains	7.5 W/m ²
Zone thermal capacitance	5 times the air thermal capacitance.
Convective heat transfer values of floor and ceiling	correlations of Awbi and Hatton [9]
Radiative heat transfer coefficient	5.6 W/m ²
Infiltration rate	0.05 ACH during AHU-operation and 0.2 ACH outside those hours
Ventilation rate	36 m ³ /h pers (EN15251 [44][Class II])

Table 7.11: Scheduled operating hours of the typical office model

	Operating hours
office hours	8 AM-6 PM
people's attendance	8 AM-12 PM, 1 PM-6 PM
Appliances	8 AM-12 PM, 1 PM-6 PM
Lights	8 AM-6 PM
Ventilation	7 AM-7 PM

The different operating hours are presented in Table 7.11.

7.6 Automated solar shading

The South zone of the office building is equipped with an automated solar shading system (shading factor = 25%). Simplifying the detailed heat transfer phenomena of solar radiation through glass, with the high quality windows having a g-value of 36% and with the solar shading having a g-value of 25%, the overall g-value for the window with solar shading is $0.36 \times 0.25 = 0.09$ (9%).

The solar shading has a controller with hysteresis which lowers the shading device when $\dot{q}_{sol} > 250 \text{ W/m}^2$ on the vertical South surface. It is raised again at a value of $\dot{q}_{sol} < 150 \text{ W/m}^2$. The North zone has no solar shading.

7.7 Conclusions

In this chapter, a 2-zone office building model was presented which will serve as the test building for the parameter study of a conventional feedback controller in Ch. 8. Furthermore, this model is used as a data generator for the procedure to estimate the parameters of a simplified building model in Ch. 9. This simplified building model is used in the formulation of a Model based Predictive Controller (MPC) in Ch. 10.

Chapter 8

CCA conventional control

8.1 Introduction

The case study presented in Ch. 2 demonstrated that changing the controller settings for room air temperature feedback control, has a major impact on the resulting thermal comfort and energy use. Non adapted settings lead to inefficient use of energy, as observed in measurements as well as in simulation results. Although a conventional on-off feedback control strategy is far from optimal in controlling CCA, analysing the controller performance subjected to different settings, yields valuable information on the transient behaviour of CCA and on the required features of a CCA controller. Furthermore, the mutual influence of controller settings and the robustness of controller performance is presented in this chapter.

8.2 Controller performance criteria

A TRNSYS model of the 2-zone office building (presented in Ch. 7) is used to evaluate the controller performance, which is assessed in terms of both thermal comfort and energy use criteria. These criteria and the simulation settings are shortly discussed in this section.

8.2.1 Thermal discomfort

Thermal discomfort is assessed in terms of the ‘Predicted Percentage of Dissatisfied’ or PPD (See Sec. 6.2.6). Comfort class B is used as motivated previously, setting $PMV_{limit} = 0.5$ and $PPD_{limit} = 10\%$. The PPD is weighted over an observed period as described in EN15251 [44, Annex F]: every time step a weighting factor $wf = PPD_{actual}/PPD_{limit}$ is calculated if the PMV exceeds the limit of 0.5. Then, the thermal discomfort DC is described as the number of PPD-hours per zone: $PPDh = \sum wf \times timestep$. Although EN15251 provides a guideline to determine how much deviation from the thermal comfort criteria can be tolerated, for simplicity, this is not used in the analysis of the results.

To clarify the value of PPDh: 10 PPDh could mean e.g. that during 5 h 20% of the people is dissatisfied instead of the allowed 10%. A PPD of 20% corresponds to approximately 1 K above or below the comfort set point.

8.2.2 Energy use

To make a correct comparison between the different energy flows in the system, the energy use is converted to specific primary energy use E (in kWh/m²). In the reference case using ideal instantaneous heating and cooling (Sec. 8.3), the heat and cold are assumed to be produced by a condensing gas boiler and a low-temperature chiller respectively. Similarly, for the CCA, the heat and cold to the AHU’s are at temperature levels imposing the use of a condensing gas boiler and low-temperature chiller. On the other hand, the CCA themselves require only low exergy heat and cold, and can be fed by a reversible air-cooled heat pump. Converting the end energy use to primary energy is therefore the only correct way to analyse the different heat flows. The primary energy conversion factors are $\eta_{gas} = 1$ for natural gas for the gas boiler and $1/\eta_{elec} = 2.5$ for electricity for the heat pump, chiller, pumps and fans.

A distinction is made between:

- Zone conditioning $E_z = E_{zh} + E_{zc} + E_{zp}$
 - Zone heating E_{zh} : boiler or heat pump
 - Zone cooling E_{zc} : high temperature or low temperature chiller
 - Circulation pump E_{zp}

- Air conditioning $E_a = E_{ah} + E_{ac} + E_{af}$
 - Air heating E_{ah} : boiler (heating coil of the AHU)
 - Air cooling E_{ac} : low temperature chiller (cooling coil of the AHU)
 - Fan E_{af}
- Appliances E_{app}
- Light E_l

For the remainder of this chapter, since only CCA control is analysed, the E_z value will be used to compare the simulation results for different control strategies on controller settings. The AHU energy use is assumed not to be affected by the CCA control and is presented for the reference case in Sec. 8.3.3.

8.2.3 Heating-cooling switching

Together with these two primary performance indicators, the simultaneous occurrence of heating and cooling in 1 day provides information on the switching behaviour between heating and cooling of the concrete slab. As indicated in Chapter 4, this leads to a huge amount of energy not being used to condition the room. A higher number of days per year for which heating-cooling switching occurs, indicates a bad controller performance (see Ch. 2).

8.2.4 Data sign convention

The thermal energy values are positive for heating (q_h , heat transferred from water to CCA) and negative for cooling (q_c , heat transferred from CCA to water). When primary energy is presented, all values are positive.

8.2.5 Meteorological data

The Typical Meteorological Year (TMY) for Uccle, Belgium, is used in the simulation model.

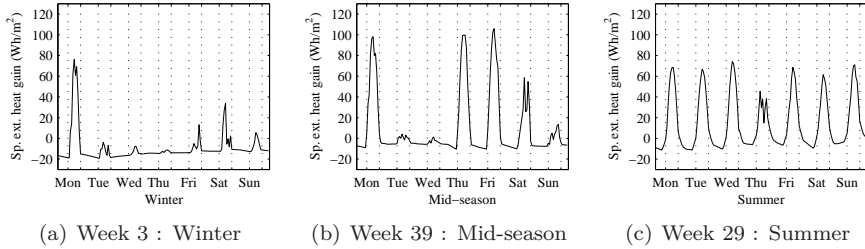


Figure 8.1: Specific static external building heat gains for winter (a), mid-season (b) and summer (c) situation.

8.2.6 Typical week

In order to analyse daily behaviour of the building, three typical weeks are investigated: a winter, mid-season and summer week (see Fig. 8.1). They are selected from the yearly data by calculating the specific static external heat gains to the building $\dot{q}_{ext,sp}$, according to Eq. 8.1. Then, the winter week is selected as the week with the lowest and the summer week with the highest $\sum_{weekdays} \dot{q}_{ext,sp}$. The mid-season week is the week with the largest difference between minimal and maximal daily maximum of $\dot{q}_{ext,sp}$, also during weekdays.

$$\dot{q}_{ext,sp} = \frac{\left(U_{av} (A_w + A_{wd}) + \frac{1}{R_{inf}} \right) (T_{oa} - T_{ia}) + \dot{q}_{sol} A_{wd} g_{wd}}{A_z} \quad (8.1)$$

8.2.7 Heating and cooling production power

In the first part of the analysis (Sec. 8.5), the available power of the water heating and cooling production units, is set to unlimited. This means that at all times the requested set point temperatures can be reached. In Sec. 8.8 the impact of limited production power is evaluated.

8.3 Reference cases: Zero Discomfort and Zero Energy Use

8.3.1 Zero Discomfort Reference: Ideal heating and cooling

As a first reference, the 2-zone office building is simulated in TRNSYS with an ideal, 100% convective heating and cooling emission system with unlimited power, as provided by the TRNBUILD building model generator [123]. As such, the heating and cooling energy flows are directly coupled to the zone air temperature node of the model. If the zone air temperature T_{ia} at the end of the time step is within the heating and cooling set points, the zone is free floating. In the other case, when heating or cooling is necessary, the exact amount of power is supplied in order to make $T_{ia,t} = T_{set,t}$ at the end of time step t .

The operative temperature T_{op} needs to be controlled within the comfort band limits $T_{op,min} - T_{op,max}$. Between 9 PM and 6 AM, night setback is applied: the comfort band is enlarged with $\pm 5^{\circ}\text{C}$. Solar shading of the South zone windows is active. The ventilation air temperature is controlled at $T_{op,min}$ throughout the year and operates from 7 AM to 7 PM.

The detailed implementation of the ideal heating and cooling in TRNBUILD is presented in App. B.

The Zero Discomfort Reference case ensures that the office zone is perfectly kept within the thermal comfort boundaries (during occupation hours, 8 AM - 6 PM on weekdays), as shown in Fig. 8.2 (a),(c) and (e) for the South zone, with the lowest possible energy use. Table 8.1 shows the resulting yearly energy use for the South and the North zone individually and for the 2-zone building. The primary energy consumption E represents the minimal energy needed to keep the 2-zone office building within the thermal comfort limits.

8.3.2 Zero Energy Use Reference: no heating and cooling

Since the performance of the control strategies will be evaluated in a discomfort-versus-energy use diagram, the complement of the Zero Discomfort Reference, is the free floating building without any heating or cooling. Ventilation is available, but only with the heat recovery being active, without the heating

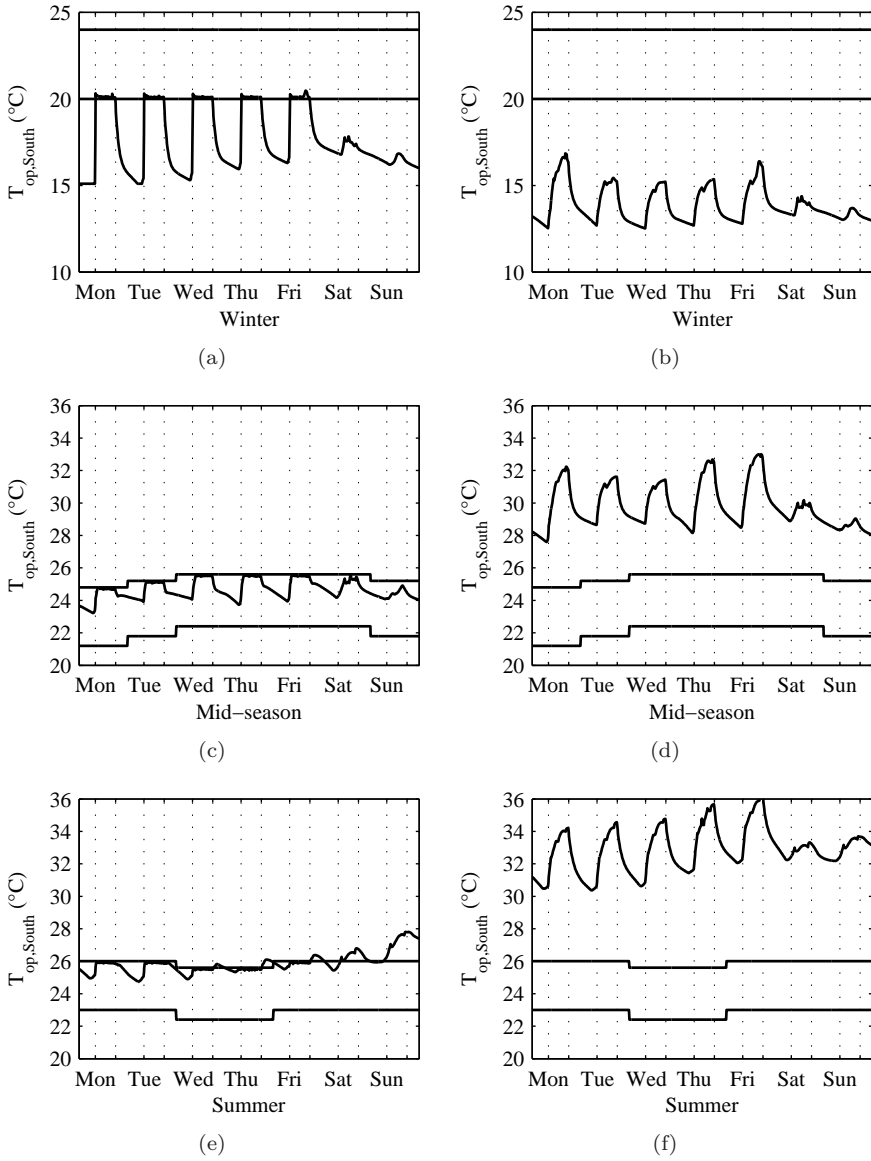


Figure 8.2: Operative temperature of the South zone for the Zero Discomfort Reference, (a), (c) and (e); for the Zero Energy Use Reference, (b), (d) and (f). The thermal comfort range is indicated, as well as the 8 AM - 6 PM occupation time during weekdays.

and cooling coil being active. The solar shading is activated. Fig. 8.2 (b)-(d) and (f) show the operative temperatures for the South zone of the office building for the three typical weeks.

8.3.3 Reference cases results

The Zero Energy and Zero Discomfort results are presented in Table. 8.1 and show the limits against which the results of the CCA building simulation will be compared. The discomfort in the Zero Energy Use case is mainly caused by too high operative temperatures. The high PPDh clearly indicates the need for comfort conditioning.

Table 8.1: Energy use for the reference ideal heating and cooling and discomfort for the free running 2-zone office building

Ideal heating/cooling		South	North	Total
q_h	kWh/m ² (thermal)	4.3	7.1	5.7
q_c	kWh/m ² (thermal)	18.4	18.1	18.3
Pump	kWh/m ² (elec)	1.3	1.5	1.4
E_z	kWh/m ² (prim)	23.3	26.4	24.8
AHU heating/cooling		South	North	Total
q_h	kWh/m ² (thermal)	6.6	6.8	6.7
q_c	kWh/m ² (thermal)	0.5	0.5	0.5
Fan	kWh/m ² (elec)	4.1	4.1	4.1
E_a	kWh/m ² (prim)	17.7	17.9	17.8
Free running building		South	North	Total
PPDh/m ²		11855	11662	11759

The yearly heat balance for heating and cooling the building shows a higher cooling demand compared to the heating demand for the ideal heating/cooling: $q_h - q_c = -12.5$ kWh/m², while the AHU with heat recovery needs more heating than cooling on an annual basis: $q_h - q_c = 6.2$ kWh/m². This will have an impact for the cases where a ground coupled heat pump-direct cooling (HPDC) system is used to supply heat and cold. However, if the ventilation energy could also be supplied by the HPDC system, this would be beneficial for the thermal balance of the ground. Without heat recovery or heat recovery with a lower efficiency, the total balance approaches unity closer than with efficient heat recovery (these results are not shown here). Of course this benefit should be

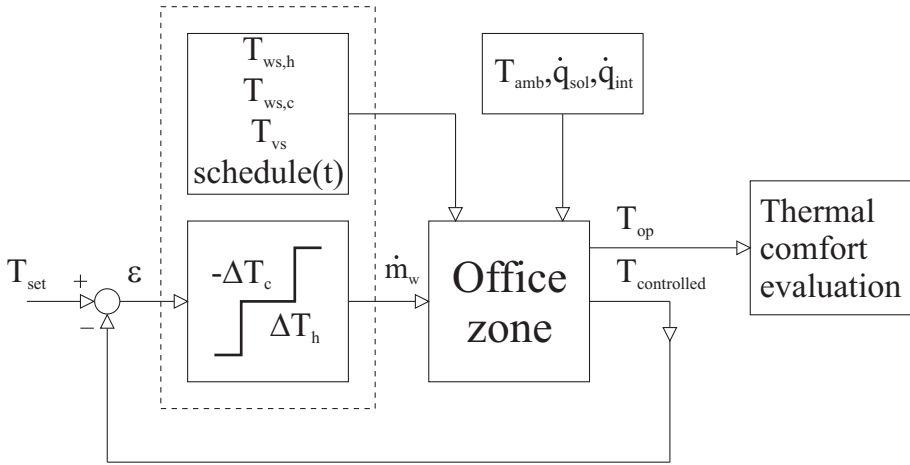
held against the increase of total energy required. Since the production system is not modelled in detail in this work, this topic falls beyond the scope of this work.

8.4 Conventional controller

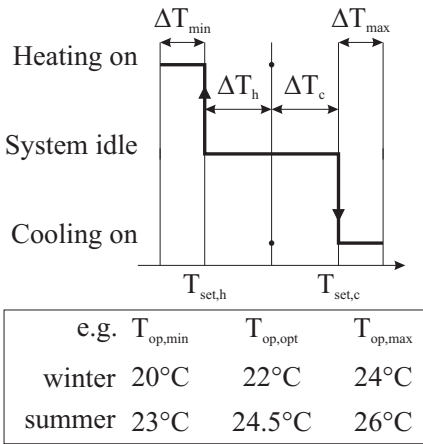
In this section, an on-off feedback control strategy for the CCA system is analysed, based on a continuously measurable temperature $T_{controlled}$, thus not dependent on pump operation (Fig. 8.3). It uses the heating and cooling curve (HCC) from the 2-zone office building (see Chap. 7) to determine the water supply temperature as a function of the running mean outdoor temperature (this temperature is defined in App. A). The following terminology is used:

- The sensor measures a temperature (= **controlled variable** $T_{controlled}$) and transmits this value to the controller.
- The **controller** compares this value to the set point T_{set} and generates a corrective action to the controlled devices. In this case a 3 stage On-Off controller is used (Fig. 8.3):
 - Heating on if $T_{controlled} < T_{set} - \Delta T_h$ or $\epsilon = T_{set} - T_{controlled} > \Delta T_h$
 - No action if $T_{set} - \Delta T_h < T_{controlled} < T_{set} + \Delta T_c$ or $-\Delta T_c < \epsilon < \Delta T_h$
 - Cooling on if $T_{controlled} > T_{set} + \Delta T_c$ or $\epsilon = T_{set} - T_{controlled} < -\Delta T_c$
- The **controlled devices** are the CCA ceiling and floor.
- The **control agent** is the heating and cooling water supplied to the CCA, of which the supply temperature ($T_{ws,hsv}$ and $T_{ws,csv}$) can vary (*sv* stands for *setpoint value*).
- The **set point** is the desired value of the controlled variable (temperature $T_{controlled}$). The band ($\Delta T_h + \Delta T_c$) around this T_{set} defines the heating and cooling setpoint: $T_{set,h}$ and $T_{set,c}$.

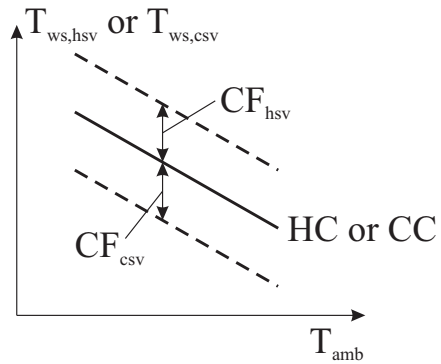
The controller parameters used in the current simulation study are listed in Table 8.2. The base heating and cooling curves are derived from the results of the heating and cooling load calculations (see Fig. 7.10). These calculations



(a)



(b)



(c)

Figure 8.3: (a) General block diagram of the 3 stage On-Off feedback controller, (b) adaptation of the temperature set point value ($\Delta T_h/\Delta T_c$) and (c) adaptation of the heating/cooling curve (CF_{hsv}/CF_{csv})

Table 8.2: Overview of controller settings

Controller settings	
Heating curve	$T_{ws,hsv} = -0.22T_{rm} + 25.1 + CF_{hsv}$
Cooling curve	$T_{ws,csv} = -0.16T_{rm} + 23.3 + CF_{csv}$
CF_{hsv} / CF_{csv}	0 / 0; 3 / -3; 6 / -6
$T_{controlled}$	T_{ia} (indoor air); T_{op} (operative) T_s (concrete ceiling surface); T_c (concrete core)
T_{set}	$T_{op,opt} = 22^\circ\text{C}$ (winter); 24.5°C (summer)
T_{max}/T_{min}	$T_{op,max}/T_{op,min}$
$\Delta T_{min}/\Delta T_{max}$	0 / 0 +1 / -1 0 / -1 0 / -1

determine the required thermal power as a function of the reference outdoor temperature. Using the CCA model as shown in Sec. 3.3, this thermal power is correlated with a required supply temperature. This results in the heating/cooling curve. These can be adapted by using correction factors CF_{hsv} and CF_{csv} , leading to the requested set point value (sv) for the water supply temperature T_{ws} for heating and cooling. T_{rm} is the running mean outdoor temperature (see App. A).

Since $T_{max} - T_{min}$ varies from winter (4°C) to summer (3°C), ΔT_{min} and ΔT_{max} are used as controller parameter instead of ΔT_h and ΔT_c :

$$T_{set,h} = T_{set} - \Delta T_h = T_{min} + \Delta T_{min} \quad (8.2)$$

$$T_{set,c} = T_{set} + \Delta T_c = T_{max} - \Delta T_{max} \quad (8.3)$$

$$(8.4)$$

The controlled temperatures are all continuously measurable variables in the control system, i.e. even with a non operating circulation pump, they can provide data to the building controller. 4 different controlled temperatures are evaluated: T_{ia} (indoor air), T_{op} (operative), T_s (concrete ceiling surface) and T_c (concrete core). These controlled temperatures are chosen because they represent the temperature path from zone air to CCA water. The ceiling surface is used in stead of the floor surface as reference for the CCA surface temperature. The drawback of these controlled temperatures is the position dependency of their reading: installation of the sensors has to be carefully accomplished so

that their reading gives a representative value. Other controlled temperatures like water supply or return temperature are dependent on pump operation, which is not included in this analysis. However they do not have the drawback of being position dependent.

Additional to these parameters and the corresponding settings, night setback is incorporated: $(T_{op,min} - 5)$ and $(T_{op,max} + 5)$ from 9 PM until 6 AM. The ventilation air temperature is controlled at $T_{op,min}$. The ventilation schedule is fixed: ON from 7 AM to 7 PM respectively. The night setback schedule is extended compared to the office hours to allow pre-heating and post-cooling of the building. However, this night setback setting will influence the peak powers required by the system, as shown at the end of this chapter, where a case is presented without night setback.

To clearly distinguish between the different controller settings, the following terminology is used hereafter:

- $T_{controlled}$: CONTR = T_{ia}, T_{op}, T_s, T_c
- CF_{hsv} / CF_{csv} : CF = 0/0, 3/-3, 6/-6
- $\Delta T_{min}/\Delta T_{max}$: SET = 0/0, 1/-1, 0/-1, 0/-2

8.5 Heating/cooling curve controller performance

8.5.1 Variation of all controller settings

Fig. 8.4 summarizes the simulation results for all combinations of controller settings as presented in Table 8.2. It can be seen that there exists a trade-off between energy use and thermal discomfort. A detailed analysis of the different subsets of these data reveals the underlying trends related to the different controller parameters. Generally, there is no difference in trends between the South zone, the North zone or the results for both zones together, due to the high quality solar shading. So, in the following results, as in Fig. 8.4, only the results for the South zone are presented.

There are a number of controller settings for which energy use is comparable to the reference point. Although the zero discomfort level is never achieved, with a minimum of around 40 PPDh, some controllers come very close.

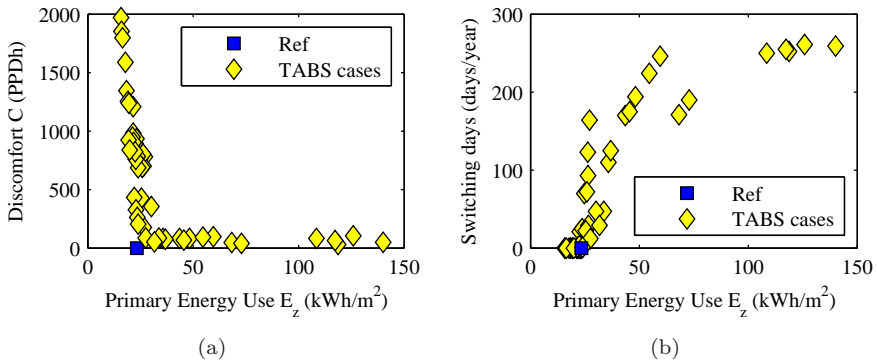


Figure 8.4: South zone energy use against (a) thermal discomfort and against (b) the number of switching days for all the controller settings investigated (see Table 8.2)

As indicated by the data for simultaneous heating and cooling in Fig. 8.4(b), an increase in energy use is directly related to the amount of days for which heating and cooling occur during the course of the same day (called ‘switching days’). This confirms the results from the analysis with the analytical transient CCA model in Sec. 4.5.9 and allows to draw a first and maybe most important conclusion for a CCA controller:

Heating and cooling of CCA during 1 day is impermissible.

8.5.2 Sensitivity to heating and cooling set points $T_{set,h}$ and $T_{set,c}$

Fig. 8.5 presents the impact of the heating and cooling set points $T_{set,h}$ and $T_{set,c}$. Fig. 8.5(a) clearly shows how CCA takes advantage from the fact that the cooling is switched on ‘before’ the comfort limit is reached. This is certainly true for T_s and T_c as the controlled temperatures. E_z is very sensitive to varying the heating and cooling setpoints $T_{set,h}$ and $T_{set,c}$; when T_{ia} and T_{op} are the controlled temperatures (\circ and \diamond in Figs. 8.5(a) and 8.5(b)). Shifting the heating set point (SET=+1/-1) does not result in an improvement (Fig. 8.5(b)). While DC decreases only slightly, E_z increases for (SET=+1/-1) compared to (SET=0/-1). The E_z -increase can be explained by the number of switching days for both settings, as presented in Table 8.3.

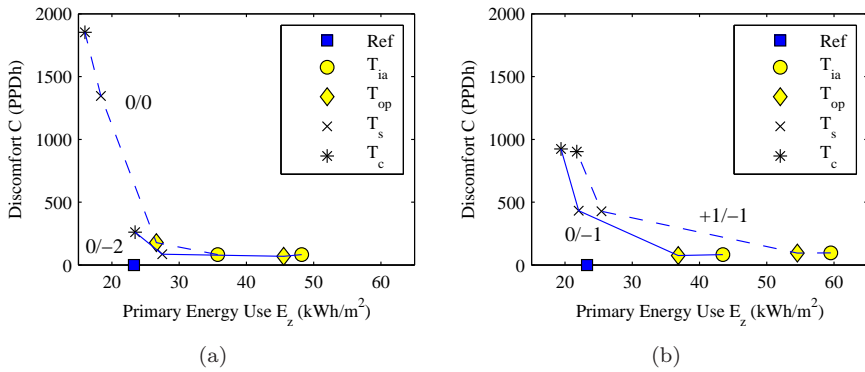


Figure 8.5: Sensitivity to heating and cooling set points $T_{set,h}$ and $T_{set,s}$ for the South zone. (a) (SET=0/0) and (SET=0/-2), (b) (SET=+1/-1) and (SET=0/-1)

HCC-correction factor (CF=+3/-3)

$T_{controlled}$: (○) T_{ia} , (◇) T_{op} , (×) T_s , (*) T_c

Table 8.3: Number of days with heating and cooling in 1 day, for heating/cooling curve correction factor (CF=3/-3).

SET/CONTR	T_{ia}	T_{op}	T_s	T_c
0/0	110	29	0	0
1/-1	246	224	22	1
0/-1	170	125	0	0
0/-2	194	175	12	0

These conclusions are equal but not as clearly observable for the heating and cooling curve correction factors (CF=0/0) and (CF=6/-6).

This means that shifting the heating setpoint upwards is not advisable for this cooling dominated building, since it will increase the risk of switching days, as shown in the (SET=1/-1)-row of Table 8.3. Shifting the cooling setpoint downwards is beneficial, but only when T_s or T_c are controlled. In general, controlling T_{ia} or T_{op} increases the risk of having switching days.

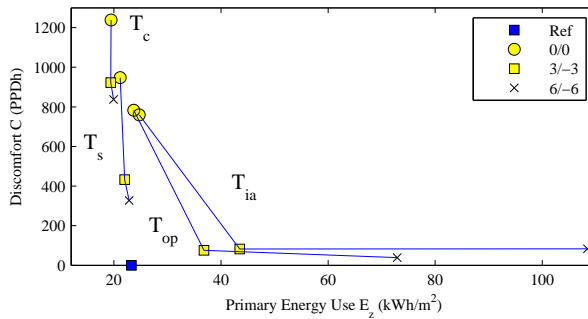


Figure 8.6: South zone energy use E_z against thermal discomfort DC for (SET=0/-1) and HCC-settings CF=0/0, 3/-3 and 6/-6

8.5.3 Sensitivity to $T_{controlled}$

Fig. 8.6 shows the results for the heating and cooling set points (SET=0/-1). The sensitivity of the controller performance to the 4 controlled temperatures T_{ia} , T_{op} , T_s and T_c is presented. Also, the influence of the HCC-settings on the results is shown (CF=0/0, 3/-3, 6/-6). This figure allows to derive conclusions regarding the HCC-controller performance as a function of $T_{controlled}$ and the heating/cooling curve.

Concerning the controlled temperatures, again, controlling T_{ia} and T_{op} is very sensitive to the heating/cooling curve settings. Due to the thermal inertia of the concrete floor, the CCA response to controller signals is characterized by a significant time delay. This is confirmed by a high switching behaviour when the air temperature T_{ia} is used as the controlled temperature: 163 days on average for the T_{ia} -points presented in Fig. 8.6, against no days with heating/cooling switching when the concrete core temperature T_c controlled. From this and the previous paragraph, it can be concluded that a CCA controller with T_{ia} or T_{op} as controlled temperature is not robust.

The reason why (CONTR= T_c) performs badly regarding thermal comfort is due to the fact that the temperature T_c reacts much faster to a heating or cooling action of the water supply, while the heat transfer towards the room air takes extra time. The circulation pump will therefore switch on and off too frequently. This was already mentioned in Chapter 4, where frequent pump switching resulted in a low amount of heat loaded or extracted from the CCA

(see Fig. 4.23)¹. This can be countered by a higher heating/cooling curve setting (Fig. 8.6): for both (CONTR= T_s) and (CONTR= T_c) the controller with (CF=3/-3) and (CF=6/-6) reduces thermal discomfort, while the energy use is hardly affected. The highest gain can be achieved with the change to the (CF=3/-3) setting of the heating/cooling curve.

Fig. 8.6 shows that using the CCA surface temperature T_s is promising for achieving low thermal discomfort at a low energy cost. Using (CF=3/-3) decreases DC without increasing E_z significantly. Increasing the HCC to (SET=6/-6) has a limited influence for T_s as controlled temperature. Physically, T_s is positioned ‘in the middle’ between T_{op} , the temperature used to evaluate thermal comfort, and T_{ws} the temperature at which the heat or cold is supplied. ($T_s - T_{ia}$) is the driving temperature difference for the CCA-to-room heat transfer. Therefore, keeping T_s at a setpoint temperature, means keeping the thermal power at a required level.

8.5.4 Heating/cooling curve correction

Modifying the heating and cooling curve, has an important impact. Still observing Fig. 8.6, for the (CF=0/0)-setting, being the initial heating and cooling curve calculated from the heating/cooling load, the controller does not perform well.

This (CF=0/0)-setting results in the highest thermal discomfort for all controlled temperatures (○ on Fig. 8.6). (CF=3/-3) improves thermal comfort (□ on Fig. 8.6), against a relatively small increase of E_z . (CF=6/-6) shows a rather small further decrease of DC for all controlled temperatures.

For T_{ia} and T_{op} as controlled temperature, an important increase of E_z is observed for the (CF=6/-6)-setting. This conclusion confirms the results in Chapter 4. Fig. 4.24 showed that with a higher heating temperature (lower for cooling), the required heat input to the room was obtained more quickly, but against a higher energy use. Moreover, since switching days will occur more frequently with (CF=6/-6), the amount of ‘unused’ energy is much larger (see also Fig. 4.31). For T_s and T_c as controlled temperatures, switching days will occur less or not at all, since the CCA are not ‘overloaded’, as addressed in Sec. 8.5.3.

¹TRNSYS does NOT take into account the effect of flow propagation on the heat transfer (see Sec. 4.4)

8.5.5 Illustration of the HCC correction effect

As an illustration of the effect of the heating and cooling curve CF-setting, the detailed results for a Thursday in September are used. This Thursday is one of the days in the selected mid-season week of Sec. 8.2.6 with a high solar radiation. The effect of controlling T_{op} is compared with controlling T_s for three different HCC-correction factors (CF=0/0, 3/-3, 6/-6). Also, the impact of the cooling setpoint $T_{set,c}$ (SET=0/-1, 0/-2) is illustrated for this day.

Firstly, the results (T_{op} , $T_{controlled}$ and \dot{q}_w) of having T_{op} as the controlled temperature are presented in Figs. 8.7(a)-(c)-(e). The vertical lines show the night setback window. The horizontal lines in Fig. 8.7(a) show the thermal comfort band ($T_{op,min} - T_{op,max}$), while the horizontal lines in Fig. 8.7(c) are $T_{set,h}$ and $T_{set,c}$, the temperature setpoints for heating and cooling. The (SET=0/-2)-setting is used here. Several observations can be made from this graph:

- Cooling from the previous day results in a lower starting T_{op} for the lower cooling curves (CF=3/-3 and CF=6/-6), since the concrete slab contains a large residual amount of cold which cools down the building after office hours. Changing the night setback schedule might solve this.
- As a consequence, heating starts up in the beginning of the day for (CF=3/-3 and CF=6/-6), which has almost no direct effect on the room air temperature. This limited effect was already observed while analysing the results of the analytical transient model in Sec. 4.5.9. Moreover, overheating is enhanced by this heating period, once heat gains come up.
- Cooling starts during the day for all CF-settings investigated. However, the (CF=6/-6)-setting is able to cool down the CCA more quickly, and stops cooling first.
- The (CF=6/-6)-setting has, using a high cooling power, loaded too much cold in the CCA. It will cool down the room too much, requiring a heating period at the end of the day.

Secondly, looking at the same results for the CCA surface temperature T_s as the controlled temperature, Figs. 8.7(b)-(d)-(f) show that for this setting the response of the controlled temperature T_s to a controller action is much faster. When the heating/cooling curve is set to (CF=+3/-3) or (CF=6/-6), the

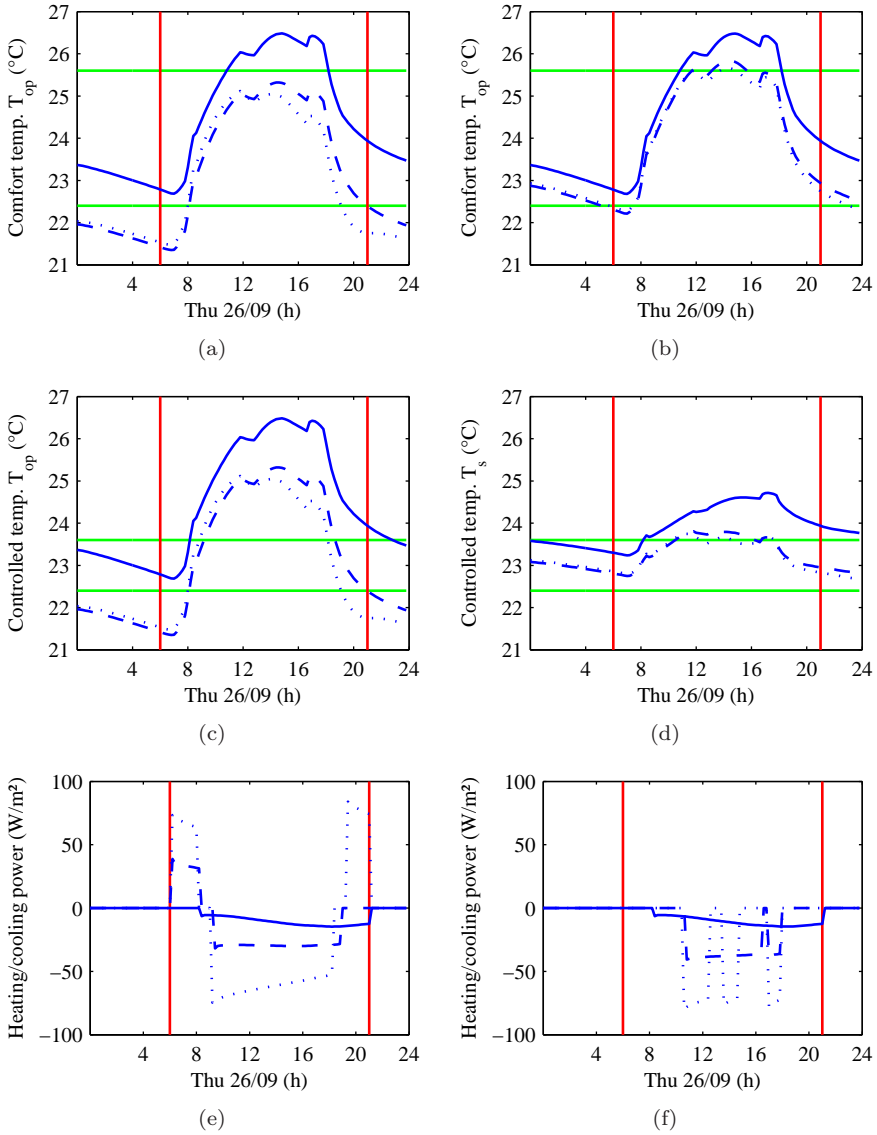


Figure 8.7: South zone T_{op} , $T_{controlled}$ and \dot{q}_w for Thursday of the mid-season week.
 (a)-(c)-(e): T_{op} as controlled temperature,
 (b)-(d)-(f): T_s as controlled temperature,
 Controller settings: SET=0/-2; CF=0/0: solid line; CF=3/-3: dashed line; CF=6/-6: dotted line,
 Vertical lines indicate the night setback window,
 (a)-(b) Horizontal lines: $T_{op,min} - T_{op,max}$ range,
 (c)-(d) Horizontal lines: $T_{set,h} - T_{set,c}$ range

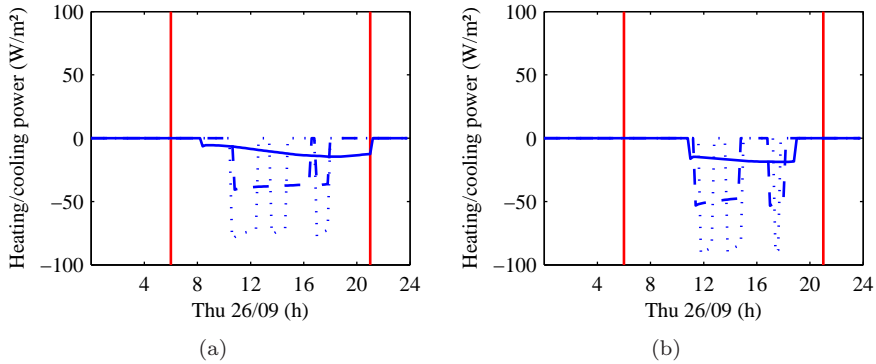


Figure 8.8: South zone thermal power \dot{q}_w for Thursday of the mid-season week.
 (a) Heating/cooling setpoint SET=0/-1,
 (b) Heating/cooling setpoint SET=0/-2 (= Fig 8.7(f)),
 Controller settings: T_s as controlled temperature,
 CF=0/0: solid line; CF=3/-3: dashed line; CF=6/-6: dotted line,
 Vertical lines indicate the night setback window.

system is able to keep T_s close to the required temperature $T_{set,c}$, as shown in Fig. 8.7(d). For the (CF=6/-6)-setting, Fig. 8.7(f) shows that this even results in intermittent pump operation, which has proven to be an energy efficient way to transfer heat to the CCA, based on the results from the transient analysis in Ch. 4. When controlling T_s combined with the heating/cooling curve settings (CF=3/-3 and CF=6/-6) and the setpoint setting (SET=0/-2), the CCA will react fast enough to compensate heat losses or loads in the office zone, resulting in a lower yearly thermal discomfort, as was shown in Fig. 8.6.

Fig. 8.7(f) also shows that the switching behaviour is no longer existing. This controller avoids to cool down the CCA too much, which results in a higher temperature at the beginning of the next day.

Thirdly, the effect of the cooling setpoint is presented in Fig. 8.8. In the (SET=0/-2)-case cooling is ON for a longer time, but using a lower power than for (SET=0/-1). This is caused by the lower concrete core temperature, due to the fact that cooling starts up earlier, and by this avoiding a high temperature difference between T_{ws} and T_c , as shown in Fig. 8.9). For (SET=0/-2) the yearly mean T_c equals 21.7°C, while this is 22.2°C for the (SET=0/-1)-setting, a difference of 0.5°C.

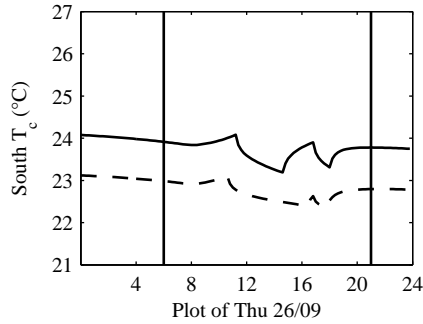


Figure 8.9: The influence of the cooling set point $T_{c,set}$ on the temperature of the concrete core T_c : SET=0/-1 (full line) and SET=0/-2 (dashed line) Controller settings: T_s as controlled parameter, CF=3/-3

8.5.6 Conclusions of the controller performance evaluation

Analysing the performance of the conventional controller learns that T_c or T_s should be used as the controlled temperature to avoid switching between heating and cooling during 1 day. This switching leads to a large portion of ‘unused’ energy.

The cooling should be switched ON at a controlled temperature which is lower than the maximum allowed operative temperature in the zone. This enables the CCA to build up cooling power and at the mean time ensures that the CCA are at a temperature lower than the zone to have cooling power stand by. This is often referred to as the ‘selfregulating effect’: $\dot{q}_{CCA-room} \propto (T_s - T_z)$, so controlling T_s implies controlling $\dot{q}_{CCA-room}$. If T_z reaches T_s , heat transfer from CCA to room stops. For heating, the same principle applies.

The heating/cooling curve (HCC) should be set higher than the value derived from the heating and cooling load calculations to enable a faster ‘loading’ of the CCA. However, a too high HCC (+6/-6 in this case) does not improve the controller performance. On the contrary, the risk of overloading exists, resulting in switching between heating and cooling in 1 day. Moreover, the required thermal power is higher for this setting.

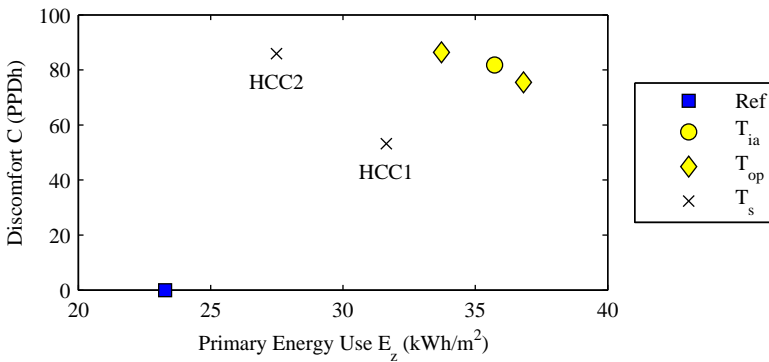


Figure 8.10: The controller performance for the ‘best’ controller settings

8.6 The best HCC controller settings

8.6.1 Controller performance

Zooming in into the simulation results of the HCC controller with different settings results in Fig. 8.10. As mentioned previously, controlling T_s results in the best controller performance. However, also T_{ia} appears in the collection of controllers performing close to the reference (see Table 8.4). This is surprising, regarding the fact that this point has 193 switching days with both heating and cooling. Although it seems a good combination, taking T_{ia} as controlled temperature has a big risk of overheating or -cooling the CCA, which was also addressed by Lehmann et al. [87]. The (CONTR= T_{ia})-setting is very sensitive to variations in the system’s temperatures. For example, taking a water supply temperature setting (CF=6/-6) instead of (CF=3/-3) results in an increase of E_z by 82%, while for T_s , this is only 11%. To a smaller extent, this is also true for T_{op} as the controlled temperature.

8.6.2 Heat/cold production power

Although the simulation results closest to the reference results are obtained with a high heating and a low cooling curve (CF=6/-6), the required production power is very high compared to the more moderate HCC-setting (CF=3/-3), as shown in Fig. 8.8. This leads to a high investment cost for the heat/cold

Table 8.4: The best controller settings

	CONTR	CF	SET	E_z kWh/m ² (prim)	C PPDh
Ref				23.3	0
HCC1	T_s	6/-6	0/-2	31.6	53
HCC2	T_s	3/-3	0/-2	27.5	86
HCC3	T_{op}	6/-6	0/0	33.7	86
HCC4	T_{op}	3/-3	0/-1	36.8	75
HCC5	T_{ia}	3/-3	0/0	35.7	82

production units. To reduce production power, it seems best not to supply too high or too low water temperatures. This consideration would make HCC2 from Table 8.4, with the moderate HCC-setting (CF=3/-3), the best controller setting.

Although here the transient CCA behaviour is analysed, this conclusion corresponds to the steady state analysis in Sec. 3.2.9, where a COP_{CCA} was defined, which was highest for $T_{ws} = 28^\circ C$ and decreased for higher water supply temperatures. Although derived in a completely different way, that optimal $T_{ws} = 28^\circ C$ is indeed higher than the base point of the CCA heating curve: $25.1^\circ C$.

The HCC2 controller will be referred to as the ‘modified-HCC controller’.

8.7 Evaluation of the modified-HCC controller

8.7.1 Controller behaviour

Comparable to Fig. 8.2, Fig. 8.11 shows the operative temperature of the South zone for the controller setting HCC2, together with the corresponding heating and cooling power for the typical winter, mid-season and summer weeks. In the winter situation a large heating power is required with this setting. Due to the internal gains, the operation time in winter will be shorter than in a summer situation. A more realistic production power would lead to longer operation times. In the summer situation, it appears that undercooling exists, leading to a heating need at the start of Tuesday and Friday.

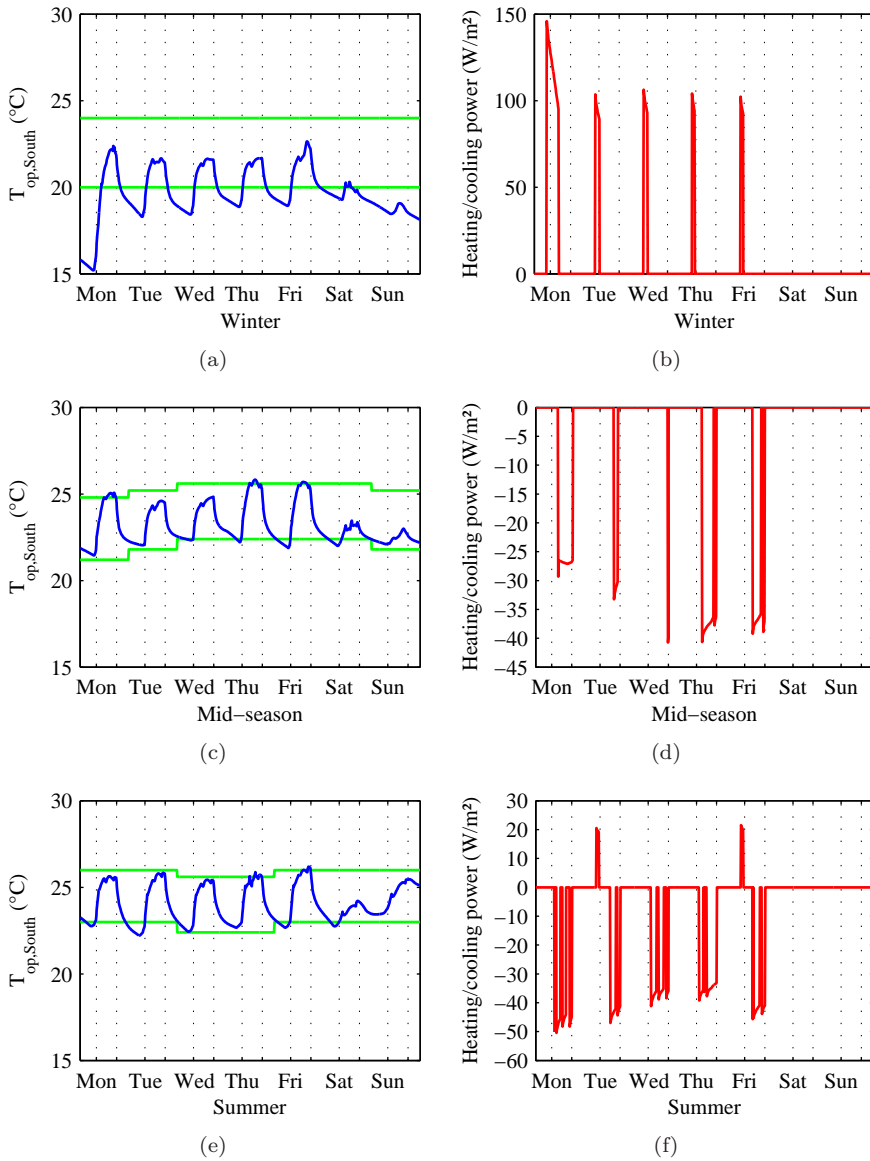


Figure 8.11: South zone results with the modified-HCC controller: Operative temperature and heating or cooling power (water circuit) (a)-(b) for a typical winter week, (c)-(d) for a typical mid-season week and (e)-(f) for a typical summer week. The thermal comfort range is indicated, as well as the 8 AM - 6 PM office hours. Note the different scales of the Y-axis for heating/cooling power.

8.7.2 CCA modified-HCC controller versus non-CCA reference case

In order to analyse the operation of the CCA controlled by the modified-HCC controller, Fig. 8.12 shows the difference between the modified-HCC controller and the Zero Discomfort Reference case for three characteristic zone temperatures T_{op} , T_s and T_c . Remember (Sec. 8.3) that this reference case has ideal heating and cooling and results in the lowest energy use to maintain thermal comfort and does not thermally activate the building mass. Therefore, this comparison illustrates the different thermal behaviour of a CCA building compared to a non-CCA building.

In Fig. 8.12, a negative ΔT_{op} (solid line) means that the operative temperature is lower in the CCA building compared to the reference case. E.g. in the winter period (Fig. 8.12(a)), where $T_{op,Ref} = T_{op,min}$, a negative ΔT_{op} means that $T_{op,CCA}$ falls below the allowed comfort band. In the summer period (Fig. 8.12(c)), where $T_{op,Ref} = T_{op,max}$, a positive ΔT_{op} means that $T_{op,CCA}$ exceeds the allowed comfort band.

In winter time, ΔT_{op} is negative ($T_{op,CCA} < T_{op,non-CCA} = T_{op,min}$) in the first hours of Monday. As a consequence, heating starts up, as shown in Fig. 8.11(b), and makes the CCA rise in temperature. After office hours, the heat loaded during the first hours is sufficient to make ΔT_{op} rise to over 3°C (in the CCA-case, the zone is 3°C warmer during the night than in the reference case, see Fig. 8.12(a)). This means that, whereas the reference controller stops heating at the end of the day, the heat loaded in the CCA keeps the zone temperature at a higher level for the modified-HCC controller. This operation is repeated for the next days, although to a minor extent. In general the concrete core temperature T_c , shown with the dashed line in Fig. 8.12(a), is $3\text{-}6^\circ\text{C}$ higher than for the reference case.

In the mid-season week Tuesday and Wednesday are days with a low external heat gain $\dot{q}_{ext,sp}$ (see Sec. 8.2.6). This results in little cooling during these days, as shown in 8.11(d). 8.12(b) shows that, for Tuesday and Wednesday, the CCA temperature T_c (dashed line) increases compared to the reference case. For Thursday and Friday, having high external heat loads, cooling has to start again to load extra cold into the CCA in order to decrease the CCA temperature again and to have sufficient power to transfer cold to the office zone. A more intelligent control strategy would be able to anticipate to this inter-day difference of the building loads. Globally, T_c is kept lower than in the

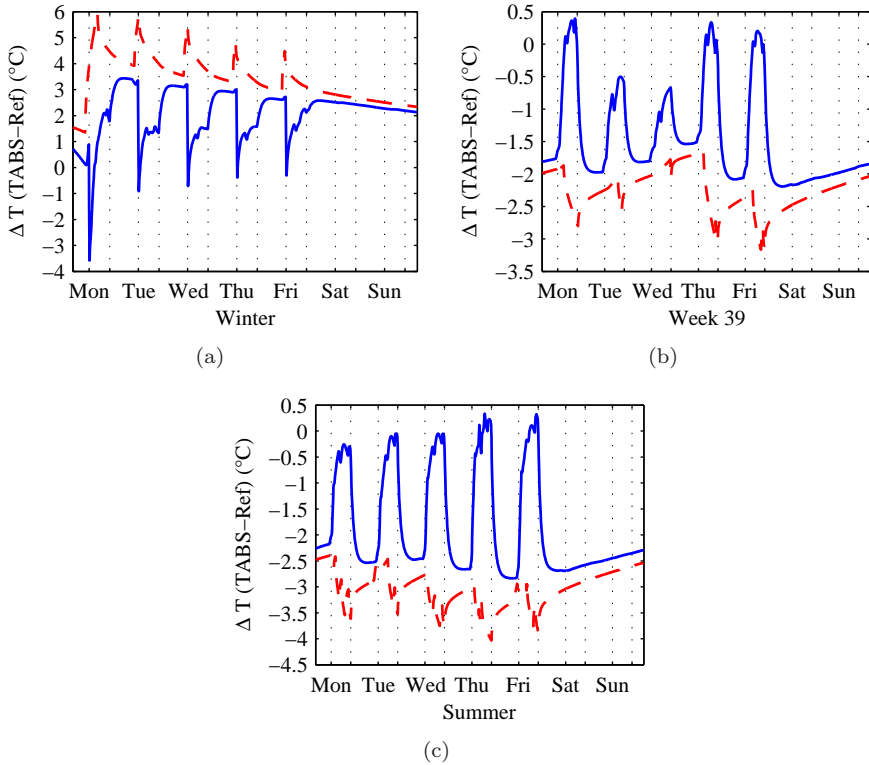


Figure 8.12: Comparison between the CCA building with the modified-HCC controller and the non-CCA building with the ideal heating/cooling (Zero Discomfort Reference case). South zone results with the difference of the operative temperature ($T_{op,CCA} - T_{op,Ref}$) (-) and of the concrete core temperature ($T_{c,CCA} - T_{c,Ref}$) (- -)

reference case, but not more than 3°C .

In summer (Fig. 8.12(c)), the CCA are kept $3\text{--}4^{\circ}\text{C}$ lower than for the reference case. Compared to this reference case, the cold loaded into the CCA is able to decrease the operative temperature T_{op} during the night. A similar effect was observed when heating the CCA in the winter situation.

In winter time, T_{op} is in general higher than for the reference case, but the difference remains within the $\Delta T = 4^{\circ}\text{C}$ of the winter thermal comfort band. In summer time, T_{op} is in general lower than the reference case, but again here, the difference remains within the $\Delta T = 3^{\circ}\text{C}$ of the summer thermal comfort band. This is a very important remark, since it means that, where the reference case kept T_{op} at the bounds of the comfort band, and therefore at a maximum difference with the optimal $T_{op,opt}$, with CCA T_{op} will float within the comfort band, and will be, on average, closer to $T_{op,opt}$ than in the reference case.

The fact that in wintertime the building is kept at a higher, and in summer time, a lower overall temperature, explains why the CCA requires a larger amount of energy than the reference system, even when it makes use of a heat pump and a high temperature chiller (see Table 8.4).

In general, this modified-HCC controller operates in such a way that it tries to keep the concrete temperature constantly at an elevated level: warmer in winter and colder in summer. This control behaviour should be pursued in a CCA controller.

8.8 Modified-HCC controller with limited production power

The required heating and cooling power which has to be delivered by the water circuit, is high: certainly for heating, where $\dot{q}_{h,max} = 146\text{ W/m}^2$, but also for cooling, where $\dot{q}_{c,max} = 69\text{ W/m}^2$. The heating and cooling load calculations resulted in respectively 26 W/m^2 and 25 W/m^2 .

This section investigates the impact of limited production power to the performance of the CCA system with the modified-HCC controller. In the next section, the impact of eliminating night setback is analysed. After all, the high heating peak powers occur at 6 AM, when the night setback is switched off.

In order to investigate the impact of a limited heating and cooling power on the performance of the controller, the modified-HCC controller is applied to a heat/cold production system with two different settings:

1. $\dot{q}_{h,2xdes} = 52 \text{ W/m}^2$ and $\dot{q}_{c,2xdes} = 50 \text{ W/m}^2$: a heating and cooling power limited to twice the design value.
2. $\dot{q}_{h,des} = 26 \text{ W/m}^2$ and $\dot{q}_{c,des} = 25 \text{ W/m}^2$: a heating and cooling power limited to the design value.

Fig. 8.13 presents the South zone load duration curve of the reference Zero Discomfort case and the three CCA cases: unlimited power, limited to twice the design value and limited to the design value.

Fig. 8.13(a) of the reference case, shows that, except for a few hours with a high thermal power, \dot{q}_{max} is limited to values around or below the design values.

The load duration curve of the modified-HCC controller with unlimited heating and cooling power is presented in Fig. 8.13(b). As explained previously, the maximum heating power is almost 6 times higher than the design heat load of $\dot{q}_{h,des} = 26 \text{ W/m}^2$. For cooling the maximum cooling power is almost 3 times the design value of $\dot{q}_{c,des} = 25 \text{ W/m}^2$. These high production powers would induce too high investment costs.

The reason for this difference in maximum heating ($6 \times \dot{q}_{h,des}$) and cooling power ($3 \times \dot{q}_{c,des}$) can be explained by looking at the CCA behaviour, as e.g. in Fig. 8.11. Heating starts up at the beginning of the day, when the building, and therefore also the concrete slab, is cold. On the other hand, cooling starts up when the zone temperature is increasing during the day. The difference between T_c and T_{ws} will therefore be larger for the heating situation compared to the cooling situation. Fig. 8.14 shows this temperature difference throughout the year when the heating or cooling starts up. The mean temperature difference at start for the whole year, $\overline{T_c - T_{ws}}$, is -5.9°C for heating but only 2.5°C for cooling.

The results show clearly that in order to control CCA appropriately, the available production power should be taken into account. The mutual interaction between design and control is very important in CCA buildings.

For the modified-HCC controller, the cooling power of the $\dot{q}_{2 \times des}$ -case is sufficient. This is derived from the load duration curve for cooling: Fig. 8.13(b)

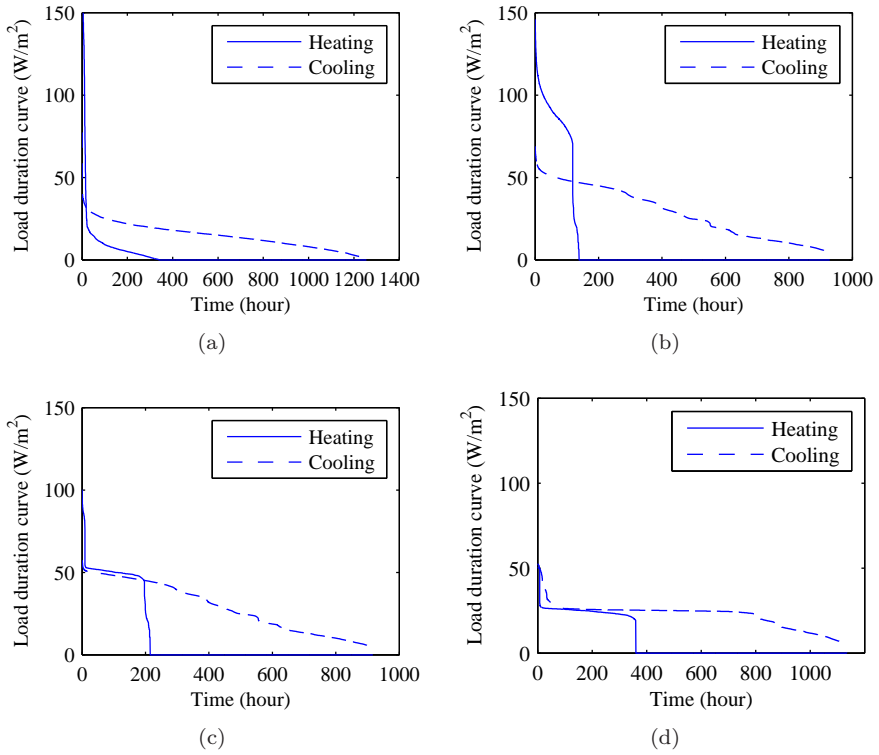


Figure 8.13: Heating and cooling load duration curve for (a) the Zero Discomfort Reference, (b) the modified-HCC controller with unlimited power \dot{q} , (c) with $2 \times \dot{q}_{des}$ and (d) with \dot{q}_{des}

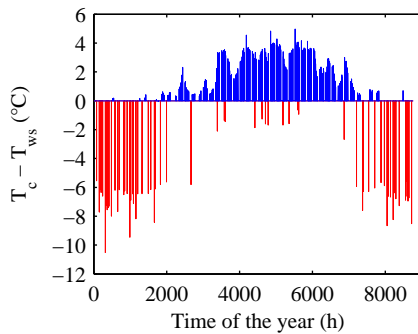


Figure 8.14: Temperature difference $T_c - T_{ws}$ at start up moments of heating (negative values) and cooling (positive values)

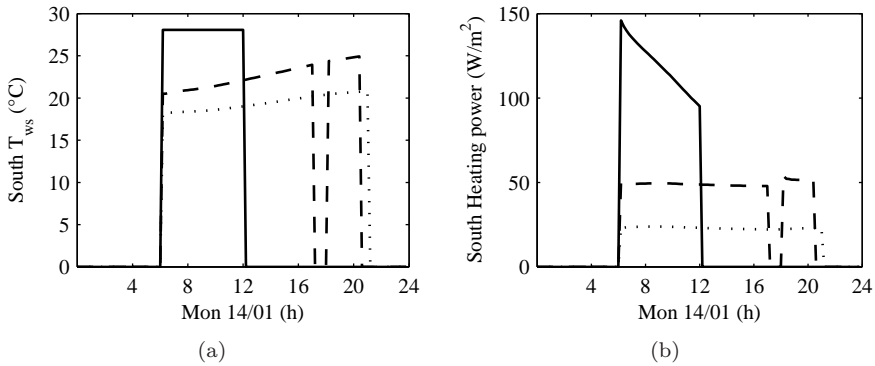


Figure 8.15: Difference between $\dot{q}_{h,des}$ (:), $\dot{q}_{h,2\times des}$ (- -) and $\dot{q}_{h,unlim}$ (-) for a typical winter day ((a) water supply temperature (the water supply set point $T_{ws,hsv} = 28^\circ C$) and (b) heating power)

and Fig. 8.13(c) are almost identical. For heating, however, this is not the case. The load duration curve for heating (Fig. 8.13(c)) is extended in time to compensate for the small heating power. If a load duration curve has a horizontal part equal to the installed power, when it is ON. This means that for those hours the production system is working at its maximum power. Heating is almost always working at its maximum power, indicating that in the heating case the production system is never able to deliver the water temperatures required by the controller.

For the \dot{q}_{des} -case, in Fig. 8.13(d), both heating and cooling power are at maximum for the most part of the operating hours. In this case, both in heating and cooling, the production system is not able to deliver the water temperatures required by the controller for the majority of the operating hours.

Fig. 8.15 shows that for the $\dot{q}_{h,2\times des}$ -case the water supply set point $T_{ws-hsv} = 28^\circ C$ is not reached anymore. This results in a longer operation time at a lower heating power. The controller performance decreases in this case, since less heating is provided compared to the $\dot{q}_{h,unlim}$ -case. The night setback switch time should be brought forward in this typical winter-Monday situation. However, the impact on the yearly thermal discomfort for the $\dot{q}_{h,2\times des}$ -case is limited (see Table 8.5), while the energy use even decreases slightly. On the other hand, limiting to the design power ($\dot{q}_{h,des}$ -case) causes the thermal discomfort to increase substantially, while the impact on the energy use is limited.

Table 8.5: Yearly energy use and maximum heating and cooling power of the South zone for the modified-HCC controller with unlimited and limited production power

	E_z kWh/m ²	C PPDh	$\dot{q}_{h,max}$ W/m ²	$\dot{q}_{c,max}$ W/m ²
\dot{q}_{unlim}	27.5	86	146	-69
$\dot{q}_{2 \times des}$	27.0	114	100	-58
\dot{q}_{des}	25.9	230	52	-50

For the case with the power limited to $\dot{q}_{2 \times des}$, the $\dot{q}_{h,max}$ -value is higher than the maximum heating production power of 52 W/m². This is caused by the alternating zone operation, which is explained in Sec. 8.9.

8.9 Alternating zone operation

When discussing the controller performance for all setting combinations in Sec. 8.6, the HCC1 option (SET=6/-6) was abandoned because of the high heating and cooling power required. Simulating the HCC1-controller with a limited power of $\dot{q}_{h,2 \times des}$ however, reveals an interesting HVAC-system behaviour. It was already mentioned in Chapter 4 that a more extreme water supply temperature was able to load heat or cold more quickly, due to a higher ΔT . The set point is reached faster. In the cooling regime, the heat gains of the South and North zone are rarely coinciding. Since the (SET=6/-6) controller setting is combined with T_s as the controlled temperature for HCC1, the setpoint is reached relatively fast.

This results in a South and North zone pump operation which do rarely coincide. Fig. 8.16(a) shows for a typical day requiring cooling, that the cooling load is alternated between South and North zone. Only around 2 PM both zones require cooling simultaneously. An important result is that, although the cooling production power is designed at 50 W/m², at times where cooling is operating for only one of the zones, this zone has the full production power at its disposal, meaning 100 W/m² for that specific zone.

The duration load curve of this HCC1 controller in Fig. 8.16(b) shows that in the case of cooling almost for 200 h the South cooling power is larger than 50 W/m², which refers to alternating zone operation. For this period, not even

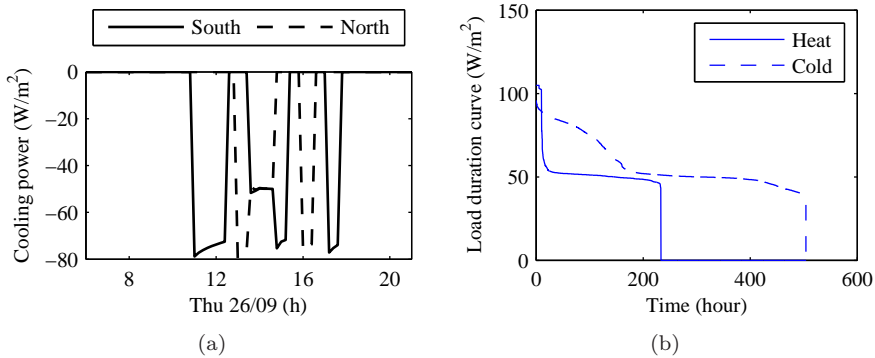


Figure 8.16: HCC1 controller performance with $\dot{q}_{2 \times des}$: (a) alternating North-South zone operation and (b) the duration load curve of the South zone

the full available power of 100 W/m^2 is required, this means that the requested set point will always be met. For heating, this load duration curve shows that almost never alternating zone behaviour occurs, because heating is typically required at 6 AM, when the night setback switches. This is the same time for both South and North zone.

The flat parts in the load duration curves are time periods in which both zones are operating and the production system is working at full power. Temperature set points are not met for these periods. For heating this appears to be almost always the case. Again, as was already derived from Fig. 8.15, the available heating power is not sufficient.

For the HCC1 controller with $\dot{q}_{2 \times des}$, the primary energy use $E_z = 29.7 \text{ kWh/m}^2$ and $C = 102 \text{ PPDh}$, which means that the energy use is slightly higher than for the modified-HCC controller (row 2 in Table 8.5) and thermal discomfort slightly lower.

8.10 Night set back settings

The modified-HCC controller still has problems due to the night set back settings. Certainly in the case of heating, switching to comfort limits at 6 AM gives rise to comfort violations and high power peaks due to the large thermal

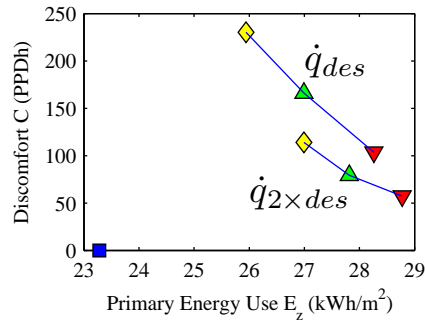


Figure 8.17: Impact of night setback settings on the controller performance for the South zone and the modified-HCC controller, for a production system sized to \dot{q}_{des} and $\dot{q}_{2 \times des}$, for a controller with night setback (\diamond), reduced night setback (\triangle) and no night setback (\blacktriangledown).

capacity of the CCA. The impact of these night setback settings is evaluated by comparing:

1. 9 PM - 6 AM night set back: original settings
2. 9 PM - 3 AM night set back: advancing the morning switch
3. No night setback

The primary energy use and thermal discomfort results are shown in Fig. 8.17 for the modified-HCC controller and for two cases: 1) the production power limited to $\dot{q}_{2 \times des}$, twice the design value, and to \dot{q}_{des} , the design value for the production power. These results show that omitting night setback clearly improves thermal comfort, but against a small increase in energy use.

Table 8.6 shows that the improved thermal comfort is mainly caused by a reduction of the number of hours when the operative temperature is too low. The impact on overheating is limited. This is as expected since the night setback was mainly causing problems in the heating regime. Consequently, this leads to a 20% to 30% increase in heating energy, while the impact on the cooling energy is limited to 3%-4%, respectively for $\dot{q}_{2 \times des}$ and for \dot{q}_{des} .

Fig. 8.18 shows that for a winter situation, Subfigs. (a)-(b), the impact of the night setback setting is large. When no night setback is applied, T_{op} is kept much higher and discomfort is reduced. Moreover, what is very important

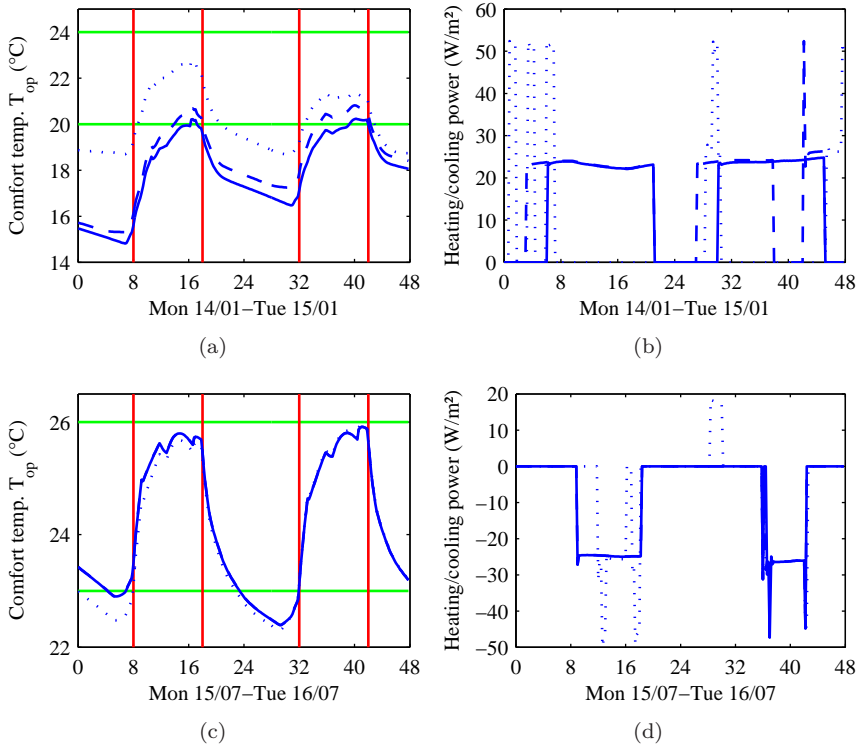


Figure 8.18: Effect of the night setback settings for the \dot{q}_{des} -case and for (a)-(b) two consecutive winter days and (c)-(d) two consecutive summer days, with (a)-(c) the operative temperature and (b)-(d) the corresponding heating power.

The horizontal lines indicate the comfort band and the vertical line indicate the office hours. NS 9 PM-6 AM: full line (—), NS 9 PM-3 AM: dashed line (- -), No NS: dotted line (...).

Table 8.6: Effect of the night setback settings on the yearly number of hours below and above the PMV-limit and the yearly thermal heating and cooling energy.

Production power	Night setback settings (NS)	Number of hours		Heating energy kWh/m ² _{th}	Cooling energy kWh/m ² _{th}
		PMV<-0.5 (Too cold)	PMV>0.5 (Too warm)		
$\dot{q}_{2 \times des}$	NS 9 PM-6 AM	240	191	10.6	26.2
	NS 9 PM-3 AM	146	174	11.3	26.6
	No NS	77	172	12.5	26.9
\dot{q}_{des}	NS 9 PM-6 AM	396	432	9.0	25.2
	NS 9 PM-3 AM	248	380	10.1	25.6
	No NS	90	343	11.9	26.1

for the sizing of the production system, the systems automatically operate by alternating between the zones. Remember that Fig. 8.18 presents the results with production sized to only \dot{q}_{des} , so a value of around 50 W/m² means that only 1 zone is operating. So, compared to the previous paragraph on alternating zone operation, this system behaviour is now achieved with \dot{q}_{des} instead of $\dot{q}_{2 \times des}$ and with a heating/cooling curve correction of (CF=3/-3) instead of (CF=6/-6), only by allowing the system to operate the whole night.

For cooling, in Figs. 8.18(c)-(d), the impact of omitting night setback is very limited. T_{op} is reduced slightly and alternating zone operation is available, but not always. For Tuesday 16/07 in Fig. 8.18(d), the \dot{q} -pattern is identical for all three night setback-settings. Moreover, heating starts up shortly around 28 h because the system is constantly working within the narrow temperature band.

This difference between heating and cooling is evidently caused by the fact that the highest heat loss occurs during the night, while the highest heat gains occur during the office hours. So, applying night setback or not, affects heating and not so much cooling.

This reflects also in the load duration curve. Fig. 8.19 shows the load duration curve of the 6 AM-9 PM night setback and of the no-night setback setting, both for heating and cooling. The cooling load duration curve is hardly affected by the night setback setting. For heating however, the impact is very large. With night setback, shown by the full line in Fig. 8.19(a), the system operates constantly at its maximum power of $\dot{q} = 26$ W/m², which means that both zones operate simultaneously. Without night setback however, shown by the dashed line in Fig. 8.19(a), the system also operates at maximum power, but

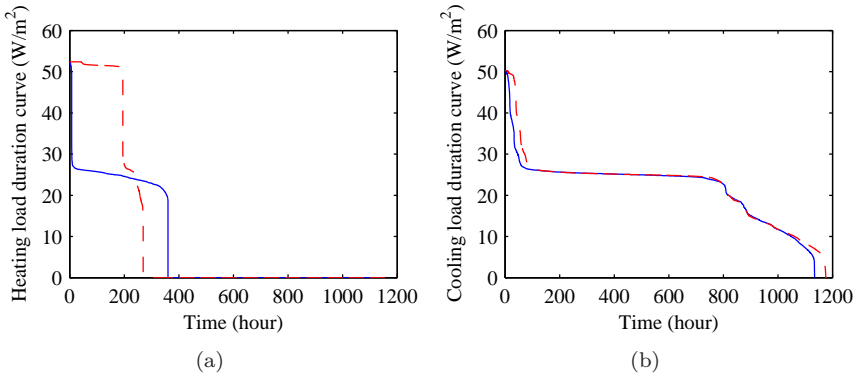


Figure 8.19: Load duration curve of (a) heating and of (b) cooling for the modified-HCC controller with 9 PM-6 AM night setback (—) and without night setback (---)

with only 1 single zone operating for the most part of the hours (where $\dot{q} = 52 \text{ W/m}^2$).

The fact that the system, both in heating and cooling, is constantly working at its thermal power limits, means that this modified-HCC controller, without night setback, is working at its maximum performance. Improving the controller performance will require a completely different control strategy.

8.11 Modified-HCC controller without solar shading

If the solar shading of the South zone is omitted, the results of the CCA building are disastrous. The number of PPDh of the South zone is multiplied by 16, while the cooling primary energy use increases with 70% and the maximum required cooling power with 45% (Table 8.7). This clearly illustrates that:

It is a prerequisite to control or prevent the solar gains of the office zones.

Table 8.7: Modified-HCC controller performance for the South zone with unlimited heating and cooling power and with and without solar shading

	E_z kWh/m ²	C PPDh	$\dot{q}_{h,max}$ W/m ²	$\dot{q}_{c,max}$ W/m ²
Solar shading	27.5	86	146	-69
No solar shading	45.8	1416	142	-100

8.12 Conclusions

The controller settings have a large impact on the required heat and cold production power, thereby proving the important mutual interaction between the design of a CCA building and the chosen control strategy.

Inappropriate control settings result in switching between heating and cooling in the same day, which on its turn results in an energy use increase. This switching behaviour has to be avoided in CCA control by taking the concrete surface or core temperature as the controlled temperature and by avoiding a too high heating curve and a too low cooling curve.

The behaviour of the HCC controller with the best energy and thermal comfort performance comes down to keeping the concrete temperature at a constant level in order to provide enough thermal power: higher in winter and lower in summer, but in both cases not too much deviating from the required comfort temperature, otherwise the self-regulating effect of CCA is lost and subcooling or overheating might occur.

The best controller performance is achieved with a 3°C higher heating curve and a 3°C lower cooling curve, together with the CCA ceiling surface temperature as the controlled temperature, and by starting up cooling 2°C lower than the maximum comfort temperature.

The night setback analysis implies that night setback is absolutely required when heating with CCA, but not beneficial when cooling.

The conclusions of Ch. 4 are confirmed in this chapter, namely that using high/low water temperatures to supply the CCA, results in a faster reaction, but with more heat stored or extracted from the slab, and therefore risking overheating or undercooling of the office zone.

A lower CCA core temperature is also beneficial for the required cooling power.

A colder concrete slab results in a smaller temperature difference between the concrete core temperature T_c and the water supply temperature T_{ws} . Therefore, a smaller production power. A similar reasoning applies to the heating regime, but, as mentioned, too high/low CCA temperatures should be avoided to prevent overheating or undercooling of the zone.

The choice of $T_{controlled}$ determines the pump-on-off times: by controlling the indoor air temperature T_{ia} , the reaction to a heating and cooling action is too slow, leading to a continuous pump operation. This will increase overheating or -cooling of the CCA. When controlling the concrete core temperature T_c however, the system reacts too quickly on a heating or -cooling action, as a result of which the CCA will not be loaded enough. Controlling the CCA surface temperature T_s seems to be a good compromise.

For heating, since on average the temperature difference between water and concrete is larger than for cooling, the required heating power must be larger than the cooling power, regardless of the outcome of the heating/cooling load calculation. It is concluded that $\dot{q}_h = 3 \times \dot{q}_{h,des}$ and $\dot{q}_c = 2 \times \dot{q}_{c,des}$ are advisable guidelines. This was already addressed in Sec. 4.5.10, where a design guideline is presented based on the Bi-numbers of the CCA.

Solar shading is a prerequisite to achieve thermal comfort with CCA.

In general, the controller's action must make sure that the CCA is continuously at a higher temperature when heating and a lower temperature when cooling. The fact that the building is kept at a higher overall temperature in winter and a lower in summer, explains why CCA requires a larger amount of primary energy than the reference system, even when it makes use of a heat pump and a high temperature chiller.

Looking at the heating and cooling load duration curves and taking in mind both South and North zone, the fact that the system, controlled without night setback, is constantly operating at full thermal power, means that this conventional feedback controller is working at its limits with the presented modified-HCC controller without night setback. In order to improve the controller performance even further, a control strategy is required which can take the state of the building, the limitations of the heating and cooling system and the future heat losses and gains into account to determine the optimal controller settings. This is addressed in the next two chapters.

Chapter 9

Simplified CCA-building model

9.1 Introduction

The detailed analysis of the conventional HCC controller of Ch. 8 revealed some important features of operational CCA behaviour, such as the effect of the large time constant and of the limited heating and cooling power but also the high peak load that is required to operate CCA. To cope with this problem, the controller should determine a future input profile for e.g. the water supply temperature T_{ws} and the water flow rate \dot{m}_w for which thermal comfort is achieved at minimal energy cost throughout the hours of occupation, while taking into account the CCA thermal properties. A Model based Predictive Controller, or MPC, is a candidate for this task. However, an MPC requires a simple but accurate thermal model of the office zone and its loads to calculate an optimal control profile. This chapter presents the methodology which is followed to derive such a simplified model. The objective is to assess the impact of the model structure and of the data set used for parameter estimation on the accuracy of this simplified model. Subsequently, in the next chapter, this model will be used to assess the added value of an MPC-based CCA operation.

The model generation and parameter estimation approach in this chapter is structured as follows. The simplified building models are Resistance-

Capacitance (RC) models, which have been widely used in building simulation [34, 91, 83, 21, 12], thereby illustrating their applicability. The order of these models ¹ should be limited in order to obtain a feasible and robust MPC-structure. Low order models result in a reduced computation time, which enables the use of receding horizon or other feedback mechanisms in the MPC-controller [90]. Two RC-model structures, a 2nd order and a 4th order model, both based on a simplified representation of the thermal processes inside a zone, are proposed. They represent one zone of the 2-zone office building, which was described in Chapter 7. The initial guess for the model parameters is based on the known building geometry and on insight in the heat transfer modes in a building zone. To avoid influence of measurement errors and to ensure the controllability of the different inputs and disturbances, the detailed TRNSYS model of the 2-zone office building is used to generate identification and validation data for the parameter estimation procedure. Using this approach, the white-box model, having parameters determined by physics, turns into a grey-box model, which has the same structure, but with parameters which are not a priori defined.

The model parameters are estimated using 5 distinct identification data sets, with different levels of information content in the excitation signal. The first group of 3 data sets is obtained with ideal, fully measurable and controllable input variables and perfectly measurable output variables. The second group of 2 data sets contains inputs which are still perfectly measurable but not controllable and, again, output variables which are perfectly measurable. The results of the first group are interesting in applications where a detailed building model is available. This is often the case for larger buildings for which there is a tendency towards simulation assisted design. The results of the second group are useful for on-line parameter estimation of the building during operation, either to fine-tune the parameters of the model identified off-line during step 1, or to start from scratch if no prior model was available.

The two model structures, the initial parameter set and 5 estimated parameter sets result in a set of 12 distinct models for which the model quality is assessed by comparing the root-mean-squared error for each of the identification data sets.

¹The expression ‘model order’ refers to the number of nodes (thermal capacitances C) in the model.

9.2 White box building model

In this work, the white-box approach is used as a starting point for model construction. As already presented in the chapter on CCA frequency analysis (Ch. 5), the model should incorporate the response of the building zone to 3 disturbances (ambient temperature T_{amb} , solar radiation \dot{q}_{sol} and internal gains \dot{q}_{int}) and to 2 control variables (water supply temperature T_{ws} and ventilation supply temperature T_{vs}).

9.2.1 Simplified CCA model structure

The CCA model is further simplified compared to the investigated model reduction in Sec. 5.4.4. The parallel heat flow path to respectively the room above and below the slab of the 2nd order model of that section, is transformed into 1 heat flow path in this 1st order CCA model (Fig. 9.1). Although, the admittances and transmittances will deviate even more from the 19th order model of Sec. 5.4.4, this approach is chosen in order to obtain a low order building model.

The parameters of the 1D-model in Fig. 9.1(c) are linked to the parameters of the 2D-model in Fig. 9.1(a) by:

$$R_a^{-1} = \frac{R_1}{2} + \frac{R_2}{2} \quad (9.1)$$

$$R_b^{-1} = \left(\frac{R_1}{2} + \frac{1}{A_1 h_1} \right)^{-1} + \left(\frac{R_2}{2} + \frac{1}{A_2 h_2} \right)^{-1} \quad (9.2)$$

$$C = C_1 + C_2 \quad (9.3)$$

9.2.2 Simplified building model structure

Constructing a T_{ra} -model (as is done in TRNSYS) still requires considerable effort in order to integrate all different zone surfaces and to attribute the occurring heat gains to the correct nodes. Especially when solar radiation plays a role or when multi-zone buildings with a more complex layout have to be controlled, this is an elaborate work. A less detailed model might as well be adequate in assessing thermal comfort and energy use, thereby increasing the

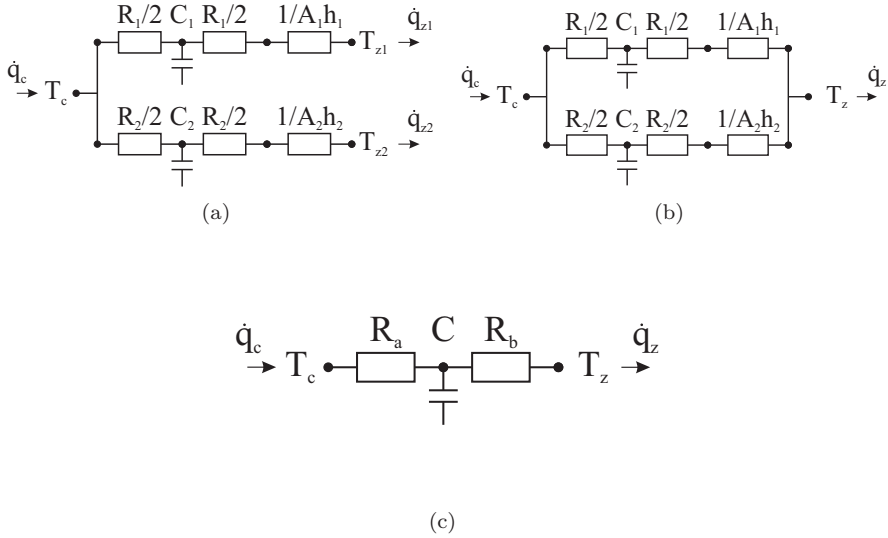


Figure 9.1: Transformation from the 2D model with (a) different room temperatures below and above and (b) equal room temperatures below and above, to (c) the 1D combined RC-network model.

simplicity and robustness of the model construction. A prerequisite for these simplified models is that they have to incorporate the 3 major disturbances T_{amb} , \dot{q}_{sol} and \dot{q}_{int} and the 2 controllable inputs T_{ws} and T_{vs} .

To take the solar radiation \dot{q}_{sol} into account, the g -value of the window has to be accounted for, which acts as a ‘resistance’ towards the \dot{q}_{sol} heat flow, in a similar way as a $1/R$ -parameter determines the heat flow caused by a ΔT . \dot{q}_{sol} is an input to the model and is defined as the incident solar radiation on the outside of the window, whereas $g_{wd}\dot{q}_{sol}$, with g_{wd} representing the solar fraction of the window, is the solar radiation passing through the office window. Because the position of the solar shading depends on the setting of the solar shading controller, its g -value is a discrete variable, which is accounted for in the MPC by preprocessing the \dot{q}_{sol} predictions (see Sec. 9.2.3).

The 2nd order model (see Fig. 9.2(a)) is an adapted version of Laret’s two-capacitances model [34]. In the latter model, the zone with temperature T_z is the first node which is coupled to the ambient temperature by a thermal resistance, representing infiltration and windows. The 2nd node is the outer wall, in between the zone node and the ambient air. However, in the

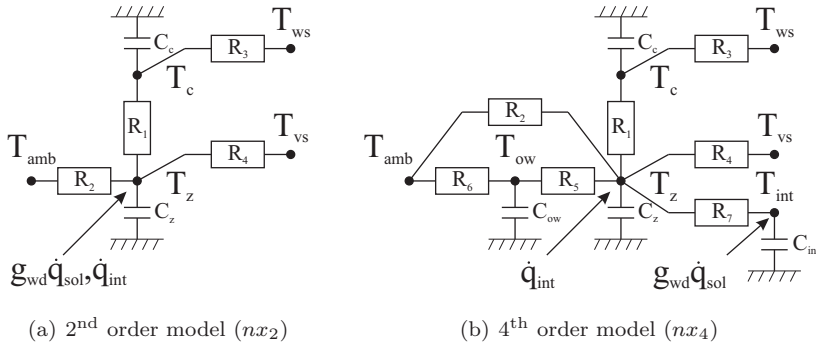


Figure 9.2: Simplified building representation by means of (a) a 2nd order model and (b) a 4th order model

investigated CCA building, heating and cooling is provided by the CCA floor and ceiling, having a considerable thermal mass which has to be taken into account when considering the heat exchange between supply water and zone node. One of the nodes is therefore the concrete slab with thermal capacitance C_c and temperature T_c , which is connected to the zone node by the thermal resistance R_1 ($= R_b$ of Fig. 9.1(c)). The zone node has a thermal capacitance $C_z = 5 \times V_{air} \rho_{air} c_{air}$. The ‘air capacity’ represents the full internal thermal energy storage of the office zone, for which Laret used a value of 4-5 times the actual thermal capacity of the air.²

On the other hand, the conduction heat loss through the windows and infiltration represent 80% of the total heat loss to the ambient. The cooling load calculation shows that the outside wall is responsible for only 9% of the cooling loads. Therefore, the 2nd order model neglects heat loss through the outside wall. This results in the model presented in Fig. 9.2(a). The thermal resistance R_2 of window and infiltration connects zone air to the disturbances T_{amb} . \dot{q}_{sol} and \dot{q}_{int} act directly on the zone air node, while the input T_{vs} influences T_z through the thermal resistance $R_4 = (\dot{m}_v c_{air})^{-1}$. The water supply temperature T_{ws} influences the zone air via the state of the concrete slab. The thermal resistance R_3 is the equivalent thermal resistance for CCA-elements, as defined by Koschenz and Lehmann [81], added by R_a of Fig. 9.1(c),

²In the TRNSYS model of the 2-zone office building, the thermal capacitance is set to 5 times the air capacitance to account for furniture and other non-modelled zone parts (see App. D).

which is half of the thermal resistance of the concrete slab. The heat exchange via the corridor to other zones of the building is neglected.

A drawback of the 2nd order model is the direct connection of the zone node to the radiative heat flows. Where in reality radiative heat flows are absorbed by the surrounding surfaces, they act now immediately on the zone air. Both Tindale (cited by Davies [34]) and Masy [91] proposed an additional internal node in order to better represent the internal storage within the zone. This leads to the 4th order model (see Fig. 9.2(b)) in which the extra internal node with thermal capacitance C_{int} and the outer wall with a thermal capacitance C_{ow} are added as additional model nodes. The thermal resistance of the outer wall, $1/U_{ow}$, is divided over R_5 and R_6 . C_{int} is determined by the combined thermal capacity of the internal walls, and connects to the zone air node by R_7 , which is the small thermal resistance between zone node and the core of the internal walls. Solar radiation now acts on the internal node, whereas the ambient temperature is connected through a parallel path to the zone node.

9.2.3 Solar radiation

Solar radiation acts as a heat input on glazings and internal surfaces depending on time, building surroundings, weather conditions, location and orientation of the building, solar shading control and properties of the different materials [34]. Depending on the reflection, absorption and transmission factors of the glazing ($\rho + \alpha + \tau = 1$), the transmitted fraction of the beam radiation is received by the interior surfaces of the zone, where it is partly reflected and partly absorbed. The reflected portion is further absorbed by other surfaces and reflected until it is completely absorbed by the interior surfaces and furnishing. A small portion might be retransmitted to the exterior.

Regarding the 2nd and 4th order model, it is assumed that the process of reflection and absorption until complete absorption is fast compared to the occurring time constants of the zone. Consequently, solar radiation transmitted to the zone and thus corrected for the solar fraction of the window g_{wd} , is modelled as a heat input to the zone node in the 2nd order model and to the interior node in the 4th order model.

9.2.4 Building model equations

The RC-models are described using the general state space formulation, where inputs and disturbances are combined in a single vector \mathbf{U} . The system is represented by

$$\dot{\mathbf{X}} = \mathbf{A}\mathbf{X} + \mathbf{B}\mathbf{U} \quad (9.4)$$

$$\mathbf{Y} = \mathbf{C}\mathbf{X} + \mathbf{D}\mathbf{U} \quad (9.5)$$

with:

$$\mathbf{X} = \begin{bmatrix} T_c \\ T_z \end{bmatrix} \text{ or } \begin{bmatrix} T_c \\ T_z \\ T_{int} \\ T_{ow} \end{bmatrix}, \mathbf{U} = \begin{bmatrix} T_{ws} \\ T_{vs} \\ T_{amb} \\ \dot{q}_{int} \\ \dot{q}_{sol} \end{bmatrix} \quad (9.6)$$

With nx the number of states, nu the number of inputs and disturbances and ny the number of outputs, the system matrices have the following dimensions:

- \mathbf{X} : $nx \times 1$, \mathbf{U} : $nu \times 1$, \mathbf{Y} : $ny \times 1$
- \mathbf{A} : $nx \times nx$, \mathbf{B} : $nx \times nu$, \mathbf{C} : $ny \times nx$, \mathbf{D} : $ny \times nu$

All parameters of the RC-models are assumed to be constant. Therefore, the energy balance for the different states in the model can be written as a set of ordinary linear differential equations.

For the 2nd order model this results in

$$C_c \frac{\delta T_c}{\delta t} = -\frac{1}{R_1} (T_c - T_z) - \frac{1}{R_3} (T_c - T_{ws}) \quad (9.7)$$

$$C_z \frac{\delta T_z}{\delta t} = -\frac{1}{R_1} (T_z - T_c) - \frac{1}{R_4} (T_z - T_{vs}) - \frac{1}{R_2} (T_z - T_{amb}) \\ + A_{zone} \dot{q}_{int} + g_{wd} A_{wd} \dot{q}_{sol} \quad (9.8)$$

while the 4th order model is described by

$$C_c \frac{\delta T_c}{\delta t} = -\frac{1}{R_1} (T_c - T_z) - \frac{1}{R_3} (T_c - T_{ws}) \quad (9.9)$$

$$C_z \frac{\delta T_z}{\delta t} = -\frac{1}{R_1} (T_z - T_c) - \frac{1}{R_4} (T_z - T_{vs}) - \frac{1}{R_2} (T_z - T_{amb}) \\ - \frac{1}{R_5} (T_z - T_{ow}) - \frac{1}{R_7} (T_z - T_{in}) + A_{zone} \dot{q}_{int} \quad (9.10)$$

$$C_{int} \frac{\delta T_{int}}{\delta t} = -\frac{1}{R_7} (T_{int} - T_z) + g_{wd} A_{wd} \dot{q}_{sol} \quad (9.11)$$

$$C_{ow} \frac{\delta T_{ow}}{\delta t} = -\frac{1}{R_5} (T_{ow} - T_z) - \frac{1}{R_6} (T_{ow} - T_{amb}) \quad (9.12)$$

In the state space notation, the R and C values are lumped into 1 parameter RC . As an example, for the 2nd order model, the A and B matrices are:

$$A = \begin{bmatrix} -\frac{1}{C_c R_1} - \frac{1}{C_c R_3} & \frac{1}{C_c R_1} \\ \frac{1}{C_z R_1} & -\frac{1}{C_z R_1} - \frac{1}{C_z R_2} - \frac{1}{C_z R_4} \end{bmatrix} \quad (9.13)$$

$$B = \begin{bmatrix} \frac{1}{C_c R_3} & 0 & 0 & 0 & 0 \\ 0 & \frac{1}{C_z R_4} & \frac{1}{C_z R_2} & \frac{A_{zone}}{C_z} & \frac{g_{wd} A_{wd}}{C_z} \end{bmatrix} \quad (9.14)$$

9.2.5 Initial parameter values

Because the model parameters have a physical meaning, initial values can be determined from the material properties and geometry of the surfaces surrounding the office zone. R is the thermal resistance - conduction and convection - of the layer connecting two states or a state and an input, while C is the thermal capacitance of the respective material layer. The RC -network is built up according to the following rules:

- \dot{q}_{sol} is multiplied by the window area A_{wd} and \dot{q}_{int} by the zone area A_{zone} .
- The outer wall is modelled by an optimised RCR-network, following the methodology proposed by Masy [91]: from outside to inside it is composed as $0.96R - 0.79C - 0.04R$ with R the total thermal resistance and C the total capacitance of the wall. With this simplified composition, the

inner heat flows correspond to results from detailed wall models. Because of the low contribution of the outer wall to the buildings heating and cooling load, this simplification will not result in large errors on the energy balance of the simplified building model.

- The CCA are modelled using the star network approach developed by EMPA [81] with a fictitious concrete core node as central point, but transformed into a 1st order model as shown in Fig. 9.1.
- the surface convective heat transfer for floor and ceiling is modelled using the natural convection coefficient correlation from Awbi and Hatton [9] (see App.D.5).
- The surface heat transfer for vertical walls is modelled through a constant heat transfer coefficient (combined convection and radiation): $h_{\text{inside}} = 7.7 \text{ W/m}^2\text{K}$ and $h_{\text{outside}} = 25 \text{ W/m}^2\text{K}$.
- The internal capacity C_i is the thermal capacitance of the lightweight separation wall of the office zone, while the thermal resistance R_i includes convection and conduction to the centre of this wall.
- Material properties are typical values, in this case taken from the Belgian building standard NBN62-002:2008.

Henceforth, the set of model parameters calculated according to these assumptions, will be referred to as parameter set *ini*. The state space matrices A_{ini} and B_{ini} for the 2nd order model are (presented in the TRNSYS units h (hour) and (kJ/h)):

$$A_{\text{ini}} = \begin{bmatrix} -0.1722 & 0.1120 \\ 2.0309 & -2.3709 \end{bmatrix} \quad (9.15)$$

$$B_{\text{ini}} = \begin{bmatrix} 0.0602 & 0 & 0 & 0 & 0 \\ 0 & 0.2400 & 0.1000 & 0.0545 & 0.0071 \end{bmatrix} \quad (9.16)$$

9.3 Parameter estimation procedure

9.3.1 Data sets for parameter estimation

Estimating the parameters of the simplified building model, requires ‘measurement data’ from the investigated building: the response of the state \mathbf{X}

against an excitation of input \mathbf{U} . When a detailed building model is available, as in this case by using the TRNSYS model, virtually all combinations of excitation signals are possible. However, gathering useful data from real building measurements, is not straightforward. The controllability of T_{ws} and T_{vs} depends on the HVAC system layout and building management system. T_{amb} is an uncontrollable input and \dot{q}_{sol} and \dot{q}_{int} are only to a certain extent controllable, for instance by adjusting the solar shading or by using electrical heaters respectively.

This work wants to compare the parameter estimation results for the case with ideal, fully measurable and controllable input variables \mathbf{U} and perfectly measurable state variables \mathbf{X} against the case where all inputs \mathbf{U} are still perfectly measurable but not controllable and where the state variables \mathbf{X} are assumed to be perfectly measurable. The detailed TRNSYS building model serves as a data generator for both cases.

In the first case, a step excitation is applied to the inputs at different times and the measured response of the zone in terms of T_z and T_c serves as data set for the parameter estimation procedure. The changes in T_z and T_c can clearly be allocated to the different changes of the inputs. Since internal gains and solar radiation are important factors influencing T_z , three subsets of data are created: (1) with a step excitation in T_{ws} , T_{vs} and T_{amb} , but without \dot{q}_{sol} and \dot{q}_{int} , (2) as in the first case including a step excitation in \dot{q}_{int} and (3) as in the first case but with both \dot{q}_{sol} and \dot{q}_{int} inputs excited.

In the second case, it is assumed that the building operates under realistic conditions. T_{ws} and T_{vs} are block functions representing the on-off behaviour of the water flow and the ventilation system respectively. T_{amb} and \dot{q}_{sol} values are chosen for a typical summer and a typical winter condition:

$$\text{Summer: } T_{amb} = 20 - 7 \sin\left(\frac{360}{24}(t - 10)\right) \quad (9.17)$$

$$\dot{q}_{sol} = 850 \sin\left(\frac{360}{24}(t - 6)\right) \text{ and } \dot{q}_{sol} \geq 0 \quad (9.18)$$

$$\text{Winter: } T_{amb} = -1.5 + 2.5 \sin\left(\frac{360}{24}(t - 10)\right) \quad (9.19)$$

$$\dot{q}_{sol} = 28 \sin\left(\frac{360}{24}(t - 6)\right) \text{ and } \dot{q}_{sol} \geq 0 \quad (9.20)$$

Table 9.1: Data sets for parameter estimation (DS1 - DS3: theoretical input profiles; set DS4 - DS5: realistic input profiles)

Data set	HVAC		Weather		Occupancy
	T_{ws}	T_{vs}	T_{amb}	\dot{q}_{sol}	\dot{q}_{int}
DS1	Step	Step	Step	0	0
DS2	Step	Step	Step	0	Step
DS3	Step	Step	Step	Step	Step
DS4	Block	Block	Summer	Summer	Block
DS5	Block	Block	Winter	Winter	Block

\dot{q}_{int} is also represented by a block function as often assumed in building simulation. Since all inputs are excited more or less simultaneously, the changes in T_z and T_c can not be allocated to the different inputs as it could in the first step.

Table 9.1 lists the 5 different data sets. Data sets DS3 and DS4 are particularly interesting because they contain \dot{q}_{sol} with a considerably high value ($\dot{q}_{sol,max} = 850 \text{ W/m}^2$), while in DS5 \dot{q}_{sol} is included, but only with a significantly lower value (maximum value of 28 W/m^2). Fig. 9.3 illustrates the response of T_z and T_c according to the first case for DS3 (theoretical input profiles) and according to the second case (realistic input profiles) for DS4.

9.3.2 Parameter estimation tool

The parameter estimation is conducted in ACADO [64], an optimisation tool adapted for non-linear optimal control problems. This toolkit, for which a Matlab interface exists, has algorithms using the specific structure of parameter estimation problems, and has a-posteriori analysis tools available.

The parameter estimation procedure converges when a KKT-tolerance of 10^{-7} is reached. The KKT-conditions, named after Karush, Kuhn and Tucker, are necessary, but not sufficient conditions for optimality for a non-linear problem with inequality constraints [82]. Additional regularity conditions have to be satisfied. The KKT-tolerance defines an allowed deviation to these conditions as a convergence criterion.

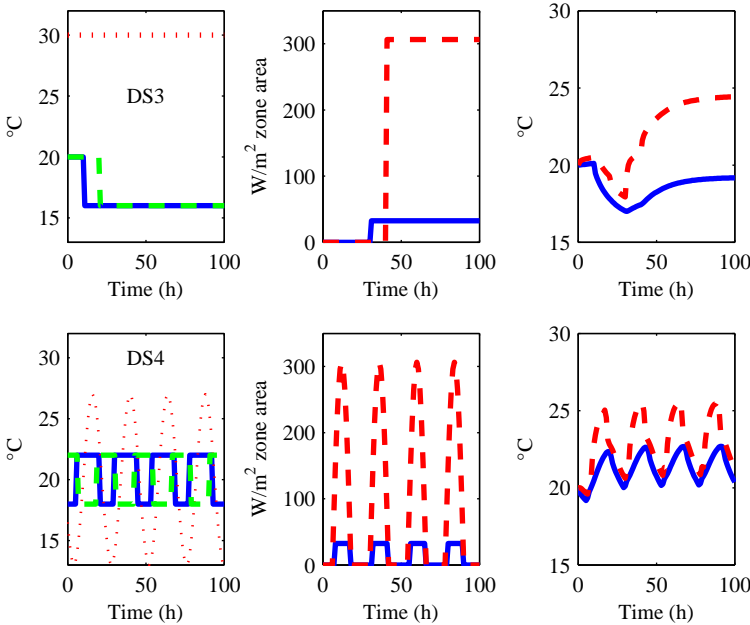


Figure 9.3: (left) T_{ws} (-), T_{vs} (- -), $T_{amb}(\cdot)$, (middle) \dot{q}_{sol} (- -) and \dot{q}_{int} (-), and (right) zone states T_c (-) and T_z (- -) for the identification sets DS3 (above) and DS4 (below), where DS3 is a representative of the theoretical and DS4 of the realistic input profiles. The step excitation of T_{amb} occurs at 0h for DS3.

9.3.3 12 simplified building models in 3 model groups

Starting from the 2nd and 4th order initial simplified building models, 10 new models are constructed using the 5 different data sets: nx_i -DS j , with $i=2,4$ and $j=1..5$. E.g. the 2nd order model of which the parameters are identified with data set 3, is referred to as $nx2$ -DS3. These models are divided in 3 groups as presented in Table 9.2.

Although PE-data set DS2 does not contain a \dot{q}_{sol} -input, for the 2nd-order simplified building model a measure is taken to enable the estimation of the \dot{q}_{sol} parameter even without measurements. Suppose the parameter representing \dot{q}_{int} in Eq. 9.8 (see Section 9.2.4) is called $p_{int} = A_{zone}/C_z$, it then follows from this same equation that the parameter representing \dot{q}_{sol} is $p_{sol} = g_{wd}A_{wd}p_{int}$.

Table 9.2: 12 simplified building models in the 3 groups: Group A are models obtained from data set 1 with T_{ws} , T_{vs} and T_{amb} as inputs (no \dot{q}_{sol} and \dot{q}_{int}), Group B are models obtained from data set 2 with T_{ws} , T_{vs} , T_{amb} and \dot{q}_{int} as inputs (no \dot{q}_{sol}), and Group C are models having all inputs in the system matrix.

	Model order	nx2	nx4
	Data set		
Initial model		C	C
Theoretical input profiles	DS1	A	A
	DS2	C	B
	DS3	C	C
Realistic input profiles	DS4	C	C
	DS5	C	C

With this measure, model nx2-DS2 shifts from model group B to model group C. For the 4th-order model (Eqs. 9.10 and 9.11) \dot{q}_{int} and \dot{q}_{sol} do not act on the same node. Therefore, the above relation between both parameters does not hold for the 4th-order model.

9.3.4 Parameter estimation as an optimisation problem

Written as a set of differential equations, the 2nd and 4th order building model have respectively 7 and 12 parameters which need to be estimated. Eqs. 9.8-9.12 are rewritten as:

$$\dot{\mathbf{X}} = \mathbf{p} \cdot \mathbf{X} + \mathbf{qT} \cdot \mathbf{UT} + \mathbf{qQ} \cdot \mathbf{UQ} \quad (9.21)$$

with \mathbf{p} the state parameter matrix having zeros at the diagonals, \mathbf{qT} the temperature input parameter matrix and \mathbf{qQ} the heat flow input parameter matrix. Written in full, the model equations become as in Eqs. 10.3.1-9.27, where the ij -indices refer to the row and columns in the parameter matrices.

For the 2nd order model this results in

$$\frac{\delta T_c}{\delta t} = p_{12} (T_c - T_z) + qT_{11} (T_c - T_{ws}) \quad (9.22)$$

$$\begin{aligned} \frac{\delta T_z}{\delta t} &= p_{21} (T_z - T_c) + qT_{22} (T_z - T_{vs}) + qT_{23} (T_z - T_{amb}) \\ &+ qQ_{21}\dot{q}_{int} + qQ_{22}\dot{q}_{sol} \end{aligned} \quad (9.23)$$

while the 4th order model is described by

$$\frac{\delta T_c}{\delta t} = p_{12} (T_c - T_z) + qT_{11} (T_c - T_{ws}) \quad (9.24)$$

$$\begin{aligned} \frac{\delta T_z}{\delta t} &= p_{21} (T_z - T_c) + p_{23} (T_z - T_{in}) + p_{24} (T_z - T_{ow}) \\ &+ qT_{22} (T_z - T_{vs}) + qT_{23} (T_z - T_{amb}) + qQ_{21}\dot{q}_{int} \end{aligned} \quad (9.25)$$

$$\frac{\delta T_{int}}{\delta t} = p_{32} (T_{int} - T_z) + qQ_{32}\dot{q}_{sol} \quad (9.26)$$

$$\frac{\delta T_{ow}}{\delta t} = p_{42} (T_{ow} - T_z) + qT_{43} (T_{ow} - T_{amb}) \quad (9.27)$$

The KKT-convergence criterion is used to decide whether a minimum least-squares error between the TRNSYS results and simplified model results is reached. In order to estimate the parameters of the simplified model, a range is specified in which the parameter set is located. This implies that the model parameters are physically constrained in order to achieve a feasible solution, as referred to by Armstrong et al. [4]. This range is based on the physical derivation of the initial parameter values. Each R_i and C_j parameter is supposed to vary with $\pm 50\%$, which results in the range (and corresponding inequality constraints) for the parameters as given in Table 9.3 (presented in the TRNSYS units h (hour) and (kJ/h)).

These inequality constraints, combined with the measured identification data m_k , the differential equations of the n states and initial conditions give rise to the optimisation problem which is minimizing the least-squares error between

Table 9.3: Initial parameter values (ini) and the assigned range for the parameter estimation problem, in units h (hour) and (kJ/h).

	2 nd order model			4 th order model			
	par _{i,min}	par _i	par _{i,max}	par _{i,min}	par _i	par _{i,max}	
p12	-0.4481	-0.1120	-0.0498	p12	-0.4481	-0.1120	-0.0498
p21	-8.1236	-2.0309	-0.9026	p21	-8.1236	-2.0309	-0.9026
qT11	-0.2406	-0.0602	-0.0267	p23	-2.6884	-0.6721	-0.2987
qT22	-0.9600	-0.2400	-0.1067	p24	-1.2826	-0.3207	-0.1425
qT23	-0.4001	-0.1000	-0.0445	p32	-2.5714	-0.6429	-0.2857
qQ21	0.0242	0.0545	0.2178	p42	-0.2998	-0.0749	-0.0333
qQ22	0.0031	0.0071	0.0282	qT11	-0.2406	-0.0602	-0.0267
				qT22	-0.9600	-0.2400	-0.1067
				qT23	-0.4001	-0.1000	-0.0445
				qT43	-0.0299	-0.0075	-0.0033
				qQ21	0.0242	0.0545	0.2178
				qQ32	0.0030	0.0068	0.0270

the measurement data and the model results:

$$\min_{\text{par}_i} \sum_k [\mathbf{X}_j(t_k) - m_k]^2 \quad \forall j \in [1 : n], \forall i \in [1 : 7] \text{ or } [1 : 12] \quad (9.28)$$

$$\text{subject to:} \quad (9.29)$$

$$\forall k \in [0 : T] : \dot{\mathbf{X}}(k) = \mathbf{A}\mathbf{X}(k) + \mathbf{B}\mathbf{U}(k) \quad (9.30)$$

$$\text{par}_{i,\min} \leq \text{par}_i \leq \text{par}_{i,\max} \quad (9.31)$$

$$\mathbf{X}(0) = \mathbf{X}_{\text{initial}} \quad (9.32)$$

9.4 Parameter estimation results

9.4.1 Root-Mean-Squared Error

Table 9.4 list the root mean squared errors (RMSE) of the zone temperature T_z for respectively the 2nd and 4th order models. The rows represent the simplified building models (identified by using the 5 data sets), while the columns contain

the corresponding validation results for each of the 5 data sets. The terminology used in this section is:

- val-DS1 refers to data set DS1 used for validation
- nx2-DS1 refers the 2nd order model with parameters estimated with data set DS1
- nx4-DS1 refers the 4th order model with parameters estimated with data set DS1
- nx-DS1 refers to both 2nd and 4th order model with parameters estimated with data set DS1

Table 9.4: RMSE on zone temperature T_z (2nd and 4th order)

(Group)Modelname	val-DS1	val-DS2	val-DS3	val-DS4	val-DS5
RMSE for the 2 nd order model					
(C)nx2-ini	0.4	0.8	6.5	3.1	0.8
(A)nx2-DS1	<i>0.5</i>	2.3	5.0	2.9	2.2
(C)nx2-DS2	1.4	<i>0.2</i>	7.6	4.7	0.6
(C)nx2-DS3	2.9	0.3	<i>0.3</i>	1.3	0.8
(C)nx2-DS4	4.4	1.2	1.3	<i>0.8</i>	1.5
(C)nx2-DS5	0.7	0.9	8.9	5.7	<i>0.5</i>
RMSE for the 4 th order model					
(C)nx4-ini	0.9	0.7	5.1	2.2	0.6
(A)nx4-DS1	<i>0.1</i>	2.2	4.9	2.9	2.1
(B)nx4-DS2	0.5	<i>0.1</i>	2.1	1.3	0.6
(C)nx4-DS3	1.0	0.4	<i>0.1</i>	0.6	0.7
(C)nx4-DS4	1.6	0.6	0.4	<i>0.6</i>	0.8
(C)nx4-DS5	0.7	0.3	34.7	17.3	<i>0.4</i>

The parameter estimation (PE) procedure converges for all data sets considered with a KKT-tolerance of 10^{-7} as convergence criterion. The values in *italic* on the diagonal in Table 9.4 are the validation results using the same data set for parameter estimation as for validation. They show that this auto-validation obtains the lowest RMSE for that respective data set. The RMSE results are used to assess the robustness of the simplified model: a model which is capable of reproducing all data sets accurately, is assumed to be robust in a wide range of circumstances. Since the simplified model is used in the MPC to predict thermal comfort, a target value of 1°C seems appropriate.

The initial white-box model, based on physics and building geometry, performs very well for all data sets except val-DS3 and val-DS4, having high solar gains. Therefore, the impact of \dot{q}_{sol} is not well reproduced by this initial model. The nx4-ini model shows a slight improvement for val-DS3 (6.5 to 5.1) and val-DS4 (3.1 to 2.2), but not sufficient to arrive at a good model.

From Table 9.4 it is concluded that the influence of the PE-data set is more pronounced than the influence of the model order. Overall, the mean of the RMSE values for the 4th order model is even 30% higher than for the 2nd order model, due to the bad RMSE of the nx4-DS5 model. The mean RMSE for all other nx4 models is 45% lower compared to the respective nx2 models.

Comparing the RMSE of nx2-DS2 with nx4-DS2 is like comparing apples and oranges, because nx2-DS2 takes into account \dot{q}_{sol} (see Sec. 9.3.3), while nx4-DS2 not. However, the bad RMSE of nx2-DS2 indicates that the measure to assign a \dot{q}_{sol} -parameter based on the \dot{q}_{int} -parameter is not correct. Apparently, the way solar radiation is absorbed in a building differs too much from the effect of \dot{q}_{int} . This is an important conclusion for real situations: a 2nd order building zone model must be identified with solar radiation known and preferably controllable.

Evidently, both group A (2nd and 4th order) models, having parameters estimated without \dot{q}_{int} and \dot{q}_{sol} as excitation signals, fail to predict T_z for validation data sets val-DS2 to val-DS5 which contain \dot{q}_{int} and \dot{q}_{sol} . Surprisingly, the same conclusion regarding \dot{q}_{sol} can be drawn for nx2-DS5 and nx4-DS5. The results of this model are even worse than the RMSE values of nx-DS1. The parameter estimation procedure for nx-DS5 fails to improve this model compared to nx4-ini. E.g. for model nx4-DS5, the impact of \dot{q}_{sol} on T_z is predicted wrong to such a degree that T_z increases to 80°C with the val-DS3 data set, where the TRNSYS models shows $T_z = 24^\circ\text{C}$ at the end of the simulated period. Although \dot{q}_{int} and, with a limited value, \dot{q}_{sol} are present in val-DS5, the oscillations and simultaneous occurrence of excitations in this data set troubles the nx4 parameter estimation, apparently.

The nx4 model was composed in order to bring the impact of \dot{q}_{sol} into line with the occurring heat transfer modes in a building zone. The nx4-ini RMSE indeed improves for the \dot{q}_{sol} data sets (DS3-DS5) compared to nx2-ini, although not significantly. Identifying nx4 with data sets having high \dot{q}_{sol} (DS3-DS4), results in the lowest RMSE for the corresponding validation data sets (val-DS3, val-DS4). However, nx4-DS3 outperforms nx4-DS4 for val-DS1 (RMSE = 1.0

Table 9.5: Input-output relation for the A and B system matrices of the 2nd order simplified building model

nx2-model: Influence			nx4-model: Influence		
	of input	on state		of input	on state
B(1, 1)	T_{ws}	T_c	B(1, 1)	T_{ws}	T_c
B(2, 2)	T_{vs}	T_z	B(2, 2)	T_{vs}	T_z
B(2, 3)	T_{amb}	T_z	B(2, 3)	T_{amb}	T_z
B(2, 4)	\dot{q}_{int}	T_z	B(4, 3)	T_{amb}	T_{ow}
B(2, 5)	\dot{q}_{sol}	T_z	B(2, 4)	\dot{q}_{int}	T_z
			B(3, 5)	\dot{q}_{sol}	T_{int}

versus RMSE = 1.6), where nx4-DS4 has the highest RMSE for val-DS1 out of all nx4-models.

9.4.2 System matrices

Analysing the A and B matrices of the different models (see Fig. 9.4) shows how the parameters of the different simplified building models vary. The reciprocal of the A-matrix eigenvalues are the model time constants: $\tau_i = -1/\lambda_i$, while B represents the influence of the inputs on the change of the states (see Table 9.5).

The parameter estimation procedure adapts the time constants of the 2nd order model (see Fig. 9.4(a)) to 12 – 14 h and 9 – 13 min for nx2-DS3 and nx2-DS4, who have the smallest RMSE values. The time constants of the nx4 models correspond less: the highest time constant varies between 15 h and 30 h. The smallest time constants are between 10 min and 23 min. Where the RMSE of nx4-DS3 and nx4-DS4 was low for all data sets, again here, their time constants agree relatively well.

The good RMSE values of nx2-DS3 and nx2-DS4 and of nx4-DS3 and nx4-DS4, apparently result in equal time constants for those models. But this is also true for the B-matrix elements of those models. Fig. 9.4(b) shows a good agreement for nx2-DS3 and nx2-DS4, except for the T_{amb} -parameter B(2,3).

For both 2nd and 4th order models, there is a big variation between the each of the B-matrix elements of the different models. The bad RMSE of the nx4-DS5 model can be explained by the value of the \dot{q}_{sol} parameter B(3,5) of this model,

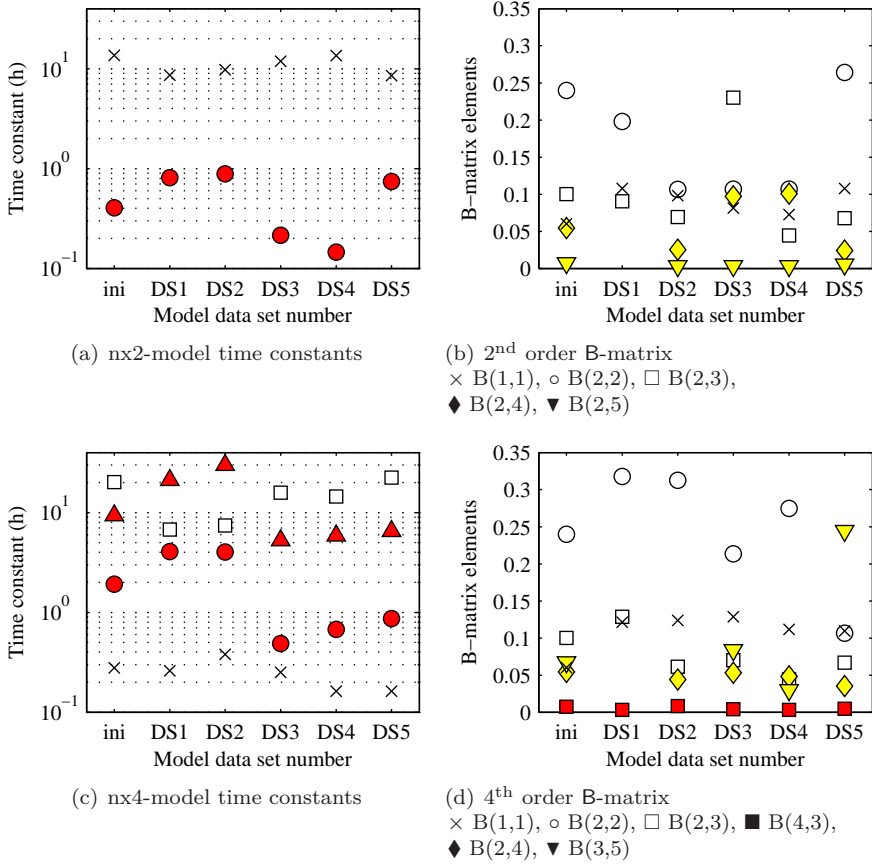


Figure 9.4: (a), (c) 2nd and 4th order model time constants and (b), (d) non-zero elements of the simplified building model B matrix, representing the initial model and the DS1 - DS5-models as abscis.

which is much higher than the corresponding parameters of the other models. Also for the 2nd order model, this conclusion holds. Moreover, the RMSE is very sensitive to the $B(3,5)$ -value: models nx2-DS2 and nx2-DS5 have an $B(3,5)$ -value which is respectively 5% and 70% larger than the $B(3,5)$ -value of models nx2-DS3 and nx2-DS4, whose $B(3,5)$ -value equals 0.0031. Even the 5% difference results in an increased RMSE value for the datasets val-DS3 and val-DS4 containing \dot{q}_{sol} .

9.4.3 Thermal capacitance of the room air node

The knowledge of the newly identified matrix parameters can be used to feed back information to the parameters of the initial model. Eqs. 9.8 and 9.10 show that the matrix element $B(2,4)$ represents $1/C_z$, the inverse of the thermal capacitance associated with the zone node. $B(2,5)$ equals $g_{wd}A_{wd}/C_z$ for the 2nd order model. Therefore, the estimated values of these parameters can be used to evaluate the hypothesis that C_z equals 4-5 times the thermal capacitance of the zone air, both for the 2nd and for the 4th order model. Table 9.6 lists the correction factor F_z for the thermal capacitance of the zone node defined by:

$$C_z = F_z V_z \rho_z c_z \quad (9.33)$$

Table 9.6: Correction factor F_z for the thermal capacity of the zone node

	DS0	nx2-DS3	nx2-DS4	nx4-DS3	nx4-DS4
$F_z (\dot{q}_{int})$	5.0	2.8	2.7	5.1	5.6
$F_z (\dot{q}_{sol})$	5.0	11.3	11.3	-	-

Table 9.6 shows that for the 2nd order model it is not correct to use an equal thermal capacitance for the inputs \dot{q}_{int} and \dot{q}_{sol} . The input \dot{q}_{int} requires a thermal capacitance of almost 3 times the zone air capacitance, while \dot{q}_{sol} requires a thermal capacitance of more than 11 times the zone air capacitance. This difference is related to the way internal gains and solar radiation interact with the building zone. Internal gains, having a large convective part, effect directly the air temperature of the zone. Solar gains on the contrary, are first absorbed by the thermal mass of the floors and walls. Only then this absorbed heat is released gradually to the zone. This is a much slower process, which explains the high F_z correction factor for the input \dot{q}_{sol} .

For the 4th order model, where the capacitance of the zone is split into C_z and C_{int} , the correction factor F_z for the input \dot{q}_{int} is a little higher than the initial value of 5.

This is an important conclusion since the dynamic response of the building zone depends largely on the thermal capacitance attributed to the zone state.

9.4.4 Influence of the initial parameter range

The parameter estimation results show a large dependency on the specified range that bounds the values of the parameters. This is demonstrated with the PE-results of the nx2 models. While the KKT-convergence criterion was nicely satisfied for the previous results, several parameters of the nx2-models lie on the boundaries of the parameter range, as shown in Table 9.7. This might indicate that the range of these parameters should be broader.

Table 9.7: Initial parameter range and the parameter estimation results of the nx2 models, in units h (hour) and (kJ/h). The underlined values lie on the boundaries of the parameter range.

	par _{i,min}	par _{i,max}	nx2-DS1	nx2-DS2	nx2-DS3	nx2-DS4	nx2-DS5
p12	-0.4481	-0.0498	<u>-0.0498</u>	-0.0530	-0.0506	-0.0813	<u>-0.0498</u>
p21	-8.1236	-0.9026	<u>-0.9026</u>	<u>-0.9026</u>	-4.2684	-6.6504	-0.9732
qT11	-0.2406	-0.0267	-0.1078	-0.0980	-0.0812	-0.0727	-0.1078
qT22	-0.9600	-0.1067	-0.1979	<u>-0.1067</u>	<u>-0.1067</u>	<u>-0.1067</u>	-0.2641
qT23	-0.4001	-0.0445	-0.0903	-0.0691	-0.2301	<u>-0.0445</u>	-0.0678
qQ21	0.0242	0.2178	0.0000	0.0254	0.0972	0.1006	<u>0.0242</u>
qQ22	0.0031	0.0282	0.0000	0.0033	<u>0.0031</u>	<u>0.0031</u>	0.0053

The influence of the range on the PE-results is investigated by gradually relaxing the inequality constraints for those parameters which have an active inequality constraint. The routine starts with a range ± 0.2 around the initial parameter value. Then the PE algorithm estimates a new parameter set. If an inequality constraint is active, the range for that parameter is increased to ± 0.3 . The routine is repeated until all inequality constraints are inactive and the KKT-condition is fulfilled. For all nx2-models, this approach leads to an updated set of parameters. However, for neither of the nx4-models, the PE-estimation algorithm did converge to a solution.

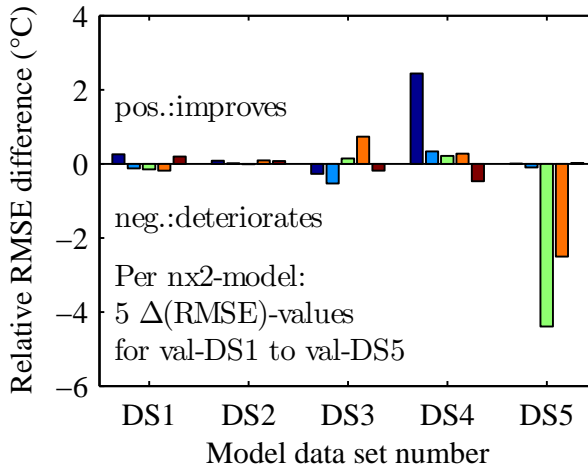


Figure 9.5: Relative difference in RMSE-values for the validation of the nx2-models with updated parameters (no active inequality constraints), compared to the original nx2-models. Positive $\Delta(\text{RMSE})$ values mean an improvement, while negative $\Delta(\text{RMSE})$ values imply a higher RMSE.

However, the updated nx2-models do not show better RMSE results, in general. Some of the parameters become even infeasible: e.g. for the nx2-DS3 and nx2-DS4 model, the T_{vs} -parameter becomes zero, meaning that the ventilation supply air does not influence the zone temperature anymore. Fig. 9.5 shows the relative improvement of the updated nx2-models compared to the original nx2-models: positive values indicate a lower RMSE, while negative values indicate a higher RMSE. For each nx2-model (DS_i in the figure) 5 bars are shown, corresponding to the 5 validation data sets $val-DS1$ to $val-DS5$. This shows that the proposed routine does not, in general, improve the model quality.

This means that the model quality can not be improved by relaxing the inequality constraints and that the physically determined ranges for the parameters are required in order to obtain a robust parameter estimation procedure. This is certainly true for the 4th order (for which this procedure did not lead to a converged solution), but also for the 2nd order models.

9.5 Conclusions

The presented approach to estimate the parameters of a white-box CCA building model, resulted in both a 2nd and 4th order building model which represents the building dynamics with an acceptable accuracy.

However, the solution of the optimisation problem is largely influenced by the constraints imposed on the parameters. The initial parameter range, defined by the white-box building model, is an important factor in the parameter estimation procedure. This observation was also made by Armstrong et al. [4], who stated that physically derived constraints should be applied in order to achieve a feasible solution.

The RMSE comparison leads to the following conclusions:

- in order to have a robust simplified zone model, the nx2-model should be identified with data containing \dot{q}_{int} and \dot{q}_{sol} .
- if real data are used as identification data set, they should contain a high amount of solar radiation and the nx4-model should preferably be used. The 2nd and 4th order model, identified with the real winter data show impermissible RMSE-values for high solar gain inputs.
- if an identification procedure is set up in a real building, both \dot{q}_{int} and \dot{q}_{sol} should be measured and preferably controllable
- the best models are obtained for the theoretical data set where all inputs (T_{ws} , T_{vs} , T_{amb} , \dot{q}_{int} and \dot{q}_{sol}) are available. The 4th order model nx4-DS3 is the only model which achieves an RMSE $< 1^\circ\text{C}$ for all validation data sets, but, as mentioned, this is a theoretical case.

The analysis of the state and input matrices of the models with estimated parameters, supports the conclusions of the RMSE comparison: the good models — nx2-DS3 and nx2-DS4 for the 2nd order models and nx4-DS3 and nx4-DS4 for the 4th order models — have comparable time constants and more or less comparable B input matrix values. They also have the lowest RMSE values. But it must be concluded from this parameter estimation analysis that it is not possible to draw clear conclusions regarding the correct model parameter values.

The analysis of the estimated parameter values shows that the thermal capacitance attributed in the 2nd order model to the inputs \dot{q}_{int} and \dot{q}_{sol} should differ: \dot{q}_{int} requires a much lower thermal capacitance than \dot{q}_{sol} .

The 2nd order model nx2-DS3 is used in the next chapter to compose a model based predictive controller for a CCA building.

Chapter 10

Model based Predictive Control for CCA buildings

10.1 Introduction

In chapter 8, careful tuning of the controller parameters has led to a controller which was able to achieve a reasonable thermal comfort against an acceptable energy cost. However, this approach did not explicitly exploit the dynamics of CCA and the building to optimize the operation with respect to energy cost and thermal comfort. An alternative is to use Model based Predictive Control (MPC), which optimizes system operation by solving at each control time step an optimal control problem (OCP). This yields a control input profile which minimizes a given cost function, using a simplified dynamic system model, updated system information and disturbances predictions (e.g. weather forecast and occupancy prediction). The cost function is typically a weighted sum of the conflicting objectives of minimizing the energy cost and minimizing thermal discomfort.

Model mismatch, prediction errors and initial state estimation introduce errors in the MPC procedure. However, since the aim of this chapter is to compare the behaviour of a Model based Predictive-controller or MPC against the tuned conventional controller of Ch. 8, these errors are not addressed.

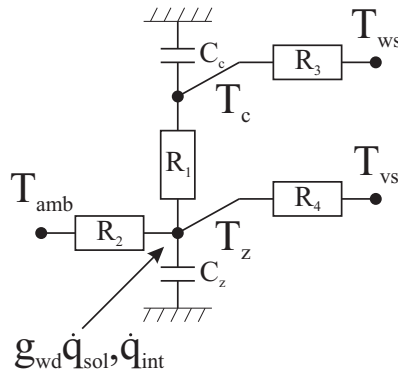


Figure 10.1: Simplified building representation by means of a 2nd order building model

10.2 Implementation of MPC

The identification of the system dynamics is perceived as a major challenge for a successful implementation of MPC (see Ch. 6). This problem was tackled in Chapter 9. The 4th order building model for which the parameters were identified with a non-realistic step sequence of the different input signals, was the best performing simplified building model. To correctly determine the response to \dot{q}_{int} and \dot{q}_{sol} , a model is required that has a separate temperature node for each of these 2 inputs.

However, since it is the aim in this chapter to analyse the behaviour of an MPC controller in a CCA building, the simple 2nd order model is chosen to be integrated in an MPC-controller (Fig. 10.1). Using this 2nd order model, the interaction between the slow reacting CCA and the fast reacting zone, can be clearly demonstrated. For the 4th order model, this interaction is more complex. The 1-zone 2nd order building model for which the validation showed the lowest RMSE of all identified models (nx2_DS3, see Ch. 9), is integrated in an MPC framework, which is implemented in ACADO [64].

This chapter focusses on the combined control of the CCA circuit and the AHU: a combination of a slow reacting, but high efficiency system with a fast reacting, but more energy intensive system.

As briefly addressed in Ch. 7, the AHU in itself is already a complex system

composed of different subsystems: heating and cooling coil, heat recovery unit, heat recovery bypass. Besides this, a recirculation system can be used to reduce fresh air intake during low occupancy periods. The AHU controller tries to reach an air supply temperature set point, CO₂ set point and possibly additional heating and cooling power to the room. Wang and Xu [143] illustrate this complex interaction by optimizing a PID-controller which reduces air flow maximally while still reaching the required set points at all times in a robust way. They estimated the number of occupants by measuring CO₂ in the return air. In the present PhD-work, the following assumptions are made regarding the AHU control:

- the AHU has a temperature control which reaches the required set point at all times. The physical limitation of the heating and cooling coil is taken into account (see Ch. 7, Sec. 7.3.4) by limiting the achievable temperature setpoints (see Sec. 10.3.4).
- CO₂ control is not addressed, since occupant attendance is simplified to a deterministic profile. The AHU operates between 7 AM and 7 PM.
- the heat recovery has a by-pass control to avoid overheating of the supply air (see Ch. 7, Sec. 7.3.4).

For the CCA circuit, the only controllable variable is the water supply temperature. As shown in Sec. 3.2.9 T_{ws} has more influence on the heat transfer between water and concrete than the water flow rate \dot{m}_w . Moreover, Lim et al. [89] stated that water flow control requires valves with high authority for these typically small flow rate systems, in order to obtain robust control. This would seriously increase the pressure drop.

10.2.1 MPC controller layout

As elaborated in Ch. 9, the system equations and matrices are:

$$\dot{X} = AX + BU \quad (10.1)$$

$$Y = CX + DU \quad (10.2)$$

with:

$$\mathbf{X} = \begin{bmatrix} T_c \\ T_z \end{bmatrix} \text{ or } \begin{bmatrix} T_c \\ T_z \\ T_{int} \\ T_{ow} \end{bmatrix}, \mathbf{U} = \begin{bmatrix} T_{ws} \\ T_{vs} \\ T_{amb} \\ \dot{q}_{int} \\ \dot{q}_{sol} \end{bmatrix} \quad (10.3)$$

having the units ($^{\circ}\text{C}$) for temperature and (W/m^2) for specific heat and cold power. g_{wd} is the shading factor of the window of the office zone.

To distinguish between the real operative temperature T_{op} of the controlled building, and the estimate of this temperature by the controller building model (Fig. 10.1), the symbol T_z is used for the latter in this chapter. It can be seen as an approximation of the operative temperature T_{op} (see Sec. 1.4.4).

This chapter focusses on the formulation of the optimal control problem and the analysis of the optimal input profile which is the output of the MPC. Fig. 10.2 presents the information flows when this MPC with the simplified building model would be integrated in the building controller. At 0 AM each night, the MPC-routine is called to provide the control signals for the heat and cold production and distribution system. The procedure contains following steps: (1) feedback of the building measurements for the concrete core temperature T_c and a measured zone temperature T_z to the MPC, (2) prediction of the disturbances T_{amb} , \dot{q}_{int} and \dot{q}_{sol} for the entire prediction horizon H_p , (3) solving the optimal control problem, (4) returning the calculated output (set points for T_{vs} , T_{ws} and the on-off signal for \dot{m}_w) to the controlled building.

The MPC calculates an optimal set point for both the supply water temperature T_{ws} and the ventilation air temperature T_{vs} .

The MPC can work in two modes:

1. MPC-CCA: The CCA operation is optimised (T_{ws}), while the ventilation operates at a constant temperature.
2. MPC-CCA-AHU: Both CCA and AHU operation are optimised (T_{ws} and T_{vs}).

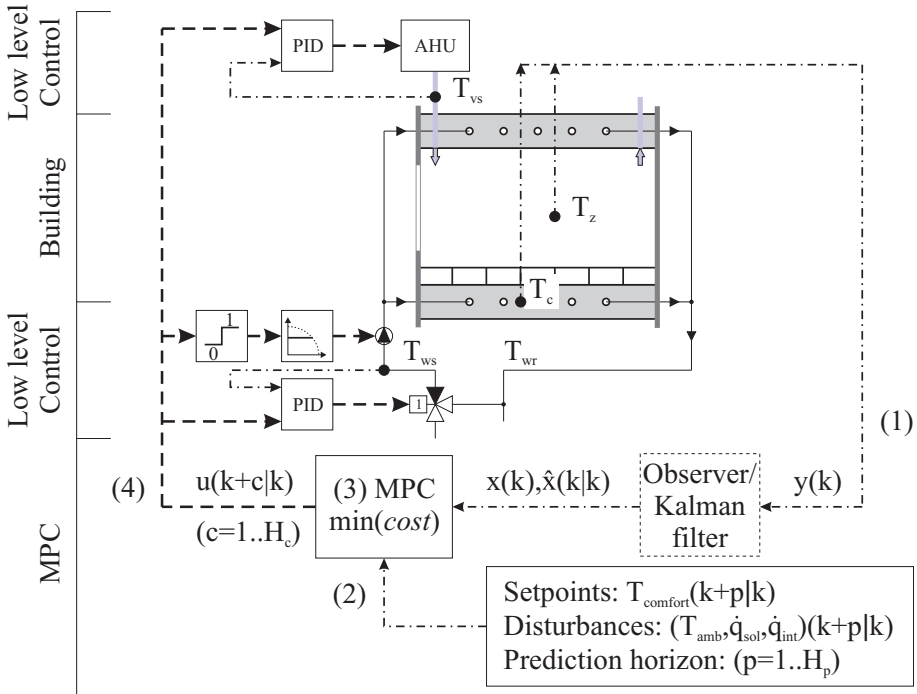


Figure 10.2: Overview of the MPC framework

10.3 Optimal control problem

The MPC determines the optimal supply water temperature and ventilation air temperature profiles for the prediction horizon H_p . By taking H_p to be two consecutive days, the MPC controller is able to account for weekend days.

The profiles are found as the solution of the optimal control problem, given by the set of Eqs. 10.4-10.13. The cost function is a weighted sum of the predicted energy cost J_{ew} , attributed to CCA, J_{ev} attributed to the ventilation heating or cooling, and the thermal discomfort cost J_d , attributed to undercooling or overheating.

The different cost factors are formulated such that they represent the real primary energy consumption (in kWh/m²) and thermal discomfort value (in Kh) which are used for the evaluation of the controllers (see Ch. 8). The

optimal profile is discretised with a control time step Δt_c of 1 hour.

$$\min_{T_{ws}, T_{vs}} \sum_{k=0}^{H_p} [J_{ew,h}(k) + J_{ew,c}(k) + J_{ev,h}(k) + J_{ev,c}(k)] F_1 \dots$$

$$\dots + [\alpha_{du} J_{du}(k) + \alpha_{do} J_{do}(k)] (1 - F_1) F_2 \Delta t_c \quad (10.4)$$

$$(10.5)$$

with:

$J_{ew,h}$ = CCA heating primary energy

$J_{ew,c}$ = CCA cooling primary energy

$J_{ev,h}$ = Ventilation heating primary energy

$J_{ev,c}$ = Ventilation cooling primary energy

J_{du} = undercooling Kelvinhour (Kh)

J_{do} = overheating Kelvinhour (Kh)

$\Delta t_c = 1$ h, control time step

subject to:

$$\mathbf{X}(k+1|k) = \mathbf{A}(k)\mathbf{X}(k) + \mathbf{B}(k)\mathbf{U}(k) \quad (10.6)$$

$$\mathbf{X}(0) = \mathbf{X}_0 \quad (10.7)$$

$$T_{ws,min} \leq \mathbf{U}(1) = T_{ws} \leq T_{ws,max} \quad (10.8)$$

$$T_{vs,min} \leq \mathbf{U}(2) = T_{vs} \leq T_{vs,max}^{(a)} \quad (10.9)$$

$$\dot{q}_{w,h} \leq \dot{q}_{w,h,max} \quad (10.10)$$

$$\dot{q}_{w,c} \geq \dot{q}_{w,c,max} \quad (10.11)$$

$$\dot{q}_{v,h} \leq \dot{q}_{v,h,max} \quad (10.12)$$

$$\dot{q}_{v,c} \geq \dot{q}_{v,c,max} \quad (10.13)$$

^(a) When the MPC is only optimizing CCA operation, this constrained reduces to the equality $U(\mathbf{2}) = T_{vs} = T_{vs,set}$

and with weighting factors F_1 , F_2 , α_{du} and α_{do} . The different terms in this OCP formulation are addressed hereafter.

10.3.1 State matrices A and B

The state matrices in the OCP are written as a function of time: $A(k)$ and $B(k)$, because the system state can change depending on the situation. Specifically, the ventilation parameter R_4 is equal to 0 when the AHU is not operating, which changes the system equations. This introduces an additional disturbance MvOnOff in the OCP formulation:

$$A = \begin{bmatrix} p12 + qT11 & 0 \\ -p21 & p21 + \text{MvOnOff } qT22 + qT23 \end{bmatrix} \quad (10.14)$$

$$B = \begin{bmatrix} -qT11 & 0 & 0 & 0 & 0 \\ 0 & -\text{MvOnOff } qT22 & -qT23 & qQ21 & qQ22 \end{bmatrix} \quad (10.15)$$

following the state space notation of Eqs. -. MvOnOff has a value of 1 during AHU operating hours (from 7 AM-7 PM) and 0 otherwise.

The water flow rate \dot{m}_w is assumed to be constantly on in the MPC formulation. However, in a postprocessing step, the circulation pump is switched off when the difference between supply and return temperature is smaller than a predefined threshold.

10.3.2 Controller tuning parameters

With the use of the weighting-factors in the objective function, the MPC has tuning parameters. The weighting factors α_{du} and α_{do} allow to tune the MPC controller with respect to overheating and undercooling. E.g. when choosing $\alpha_{du} < \alpha_{do}$, the MPC will tolerate undercooling, when, in a summer situation undercooling during the first office hours is less important than overheating. The weighting factor F_1 is used to balance on the trade-off curve between energy cost and discomfort cost. The weighting factor F_2 is used to attribute a cost to thermal discomfort in relation to the energy cost. A high value of

F_2 will turn the thermal discomfort from a soft constraint into a quasi hard constraint.

For the examples shown below, the following weighting factors are used:

- $\alpha_{du} = 1$
- $\alpha_{do} = 1$
- $F_1 = 0.5$
- $F_2 = 0.01$: this value is chosen to make thermal discomfort cost and energy cost from CCA or AHU of the same order of magnitude.

10.3.3 Solar shading

To include the effect of solar shading (for the South zone), the data vector with the $\dot{q}_{sol,South}$ prediction is preprocessed for the prediction horizon H_p before it is applied to the MPC. The \dot{q}_{sol} prediction is corrected with $g_{solshade}$ at times when the solar shading is down, according to the device's controller settings (see Sec. 7.6). Solar shading is not implemented as an optimisation variable.

10.3.4 Power limitations

In order to limit initial investment cost, the heating and cooling power are limited to the values determined by the static heating and cooling load calculations. This is beneficial for the production units, but, additionally in the case of a ground coupled heat pump and ground cooling system, limits borefield investments. In general, any renewable energy source is limited in power and energy content.

The fact that the limited power is integrated in the MPC formulation, makes sure that the power peaks, which were observed with the conventional controller with unlimited production power, are avoided. The MPC provides a profile for T_{ws} and T_{vs} , which can always be met, given the system constraints are accurate. In this way, the systems power or energy content potential is fully exploited by the MPC.

The CCA is assumed to be connected to a low-temperature heating and high temperature cooling reversible air cooled heat pump. In this way, the presented

results can also be reached with a ground coupled heat pump and ground cooling system.

This results in limitations of both the temperature levels and the maximum power (see Sec. 3.3):

- $T_{ws,min} = 17^{\circ}C$
- $T_{ws,max} = 40^{\circ}C$
- $\dot{q}_{w,h,max} = 25 \text{ W/m}^2$
- $\dot{q}_{w,c,max} = 26 \text{ W/m}^2$

The heating and cooling coil in the AHU are connected to a backup system, consisting of a gas-fired boiler and a low temperature chiller. Therefore, a power limitation is not a matter in this case. However, a temperature limitation definitely is. In Sec. 7.3.5 it was stated that, due to the design of the heating and cooling coil, not every ventilation supply temperature can be reached. In order to limit the temperature drop in the AHU, the following limitations are imposed in the MPC controller:

- $T_{vs,min} = 20^{\circ}C$ (Winter), $18^{\circ}C$ (Summer)
- $T_{vs,max} = 35^{\circ}C$

These limits can be adapted depending on the actual state of the AHU.

10.3.5 Slack variables

The different terms of the objective function — thermal discomfort, CCA primary energy use and AHU primary energy use — all have two things in common: they are driven by a temperature difference and occur in two modes, as explained in Table 10.1.

Because for all three objectives, each time the same temperature difference is used in two distinct modes, slack variables are introduced to distinguish the two modes with respect to this temperature difference. In general, a slack variable is introduced in an optimization problem to transform an inequality

Table 10.1: Thermal discomfort, CCA and AHU primary energy use in the OCP objective function

Thermal discomfort	
ΔT	T_{op} vs. $T_{op,opt}$
Mode 1	Too cold: $T_{op} < T_{op,opt} - \Delta T_h$
Mode 2	Too hot: $T_{op} > T_{op,opt} + \Delta T_c$
CCA	
ΔT	$T_{water,supply}$ vs. $T_{concrete\ node}$
Mode 1	Heating: $T_{water,supply} > T_{concrete\ node}$
Mode 2	Cooling: $T_{water,supply} < T_{concrete\ node}$
AHU	
ΔT	$T_{air\ before\ coil}$ vs. $T_{air,set}$
Mode 1	Heating: $T_{air\ before\ coil} < T_{air,set}$
Mode 2	Cooling: $T_{air\ before\ coil} > T_{air,set}$

constraint into an equality constraint and a non-negativity constraint: $\mathbf{Ax} \leq \mathbf{b}$ or $\mathbf{Ax} - \mathbf{b} \leq 0$ becomes $\mathbf{Ax} - \mathbf{b} + \epsilon = 0$ with the help of the slack variable $\epsilon \geq 0$.

The slack variables for CCA primary energy, AHU primary energy and thermal discomfort are addressed in the following sections.

10.3.6 Discomfort cost

As elaborated in Ch. 6.2 and already applied in the evaluation of the conventional controller in Ch. 8, thermal discomfort is expressed as a function of PPD or the ‘Predicted Percentage of Dissatisfied’ with thermal comfort. However, since the calculation of the PPD requires an iterative procedure [93] and the knowledge of several hard to determine comfort parameters is required [96], a more simplified approach is required for the OCP discomfort cost. In the literature [83, 21, 148] the squared deviation between the operative temperature and the optimal operative temperature $T_{op,opt}$ is often used to implement the thermal discomfort cost in the OCP objective function, whether or not taking into account a neutral zone with zero discomfort cost around $T_{op,opt}$.

Using this ΔT^2 overestimates thermal discomfort due to its quadratic nature: for a 1 K exceeding of the comfort limits, it already yields a 30% higher value than the PPDh value. Applying this in the MPC controller will therefore

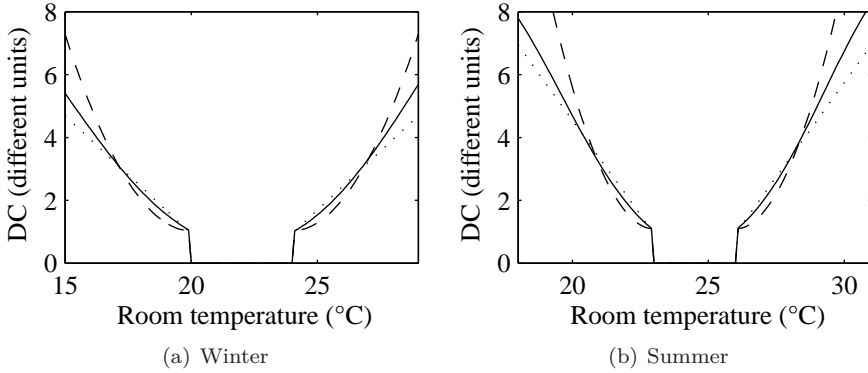


Figure 10.3: Thermal discomfort (DC) values for PPD (PPDh, —), linear (Kh, :) and quadratic (Kh², --) approach for winter ((a)) and summer ((b))

punish temperature violations more than would be expected from the PPD-theory. Introducing a correction factor f_{quad} (Fig. 10.3) to fit both approaches over a larger temperature interval can compensate for this. However, this $f_{quad}\Delta T^2$ -approach underestimates thermal discomfort for small violations of the operative temperature limits $T_{comf,min}$ and $T_{comf,max}$. Fig. 10.3 shows the result of the ‘PPDh’ thermal discomfort (DC) approach against a linear and a quadratic Kh-approximation, fitted to minimize deviation from the PPDh results. The figures are composed for the following settings:

- Reference DC: PPDh (see Ch. 6.2)
- Linear DC approximation: $DC = f_{lin} \|T_z - T_{comf,lim}\|$
- Quadratic DC approximation: $DC = f_{quad} (T_z - T_{comf,lim})^2$
- $T_{comf,lim}$: $T_{comf,min}$ or $T_{comf,max}$
- f_{lin} : 0.75 for winter conditions, 1.2 for summer conditions
- f_{quad} : 0.25 for winter conditions, 0.5 for summer conditions

Although the difference between the three discomfort approaches does not seem large, it does make a difference, since a large part of the discomfort is caused by a minor violation of the temperature limits $T_{comf,lim}$. This is observed in the results of the conventional controller (Ch. 8) and was also noticed e.g.

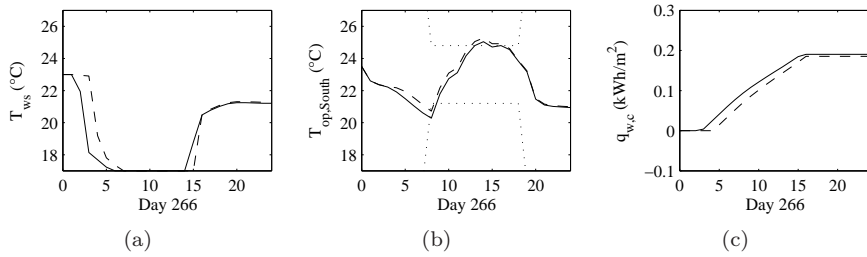


Figure 10.4: Comparison between the linear (—) and quadratic DC-fit (- -), (a) T_{ws} , (b) T_{op} and (c) \dot{q}_w for a summer day

in the OptiControl project [57]. In the quadratic DC-fit, a small violation of $T_{comf,lim}$, will be accounted for less severe than in the linear approach of the PPDh-value.

The fact that the chosen DC-fit does make a difference, is shown in Fig. 10.4, where the optimal profile for a summer day is calculated by the MPC controller with both the linear and the quadratic DC-fit. For both the linear and the quadratic fit, the first occupation hour is too cold, but in the afternoon there are several hours with a too high operative temperature. In the linear DC-fit, the MPC chooses to cool down the CCA more extensively compared to the quadratic fit, in order to avoid the afternoon high temperatures.

Table 10.2 shows that the linear and the quadratic DC-fit use the same amount of primary energy, but due to the different T_{ws} -profile, the afternoon discomfort is reduced with 60% for the linear approximation. In the remainder of the text, the linear DC-fit is chosen to model the PPD thermal comfort in the cost function of the OCP. Thermal discomfort is therefore expressed in Kelvinhour (Kh).

Table 10.2: Energy use (kWh/m²) and afternoon discomfort (Kh overheating) for the linear and quadratic thermal discomfort approach.

DC approach	E_{prim} (kWh/m ²)	DC (Kh)
DC _{linear}	0.19	0.24
DC _{quadratic}	0.19	0.56

10.3.7 CCA-water heating and cooling cost

The cost for heating up or cooling down the CCA is determined by the amount of heat transferred from the water in the tubes to the concrete slab: $\dot{q}_{CCA} = \dot{m}_w c_{p,w} (T_{ws} - T_{wr})$. In the simplified building notation, this is equal to: $\dot{q}_{CCA} = (T_{ws} - T_c) / R_3$, where R_3 is the thermal resistance from T_{ws} to the lumped capacitance of the concrete slab at the temperature state T_c . In Ch. 9 it was shown that the identification procedure provides information on the lumped parameter RC_{ws-c} , but not on the R -parameter itself. Therefore, the value coming from the initial model with physically defined parameters is used hereafter: $R_3 = R_c + 0.5(R_1 || R_2) = 0.18 \text{ m}^2 \text{ K/W}$ ¹ for the CCA with raised floor used in the office building model. Eqs. 10.16-10.17 present the implemented energy cost function for the water circuit in the CCA:

$$J_{ew} = F_{ew} \dot{m}_w c_{p,w} (T_{ws} - T_{wr}) \quad (10.16)$$

$$= F_{ew} \frac{(T_{ws} - T_c)}{R_3} \quad (10.17)$$

with:

- T_{ws} (K): requested water supply temperature.
- T_c (K): concrete core temperature.
- J_{ew} (kWh/m²): cost function for the CCA water circuit, presented as primary energy
- F_{ew} (-): conversion factor containing production efficiency and the primary energy factor.
- Heat and cold are supposed to be supplied by a reversible air cooled heat pump with $SPF = 3.9$ and $SEER = 3.5$.
- The primary energy conversion factor $1/\eta_{elec} = 2.5$ for electricity (based on the Belgian electricity park).

The distinction between heating and cooling is made based on the sign of the temperature difference ($T_{ws} - T_c$), resulting in Eqs. 10.18-10.19 for respectively

¹($R_1 || R_2$) refers to the parallel thermal resistances R_1 and R_2

heating and cooling.

$$(T_{ws} - T_c) \geq 0 \Leftrightarrow J_{ew,h} = \frac{\epsilon_{w,h}\eta_{elec}}{1000R_3 \text{ SPF}}, J_{ew,c} = 0 \quad (10.18)$$

$$\epsilon_{w,h} = T_{ws} - T_c \Rightarrow T_c - T_{ws} + \epsilon_{w,h} = 0, \text{ with } \epsilon_{w,h} \geq 0$$

$$(T_{ws} - T_c) \leq 0 \Leftrightarrow J_{ew,c} = \frac{\epsilon_{w,c}\eta_{elec}}{1000R_3 \text{ SEER}}, J_{ew,h} = 0 \quad (10.19)$$

$$\epsilon_{w,c} = T_c - T_{ws} \Rightarrow T_{ws} - T_c + \epsilon_{w,c} = 0, \text{ with } \epsilon_{w,c} \geq 0$$

10.3.8 Ventilation heating and cooling cost

The cost for heating or cooling the ventilation air is determined by the heat transferred from water to air in the heating and cooling coil of the air handling unit. In Chapter 7, Sec. 7.3.4 and in App. C it is shown that for cooling, the dehumidification is an important factor influencing the heat transferred. However, in order to simplify the ventilation cost in the objective function, only the sensible heat is taken into account, both for heating and cooling.

The heating and cooling coil make sure the ventilation set point temperature $T_{vs,set}$ is reached, starting from the air exiting the heat recovery. Using the simplified building model nomenclature, the simplified expression for the energy cost associated with the heating or cooling coil is given by Eqs. 10.20-10.21:

$$J_{ev} = F_{ev}\dot{m}_{vs}c_{p,a}(T_{vs} - T_{HR,out}) \quad (10.20)$$

$$= F_{ev}\dot{m}_{vs}c_{p,a}[T_{vs} - (T_{amb} + 0.95\epsilon_{HR}(T_z - T_{amb}))] \quad (10.21)$$

with:

- \dot{m}_v (kg/sm²): ventilation flow rate,
- $c_{p,a}$ (J/kgK): specific heat capacity,
- ϵ_{HR} (-): efficiency of the AHU heat recovery unit,
- $T_{HR,out}$ (K): the ventilation air temperature after the heat recovery (T_{s2} in the nomenclature of Fig. 7.5),

- T_{vs} (K): requested ventilation supply temperature (T_{s4} in the nomenclature of Fig. 7.5),
- T_{amb} (K): ambient temperature (T_{s1} in the nomenclature of Fig. 7.5),
- T_z (K): room temperature (T_{r1} in the nomenclature of Fig. 7.5),
- J_{ev} (kWh/m²): cost function for heating and cooling the ventilation air, presented as primary energy,
- $F_{ev}(-)$: conversion factor containing production efficiency and the primary energy conversion factor,
- heat is supposed to be supplied by a gas-fired boiler with efficiency $\eta = 0.9$ and cold by an air cooled chiller with $SEER = 3$ and
- the primary energy conversion factors are $\eta_{gas} = 1$ for natural gas and $1/\eta_{elec} = 2.5$ for electricity.

Two simplifications for the ventilation cooling energy induce deviations from the real situation. Firstly, using only sensible cooling energy results in an underestimation of the real cooling energy use. Secondly, since the bypass of the heat recovery is neglected (see Sec. 7.3.4), the MPC may wrongly think the incoming air needs to be cooled, while, due to the activation of the bypass, this is not the case.

Distinction between heating and cooling is introduced by the slack variables $\epsilon_{v,h} \geq 0$ and $\epsilon_{v,c} \geq 0$, resulting in Eqs. 10.22-10.23 for respectively heating and cooling:

$$(T_{vs} - T_{HR,out}) \geq 0 \Leftrightarrow J_{ev,h} = \frac{\epsilon_{v,h} \dot{m}_{vs} c_{p,a} \eta_{gas}}{1000 \eta}, J_{ev,c} = 0 \quad (10.22)$$

$$\epsilon_{v,h} = T_{vs} - T_{HR,out} \Rightarrow T_{HR,out} - T_{vs} + \epsilon_{v,h} = 0, \text{ with } \epsilon_{v,h} \geq 0$$

$$(T_{vs} - T_{HR,out}) \leq 0 \Leftrightarrow J_{ev,c} = \frac{\epsilon_{v,c} \dot{m}_{vs} c_{p,a} \eta_{elec}}{1000 SEER}, J_{ev,h} = 0 \quad (10.23)$$

$$\epsilon_{v,c} = T_{HR,out} - T_{vs} \Rightarrow T_{vs} - T_{HR,out} + \epsilon_{v,c} = 0, \text{ with } \epsilon_{v,c} \geq 0$$

The AHU operates with a hygienic flow rate of 36 m³/h pers and only from 7 AM-7 PM, as provided in the basic control strategy of the building. The

limited operation period of the ventilation limits its contribution to control thermal comfort.

10.3.9 Initialisation of the system state

The state vector is initialized with \mathbf{X}_0 . For this 2nd order model, $T_{op,0}$ and $T_{c,0}$ are measured room and concrete core temperature of the room or zone to be controlled. Obtaining these two values from a real building is not straightforward.

T_{op} should be the representative operative temperature for the whole room, or even more difficult, for a group of rooms making up one control zone. In reality this temperature can be measured, but is location dependent: close to a colder window, the mean radiative temperature is lower than more centrally in the room. Certainly for CCA, which depends strongly on radiative heat transfer, this is crucial.

A measurement of T_c should reflect the ‘temperature of the concrete slab’. However, in the grey-box 2nd order model with the parameters estimated using data from the detailed 2-zone office model, this temperature is not related to a certain location in the slab, determined by the thermal resistances to the surrounding states or inputs. Due to the parameter estimation procedure, this information is lost.

10.4 Evaluation of the MPC controller

Firstly, the behaviour of the MPC controlling only the CCA (MPC-CCA) is investigated for a typical heating situation and a typical cooling situation. In both situations, a sequence of Sunday-Monday is chosen in order to observe the week start up, which gave rise to peak power and discomfort problems with the conventional heating/cooling curve controller (HCC). Secondly, the effect of incorporating the ventilation energy in the OCP, is evaluated (MPC-CCA-AHU). This provides insight in the cooperation between the slow reacting CCA system and the fast reacting AHU.

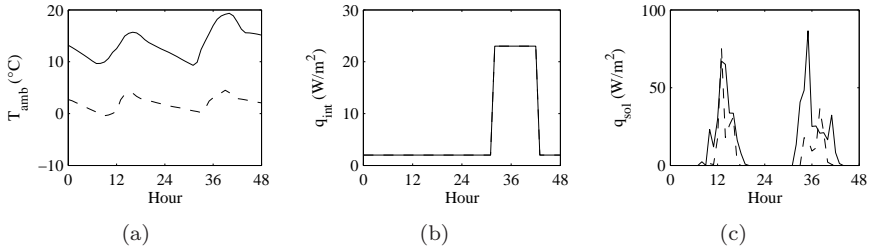


Figure 10.5: Heating (---) and cooling (—) evaluation period for the MPC controller with (a) ambient temperature T_{amb} , (b) internal gains \dot{q}_{int} and (c) solar gains \dot{q}_{sol} , both relative to the office floor area.

10.4.1 Evaluation period

For the cold period, Sunday, January 6th and Monday, January 7th represent two consecutive days with low solar radiation combined with low outdoor temperatures. For the hot period, Sunday, September 22nd and Monday, September 23rd, are two days with a high solar load and high outdoor temperatures. Due to the lower position of the sun, these September days have typically a higher solar load on a South facing vertical surface than real summer days.

Fig. 10.5 shows the ambient temperature, internal gains and solar radiation for these two periods. The chopped off profile of the solar radiation in the cooling period is caused by the solar shading being active at high solar radiation values ($\dot{q}_{sol} > 250 \text{ W/m}^2$ window area or $> 90 \text{ W/m}^2$ floor area).

10.4.2 Heating operation

As a reference for the behaviour of the conventional controller, the modified-HCC (HCC2) strategy from Ch. 8 is taken, with a heating and cooling power limited to the static design value and without night set back. The behaviour of this controller for the South zone will be compared with the MPC with and without ventilation control. The system behaviour with the HCC2 controller in the heating situation is presented in Fig. 10.6. When heating is on, it is operating at 50 W/m^2 , which is the double of the design power. As explained in Ch. 8, this is due to the switching between the South and the North zone.

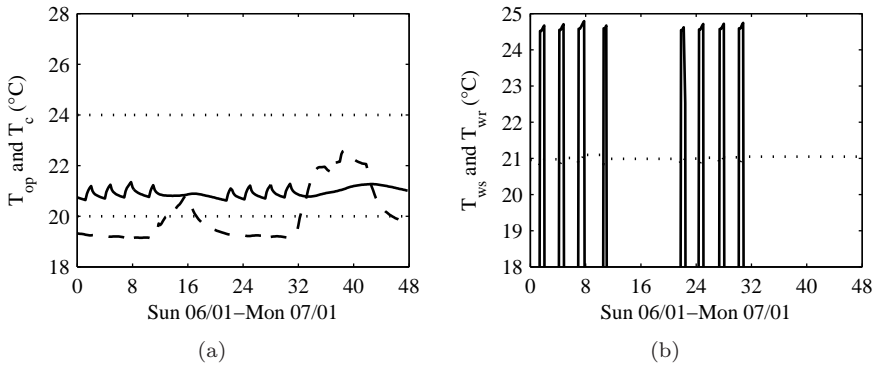


Figure 10.6: System heating behaviour with the reference modified-HCC controller: (a) T_{op} (---) and T_c (—). The comfort band is shown by the dotted lines. (b) T_{ws} (—) and T_{wr} (·)

Due to the absence of night setback, the 20–24°C comfort band is active during the whole period, including Sunday.

Modified-HCC controller behaviour

Applying the modified-HCC controller, the CCA ceiling surface temperature $T_{CCA,surf}$ is controlled at 20°C. When heating starts up, approximately 1 h later the set point is reached and the heating stops. This cycle is repeated during night periods, which makes that the modified-HCC controller is actually keeping the CCA core at a constant temperature with an average of 20.9°C. The reason why this is a good controller lies in the fact that when the building is cooling down, the CCA are heating the zone. However, the surface temperature is moderate so that when T_{op} increases due to heat gains, the CCA automatically start cooling.

Ventilation air is supplied at 20°C during office hours.

MPC-CCA control

When the MPC controls the office building, heating starts up at 9 PM on Sunday evening in order to have the air temperature at 20°C on Monday morning at 8 AM (Fig. 10.7). Since the heating power limited to 25 W/m²,

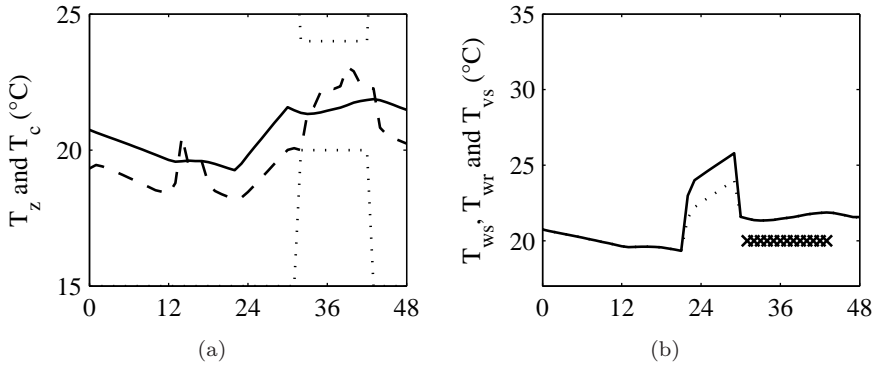


Figure 10.7: System heating behaviour with the MPC-CCA controller: (a) T_z (- -) and T_c (—). The comfort band is shown by the dotted lines. (b) T_{ws} (—), T_{wr} (:) and T_{vs} (×)

T_{ws} can only increase gradually. Equal to the TRNSYS case, ventilation air is supplied at 20°C during office hours.

The self regulating effect of the CCA is visible, with the CCA being warmer during the heating period, but colder than T_z during the hours with heat gains. Different from the modified-HCC controller, the CCA are not kept at a constant temperature anymore, but the MPC-CCA acts as an optimal start-up controller.

MPC-CCA-AHU control

In this case, the AHU is operating during office hours, but the ventilation supply temperature T_{vs} can be freely chosen by the MPC controller. Of course, T_{vs} is constrained as stated in Sec. 10.3.4.

The behaviour of the MPC-CCA-AHU controller shows an interesting effect (Fig. 10.8). The CCA start up heating only at 0 AM, so 3 h later than with the MPC-CCA controller. T_{vs} is raised to its maximum value of 35°C during the first hour of AHU operation, in order to get T_z at comfort level at 8 AM. Afterwards, T_{vs} drops to its minimum value in order to save heating energy. T_z is slightly lower during the office hours compared to the MPC-CCA controller, but remains within the comfort band.

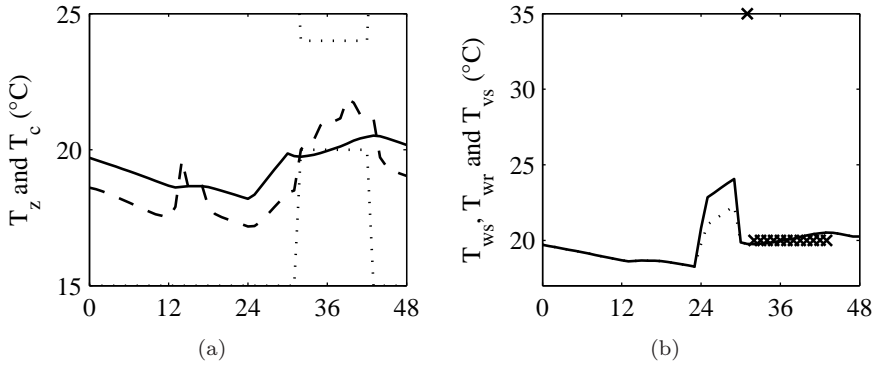


Figure 10.8: System heating behaviour with the MPC-CCA-AHU controller: (a) T_z (---) and T_c (—). The comfort band is shown by the dotted lines. (b) T_{ws} (—), T_{wr} (·) and T_{vs} (+)

Table 10.3: Comparison of energy use (kWh/m^2) and thermal discomfort (Kh) between the MPC-CCA and MPC-CCA-AHU controllers from the OCP

Controller	$E_{CCA,prim}$ (kWh/m^2)	$E_{AHU,prim}$ (kWh/m^2)	$E_{TOT,prim}$ (kWh/m^2)	DC (Kh)
MPC-CCA	0.16	0.08	0.24	-0.00
MPC-CCA-AHU	0.09	0.11	0.20	-0.00

Again here, the self regulating effect is visible, with the CCA cooling down the office zone during office hours. CCA energy use is lower due to the lower average T_c compared to the MPC-CCA-controller.

Energy use and thermal discomfort

Table 10.3 presents the primary energy used by the CCA and to heat up the ventilation air, together with the discomfort level, expressed in Kh. The T_{vs} increase at 8 AM with the MPC-CCA-AHU controller cost 38% more ventilation energy, while the CCA-energy cost reduces with 44%. The total primary energy consumption is the lowest for the MPC-CCA-AHU controller, indicating that a combination of CCA and ventilation yields an optimal result.

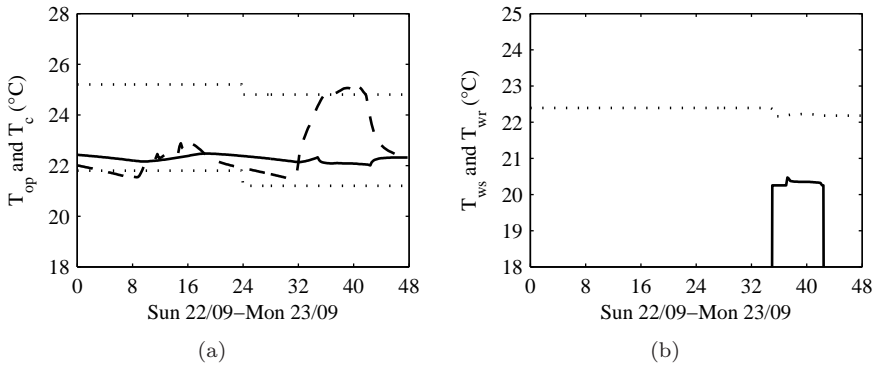


Figure 10.9: System cooling behaviour with the reference modified-HCC controller: (a) T_{op} (---) and T_c (—). The comfort band is shown by the dotted lines. (b) T_{ws} (—) and T_{wr} (:)

10.4.3 Cooling operation

For the cooling situation, the behaviour of the reference HCC2 controller is presented in Fig. 10.9. When cooling is on, the system is operating at 26 W/m^2 .

Modified-HCC controller behaviour

In the modified-HCC controller the CCA ceiling surface temperature $T_{CCA,surf}$ is controlled at 22.8°C . Unlike in the heating case, cooling starts up at 10 AM on Monday morning and stops at 6 PM, working constantly during the whole day. On Sunday, there are no internal gains, therefore cooling is not needed. But again, the modified-HCC controller is actually keeping the CCA core at a nearly constant temperature with an average of 22.3°C . The reason why this is a good controller lies in the fact that the self regulating effect is also working in this case. During the night, the CCA is mildly heating the office, while cooling starts up when the T_z starts to increase due to heat gains.

Ventilation air is supplied at 20°C during office hours.

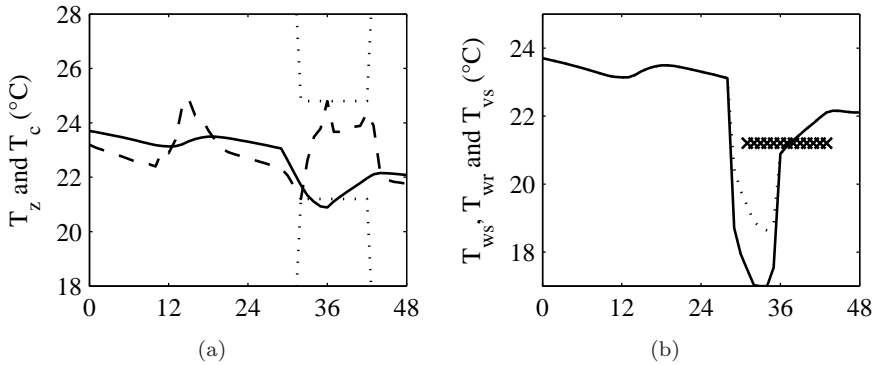


Figure 10.10: System cooling behaviour with the MPC-CCA controller: (a) T_z (- -) and T_c (—). The comfort band is shown in the dotted lines. (b) T_{ws} (—), T_{wr} (:) and T_{vs} (+)

MPC-CCA control

When the MPC controls the office building, cooling starts up at 5 AM on Monday morning to obtain two results: preventing T_z to become too low at 8 AM, but even so preventing an overshoot of T_z , particularly due to solar gains (Fig. 10.10). Since the cooling power is limited to 26 W/m^2 , T_{ws} can only decrease gradually. Unlike with the modified-HCC controller, cooling already stops at 12 PM. Equal to the modified-HCC case, ventilation air is supplied at 20°C during office hours.

The self regulating effect of the CCA is visible, with the CCA being warmer during the night, but colder than T_z during the hours with heat gains. This behaviour is similar as with the modified-HCC controller. Again, the MPC-CCA acts as an optimal start-up controller. In the first 3 hours of cooling operation, from 5 AM until 8 AM, T_c remains higher than T_z , although cooling is on and T_z decreases. This is due to the rather low ambient temperature at this moment (see Fig. 10.5(a)). Therefore, operating the cooling comes down to reducing the heating power of the CCA which is compensating the heat loss to the ambient at that time. The CCA really starts cooling when $T_c < T_z$.

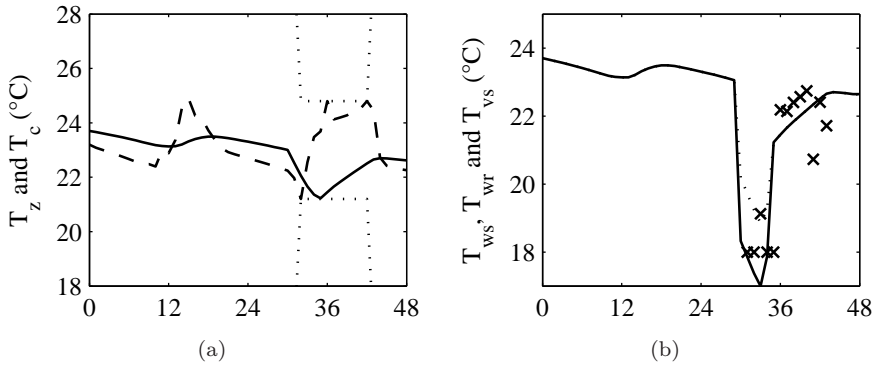


Figure 10.11: System cooling behaviour with the MPC-CCA-AHU controller: (a) T_z (- -) and T_c (—). The comfort band is shown in the dotted lines. (b) T_{ws} (—), T_{wr} (:) and T_{vs} (+)

MPC-CCA-AHU control

In this case, the AHU is operating during office hours, but the ventilation supply temperature T_{vs} can be freely chosen by the MPC controller. Again here, T_{vs} is constrained as stated in Sec. 10.3.4.

The behaviour of the MPC-CCA-AHU controller is shown in Fig. 10.11. The CCA starts to be cooled only at 6 AM, so 1 h later than with the MPC-CCA controller. Cooling stops 1 h earlier, at 11 AM.

Immediately at the start up of the AHU, T_{vs} is decreased to its minimum value of 18°C. This guarantees that T_z is at minimum comfort value at 8 AM, so the full comfort range is available for T_z to cope with the heat gains during the day. For the remainder of the day, starting from 12 AM, the AHU operates at a higher T_{vs} than in the MPC-CCA-case. Even so, the peak of solar gains at 3 PM, due to raising the solar shading, is compensated by the AHU and not by the CCA: T_{vs} is lowered to 21°C at this moment.

Again here, the self regulating effect is visible, with the CCA cooling down the office zone during office hours. CCA energy use is lower due to the higher average T_c compared to the MPC-CCA-controller.

Table 10.4: Comparison of energy use (kWh/m²) and thermal discomfort (Kh) between the MPC-CCA and MPC-CCA-AHU controllers from the OCP

Controller	$E_{CCA,prim}$ (kWh/m ²)	$E_{AHU,prim}$ (kWh/m ²)	$E_{TOT,prim}$ (kWh/m ²)	DC (Kh)
MPC-CCA	0.12	0.02	0.14	-0.00
MPC-CCA-AHU	0.09	0.01	0.10	0.00

Energy use and discomfort

Table 10.4 presents the primary energy used by the CCA and to heat up the ventilation air, together with the discomfort level, expressed in Kh.

The T_{vs} decrease observed with the MPC-CCA-AHU controller does not require more AHU primary energy. This might look surprisingly, but it is due to the fact that $E_{AHU,prim}$ is heating energy instead of the expected cooling energy. In fact, the MPC is optimally using free cooling with the ventilation air. Since a September day is considered, T_{amb} is already low. The heat recovery unit can not fully heat up the air to set point, and therefore it requires less primary energy to heat up the air to 18°C with the MPC-CCA-AHU controller than to 20°C with the MPC-CCA controller. The total primary energy consumption still remains the lowest for the MPC-CCA-AHU control, indicating that a combination of CCA and AHU also yields an optimal result here.

10.5 Conclusions

This chapter presents a formulation for the objective function in a Model based Predictive Controller, which is trying to minimize thermal discomfort, expressed in PPDh and primary energy use of both CCA and AHU. Tuning parameters can be used to give more or less weight to the different terms in the objective function. The MPC formulation is flexible and can be freely adapted, e.g. to incorporate financial cost.

Since the PPDh-approach used in the evaluation of the conventional controller (Ch. 8) is non-linear, a Kelvinhour-approach (Kh) is implemented in the OCP-formulation. A linear Kh function corresponds best with the general PPDh value.

The primary energy cost for both CCA and AHU is taken into account in the MPC objective function. The MPC fully exploits the temperature band provided by the comfort range, thereby taking into account the dynamics of CCA and building. When the ventilation supply temperature T_{vs} is a controlled variable, the MPC will use the AHU to compensate heat gain peaks in a cooling regime, e.g. due to solar radiation, while the CCA is used in night time to precool the building.

Both for heating and cooling, the MPC controls the CCA as an optimal start-up controller. In heating, when T_{vs} is controlled, the AHU will be used to achieve thermal comfort during the first office hours. The implemented MPC formulation is capable to combine the slow reacting CCA with the fast reacting AHU, when controlling thermal comfort at the lowest possible energy cost.

Looking at the concrete core temperature, the MPC does not try to keep the concrete core temperature at a constant level. This was however the result of the conventional controller with the best settings. On the contrary, in order to save energy, the MPC only heats up or cools down the CCA as much as required (but not more) to obtain thermal comfort.

Both energy use and thermal discomfort can potentially be reduced compared to the conventional controllers, both in heating and cooling. However, implementation in a real building introduces important errors, due to building model mismatch, cost function mismatch and weather prediction uncertainties.

Part IV

Conclusions and outlook

Chapter 11

Summary and Conclusions

11.1 Summary

In this work, the dynamic behaviour of Concrete Core Activation (CCA) is analysed and incorporated into the control strategy of an office building. With CCA, the concrete slabs of an office building are actively conditioned using embedded water tubes.

The case study of a 1000m² office building with CCA demonstrates the overwhelming importance of measuring the building's HVAC system as well as analysing the measurement data thoroughly: an efficiently working heat pump and ground cooling system was masking inefficient CCA controller operation. Due to switching between heating and cooling during one day, the CCA was loaded and unloaded with heat without a substantial contribution to the thermal conditioning of the office zone.

Moreover, a simplified, 2nd-order building model was able to reproduce the measured control behaviour and to estimate the amount of energy which was squandered by the heating/cooling switching. These qualitative results showed that only a quarter of the produced heating energy and one half of the produced cooling energy was effectively used to condition the office zone.

By means of the EMPA CCA model [81], a static analysis of the heat transfer from water to the zones above and below reveals that the thermal resistance of the plastic tubing — up to 10% of the total thermal resistance from water to

zone — should not be neglected. Moreover, this analysis identifies the water supply temperature as the preferred control variable over the flow rate, taking into account heat/cold production and pump efficiency.

This static analysis shows that in steady state CCA heating power is sufficient to compensate the heating loads of a high-quality office building. However, for office buildings which are typically characterised by high internal gains, CCA can not generate enough cooling power to compensate the cooling loads. Nevertheless, from the static CCA model, the heating and cooling curve can be derived, which serves as the reference point of the CCA control algorithm, conventional or advanced.

Lab scale measurements of the transient CCA behaviour evidently show a large delay and damping of changes in water supply temperature when monitoring CCA surface temperatures. Moreover, a relevant flow propagation effect is monitored, which is important for short term pump cycling: a change in water supply temperature requires time to propagate through the whole tube in the CCA. Furthermore, high power peaks are observed when changing the water supply temperature: more than double of the steady state heat power.

An analytical expression is derived to grasp these effects. Again starting from the EMPA model and using the analytical solution of transient heat transfer in a slab, a solution is found to describe the time- and 1D-place-dependent temperature profile inside the concrete slab of the CCA. From this, an analytical expression for the transferred thermal power and thermal energy can be derived. The effect of flow propagation is incorporated by using an Equivalent Supply Temperature, which compensates for the lower mean water temperature while a change in water temperature is propagating through the tubes. Validation by a finite difference approach shows the accuracy of this measure.

Simplifying this analytical expression, by only taking the first term of the infinite sum, results in an expression which determines the required time to reach a certain amount of thermal energy transferred from the water to the zone, while taking into account the initial condition of the concrete slab and the heat transfer parameters. This expression is useful to determine start-up times of the CCA installation.

The analytical expression is used to quantify CCA control behaviour. The controller should keep the CCA 'loaded' with heat or cold in order to avoid start-up effects which require a huge amount of energy: regardless of the pump

control, over 50% of the thermal energy supplied to the CCA by the water, is used to increase the temperature of a 20 cm thick slab, and therefore not transferred to the zone. This agrees with the results of the qualitative case study analysis. Switching between heating and cooling should absolutely be avoided: an example shows that with less than 1/3rd of the energy, a ‘cooling-only’ case extracts more than double the amount of thermal energy from a room compared to a case where the CCA were heated at the beginning of the day and cooled at the end, as was observed in the case study. Also, loading the CCA with a higher (for heating) and lower (for cooling) water supply temperature, decreases the loading time of the CCA.

Evidently, the dynamic behaviour of CCA can not be decoupled from the dynamic behaviour of the building. A frequency response analysis shows that the control range of CCA does not correspond to a large part of the frequency range of the zone disturbances: ambient temperature, solar radiation and internal gains. Strictly speaking, CCA can only fully control effects with a periodicity of 1 week or more. The heat transfer coefficient from CCA surface to the zone, is identified as a critical parameter, which should be assessed with care. A 3rd-order CCA model proves to be accurate in representing the dynamic behaviour of a CCA slab.

A detailed CCA building model, set up in the dynamic simulation environment TRNSYS, consisting of two office zones separated by a corridor, is used as a test-case to analyse control strategies. In a first step, an analysis of a conventional feedback controller with a heating/cooling curve, shows that, although this controller lacks a dynamic CCA-and-building model, it achieves adequate control behaviour when using appropriate controller parameters: it comes down to keeping the CCA at the temperature required by the heating/cooling curve, this means, keeping the CCA ‘loaded’. This behaviour was already predicted by the analysis of the transient behaviour using the analytical expression. By using a respectively higher and lower heating/cooling curve, this controller automatically achieves alternating zone operation: the thermal inertia of the CCA is used to operate the zones one-by-one. This is an important controller feature which should be implemented in real buildings since it allows to direct the full power of the production units to only 1 zone. Therefore, a lower production power can be installed compared to the case where all zones are operating simultaneously. Night setback of the temperature setpoints should be avoided in heating regime.

In order to integrate a dynamic model of a CCA building in a controller,

a simplified model of not only CCA but of CCA-and-building is required. Using an automated MATLAB procedure, a state-space grey-box model is constructed having a predefined layout. Identification of the model parameters using 'measurement data' of the TRNSYS 2-zone building model, reveals the importance of setting constraints on the allowed parameter range, in order to obtain physically meaningful parameter values. Realistic data sets, for which the different disturbances occur simultaneously, hamper the identification process. In-situ excitation tests appear necessary to obtain an accurate building model. The identification results show that solar radiation requires a separate temperature node for the simplified building model to reproduce the building dynamics with an acceptable accuracy.

Using this CCA-and-building controller model, the framework of an optimal Model based Predictive Controller (MPC) is proposed in which CCA and ventilation cooperate to condition the office zone. The operational cost of CCA and ventilation are weighted against the cost of thermal discomfort. Thermal power limitations are set to the production units and temperature limitations to the water and air supply temperatures. Cost function errors, model errors, weather and other disturbance prediction uncertainties are not taken into account. As can be expected, this MPC gives priority to the CCA, but uses the ventilation to cover cooling load peaks. The MPC determines the required start-up time of the CCA, taking into account the limited power of the production units.

11.2 Conclusions

It is the aim of this work to analyse the dynamic thermal behaviour of CCA in buildings and to derive guidelines for the design of a CCA controller. This problem is addressed in different ways: by investigating a CCA element and by investigating the interaction between CCA and building. Although each of these subdivisions does not contain an elaborate sensitivity study on its own showing the robustness of their conclusions, these subdivision conclusions correlate which shows their generality.

If energetic building performance is a key factor, CCA is a useful technique because it requires an energetically well designed building: heat loads and losses should be limited because of the intrinsic low available thermal power of CCA and its slow reaction time caused by the large thermal mass.

CCA can be favourable over competing fast reacting systems, because it enables the use of energy efficient production systems such as heat pumps and ground cooling. CCA operates at high heating temperatures and low cooling temperatures. Moreover, too high heating temperatures and too low cooling temperatures must be avoided to prevent thermal overload of the CCA.

It is possible to actively control thermal comfort with CCA, both by a conventional feedback controller as in an optimal way with an enhanced model based predictive controller (MPC). However, for the latter, tackling the problem of the large amount of required engineering work and of its sensitivity to model errors, cost function errors, prediction uncertainties and measurement errors, will be crucial for a widespread implementation of this MPC.

The control strategy can turn the large thermal mass of CCA into a benefit. With alternating zone control, the building can be operated zone-by-zone, requiring a production system with an installed thermal power that is lower than the whole building load. Changing the intermittence of the water circulation pump operation, enables to choose between transferring thermal energy to the building zone and storing thermal energy in the concrete slab.

The analysis of CCA dynamic thermal behaviour does not always require complex numerical techniques. An analytical expression is formulated and used to evaluate CCA operation and to derive simplified guidelines for CCA design and control.

An important transient CCA feature is that the required thermal power to

operate CCA at a set water supply temperature is always higher than the thermal power calculated for steady state conditions. This counteracts partially the CCA benefit of alternating zone operation and its resulting lower installed thermal production power.

Neglecting the effect of the water flow propagating through the CCA-tube is identified as the possible source of model error in currently used CCA thermal models.

The results of this work enable to draw the following conclusions regarding the features a conventional CCA controller should have. These features are derived taking into account thermal discomfort and primary energy use.

- Adapt the controller settings to the specific case.
- Apply solar shading and reduce heat gains and losses in general.
- Think about the control strategy when sizing the production system.
- Avoid switching between heating and cooling during the same day.
- Keep the CCA temperature at level: higher in winter and lower in summer, to avoid power peaks and long start-up times
- Apply elevated water temperatures to ‘load’ the CCA more quickly: $+3/-3^{\circ}C$ compared to the conventional heating/cooling curve is a good setting for the example shown in this work.
- Avoid to ‘overload’ the CCA by using too high/low water temperatures or long pump operation times.
- Benefit from the large thermal capacity of CCA by achieving alternating zone operation, in order to have lower building-level production power
- Do not apply night setback for heating (night setback can be applied for cooling)

These features should be either inherent to the controller operation or imposed ‘manually’ by restricting the system operation while programming the controller.

Chapter 12

Further research

This work shows that the dynamic behaviour of CCA can be analysed using relatively simple expressions and dynamic models. However, several steps still have to be taken before a model based controller can be integrated in a real building.

Although the analytical expression can predict the dynamic phenomena which are encountered in measurements, it still needs a thorough validation in order to assess the accuracy and the validity range. Also, adaptation of the expression in case of non-homogeneous concrete slabs needs to be investigated.

Where the simplified analytical expression, presented in this work, can predict the start-up time of CCA while taking into account the initial condition of the slab and the heat transfer parameters, it should be investigated how this initial condition of the concrete slab can be monitored in reality: which sensors should be placed at which position and how should measurement errors be addressed?

Further research efforts are certainly required to improve the parameter estimation of the simplified building models. Results of parameter estimation procedures should be analysed to obtain better and more accurate initial building models. Off-line and on-line parameter estimation procedures should be standardised in order to have a wide-spread implementation of model based controllers in buildings.

The cost function of an optimal Model based Predictive Controller (MPC) should be addressed with care and adapted to each specific situation. If the

weights of the different costs — CCA operation, air handling unit (AHU) operation and thermal discomfort — do not agree with reality, the MPC is looking for an optimal operation which will not be optimal in reality. The operational cost of the CCA water system, with circulation pumps and heating and cooling production units, and of the AHU, with the fan consumption and the heating and cooling coils, should be defined and integrated into the MPC using a robust procedure. For a successful implementation of MPC, finding the correct value behind each symbol, is crucial.

The implementation of the MPC in a building, dealing with model errors, cost function errors, disturbance prediction uncertainties, measurement errors, integrating the long-term effect of the ground thermal balance in a ground coupled heat pump system, . . . is not addressed in this work, but will decrease the potential savings of the MPC. Further details on this implementation can be found in Verhelst [140]. Assessing the large implementation effort against the benefits on thermal comfort and energy use, is certainly a point of special interest.

Also, the integrated design is an important issue while assessing the potential of CCA, ground coupled heat pump systems with direct ground cooling and air handling units. If MPC of CCA demands other than heating/cooling curve temperatures, the ground coupled heat pump system should be able to produce these. When the AHU is deployed to compensate load peaks, the design of its heating and cooling coils should allow the required air supply temperatures. Furthermore, if the heating and cooling coil of the AHU is coupled to the heat pump system, the thermal balance of the ground can be improved. Moreover, when the heat recovery unit of the AHU is reduced or even omitted, the excess heat demand of the AHU might compensate even more a potential excess cold demand of the building. But is the efficiency loss by reducing the heat recovery compensated by the increased efficiency of the heat pump system? Reducing the heat recovery will also reduce the pressure drop which the fans have to compensate, thereby reducing the fan energy use. One might think of actively controlling the heat recovery by using a bypass. If the MPC requires the ground to be pre-cooled to condition it for the next day, which solution is the most cost-effective and feasible to realise? This question asks for a fully integrated system approach.

Part V

Appendices

Appendix A

Adaptive versus non-adaptive thermal comfort models in moderate climates

A.1 Introduction

CCA is regarded as a top-cooling system rather than as a full air-conditioning system. Therefore, adaptive thermal comfort models (ASHRAE55, ISSO74 or EN15251) are supposed to be applicable to CCA buildings, although the comfort model conditions are not necessarily satisfied. This appendix investigates whether, for a moderate climate and with the heating and cooling set points chosen according to the adaptive models, the building's energy use reduces. After all, applying adaptive models, if appropriate, is thought to lower energy use because higher maximum operative zone temperatures $T_{op,max}$ are allowed in summer, compared to the conventional ISO7730 model. For purpose of generality, a building with an ideal heating and cooling system is considered.

This appendix is based on the paper: 'Evaluation of adaptive thermal comfort models in moderate climates and their impact on energy use in office buildings' by Sourbron and Helsén [125].

A.2 Thermal comfort

Thermal comfort being “that condition of mind which expresses satisfaction with the thermal environment” [6] is a definition much encountered in the literature. But what is often omitted is the affix “and is assessed by subjective evaluation”, meaning that translating the conditions for achieving thermal comfort into universally applicable equations – a task which engineers very much like to perform – is a difficult, if not impossible task. Several thermal comfort standards [6, 44, 68, 136] provide information to the building designer on defining a good indoor climate. Subsequently, the choice of this thermal comfort model results in set points to be used in the HVAC installation. And therefore, this choice will influence the resulting energy use of the building meaning that the thermal comfort model chosen will be one of the factors determining the sustainability of the building.

The question on how the choice of thermal comfort model influences the energy use, presents itself. Which HVAC set points result from the adaptive thermal comfort models of ASHRAE55 [6], ISSO74 [136] and EN15251 [44] for the moderate climate of Western and Central Europe, compared to the conventional PMV-PPD model given by ISO7730 [68]? And which impact has the choice of comfort model on the energy use? This appendix intends to respond to these questions.

A.3 Thermal comfort theory

A.3.1 Basic thermal comfort theory

The basic theory of thermal comfort, developed by Fanger and translated in the international standard ISO7730 [68], is based on the prediction of the number of dissatisfied people (PPD or Predicted Percentage of Dissatisfied). Literature on this theory is abundant, an excellent summary amongst others is given by Olesen and Parsons [99]. Annex A of this standard defines three categories of thermal environment – A, B and C – with prescribed limits for both global as well as local discomfort (Table A.1 and A.2).

Table A.1: Categories for global thermal environment from ISO7730, Annex A. (PPD: Predicted Percentage Dissatisfied; PMV: Predicted Mean Vote)

Category	Thermal state of the body as a whole	
	PPD (%)	PMV
A	≤ 6	$-0.2 \leq PMV \leq +0.2$
B	≤ 10	$-0.5 \leq PMV \leq +0.5$
C	≤ 15	$-0.5 \leq PMV \leq +0.5$

Table A.2: Categories for local thermal environment from ISO EN 7730, Annex A. (DR: draught rate, percentage of people bothered by draught; PD: percentage dissatisfied)

Category	Local discomfort			
	DR (%)	PD (%) caused by		
		Vertical air temperature difference	Warm or cold floor	Radiant asymmetry
A	≤ 10	≤ 3	≤ 10	≤ 5
B	≤ 20	≤ 5	≤ 10	≤ 5
C	≤ 30	≤ 10	≤ 15	≤ 10

A.3.2 Operative temperature

As elaborated in Ch. 1, the operative temperature T_{op} , defined in a simplified form as the mean of the indoor air temperature and the mean radiant temperature in a room, is a simple but well performing index to evaluate thermal comfort.

Depending on the activity (MET) and the clothing level of the occupants (CLO), an optimal operative temperature $T_{op,opt}$ exists, corresponding to $PMV = 0$. Each comfort category has the same $T_{op,opt}$, but has a different permissible range around this optimal point. Table A.3 summarizes $T_{op,opt}$ -values and the allowed temperature range for the different categories, as prescribed by the PMV-PPD thermal comfort model. The thermal comfort models define three categories which describe the quality of the thermal comfort. A lower quality corresponds to a lower thermal comfort. Table A.3 presents the classification of the PMV-PPD thermal comfort model, expressed in % PPD.

Table A.3: Optimal operative temperature and operative temperature band for thermal comfort in office environment for the different categories according to ISO7730 [68]

Category	PPD (PMV)	Operative temperature (°C)	
		Winter	Summer
A	6% (± 0.2)	$22.0 \pm 1.0^{\circ}C$	$24.5 \pm 1.0^{\circ}C$
B	10% (± 0.5)	$22.0 \pm 2.0^{\circ}C$	$24.5 \pm 1.5^{\circ}C$
C	15% (± 0.7)	$22.0 \pm 3.0^{\circ}C$	$24.5 \pm 2.5^{\circ}C$

A.3.3 Adaptation

Theory of adaptation

The static thermal comfort model described in ISO7730 is often criticized as to recognize too little the outdoor climatic context and a person's ability to "fit" the indoor climate to its personal requests [37]. Therefore the static thermal comfort approach would contribute to an increased reliance on mechanical cooling. Since the energy use in office buildings is often dominated by the cooling requirements, the assumed lower energy use by using the adaptive thermal comfort models, is caused by their higher allowed operative temperatures.

Adaptive thermal comfort models assume that people adapt their thermal requirements because of three different mechanisms:

- Behavioural adaptation: clothing, activity, opening windows, operating fans, other time schedules, ...
- Physiological adaptation: acclimatization over a period of days or weeks to changing thermal stress factors
- Psychological adaptation: more relaxed indoor climate expectations make occupants more tolerant to temperature swings

de Dear and Brager summarized several extensive field studies [37] and concluded that in naturally ventilated buildings occupants seem capable of adapting to a broader range of conditions. They both accept higher indoor summer temperatures and lower indoor winter temperatures than predicted by ISO7730. Several attempts have been made to incorporate this adaptation into thermal comfort standards. They all relate the indoor operative temperature

to a reference outdoor temperature. When using this outdoor temperature approach though, either adaptive or non-adaptive, care should be taken to assess local thermal discomfort when necessary [6]: local draft, cold floor, . . .

Adaptive thermal comfort models

Olesen and Parsons [99] propose to use the category C criteria of ISO7730 for a non-air conditioned, 'free-running' building. The set points as summarized in Table A.3 already implicitly take into account adaptive behaviour, namely changing clothing from summer (0.5 clo) to winter period (1 clo).

de Dear and Brager's proposal for adaptive comfort criteria [36] is incorporated into the most recent version of the ASHRAE standard 55 on thermal comfort [6]. It is limited to summer conditions only though (mean monthly outdoor temperature $> 10^{\circ}\text{C}$). Furthermore, ASHRAE limits its application to "spaces where the thermal conditions are controlled primarily through opening and closing windows by occupants" (naturally ventilated buildings). Unconditioned mechanical ventilation is allowed, but opening and closing windows must be the primary means of controlling thermal conditions. Occupants have to be allowed to freely adapt their clothing.

In the Dutch guideline ISSO74, described by van der Linden et al. [136], two building types ALPHA and BETA are defined as an alternative to the, in their opinion, confusing terms of 'Naturally ventilated' and 'Air-conditioned' buildings. An ALPHA building has an operable façade with at least one operable window or at least one temperature adjustment tool per two occupants and possibilities to adjust clothing to outdoor and indoor conditions. All other buildings are BETA buildings. Comfort limitations vary more for the ALPHA building than for the BETA building, although even the BETA building's thermal comfort criteria are linearly changing with the reference outdoor temperature. This is in contrast with the ISO7730 requirements. Compared with the de Dear and Brager criteria, they also define clear criteria for winter conditions.

The European standard EN15251 adopts the non-adaptive comfort model of ISO7730, and adds an adaptive model comparable to the de Dear and Brager's model. However, the recommended indoor operative temperature as a function of the reference outdoor temperature is shifted 1°C higher. This results in a very high T_{op} for summer outdoor temperatures (Table A.5). The fact whether

Table A.4: Building's thermal comfort classification comparison

Class	ISO7730 PPD (PMV)	EN15251 _{adap} PPD (PMV)	ASHRAE _{adap} PPD (PMV)	ISSO74 _{adap} PPD (PMV)
A (I)	6% (± 0.2)	6% (± 0.2)	10% (± 0.5)	10% (± 0.5)
B (II)	10% (± 0.5)	10% (± 0.5)	20% (± 0.85)	20% (± 0.85)
C (III)	15% (± 0.7)	15% (± 0.7)		35% (± 1.76)

this is still comfortable might be questioned (e.g. a running mean outdoor temperature of 21°C results in a $T_{op,max}$ of 28.7°C compared to 26.8°C for the ASHRAE55 model). However, this thermal comfort model is based on extensive measurement data analysis, described by Nicol and Humphreys [96], who also indicated the reasons for the shifted $T_{op,max}$ -line. The conditions of building use are identical to the ASHRAE55 adaptive model. Annex G specifies deviations from the recommended limits stating that in 95% of the occupied space, a parameter can be outside the limits during 3% or 5% of the occupied hours. It is left to the designer to choose the time scale to which this is assessed.

Analogous to ISO7730, the ISSO74 model defines three classes of buildings, but with different levels of dissatisfied people, compared to ISO7730 (Table A.4). The ISSO74 model uses the same classification as de Dear and Brager [36] — class A with a PPD of 10% and class B with a PPD of 20% — but adds a class C with a 65% level of acceptability (35% dissatisfied). In this way the model can also deal with renovation projects of older buildings or temporary buildings with lower comfort criteria. An ISSO74 class A building must meet its comfort criteria during 90% of the time, the ISSO74 class B building must meet its requirements all the time and the same goes for the ISSO74 class C building. Tödli et al. ([132], section 2.1.2) state correctly that this strict requirement should be subject to pre-design discussions between building designer and client. A limited violation of these limits, expressed in Kh, can be tolerated.

In order to allow comparison of the different models in this appendix, the 10% PPD criteria are used in this appendix, being class B for ISO7730 and EN15251 and class A for ASHRAE55 and ISSO74.

A.3.4 Thermal comfort boundaries in terms of outdoor temperature: overview

The different guidelines and standards relate the comfort temperature to an outdoor temperature $T_{\text{ref,out}}$. As already stated in Section A.3.2 each category is no more than a certain temperature band around the optimal operative room temperature $T_{\text{op,opt}}$ in relation to the outdoor temperature. It should be noted that not every method uses the same definition for the outdoor temperature. Table A.5 gives an overview. For the sake of completeness, the non-adaptive comfort model as defined by de Dear and Brager [37] and the non-adaptive model of the ISSO74 standard are also included in this table.

In several cases the available standards do not give information about the full scale of outdoor reference temperatures appearing in a year. Therefore, some kind of extrapolation is provided.

The ISO7730 standard gives information on comfort temperatures in the 'heating' season and in the 'cooling' season, without specifying when these seasons start or end, or how the comfort temperature is related to the outdoor temperature. In this work the EN15251 approach from Olesen et al. [99] is applied to the ISO7730 case:

- Heating season: Outdoor running mean temperature $T_{\text{rm}} < 10^{\circ}\text{C}$
- Cooling season: Outdoor running mean temperature $T_{\text{rm}} > 15^{\circ}\text{C}$

Annex 2 of EN15251 states that the upper limit should change from winter to summer at $T_{\text{rm}} = 10^{\circ}\text{C}$ and the lower limit at $T_{\text{rm}} = 15^{\circ}\text{C}$. To avoid this step change from winter to summer conditions, a linear interpolation is applied between 10°C and 15°C . This assures a more gradual evolution of indoor temperatures, which is more in line with the idea of adaptation between winter and summer conditions [137].

ASHRAE55 very clearly states that for the naturally ventilated buildings no specific guidance is included outside the given boundaries (mean monthly outdoor temperature $< 10^{\circ}\text{C}$ and $> 15^{\circ}\text{C}$). de Dear and Brager [36] admit that using this approach results in a step change in T_{op} if outside these limits the PMV model would be applied. In order to incorporate the adaptive ASHRAE55 model in the comparison, the following approach is used:

Table A.5: Outdoor temperature definition and operative temperature band for thermal comfort in office environment according to different comfort models (T_{op} : operative temp.; T_{rm} : running mean outdoor temp.; T_{ed-i} daily mean outdoor temp. of the i^{th} day before today; $t_{a,out}$: mean monthly outdoor air temp.; $T_{e,ref}$: running mean outdoor temp., defined differently from T_{rm} ; T_{today} : mean of maximum and minimum outdoor temp. of the specified day; T_{switch} : see footnote 4)

Thermal comfort model	Reference outdoor temp. $T_{ref,out}$	Optimal operative temp. $T_{op,opt}$	Allowed temp. range $T_{op,range}$ ¹
ISO7730	Not used: $T_{op} = f(\text{winter, summer})$	Winter: 22.0°C Summer: 24.5°C	A,winter: 2°C B,winter: 4°C C,winter: 6°C A,summer: 2°C B,summer: 3°C C,summer: 5°C
EN15251 _{non-adap}	$T_{rm} = \frac{1}{38}(T_{ed-1} + 0.8T_{ed-2} + \dots + 0.6T_{ed-3} + 0.5T_{ed-4} + 0.4T_{ed-5} + \dots + 0.3T_{ed-6} + 0.2T_{ed-7})$	See ISO7730	See ISO7730
EN15251 _{adap}	see EN15251 _{non-adap}	Winter: see ISO7730 Summer ² : $T_{op,opt} = 18.8 + 0.33T_{rm}$	A,B,C,winter: see ISO7730 A,summer: 4°C B,summer: 6°C C,summer: 8°C
ASHRAE55 _{adap}	$t_{a,out}$: mean monthly outdoor air temperature	$T_{op,opt} = 17.8 + 0.31t_{a,out}$ $+10^\circ C \leq t_{a,out} \leq 33.5^\circ C$	A: 5°C B: 7°C
de Dear-Brager for airco buildings	see ASHRAE55 _{adap}	$T_{op,opt} = 22.4 + 0.05t_{a,out}$ ³ $-5^\circ C \leq t_{a,out} \leq 33^\circ C$	A: 5°C B: 7°C
ISSO74 _{adap}	$T_{e,ref} = \frac{1}{24}(T_{today} + 0.8T_{today-1} + \dots + 0.4T_{today-2} + 0.2T_{today-3})$ ($-5^\circ C \leq T_{e,ref} \leq 30^\circ C$)	$T_{e,ref} < T_{switch}$: ⁴ $T_{op,opt} = 21.45 + 0.11T_{e,ref}$ $T_{e,ref} > T_{switch}$: $T_{op,opt} = 17.8 + 0.31T_{e,ref}$	$T_{e,ref} < T_{switch}$ see ISSO74 _{non-adap} $T_{e,ref} > T_{switch}$ $T_{op,min}$: see ISSO74 _{non-adap} A, $T_{op,max}$: +2.5°C B, $T_{op,max}$: +3.5°C C, $T_{op,max}$: +4.2°C
ISSO74 _{non-adap}	see ISSO74 _{adap}	$T_{op,opt} = 21.45 + 0.11T_{e,ref}$	A: 2.5°C B: 4°C C: 5°C

¹ Class A, B and C is not defined equally in each method, see Table A.4

² Change of winter to summer conditions in EN15251_{adap}: the upper limit changes for $T_{rm} > 10^\circ C$, the lower limit changes for $T_{rm} > 15^\circ C$

³ Originally, de Dear and Brager formulated this equation [22] as a function of the outdoor effective temperature, where the effective temperature is the operative temperature of an enclosure at 50% relative humidity which would cause the same sensible plus latent heat exchange from a person as would the actual environment. This was found to be a too impractical expression. For naturally ventilated buildings, it was reformulated in terms of $t_{a,out}$ [6, 36]. The same reformulation was used here for the de Dear-Brager's airconditioned buildings equation.

⁴ T_{switch} in the ATL method depends on the thermal comfort class, Class A: $T_{switch} = 12^\circ C$; Class B: $T_{switch} = 11^\circ C$; Class C: $T_{switch} = 10^\circ C$.

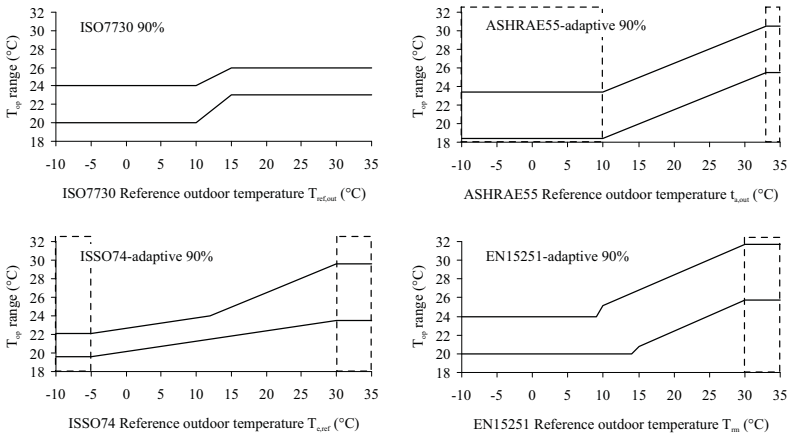


Figure A.1: Operative temperature range as a function of the reference outdoor temperature, according to the different thermal comfort models (boxed areas indicate the extrapolated values)

- Since mean monthly outdoor temperatures higher than 33.5°C do not occur for a typical moderate climate year, comfort limits do not need to be defined for these high temperatures.
- For temperatures lower than 10°C, it is assumed that the comfort range remains constant for the lower temperatures: $18.4^{\circ}C \leq T_{op,opt} \leq 23.4^{\circ}C$ for the 90% buildings.

As a result, for these low outdoor temperatures, $T_{op,max}$ is 0.6°C lower than for the class B buildings of ISO7730. $T_{op,min}$ is considerably lower though. However, it should be clearly stated that, by strict definition, this adaptive model can not be applied to buildings in moderate climates (see also Section A.4.2). Although the adaptive ASHRAE55 model will be used in the comparison with other models, this fact is kept in mind when analysing the results.

Figure A.1 gives an overview of the operative temperature ranges for the four thermal comfort models. The dashed box areas indicate the extrapolated values compared to the definition in the respective standards.

A.4 Thermal comfort limits for a moderate climate

A.4.1 Yearly comfort band

With the different limits for thermal comfort, it is possible to produce an annual view of the thermal comfort limits based on a typical meteorological year (TMY), in this case for Maastricht, located in the south of the Netherlands. This site is chosen because of the availability of real weather data from the Royal Dutch Meteorological Institute (KNMI) [80]. With these data the TMY results are compared to results for warmer years during the last decade further on in this appendix.

Figure A.2 relates the comfort limits of Table A.5 to the outdoor temperature data of Maastricht and shows that in summer time, compared to $T_{op,max}$ as prescribed by ISO7730, $T_{op,max}$ as determined by ASHRAE55 is almost never higher and $T_{op,max}$ as determined by ISSO74 is only at some points higher. Only the maximum operative temperatures as prescribed by EN15251 are never lower than ISO7730. Additionally, the maximum operative temperatures in wintertime are lower for the ASHRAE55 and the ISSO74 model. Taking in mind that the upper and lower comfort limits are the set points of respectively the cooling and heating system, based on Figure A.2, it is not straightforward that, for a moderate climate, the energy use for cooling will be lower for the adaptive comfort models. Whether or not this statement holds, is dependent on the properties and use of the building in question.

A.4.2 Quantified benefit of the adaptive comfort models

With respect to the weather data, the hypothesis formulated in the previous section can be checked and quantified. For the adaptive thermal comfort models, based on the data of Figure A.2, the number of *Degree Days* exceeding the ISO7730 $T_{op,max}$ value is an indicator for the potential energy savings attributed to the cooling system of the building.

Consequently, if a certain climate shows little or no 'ISO7730-exceeding Degree Days', using the corresponding adaptive comfort model will hardly allow higher operative temperatures than the ISO7730 model would do. On the contrary, with the lower winter set points for cooling for the ASHRAE55 and the ISSO74

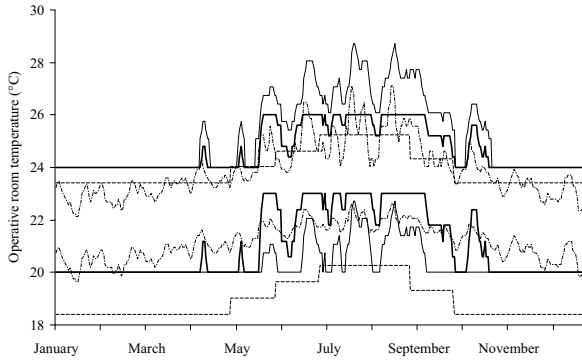


Figure A.2: Comfortable operative temperature range as a function of the corresponding reference outdoor temperature for the reference year of Maastricht, the Netherlands (‘90% satisfied’ thermal comfort models; ISO7730: thick line; ASHRAE55: dashed line; ISSO74: dash-dotted line; EN15251: solid line)

model, a building with a cooling need in winter and mid season will be cooled to lower operative temperatures than with the ISO7730 model.

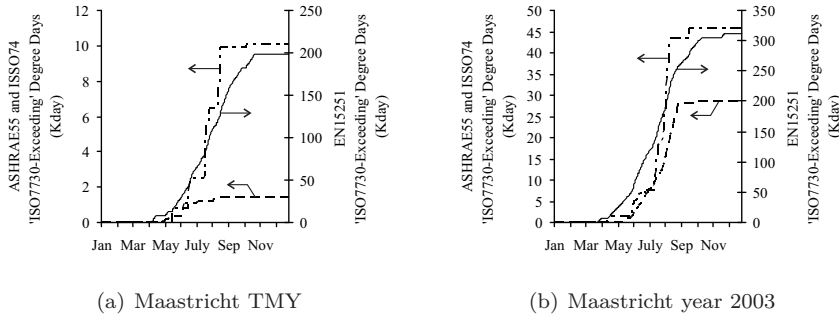


Figure A.3: Adaptive thermal comfort models Degree Days exceeding the ISO7730 $T_{op,max}$ value for the Maastricht TMY (a) and for the Maastricht year 2003 (b) (ASHRAE55: dashed line; ISSO74: dash-dotted line; EN15251: solid line)

For the Maastricht TMY, this is quantified in Figure A.3(a). Compared to the ISO7730 $T_{op,max}$ value, the ASHRAE55 model has 1.4 Kday and the ISSO74 model has 10.1 Kday for the Maastricht TMY. The adaptive EN15251 model has a higher operative temperature starting from a reference outdoor

Table A.6: Mean outside temperature and global solar radiation on horizontal for Maastricht TMY and the years 2001 to 2008

Year	$T_{\text{mean, outdoor}} (^\circ\text{C})$	$I_{\text{global, horizontal}} (\text{kWh/m}^2)$
TMY	9.5	1017
2001	10.6	1033
2002	11.1	1020
2003	11.0	1176
2004	10.4	1046
2005	10.8	1064
2006	11.2	1036
2007	11.2	1012
2008	10.5	1024

temperature of 10°C , resulting in a high number of Degree Days: 199.0 Kday. As a reference value, a whole year round 1°C higher $T_{\text{op, max}}$ -value would give 365 Kday.

These values show that the benefit of the ASHRAE55 and the ISSO74 adaptive model – \dot{U} allowing higher summer indoor temperatures – \dot{U} is very limited if applied to a moderate climate. This was already indicated by van Hoof et al. [137] for the ISSO74 model. Moreover, because of the lower maximum operative winter and mid-season temperatures for ASHRAE55 and ISSO74 compared to ISO7730, the required cooling energy during these seasons might be higher if a cooling load is existing. Using EN15251, with a maximum operative temperature never being lower than ISO7730, a building will evidently end up with a lower required cooling energy.

A.4.3 Real weather data analysis for Maastricht

The last decade has had several years with substantially higher outdoor temperatures than the typical meteorological year. Consequently, the analysis of buildings with real weather data can deviate substantially from the TMY data. Table A.6 shows the higher outdoor temperatures and demonstrates also that this does not automatically correspond to a higher solar radiation level. Data are taken from KNMI [80].

The year 2003 has a high mean temperature and a high amount of solar radiation. Therefore, this year will be used to compare the comfort model results with the TMY. Figure A.3(b) shows the 2003 results equivalent to

Table A.7: Comparison of Maastricht TMY and the year 2003 ‘ISO7730-Exceeding’ Degree Days (Kday)

ASHRAE55		ISSO74		EN15251	
TMY	2003	TMY	2003	TMY	2003
1.4	28.2	10.1	45.8	199.0	310.9

Table A.8: Number of days with $T_{op,min}$ and $T_{op,max}$ in the indicated range for Maastricht TMY and the year 2003

Range	$T_{op,min}$		Range	$T_{op,max}$	
	TMY	2003		TMY	2003
$< 20^{\circ}C$	209	185	$< 24^{\circ}C$	209	185
$20.5^{\circ}C$	0	0	$24.5^{\circ}C$	14	10
$21^{\circ}C$	14	10	$25^{\circ}C$	15	18
$21.5^{\circ}C$	15	18	$25.5^{\circ}C$	25	21
$22^{\circ}C$	25	21	$26^{\circ}C$	102	131
$22.5^{\circ}C$	22	21			
$23^{\circ}C$	80	110			

Figure A.3(a) and Table A.7 shows the difference between the TMY and the real weather data of 2003. From these weather data, it can be concluded that the HVAC set points will deviate substantially, as can be seen from Table A.8.

A.4.4 Weather data evaluation based on allowed operative temperatures

While in Section A.4.2 the weather data were related to the different comfort models by the $T_{op,max}$ difference between the non-adaptive and adaptive models, in this section, the number of days a minimum and maximum operative temperature occurs, is evaluated for the TMY weather data file.

Figure A.4 presents the number of days that the minimal and maximal operative room temperature is equal or lower than the indicated abscissa temperature, according to the different comfort models. A steep curve indicates a requested operative room temperature that does not change much during the whole year. In other words, a steep curve relates to a method that is little adaptive to the outside temperature, a gradually increasing curve to a

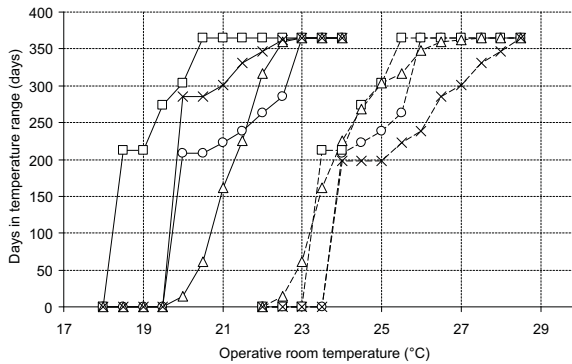


Figure A.4: Number of days the allowed lower (full line) and upper (dashed line) operative temperature is equal or smaller than the abscissa temperature, according to the different thermal comfort models (circle: ISO773; square: ASHRAE55; triangle: ISSO74; cross: EN15251)

highly adaptive method. A building will have a low energy use for heating, the more the thermal comfort model allows low minimum operative temperatures. For the cooling energy use, the opposite holds: a lower cooling energy use results if the thermal comfort model allows more days with higher operative temperatures. Evidently, this is only indicative, because the real energy use of the building will depend on the dynamics occurring at the specified time.

The following conclusions can be drawn from Figure A.4:

- ISO7730 shows for both $T_{op,min}$ and $T_{op,max}$ a gradually increasing curve;
- Although the adaptive ASHRAE55 model is by far the least stringent for $T_{op,min}$, with the temperature data of Maastricht, it asks for a lower maximal operative room temperatures $T_{op,max}$ compared to ISO7730. As a result, a building zone will possibly show a higher cooling need for the adaptive ASHRAE55 model than for the ISO7730 model;
- EN15251 shows low temperature limits for $T_{op,min}$, but, as already shown in the previous section, allows very high temperatures in the summer situation. This is caused by the adaptive curve being 1°C higher than the other adaptive methods.

Again, also using this approach, it must be concluded that the non-adaptive ISO7730 model will not necessarily result in higher energy use.

Table A.9: Analysis of the ISO7730 interpolation assumption

Range	$T_{op,min}$		Range	$T_{op,max}$	
	w interpol	w/o interpol		w interpol	w/o interpol
$< 20^{\circ}C$	209	285	$< 24^{\circ}C$	209	209
$20.5^{\circ}C$	0	0	$24.5^{\circ}C$	14	0
$21^{\circ}C$	14	0	$25^{\circ}C$	15	0
$21.5^{\circ}C$	15	0	$25.5^{\circ}C$	25	0
$22^{\circ}C$	25	0	$26^{\circ}C$	102	156
$22.5^{\circ}C$	22	0			
$23^{\circ}C$	80	80			

A.4.5 Analysis of the ISO7730 interpolation assumption

One of the assumptions in Section A.3.4 was the linear interpolation between $10^{\circ}C$ and $15^{\circ}C$ for both $T_{op,min}$ and $T_{op,max}$ of the ISO7730 model. Strictly following the EN15251 standard $T_{op,max}$ changes at $10^{\circ}C$ and $T_{op,min}$ at $15^{\circ}C$. Using these temperature limits, the number of days that $T_{op,max}$ and $T_{op,min}$ are in a certain temperature range changes, which is shown in Table A.9.

In the case without interpolation, there will be more days with a lower $T_{op,min}$ which will lower the required heating energy. $T_{op,max}$ has 54 days extra at $26^{\circ}C$, which will be beneficial to the required cooling energy. Therefore, for ISO7730, the interpolation assumption will result in a higher energy demand, compared to the case without interpolation.

A.5 Building zone energy use as a function of the thermal comfort model applied

To evaluate the effect of the thermal comfort model and the effect of a real warm year on the energy use of an office building, a TRNSYS [122] simulation is run on a typical office building zone.

A.5.1 2 zone building section description

The 2-zone building section (Fig. A.5) is a cut-out of a typical office building with South and North orientated offices separated by a corridor. This is a copy

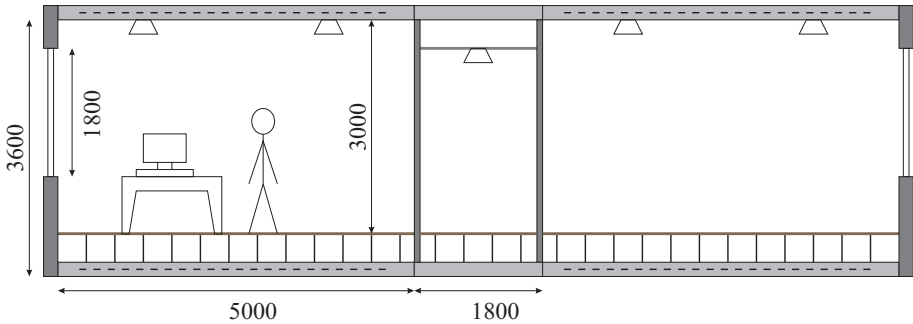


Figure A.5: 2D view of the 2-zone building section

of the office building used in the text (Ch. 7), with the difference that initially, in this appendix, the building is simulated with higher internal heat gains \dot{q}_{int} . In Sec. A.5.5, the \dot{q}_{int} -value used in Ch. 7 evaluated.

A.5.2 Simulation assumptions

The office zones in this simulation are heated and cooled by means of ideal heat and cold emitters with sufficient power to keep the room continuously at the required temperature. No night setback is used. The set points for heating and cooling are defined by the respectively lower and upper temperature limits as imposed by the different thermal comfort models. Because the set points in the simulation model are compared with air temperatures, the upper operative temperature limit from the comfort model is decreased with 0.5°C and the lower limit is increased with 0.5°C to compensate for the difference between air and operative temperature [70].

The office is occupied from Monday to Friday from 8 AM till 6 PM. The occupants have a lunch break during 1 hour, but appliances and light remain on during this period. People perform sedentary office activity with a sensible heat output of 90 W/pers (40% convective, 60% radiative) ([139]; for an air temperature of 22°C). Latent heat is not taken into account for these simulations, because this will not be influenced by the heating or cooling set points, apart from the small temperature dependency of the latent heat output of people.

For each person 150 W of electric power is consumed for appliances such as PC, printer, etc . . . , according to the ASHRAE recommendations [8]. In reality the

Table A.10: Heating and cooling energy use for the South and North zone (with q_{heat} and q_{cool} in kWh/m² and relative to ISO7730)

	South zone		North zone		Total	
	q_{heat}	q_{cool}	q_{heat}	q_{cool}	q_{heat}	q_{cool}
ISO7730	32	57	40	26	36	42
	100%	100%	100%	100%	100%	100%
ASHRAE55 _{adaptive}	28	62	34	30	31	46
	87%	107%	85%	115%	86%	110%
ISSO74	40	69	47	34	43	51
	122%	119%	117%	132%	119%	123%
EN15251 _{adaptive}	32	52	40	21	36	36
	100%	91%	99%	80%	100%	88%

consumption of PC's might be more than 2 times higher though [39], so this can be seen as a rather conservative value. Diversity factors are applied: 150 W/person is the heat gain from 1 PC and monitor [39] with a diversity factor of 0.75 and 1 desk printer with a diversity factor of 0.5. Lights have an electric power of 10 W/m² of which 80% enters the zone as a radiative heat flux, while 20% is convective. During the night, a residual electric power of 1 W/m² enters the office zone as a pure convective heat flux.

Hygienic ventilation is provided at a rate of 36 m³/h.person during occupation hours and enters the room at a constant temperature of 18°C.

The typical meteorological file of Maastricht (The Netherlands) is used.

For this simulation it is explicitly chosen not to use real heating and cooling equipment in the building, since the energy use would largely depend on the applied control strategy. This would hamper the allocation of the differences in energy use to the thermal comfort models applied.

A.5.3 Simulation results

Depending on the thermal comfort model applied the net heating energy use ranges from 30 kWh/m² to almost 50 kWh/m² (Table A.10). For cooling, the net energy use range is wider, going from 20 kWh/m² to 70 kWh/m². Heating and cooling of the ventilation air is included in the net energy values presented.

Figure A.6 shows the results relative to the energy use with the ISO7730 model applied. This figure demonstrates that the use of adaptive thermal comfort

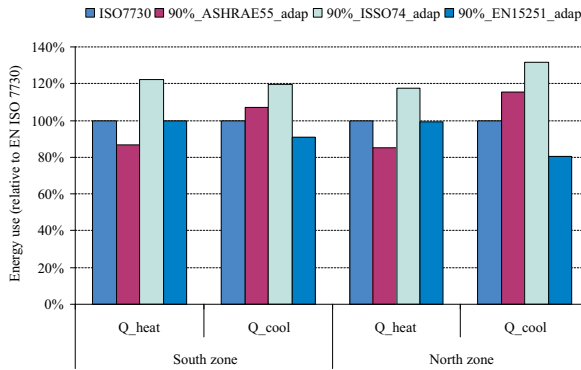


Figure A.6: Required net energy for heating and cooling to keep the zone temperature within the imposed temperature range (relative to the ISO7730 energy need)

models does not necessarily result in relevant energy savings. For heating, only the ASHRAE55 model results in a substantially lower energy use. This is hardly surprising, given its much lower minimum operative temperature compared to the other models. Questions could be raised whether this low winter temperature is still comfortable, taking into account e.g. Oseland's [100] conclusions of a minimal winter temperature of a little lower than 20°C in office environments, which is equal to the ISO7730 minimum temperature. Also, according to de Dear and Brager's own discussion [36], the ASHRAE55 thermal comfort model is not applicable when $T_{ref,out}$ drops below 10°C.

None of the other adaptive models results in a lower heating energy use, which in fact is not surprising. First of all, adaptive models aim at a different approach of the summer comfort and do not focus on winter criteria. Secondly, all but the adaptive ASHRAE55 model, show higher or equal winter temperatures (for $T_{ref,out}$ below 10°C). Only the ISSO74 model drops below the ISO7730 limit for $T_{ref,out}$ lower than -2°C. For the Maastricht TRY this happens in only 2.5% of the days, while 50% of the days have a reference outdoor temperature between -2°C and 10°C. Regarding the heating regime, it should be noted that a major part of the heating energy (> 3/4) is required to heat the ventilation air to the specified inlet temperature of 18°C.

Regarding cooling only the EN15251 model results in a substantially lower energy use, caused by the much higher maximum operative temperatures compared to the other comfort models (see Figure A.2). Both the ASHRAE55

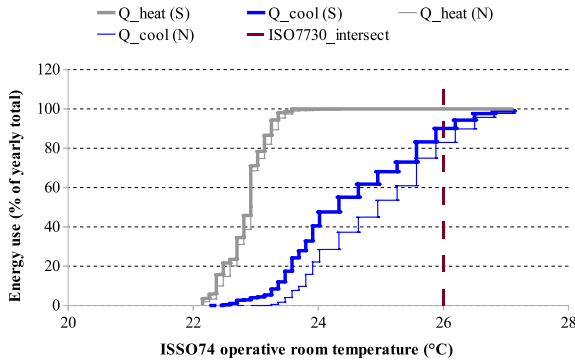


Figure A.7: Cumulative net energy for heating and cooling as a function of the prescribed operative temperature by the ISSO74 comfort model for the North (N) and South (S) zone of the office building

and the ISSO74 model result in a higher energy use. There are few warm days present in the Maastricht TRY, which reduces the potential benefit of these adaptive models, but more important, they impose lower operative temperatures during winter and mid-season period. Because the office building considered requires cooling practically the whole year round, these winter and mid-season limits effect the final result significantly.

Figure A.7 shows that 90% (for the South zone) and 83% (for the North zone) of the cooling energy need is generated during days where $T_{op,max}$ as prescribed by ISSO74 is lower than 26°C, the maximum of ISO7730. Where de Dear and Brager allot ‘their’ adaptive ASHRAE55 model to the warm and humid climates [36] — making it less applicable to the investigated situation — for the ISSO74 model this is not expected, because this comfort model is explicitly designed for use in moderate climate zones.

Figure A.8(a) demonstrates the distribution of the required cooling energy throughout the year. For the ISO7730 model this is 7% in Winter (Dec-Feb), 26% in Spring (Mar-May), 41% in Summer (Jun-Aug) and 27% during Autumn (Sep-Nov). The EN15251 model with equal winter temperatures and higher summer temperatures results in the same absolute value for winter, but lower values for the other seasons. The ASHRAE55 model has a comparable winter value but higher values for the other seasons, while the ISSO74 model shows higher absolute values for all seasons. The largest difference occurs in winter: the required cooling energy more than doubles compared to ISO7730. For the

ISSO74 model, a shift in the distribution of the required cooling energy is noticeable from summer to winter season: 12% in Winter, 26% in Spring, 36% in Summer and 26% during Autumn. The low operative winter temperatures raise the winter part to a higher extent than the high allowed operative summer temperatures reduce the summer part.

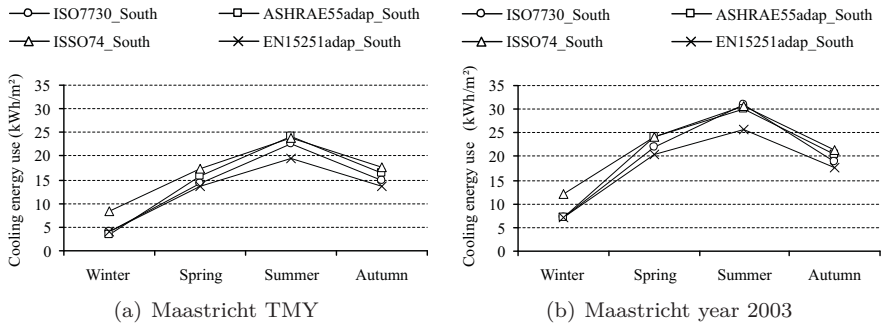


Figure A.8: Net cooling energy throughout the year for the South zone ((a) Maastricht TMY; (b) Maastricht year 2003)

A.5.4 Building zone energy use for the Maastricht year of 2003

As indicated in Section A.4.3, a warm year like 2003 can largely affect the heating and cooling set points determined by the thermal comfort model applied. This, on its turn, will influence the required heating and cooling energy to condition the building. Henze et al. [61] for instance concluded that for an extreme summer, an energy use reduction is observed by applying an adaptive comfort model (EN15251) compared to the non-adaptive ISO7730 model. When the same procedure is applied to the 2-zone office building of Section A.5.1 as for the TMY weather data, the results (Table A.11) indicate that, compared to the ISO7730 model, the net cooling energy remains higher for the ASHRAE55 and ISSO74 model and is lower for the adaptive EN15251 model. This is the same conclusion as for the TMY of Maastricht, although the differences between ASHRAE55 and ISSO74 on the one hand and ISO7730 on the other hand are smaller.

Figure A.8(b) learns that for the warm year of 2003, the adaptive thermal comfort models of ASHRAE55 and ISSO74 are able to lower the net cooling

Table A.11: Heating and cooling energy use for the South and North zone (with q_{heat} and q_{cool} in kWh/m²) for the 2003 weather data of Maastricht

	South zone		North zone		Total	
	q_{heat}	q_{cool}	q_{heat}	q_{cool}	q_{heat}	q_{cool}
ISO7730	26	84	34	41	30	63
	100%	100%	100%	100%	100%	100%
ASHRAE55 _{adaptive}	23	86	28	43	26	65
	90%	103%	84%	104%	86%	104%
ISSO74	32	93	41	48	36	70
	124%	111%	120%	116%	122%	112%
EN15251 _{adaptive}	26	76	34	34	30	55
	100%	90%	99%	81%	100%	87%

energy use for the summer period compared to the ISO7730 model, but this does not compensate for the higher energy demands for the other seasons. Therefore, the overall net cooling energy use remains higher.

To conclude, although the year 2003 is warmer (see Table A.6) than the TMY, the cooling energy requirements during winter and mid-season are still dominant and consequently, the adaptive models of ASHRAE55 and ISSO74 do not result in a lower overall energy use for cooling.

A.5.5 Influence of heat gains on energy use

Sections A.4.2 and A.5.3 demonstrate that the difference in outcome between the ISO7730 and the adaptive models is primarily determined by the high cooling need of the office building in the winter and mid season period. This raises the question whether this can be lowered. In the current simulation set-up, the internal gains are realistically based on a 10 m²/pers occupation and heat gain data from ASHRAE [8] and VDI2078 [139]. The electricity consumption of modern desktop stations can be more than 2 times higher though [39], so the current simulation model is conservative at that point.

People are simulated with a constant sensible heat output of 90 W, as indicated by VDI2078 [139] for a room temperature of 22°C. Lowering this value to 75 W/person lowers the net cooling energy use with 5% and 9% for the South and North zone respectively. The reduction is equal for all seasons though, so this will not influence the conclusions with regard to the thermal comfort models.

Office appliances are now simulated as a 100% convective heat source. Bringing the radiant convective split to 50%-50%, which is higher than recommended by ASHRAE for all types of office appliances, has a small effect on the simulation results: the net cooling energy use decreases with 2.5% and 4.5% for the South and North zone respectively. Again, the reduction is equal for all seasons.

Lighting energy use is also estimated low, with its 10 W/m² power consumption. On the other hand, in the simulation model the window area is 50% of the total building façade, which is high for modern high quality office buildings.

Since the combined internal gains account for 2/3th of the total heat gains, influencing the solar gains will not affect the results of the simulation drastically. Simulating the same building with 30% window area lowers the overall net cooling energy use in the order of 10%, but the distribution throughout the year remains equal. Therefore, the conclusions regarding the adaptive thermal comfort models remain.

A.6 Conclusions

Different commonly used thermal comfort models are described in terms of outdoor temperature: the non adaptive and widely used Fanger model (ISO7730) and the adaptive models of ASHRAE55, ISSO74 and EN15251. When applying these models, care should be taken to use the correct outdoor temperature definition. The high $T_{op,max}$ curve for the adaptive EN15251 model is remarkable compared to the ASHRAE55 and ISSO74 thermal comfort models, which raises question regarding thermal comfort.

Thorough analysis of the different models applied to the moderate climate of Maastricht (The Netherlands), reveals that there are very few periods for which $T_{op,max}$ of the ASHRAE55 and the ISSO74 adaptive model is higher than for the non adaptive ISO7730 model. For a moderate, this reveals the low potential of the ASHRAE55 and ISSO74 adaptive thermal comfort models to lower the cooling energy use due to higher temperature set points.

On the contrary, these two models show lower winter and midseason maximal operative temperatures compared to the ISO7730 model. The energy use for cooling is higher when the indoor operative temperature limits are set by the ASHRAE55 and ISSO74 adaptive models compared to the non adaptive ISO7730 model. This result is caused due to the fact that even during winter

time a relevant cooling need remains. This is not observed for the adaptive EN15251 model, which results in a cooling energy reduction of 12%.

Applying the same procedure to real weather data of exceptionally warm years like 2003, does not change the conclusions. Simulating the office zones with lower internal or external gains, does not alter the conclusions either.

Considering the fact that the ASHRAE55 and the ISSO74 adaptive thermal comfort models do not result in energy savings, for a moderate climate and for office buildings with a cooling load throughout the year, it can be concluded that adaptive thermal comfort models do not offer benefits compared to the basic ISO7730 thermal comfort model for cooling dominated office buildings in moderate climates.

Appendix B

Ideal heating and cooling in TRNSYS

As a reference case, the 2-zone office building is simulated in TRNSYS with an ideal, 100% convective heating and cooling emission system with a zero time constant and an unlimited power. The TRNBUILD building model provides this feature. With these settings, the heating and cooling energy flows are directly coupled to the air node T_{ia} of the zone model. If the T_{ia} at the end of a time step is within the heating and cooling set points, the zone is free floating. In the other case, when heating or cooling is necessary, the exact amount of power is supplied in order to make $T_{ia,t} = T_{set,t}$ at the end of time step t .

This procedure poses a problem when evaluating thermal comfort of the zone, which is based on the operative temperature T_{op} of the zone. Since the TRNBUILD ideal heating and cooling feature is controlled by the air temperature T_{ia} , this temperature is kept within the temperature set points $T_{set,h}$ and $T_{set,c}$. T_{op} will deviate from T_{ia} in the sense that it will be lower in the heating regime and higher in the cooling regime. With $T_{set,h} = T_{op,min}$ and $T_{set,c} = T_{op,max}$, thermal comfort evaluation based on T_{op} will therefore show considerable deviation from the expected ideal situation. Since the TRNBUILD building model cannot be modified, the approach, described in Table B.1, is followed: a corrected T_{set} is calculated based on the definition of the operative

Table B.1: Simulation model settings for ideal heating and cooling

	Standard settings	Corrected settings
Thermal comfort evaluation	$T_{op,min} < T_{op} < T_{op,max}$	$T_{op,min} < T_{op} < T_{op,max}$
Heating on	$T_{ia} < T_{set,h} = T_{op,min}$	$T_{ia} < T_{set,h} = 2T_{op,min} - T_{surf,mean}$
Cooling on	$T_{set,c} = T_{op,max} < T_{ia}$	$T_{set,c} = 2T_{op,max} - T_{surf,mean} < T_{ia}$

temperature (adapted from Eq. B.1).

$$T_{op} = \frac{T_a + T_{surf,mean}}{2} \quad (\text{B.1})$$

with $T_{surf,mean}$ the area weighted mean surface temperature of the office zone.

This modification enables the use of the default ideal heating and cooling of TRNBUILD while allowing thermal comfort evaluation based on T_{op} .

The implemented procedure to correct the model settings for the default ideal heating and cooling, as presented in Table B.1, results in a small thermal discomfort, whereas a zero discomfort is expected. This deviation is caused by the time discretisation and is therefore time step dependent, since $T_{h,set}$ of time step t is calculated with the $T_{surf,mean}$ value of time step $(t - 1)$.

To compensate for this error, the thermal comfort boundaries $T_{op,min}$ and $T_{op,max}$ are corrected with 0.1°C . The results from this TRNSYS simulation are used as a reference for the thermal comfort evaluation of the other simulated cases.

Appendix C

Heating and cooling coil design and control

The heating and cooling coils of the AHU are modelled using a simplified bypass method to speed up the simulation. This method does not bound the performance of the coils to any physical constraint. In reality, however, the coil design with its fin configuration and its number of rows limits the achievable temperature rise or drop by the coil. To take this into account, a limit ventilation supply set point $T_{vs,lim}$ is determined from a simplified method based on the bypass factor approach, which is presented in this appendix

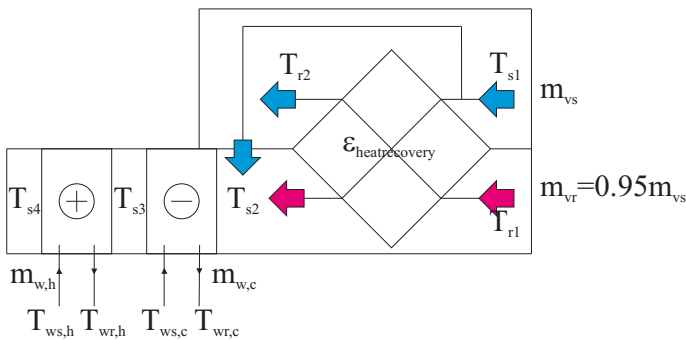


Figure C.1: Schematic presentation of the implemented air handling unit

C.1 Heating coil and sensible cooling coil design

When no condensation is involved, the coil design is rather straightforward based on typical cross flow heat exchanger theory (symbols see Fig. C.1). After the heat recovery, T_{s2} determines the inlet conditions for the coils, while T_{s4} must meet the required $T_{vs,set}$. The moist air properties are given by the typical equations and additional correlations as published by ASHRAE [8]. With an unchanged water content ($x_{s4} = x_{s2}$), the properties of $s4$ are fully known and the required coil power is determined by :

$$\dot{Q}_{coil} = \dot{m}_{da} (h_{s4} - h_{s2}) \quad (C.1)$$

with h the air enthalpy per unit dry air mass. If T_{ws} and T_{wr} are predefined:

$$\dot{m}_w = \frac{\dot{Q}_{coil,design}}{c_w (T_{ws} - T_{wr})} \quad (C.2)$$

The following equations lead to the required number of coil rows :

$$\dot{Q}_{coil,design} = U_0 A_0 \text{LMTD} \quad (C.3)$$

with :

$$\text{LMTD} = \frac{(T_{s4} - T_{ws}) - (T_{s2} - T_{wr})}{\ln \left(\frac{T_{s4} - T_{ws}}{T_{s2} - T_{wr}} \right)} \quad (C.4)$$

$$U_0 = \frac{1}{(1/\eta f_a) + (B/f_w)} \quad (C.5)$$

$$A_0 = F_s A_f N_r \quad (C.6)$$

leading to :

$$N_r = \frac{|\dot{Q}_{coil,design}|}{U_0 F_s A_f \text{LMTD}} \quad (\text{C.7})$$

with :

- η : fin effectiveness [-] (= 0.85 [63], = 0.9 [8]),
- f_a : air side heat convection coefficient [W/m²K] (= 0.80, value in between wet and dry value. ASHRAE [7] gives 8% difference between dry and wet value, VDI [138] uses this value),
- B : ratio external to internal surface area of coil for a finned coil [-] (= 20 [8]),
- f_w : water side convection coefficient [W/m²K] (= 3500, values found between 2400 and 4500 [8, 138, 63]),
- $A_f = \dot{m}_{ha}/v_{max}$: air handling unit face area [m²],
- \dot{m}_{ha} : volumetric humid air flow rate (m³/s),
- v_{max} : maximum air air speed in the AHU (m/s),
- F_s : ratio external surface area per coil row to air handling unit face area [-] (= 25 for finned coil [8]),
- N_r : number of coil rows [-].

The next real value to N_r is the number of coil rows to be installed in the air handling unit.

C.2 Heating coil and sensible cooling coil control

Once the number of coil rows is determined, the control of the coil is performed by using the ϵ -NTU method, leading to the following information:

1. T_{ws} for $\dot{Q}_{coil,design}$ and the installed N_r by using Eqs. C.8-C.12,

2. T_{s4} for T_{ws} and T_{s2} known, and the corresponding $\dot{Q}_{coil,control}$ by using Eqs. C.13-C.15.

$$NTU = \frac{UA}{C_{min}} = \frac{U_0 A_0}{C_{min}} \quad (C.8)$$

$$C_{min} = \min(m_{da}(c_a + x_{s2}c_w), m_w c_w) \quad (C.9)$$

$$C_{max} = \max(m_{da}(c_a + x_{s2}c_w), m_w c_w) \quad (C.10)$$

$$\epsilon = \frac{1 - e^{-NTU(1 - \frac{C_{min}}{C_{max}})}}{1 - \frac{C_{min}}{C_{max}} e^{-NTU(1 - \frac{C_{min}}{C_{max}})}} \quad (C.11)$$

$$= \frac{m_{da}(c_a + x_{s2}c_w)(T_{s2} - T_{s4})}{C_{min}(T_{s2} - T_{ws})} \quad (C.12)$$

Giving T_{ws} for $\dot{Q}_{coil,design}$ and the installed N_r

$$T_{ws,design} = T_{s2} + \frac{\dot{Q}_{coil,design}}{\epsilon C_{min}} \quad (C.13)$$

Giving T_{s4} for T_{ws} and T_{s2} known, and the corresponding $\dot{Q}_{coil,control}$

$$T_{s4} = T_{s2} - \epsilon \frac{C_{min}}{m_{da}(c_a + x_{s2}c_w)} (T_{s2} - T_{ws}) \quad (C.14)$$

$$\dot{Q}_{coil,control} = m_{da}(h_{s4} - h_{s2}) \quad (C.15)$$

During the simulation run, Eq. C.14 determines the maximum (minimum) feasible air exit temperature for the given heating (sensible cooling) coil.

C.3 Dehumidifying cooling coil design

While sensible heat exchange calculations can be made based on temperature differences of air and water, for dehumidifying cooling coils, however, the air side calculation should be based on enthalpy differences instead.

Again, after the heat recovery, T_{s2} determines the inlet conditions for the coils, while T_{s4} must meet the required $T_{vs,set}$. In this case, however, if $T_{vs,set} < T_{dp,s2}$ RH_{s4} equals 1 to make a first guess of the cooling coil power:

$$\dot{Q}_{coil,design} = m_{da} (h_{s4} + (x_{s2} - x_{s4}) 4.185 T_{s4} - h_{s2}) \quad (C.16)$$

with T_{s4} expressed in °C.

ASHRAE [7] provides a design method for dehumidifying cooling coils. The same method can also be found in VDI's Wärmesatlas [138]. Without going into detail, the procedure of this method is summarized below:

- The dry-wet boundary condition is determined using coil heat transfer parameters and water and air flow characteristics.
- The dry and the wet part of the coil are calculated separately. The dry part is calculated using the equations of the sensible coils.
- The wet part surface conditions are determined using the coil heat transfer parameters.
- The logarithmic mean enthalpy difference between air stream and coil surface is used to determine the required coil surface and subsequently the number of coil rows.
- The real coil leaving air condition (T_{s3} or T_{s4}) is determined assuming a constant effective surface temperature of the coil and using standard $\epsilon - NTU$ approach.

C.4 Dehumidifying cooling coil control

Since the dehumidifying cooling coil design method requires a number of iterations to determine the state of the coil, it would slow down the simulation

if it was used for control purposes. Therefore, for use in the building simulation controller, an alternative method is proposed based on the Bypass Factor approach, which is also used in the TRNSYS heating and cooling coil models types 754 and 752.

The Bypass Factor (BPF) approach, originally defined by Carrier, is based on the fact that a cooling coil not just brings air to saturation. A part of the air does not come in contact with the cold metal surface. Its condition remains unchanged and the result is the same as if a part of the air is bypassed around the coil. The remainder of the air is cooled to saturation at surface temperature. The BPF is a function of the coil depth and the air speed. Harris and Condé [58] defined $BPF = 0.56^n$ with n the number of coil rows for an air speed of approximately 2.5 m/s. This approach leads to a straightforward method to determine leaving air conditions when the coil configuration and incoming air and water temperatures and mass flow rates are given.

$$NTU = \frac{UA}{C_{min}} \quad (C.17)$$

$$\epsilon = \frac{1 - e^{-NTU\left(1 - \frac{C_{min}}{C_{max}}\right)}}{1 - \frac{C_{min}}{C_{max}}e^{-NTU\left(1 - \frac{C_{min}}{C_{max}}\right)}} \quad (= \text{Eq. C.11})$$

ϵ determines the maximal cooling power of the coil and the minimal enthalpy of the leaving air stream.

$$\dot{Q}_{coil,max} = \epsilon C_{min} (T_{ws} - T_{s2}) \quad (C.18)$$

$$h_{s4} = h_{s2} + \frac{\dot{Q}_{coil,max}}{m_{da}} \quad (C.19)$$

Since the BPF-approach assumes mixing of unconditioned and saturated air, the effective surface temperature of the coil can be determined by Eqs. C.20-C.21

$$\text{BPF} = 0.56^{Nr} = \frac{h_{s4} - h_{surf}}{h_{s2} - h_{surf}} \quad (\text{C.20})$$

$$T_{surf} = \text{temperature of saturated air with } h = h_{surf} \text{ and RH} = 1 \quad (\text{C.21})$$

Since the BPF-ratio can also be applied to temperatures and moisture ratios (see humid air x-T diagram), this results in the conditions of the leaving air stream.

$$T_{s4} = \text{BPF } T_{s2} + (1 - \text{BPF}) T_{surf} \quad (\text{C.22})$$

$$x_{s4} = \text{BPF } x_{s2} + (1 - \text{BPF}) x_{surf} \quad (\text{C.23})$$

$$(\text{C.24})$$

The results of the two methods, the detailed ASHRAE method and the proposed simplified Bypass Factor method, are compared in Fig. C.2. Some conclusions can be drawn:

- A larger deviation is observed when the inlet condition approaches saturation (lower sensible heat contribution)
- Both methods show that for more saturated inlet conditions (lower sensible heat contribution) the coil surface area increases. This can be explained by the fact that the same temperature difference (which is the driving force for the heat transfer), has to ensure a higher heat removal.
- The previous conclusions suggest that including a heat recovery unit in the air handling unit, which mainly extracts sensible heat from the air stream, implies a larger cooling coil, and therefore a higher pressure drop for the supply fan. Without going further into detail in this work, this trade-off should be taken into account when optimising an AHU for a specific building and aeraulic network.

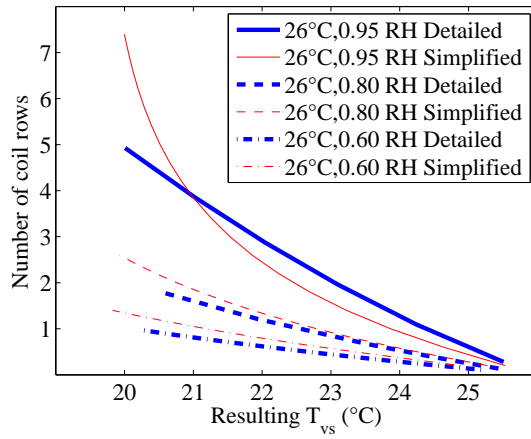


Figure C.2: Cooling coil design results for the detailed ASHRAE/VDI method and the simplified procedure (the legend gives the inlet conditions)

Appendix D

Parameters of the 2-zone office building

In this appendix, the origin of the different parameters of the 2-zone office building model is presented. Since many of them have a considerable impact on the dynamic behaviour of the office zone, it is important to make a well considered choice case-by-case. At the end of this appendix, some TRNSYS related topics are treated which might be useful for future users.

D.1 Internal gains: heat gains from people

Table D.1 presents the specific values for heat gains from people.

Sensible heat loss from skin is the heat exchange from the skin, through the clothing to the surroundings and is partly convective and partly radiative [8][sec. 8.2]. Evaporative heat loss from skin depends on the amount of moisture on the skin and the difference between the water vapour pressure at the skin and in the ambient environment.

Respiratory losses are both sensible and latent losses from the respiratory tract to the inhaled air.

Table D.1: Heat gains from people and occupation density

Parameter	Value	Remark
Sensible	73 W/pers	ASHRAE Fundamentals [8][Ch18, Table 1]: moderately active office work, low air velocity, 42% convective, 58% radiant. VDI 2078 [139][App. A, Table A1] provides values as a function of room air temperature.
Latent	55 W/pers	
occupation density	1 pers/ 10 m ²	for single office (EN15251 [44][Table B.2]). A landscape office would give 1 pers/15 m ² .

Sensible heat is directly added to the TRNSYS building models in the form of convective and radiative heat gains.

Latent heat is usually given in the form of power \dot{Q} (W) or mass flow rate \dot{m} (kg/s). The two are related by Eq. D.1 (with t in °C).

$$\dot{Q} = H \dot{m} = (2501.6 + 1.867 t) \dot{m} \quad (\text{D.1})$$

D.2 Internal gains: appliances

Several sources [8, 139, 44, 39] supply data for energy use of appliances such as PC, printer and copy machines in offices. Because this simulation model is set up to analyse real building behaviour, relatively low appliances heat gain values are used. Conservative, higher values are more suitable for design purposes. Table D.2 presents the values which are used in the simulation model.

The resulting value is lower than typical reference values for appliances in operation (15 W/m²[69], 14 W/m²[20]), but these are values which are meant for design purposes and not for energy use evaluation. A survey from the Swedish Energy Agency [129] presents data for all relevant energy flows in a large number of buildings. Looking at the appliances energy use of the air conditioned buildings (Fig. D.1), with heat recovery in the AHU, and with an heating energy use less than 100 kWh/(m².y), an average value of 17.2 kWh/(m².y) is calculated. This results in an average heat gain of 6.6 W/m², based on 2600 typical yearly heating operating hours.

Table D.2: Heat gains from office appliances

Parameter	Value	Remark
Monitor	30 W	60% convective, 40% radiative, diversity factor 0.75 [8][Ch. 18, Table 8]
Desktop PC in operational mode	65 W	90% convective, 10% radiative, diversity factor 0.75 ^(a) [8][Ch. 18, Table 8]. Duška et al. [39] suggest that PC power tends to increase in recent years and they find an average value of 110 W.
Desktop laser printer	110 W	70% convective, 30% radiative, 1 printer/8 pers, diversity factor 0.5 [8][Ch. 18, Table 9]
Resulting power	7.8 W/m ²	
Weighted convective - radiative split	80% convective - 20% radiative	
Residual night and weekend power	2 W/m ² K	[69] This value also incorporates the residual lighting gains

^(a) A diversity factor is introduced to take into account that appliances are not working constantly

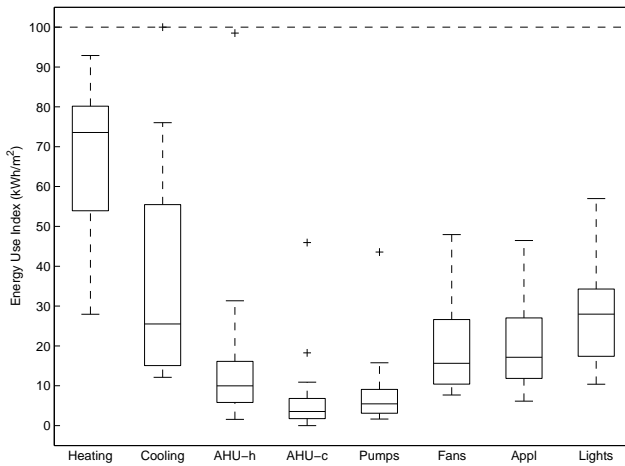


Figure D.1: Energy use values of 32 air conditioned buildings with heat recovery in the AHU and with an heating energy use less than 100 kWh/m².y from the Swedish Energy agency survey [129]

Table D.3: Heat gains from lighting

Parameter	Value	Remark
Offices	500 lux (10 W/m ²)	50% convective, 50% radiative, EN15251 [44][Table D1]
Corridors	100 lux (2 W/m ²)	idem
Diversity factor	75%	for the offices
Residual night and weekend power		the residual lighting gains are incorporated into the non occupancy appliances gains

D.3 Internal gains: lighting

Data for lighting energy use are based on the European standard EN15251 [44][Table D1] (50% convective, 50% radiative): 500 lux for (10 W/m²).

In real building situation lighting is not always on at full power. Several studies have been made on user behaviour and automated control influence lighting energy use. Reinhart [107] obtains values for an example office down to 50% or lower of the nominal power. A comparable strategy is also used by Saelens et al. [114].

Investigation of the results from a large office building survey in Sweden [129] reveals a corrected mean lighting power of 74% ($\sigma = 20\%$) of the installed power for single offices. For the landscape offices in this survey there appears to be no correction factor. A reason could be that in landscape offices users influence on lighting is very limited. The UK Energy Consumption Guide [20] assumes a utilisation factor between 85% and 70%.

When stochastic user behaviour is implemented, the incorporated lighting gains for the office spaces are defined by the ‘integrated methodology’ by Parys et al. [101], with a maximum gain of 10 W/m². In the corridor the fixed lighting gain of 2 W/m² remains in this case.

D.4 Zone capacitance value

The TRNBUILD building model (or any equivalent building model) requests a value for the zone capacitance. This value, which is also used in the

Table D.4: Overview of zone thermal capacitance values from literature

Source	Value	Remark
EN13790 [69]	80 kJ/m ² K	per m ² floor area, including a maximum of 10 cm thermal mass from the zone walls, for the lightest building type
Belgian energy performance directive	55 kJ/m ² K	per m ² floor area, including a maximum of 10 cm thermal mass from the zone walls, for the lightest building type
Masy [91]	19.55 kJ/m ² K	per m ² floor area, she multiplies the air capacitance with a factor 5 to include effects of non homogeneous air layers (Masy refers to Laret) and takes into account furniture capacitance; $5 \times 3607 \text{ J/m}^2\text{K} + 1515 \text{ J/m}^2\text{K} = 19550 \text{ J/m}^2\text{K}$ (1515 J/K per m ² floor area is the furniture capacitance)
Kummert [83]	18 kJ/m ² K	per m ² floor area, he states that the factor 5 does also include furniture capacitance.
Davies [34]	$4 - 5 \times C_{air}$	4 - 5 times the real thermal capacity of the air (taken from L. Laret, Contribution au développement de modèles mathématiques du comportement thermique transitoire de structures d'habitation, Thèse de doctorat, Université de Liège, 1981)
Tödli et al. [132]	3607 J/m ² K	per m ² floor area

simplified controller models, is of utmost importance, since it has a large impact on the thermal behaviour of the room. In a detailed dynamic building model like TRNBUILD [123], this value does not include wall capacitance, unlike the simplified zone models used in energy performance calculations ([69], Belgian energy performance directive), which assume the wall capacitances to be included.

The question whether furniture thermal capacitance is to be included into this zone capacitance is seldom answered in the literature. Masy [91] gives values for both air and furniture capacitance. However, lacking other useful data, this leads to the conclusion that for the furniture capacitance better references are needed. The different references are summarized in Table D.4.

Since no clear conclusion can be drawn from the different literature sources, the following assumption is made: furniture and other objects in the office zone are

taken into account by using a value of 5 times the real thermal capacity of the air as the thermal capacitance of the room air temperature node in the CCA office building model.

D.5 Convective heat transfer values of floor and ceiling

The use of CCA implies a varying temperature difference between room air and surface. To model the heat transfer in a correct way, the heat transfer coefficient is an internal parameter in the simulation model, which is calculated each internal iteration of the building model. Several correlations for the natural heat convection coefficient, which depends on the temperature difference between air and ceiling or floor surface temperature, are available in the literature and summarised in Table D.5.

With the room dimensions as specified in Table 7.3, an air temperature of 20°C and an assumed temperature difference of 5°C, the dimensionless convective heat transfer values for the room are :

- $Pr = 0.71$
- $Gr = 2.91 \cdot 10^{10}$ (based on the room height)
- $Ra = 2.06 \cdot 10^{10}$ (based on the room height)

The results are summarised in Figure D.2, showing clearly that the standard floor heating coefficient of TRNSYS corresponds well with other sources, but the ceiling heating coefficient does not. Although Awbi and Hatton [9] comment themselves on the ceiling heating value, stating that this value depends on the temperature stratification, which largely depends on the room geometry, the Awbi and Hatton-correlation [9] is retained for the simulation in this PhD-work.

Causone et al. [28] derived similar values. Calay et al. [25] an Awbi and Hatton [9] argument that the TRNSYS coefficient was experimentally derived using isolated surrounding surfaces and small free-edge heated plates, which does not correspond with real building applications as the air movement in a room will be different.

Table D.5: Literature review of natural convection correlations

$(\theta = T_{surface} - T_{air} \text{ (}^\circ\text{C)}, D = \text{room hydraulic diameter} = \frac{4 \text{ room area}}{\text{room perimeter}} \text{ (m)},$ $H = \text{room height (m)}, L = \text{room length (m)})$		
Source	Floor cooling Ceiling heating [W/m ² K]	Floor heating Ceiling cooling [W/m ² K]
Trnsys Type 56 [123]	$1.08 \theta^{0.31}$	$2 \theta^{0.31}$
Empa [81] ¹		$\alpha_c 8.92 \theta^{0.1}$
Causone et al. [28]	0.5 for $\theta = -10$ 0.3 for $\theta = -8$	4.4 for $\theta = 4$
Awbi and Hatton [9] ²	$\frac{0.704}{D^{0.601}} \theta^{0.133}$	$\frac{2.175}{D^{0.076}} \theta^{0.308}$
Min et al. (from Khalifa [77])	$\frac{0.203}{D^{0.24}} \theta^{0.25}$	$\frac{2.416}{D^{0.08}} \theta^{0.31}$
Schlapmann et al. (from Khalifa [77])		$(0.33 \frac{H}{L} + 0.75) \theta^{1/3}$

¹ α_c is the convective part of the total heat transfer coefficient and varies between 20% for $\theta = 1$ and 30% for $\theta = 4$

² According to the authors own comparison these correlations correspond well with other data for the floor, but not for the ceiling (ASHRAE and CIBSE obtain up to two times higher values)

D.6 Radiative heat transfer

Radiative heat transfer is governed by the difference in temperature to the 4th power between the two receiving bodies. However, this can be linearised to accommodate the form $\dot{q} = h_r(T_s - T_{rs})$ by using :

$$\dot{q}_{rad} = \sigma \epsilon (T_s^4 - T_{rs}^4) \tag{D.2}$$

$$= \sigma \epsilon 4 \left(\frac{(T_s + T_{rs})}{2} \right)^3 (T_s - T_{rs}) \tag{D.3}$$

$$= \sigma \epsilon 4 T_m^3 (T_s - T_{rs}) \tag{D.4}$$

$$= h_r (T_s - T_{rs}) \tag{D.5}$$

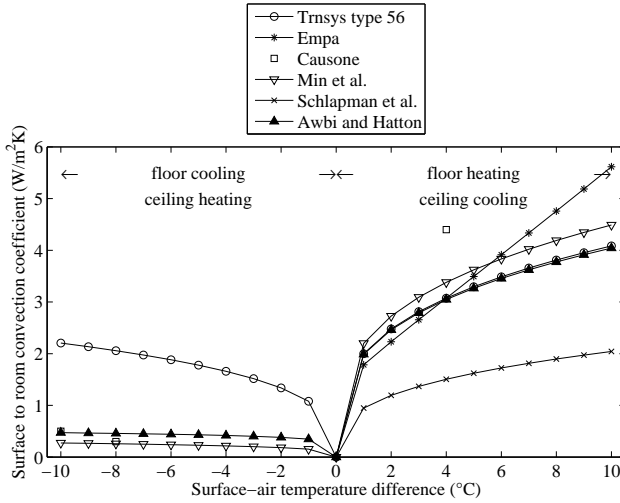


Figure D.2: Natural convection coefficient for floor cooling/ceiling heating (left hand side) and for ceiling cooling/floor heating (right hand side)

with T_m the arithmetic mean of the surface temperature T_s and the radiant temperature for that surface $T_{r,s}$. The origin of this radiant temperature is elaborated in Ch. 1. Although radiative heat transfer is not linear, h_r can be approximated by a linear function if T_m does not change too much, which is the case in a building zone, as shown in Fig. D.3. For $T_m = 23^\circ\text{C}$ and an emissivity of 0.95, this results in $h_r = 5.6$ which is also found experimentally by Causone et al. [28]. Davies [34] used a constant of 5.7, while Feustel and Stetiu [48] referred to 5.5.

D.7 Convective versus radiative heat transfer coefficients

Using the known values for convective and radiative heat transfer coefficients, the difference between those two parameters is shown in Fig. D.4. The value of h_c and h_r is plotted against the surface-to-zone temperature difference $T_s - T_z$.

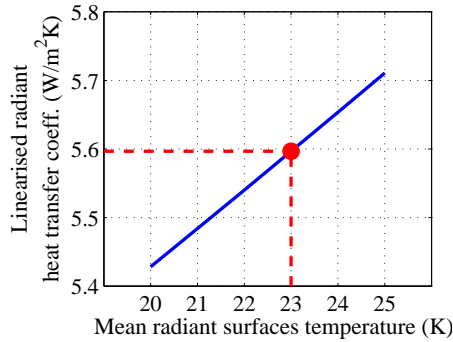


Figure D.3: Variation of the linearised radiative heat transfer coefficient h_r for a limited range of T_m

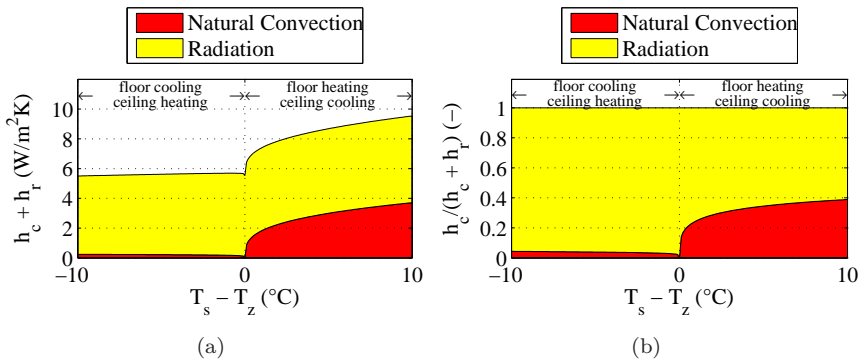


Figure D.4: Convective versus radiative heat transfer coefficient as a function of the surface-to-zone temperature difference $T_s - T_z$ with (a) showing absolute values and (b) showing values relative to the total value of $h_c + h_r$

D.8 Infiltration rates

VanBronkhorst et al. [135] use, for a building with 5 floors or less, the approach to cut infiltration rates to 25% during system operation, compared to the ‘fans off’ situation. They also use a 90% correction factor on the building volume for the presence of unoccupied spaces, furniture and walls.

Emmerich et al. [40] present measured infiltration data for a large set of

Table D.6: Ventilation parameters

Source	Value	Remark
Office	43.2 m ³ /h	1 l/s.m ² = 36 m ³ /h.pers or 43.2 m ³ /h (Class 2 of EN 15251 [44]). Class 1 would be: 1.5 l/s.m ² = 54 m ³ /h.pers
Corridor	10.1 m ³ /h	1 toilet per 12 people and 50 m ³ /h (EN15251, Table B.5, Class I) air per toilet
Other assumptions regarding the AHU		
Return air temperature: South, Corridor and North flow temperatures weighted with flow rates		
Return air flow rate: sum of South, Corridor and North flow rates (in kg/h)		
Return air absolute humidity: $\frac{\sum_{S,C,N} AH.AF}{\sum_{S,C,N} AF} \frac{kg-water}{kg-dryair}$		

buildings, stating that 6% fullfills their target 'good practices' level of air tightness. Resulting infiltration air changes ranged from 0.02 h⁻¹ to 0.05 h⁻¹ in an overpressurized case (95% return air flow, EN13779 category PC3)).

In this PhD-work, the simulated CCA building is assumed to meet these criteria and an air leakage rate of 0.05 h⁻¹ is used. During system shut down the infiltration rate is 0.2 h⁻¹. A 90% correction factor on the building volume is also incorporated.

D.9 Ventilation

The ventilation rate applied in the CCA building simulation model corresponds to Class 2 of EN 15251 [44] (see Table D.6). For the corridor it is assumed that the ventilation needed for the toilets is blown into the corridor from the South and North office zone.

D.10 Maximum specific heat gains and heat losses

From the building data, the meteorological data and the information on the internal heat gains, the maximum heat gains, \dot{q}_{sol} and \dot{q}_{int} , and heat losses, $UA(T_{comf} - T_{amb})$ can be determined related to the office zone floor area. Table D.7 summarizes these results.

Table D.7: Maximum heat gains and heat losses related to the office floor area. UA incorporates conduction through outside wall and window and infiltration.

	W/m ²
$\max(\dot{q}_{sol})$	116
$\max(\dot{q}_{int})$	23 (58% convective, 42% radiative)
$\max(UA(T_{amb} - T_{comf}))$	-20

D.11 Model Excitation

The TRNSYS model *TypicalOffice2Zone.tpf* is fitted with an option to apply userdefined excitation input signals to the model. The model response to these input signals can be used for evaluating model parameter estimation procedures.

The equation card *Response* generates the required input signals. To activate the ‘Response’-feature of the model, set the parameter $Response = 1$ in the ‘Simulation Cards’.

7 inputs can be defined by the user, as presented in Table D.8.

Two options are provided to generate excitation input signals: by user defined equations or by a file read by the TYPE 9 Data Reader *RespReader*. The user can choose between these two options by using the parameter *RespFromFile* in the ‘Simulation Cards’: the value 0 indicates that the model takes the user defined equations as excitation signals, while the value 1 means that the datafile is read to generate excitation signals. This choice is made in the equation card *Response*, defining the 7 Response-parameters.

Table D.8: Definition of the 7 excitation inputs signals to the TRNSYS model
TypicalOffice2Zone.tpf

Excitation signal	TRNSYS parameter	Unit or value
Water supply temperature	<i>TwsResponse</i>	°C
Water flow rate On or Off	<i>FwsResponse</i>	[0 – 1]
Ventilation supply temperature	<i>TvsResponse</i>	°C
Air Handling Unit On of Off	<i>FvsResponse</i>	[0 – 1]
Ambient air temperature	<i>TambResponse</i>	°C
Internal gains	<i>QintResponse</i>	kJ/h/m ² (floor area)
Solar gains	<i>QradResponse</i>	kJ/h/m ²

D.11.1 Water supply

When the water supply is controlled, the TRNSYS parameters *TwsResponse* and *FwsResponse* disconnect the North and South 3-way valve from the production unit (in macro ‘Production’) and directly set the 3-way valve parameters for the supply temperature $TsS = TsN = TwsResponse$ and for the flow rate $FS = FN = Nominal_flow_rate \times FwsResponse$.

D.11.2 Ventilation supply

When the ventilation air flow is controlled by the ‘Response’-feature, the control of the two AHU’s of the building, for the North and for the South zone, is set by the parameters *TvsResponse* and *FvsResponse*.

When $Response = 1$ the normal ventilation schedule parameter is set to zero in the macro *VentilationSchedule*. In the equation card *AHUControl*, the ventilation air flow, through the parameter *AHUOnOff*, is now defined by the value of *FvsResponse*. The ventilation supply temperature is defined by *FvsResponse*.

D.11.3 Weather conditions

The weather conditions in the ‘Response’-case are set in the equation card *Weather* in the macro *WeatherData*. The parameter *Response* again defines

which data source is used.

The ambient temperature is set to *TambResponse*. The sky temperature is equally set to *TambResponse*, which is not completely accurate, but implemented as simplification.

The total solar radiation is split into beam and diffuse by the parameter *RatioBeamToTotal*. For the moment it is implemented only for the planes horizontal, South vertical and North Vertical. The values of this parameters are the yearly ratio of beam-to-total solar radiation for the respective planes, as elaborated in the Matlab-script *AnalyseVerhoudingTotvsDirecteStraling.m*. These ratios are different for the North and the South zone! In the ‘Response’-case, the angle of incidence of the beam radiation is always zero, which means perpendicular to the plane. The units of solar radiation for the excitation signals is [kJ/h/m²].

It is important to understand this solar radiation implementation to evaluate the results of the excitation signal simulations.

D.11.4 Files

Ratio Beam tot Total solar radiation:

*N:\TME\TME\MSourbron\Data\Weather\
AnalyseVerhoudingTotvsDirecteStraling.m*

Generating excitation input files:

N:\TME\TME\MSourbron\TypicalOffice\Data\ResponseDataGenerator.m

D.12 Procedure for parameter estimation

All files are located in *N:\TME\TME\MSourbron\TypicalOffice\Identificatie*

1. Generate data-sets with the ‘Response’-feature of *TypicalOffice2Zone.tpf*. The TRNSYS model generates a file *Output\1001Response.out*. Copy

this into ... \IdData and rename appropriately.

2. Process this output file with ... \Mfiles\MPCTABS_Read_data.m to prepare the identification files.
3. Generate initial model with M:\Doctoraat\Modellen\MATLAB\work\Zone\RC_nx2.m or RC_nx4.m.
4. Perform PE-identification with ... \PE_TABSbuilding \ PE_TABSbuilding_nx2.m or ..._nx4.m. To start ACADO in Matlab, check www.acadotoolkit.org.
5. Validate the model with ... \Mfiles\validate_model.m

The tables in the PhD-text are generated with *IDfortext.m*.

D.13 TRNSYS related topics

D.13.1 Floor and ceiling boundary condition

The floor and the ceiling of the building model have the boundary condition 'Identical', meaning that the heat flows interacting on both sides are identical. This useful TRNBUILD [123] option — avoiding the need to model zones above and below — has the annoying drawback that an error is introduced since boundary conditions are not really identical.

The TRNSYS CCA building model has two CCA-slabs, one is the floor and the other is the ceiling slab. A first fictive zone is assumed to be under the considered office room and a second above. Solar gains are assumed to interact with the floor only. This means that the ceiling of the fictive lower zone also receives these solar gains while the floor of the fictive upper zone receives none. This should evidently be reversed.

Also, the absorption factor of the inside of the building element is copied to the outside. Troch [133] has extensively investigated the impact of the erroneous boundary conditions on the model results and concludes that the effect on the heat exchange in the active layer is not negligible. The year simulation of the Typical Office Building shows that the floor, receiving radiation both at the upper and at the lower surface will have a higher temperature than the ceiling ($\Delta T_{core,mean,year} = 0.07K$ for the reference controller in the South zone) and

will extract more heat from the zone than the ceiling. The resulting yearly heat exchanged by the two building elements with the zone are presented in Table D.9:

Table D.9: Impact of the erroneous radiation boundary conditions on the heating and cooling of floor and ceiling

	Floor (kWh/m ²)	Ceiling (kWh/m ²)	Difference (%)
Heating	11.26	11.59	-2.9
Cooling	-19.99	-18.86	6.0

With perfectly implemented boundary conditions, the results for either floor or ceiling would satisfy.

D.13.2 Pre-simulation time

Since the initial conditions have an influence on the building behaviour during the first days, a pre-simulation time of 48 hours is taken into account. This measure eliminates e.g. high peak powers occurring in the start up phase.

When the MPC is implemented on the building zone, the MPC is not running during the first day of the pre-simulation phase.

In TRNSYS, this pre-simulation period is implemented by starting the simulation at *hour 8712* (day 364 of the previous year). The simulation ends at *hour 17520* (day 365 of the simulated year). Since TRNSYS assumes that a simulation, starting at *hour 0*, starts on a Monday, *hour 8760*, which is the first hour of the simulated year, is then the first hour of a Tuesday.

Because the simulation results are processed in Matlab and the MPC controller is implemented in Matlab, these algorithms need to take into account that the first simulation day is a Tuesday. Since Matlab uses real data in its time and date processing functions, since in Matlab 'Day 1' is assumed to be Saturday Januari 1th, 2000 and since the year 2000 was a leap year, 'Day 366+365+1' is Tuesday Januari 1th 2002, which is assumed to be the starting day of the simulated year. The pre-simulation phase starts at 'Day 366+364'.

D.13.3 Batch file in TRNSYS

Creating a batch file executing different .dck files successively is done in the following way in a Microsoft Windows environment:

1. Open Notepad
2. Type '@echo off' : this will prevent DOS from typing the batch files commands
3. Type ' "C:\Program Files\Trnsys16_1\Exe\Trnexe.exe" "C:\Program Files\Trnsys16_1\MyProjects\Folder1\TrnsysFile1.dck" /N '. The '/N' means that TRNSYS will not ask for the 'Continue Yes or No' question at the end of the simulation.
4. Retype the above command for every other .dck file you want to execute
5. Save the Notepad file as 'TrnsysBatch.bat'
6. Execute the batch file by double clicking it in the Windows Explorer
7. Edit the batch file with the right mouse button and click on 'Edit'

Documentation on batch files can be found on
'<http://www.computerhope.com/batch.htm>' or
'<http://www.allenware.com/icsw/icswidx.htm>'

Appendix E

Automatic state space matrix construction from RC-network

A generalised procedure is used to obtain the state space matrix from the drawing of the RC-network of the simplified building model. This procedure is written in Matlab and is usable for every RC-network. It results in the matrices A, B, C and D from the general state space formulation :

$$\dot{X} = AX + BU \quad (\text{E.1})$$

$$Y = CX + DU \quad (\text{E.2})$$

The working method is described below and illustrated for the CCA building model with 2 states.

E.1 Step 1 : drawing the RC-network

A first step is to construct a drawing for the desired RC-network. In this way, the states, inputs, outputs and the interconnections between states and the

connections between states and inputs are defined graphically (Fig. E.1). The two differential equations describing this system are:

$$C_c \frac{\delta T_c}{\delta t} = -\frac{1}{R_2} (T_c - T_z) - \frac{1}{(R_z + R_1)} (T_c - T_{ws}) \tag{E.3}$$

$$C_z \frac{\delta T_z}{\delta t} = -\frac{1}{R_2} (T_z - T_c) - \dot{m}_v c_a (T_z - T_{vs}) + Q \tag{E.4}$$

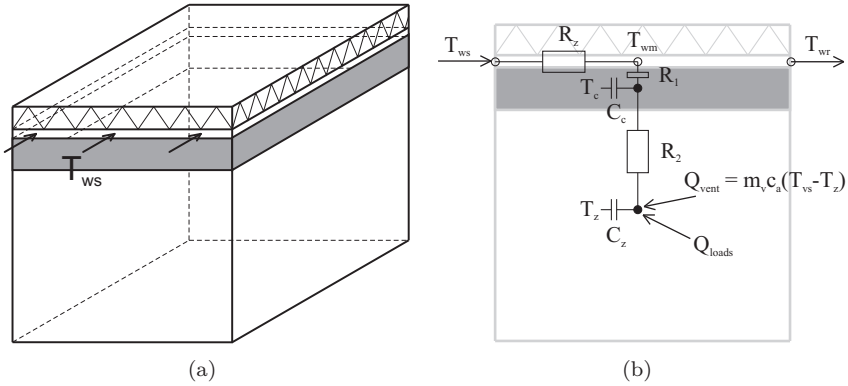


Figure E.1: (a) Layout of the simplified building and (b) 2nd order RC-model of the simplified building.

E.2 Step 2 : Defining states, inputs and additional outputs

In step 2 the number and the names of the states, inputs and the outputs are defined:

- xn : number of states
- X : states vector
- uTn : number of temperature inputs
- uQn : number of heat flow rate inputs
- $un = uTn + uQn$: number of inputs

- UT : temperature inputs vector
- UQ : heat flow rate inputs vector
- $yUDn$: number of userdefined outputs
- Y : output vector

The output vector Y has $xn+xn.(xn-1)+uTn.xn+uQn.xn+yUDn$ elements and contains a predefined and a userdefined part. It is constructed in the following order:

1. xn state temperatures
 $Y(1, xn) = X(i), i = 1 \dots xn$
2. $xn(xn-1)$ heat flows between states
 $Y(xn+1, xn+xn.(xn-1)) = \dot{Q}_{X(i)-to-X(j)},$
 $i = 1 \dots xn, j = 1 \dots xn, i \neq j$
3. $uTn.xn$ heat flows between temperature inputs and states
 $Y(xn+xn.(xn-1)+1, xn+xn.(xn-1)+uTn.xn)$
 $= \dot{Q}_{uT(i)-to-X(j)}$
 $i = 1 \dots uTn, j = 1 \dots xn$
4. $uQn.xn$ heat flows between heat flow inputs and states
 $Y(xn+xn.(xn-1)+uTn.xn+1, xn+xn.(xn-1)+uTn.xn+uQn.xn) = \dot{Q}_{uQ(i)-to-X(j)},$
 $i = 1 \dots uQn, j = 1 \dots xn$
5. $yUDn$ userdefined outputs
 $Y(xn+xn.(xn-1)+uTn.xn+uQn.xn+1, xn+xn.(xn-1)+uTn.xn+uQn.xn+yUDn)$

For the 2nd order building model, this leads to:

- $xn = 2$

$$X = \begin{bmatrix} T_c \\ T_z \end{bmatrix} \quad (E.5)$$

- $uTn = 2, uQn = 1$

$$U = \begin{bmatrix} T_{ws} \\ T_{vs} \\ Q \end{bmatrix} \tag{E.6}$$

- $yUDn = 5, yn = 15$

$$Y = \begin{bmatrix} T_c \\ T_z \\ Q_{T_c-T_z} \\ Q_{T_z-T_c} \\ Q_{T_{ws}-T_c} \\ Q_{T_{ws}-T_z} \\ Q_{T_{vs}-T_c} \\ Q_{T_{vs}-T_z} \\ Q_{Q-T_c} \\ Q_{Q-T_z} \\ T_{w,mean} \\ T_{wr} \\ T_{core} \\ T_s \\ T_{op} \end{bmatrix} \tag{E.7}$$

E.3 Step 3 : State space matrices A, B, C and D

In this step, the values of the resistances between the states and between the temperature inputs and states and the values of the capacitances of the states are used to construct the state space matrices.

E.3.1 Capacitance matrix Cap

The capacitance matrix Cap (1 by xn) contains the capacitance of the different states in the model

$$Cap(i) = C(X(i)), i = 1 \dots xn, [J/K] \tag{E.8}$$

E.3.2 Resistance matrices R_X and R_U

The matrix R_X (xn by xn) with resistances between the states is symmetrical. $R_X(i, j)$ is the resistance between state i and state j .

$$R_X(i, j) = R_{X(i)-X(j)} = R_{X(j)-X(i)}, i = j = 1 \dots xn, i \neq j, [K/W] \tag{E.9}$$

The diagonal and the positions in R_X where there is no connection between the states are defined as *Inf*.

The matrix R_U (un by xn) with resistances between the inputs and the states consists of a part from the temperature inputs and a part from the heat flow inputs. $R_{UT}(i, j)$ is the resistance between temperature input i and state j . R_{UQ} shows a 1 at positions where a heat flow input acts on a state.

$$R_{UT}(i, j) = R_{UT(i)-X(j)}, i = 1 \dots uTn, j = 1 \dots xn, [K/W] \tag{E.10}$$

$$R_{UQ}(i, j) = 1 \text{ if } UQ(i) \text{ acts on } X(j), i = 1 \dots uQn, j = 1 \dots xn, [K/W] \tag{E.11}$$

$$R_U = [R_{UT}; R_{UQ}] \tag{E.12}$$

The positions in R_{UT} and R_{UQ} where there is no connection between inputs and states are defined as *Inf*.

E.3.3 System matrix A

The system matrix A defines the relation between the states and their derivatives:

$$A(i, i) = -\frac{1}{Cap(i)} \left(\sum_{k=1}^{xn} \frac{1}{R_X(k, i)} + \sum_{k=1}^{xn} \frac{1}{R_{UT}(k, i)} \right), i = 1 \dots xn \tag{E.13}$$

$$A(i, j) = \frac{1}{Cap(i)R_X(i, j)}, i = 1 \dots xn, j = 1 \dots xn, i \neq j \tag{E.14}$$

For the second order CCA building model, this leads to

$$A = \begin{bmatrix} -\frac{1}{C_c R_2} - \frac{1}{C_c(R_z + R_1)} & \frac{1}{C_c R_2} \\ \frac{1}{C_z R_2} & -\frac{1}{C_z R_2} - \frac{\dot{m}_v c_a}{C_z} \end{bmatrix} \quad (\text{E.15})$$

E.3.4 Input matrix B

The input matrix B defines the relation between the derivatives of the states and the inputs:

$$B(i, j) = \frac{1}{(Cap(i)R_U(j, i))}, i = 1 \dots xn, j = 1 \dots un \quad (\text{E.16})$$

For the second order CCA building model, the input matrix is:

$$B = \begin{bmatrix} \frac{1}{C_c(R_z + R_1)} & 0 & 0 \\ 0 & \frac{\dot{m}_v c_a}{C_z} & \frac{1}{C_z} \end{bmatrix} \quad (\text{E.17})$$

E.3.5 Output matrix C and transmission matrix D

The output matrix C defines the relation between the outputs and the states. According to the definition of Y in E.2, the output matrix is composed of 5 parts. The transmission matrix D defines the relation between the outputs and the inputs and is likewise composed of 5 parts.

The state temperatures are output of the system and therefore, the first part of the output matrix C ($xn - by - xn$) shows 1 on the diagonal and 0 elsewhere. D is an $xn - by - un$ zero matrix.

The part of C describing the heat flow between the states is an $xn.(xn-1)-by-xn$ matrix and is determined by $\dot{Q}_{X(i)-to-X(j)} = 1/R_X(i, j)(X(i) - X(j))$, $i = 1 \dots xn$, $j = 1 \dots xn$, $i \neq j$. The equivalent part of D is an $xn - by - un$ zero matrix.

The part of C describing the heat flow between the temperature inputs and the states is an $uTn.xn - by - xn$ matrix and the equivalent part of D is an $uTn.xn - by - un$ matrix. They are determined by the equation $\dot{Q}_{uT(i)-to-X(j)} = 1/R_{UT}(i, j)(UT(i) - X(j))$.

Likewise, the part of D describing the heat flow between the heat flow inputs and the states is an $uQn \cdot xn - by - un$ matrix. The elements are 1 when the heat input acts on the corresponding node and 0 otherwise. The corresponding part of C is an $uQn \cdot xn - by - xn$ zero matrix.

The user defined parts of C and D are composed according to the corresponding equations.

For the second order CCA building model, the output and direct transmission matrices are:

$$C = \begin{bmatrix} 1 & 0 \\ 0 & 1 \\ \frac{1}{R_2} & -\frac{1}{R_2} \\ -\frac{1}{R_2} & \frac{1}{R_2} \\ -\frac{1}{(R_z+R_1)} & 0 \\ 0 & 0 \\ 0 & 0 \\ 0 & -(\dot{m}_v c_a) \\ 0 & 0 \\ 0 & 0 \\ \frac{R_z}{(R_z+R_1)} & 0 \\ \frac{\dot{m}_w c_w (R_z+R_1)}{(R_z+R_{wt}+R_x)} & 0 \\ \frac{1}{(R_z+R_1)} & 0 \\ \frac{R_a}{R_2} & \frac{R_c/2}{R_2} \\ \frac{R_a}{2R_2} & \frac{R_c/2}{2R_2} \end{bmatrix}, D = \begin{bmatrix} 0 & 0 & 0 \\ 0 & 0 & 0 \\ 0 & 0 & 0 \\ 0 & 0 & 0 \\ \frac{1}{(R_z+R_1)} & 0 & 0 \\ 0 & 0 & 0 \\ 0 & 0 & 0 \\ 0 & \dot{m}_v c_a & 0 \\ 0 & 0 & 0 \\ 0 & 0 & 1 \\ \frac{R_1}{(R_z+R_1)} & 0 & 0 \\ (1 - \frac{1}{\dot{m}_w c_w (R_z+R_1)}) & 0 & 0 \\ \frac{R_c/2}{(R_z+R_1)} & 0 & 0 \\ 0 & 0 & 0 \\ 0 & 0 & 0 \end{bmatrix}$$

(E.18)

E.4 State space representation of the 2nd order CCA building model

The state space representation now becomes:

$$\begin{bmatrix} \dot{T}_c \\ \dot{T}_z \end{bmatrix} = \begin{bmatrix} -\frac{1}{C_c R_2} - \frac{1}{C_c(R_z+R_1)} & \frac{1}{C_c R_2} \\ \frac{1}{C_z R_2} & -\frac{1}{C_z R_2} - \frac{\dot{m}_v c_a}{C_z} \end{bmatrix} \begin{bmatrix} T_c \\ T_z \end{bmatrix} + \begin{bmatrix} \frac{1}{C_c(R_z+R_1)} & 0 & 0 \\ 0 & \frac{\dot{m}_v c_a}{C_z} & \frac{1}{C_z} \end{bmatrix} \begin{bmatrix} T_{ws} \\ T_{vs} \\ Q \end{bmatrix} \tag{E.19}$$

$$\begin{bmatrix} T_c \\ T_z \\ Q_{T_c-T_z} \\ Q_{T_z-T_c} \\ Q_{T_{ws}-T_c} \\ Q_{T_{ws}-T_z} \\ Q_{T_{vs}-T_c} \\ Q_{T_{vs}-T_z} \\ Q_{Q-T_c} \\ Q_{Q-T_z} \\ T_{w,mean} \\ T_{wr} \\ T_{core} \\ T_s \\ T_{op} \end{bmatrix} = \begin{bmatrix} 1 & 0 \\ 0 & 1 \\ \frac{1}{R_2} & -\frac{1}{R_2} \\ -\frac{1}{R_2} & \frac{1}{R_2} \\ -\frac{1}{(R_z+R_1)} & 0 \\ 0 & 0 \\ 0 & 0 \\ 0 & -(m_v c_a) \\ 0 & 0 \\ 0 & 0 \\ \frac{R_z}{(R_z+R_1)} & 0 \\ \frac{1}{(R_z+R_{wt}+R_x)} & 0 \\ \frac{R_a}{(R_z+R_1)} & \frac{R_c/2}{R_2} \\ \frac{R_a}{R_2} & \frac{R_c/2}{2R_2} \\ \frac{R_a}{2R_2} & \frac{R_c/2}{2R_2} \end{bmatrix} \begin{bmatrix} T_c \\ T_z \end{bmatrix} + \begin{bmatrix} 0 & 0 & 0 \\ 0 & 0 & 0 \\ 0 & 0 & 0 \\ 0 & 0 & 0 \\ \frac{1}{(R_z+R_1)} & 0 & 0 \\ 0 & 0 & 0 \\ 0 & 0 & 0 \\ 0 & m_v c_a & 0 \\ 0 & 0 & 0 \\ 0 & 0 & 0 \\ 0 & 0 & 1 \\ \frac{R_1}{(R_z+R_1)} & 0 & 0 \\ (1 - \frac{1}{m_w c_w (R_z+R_1)}) & \frac{R_c/2}{(R_z+R_1)} & 0 \\ 0 & 0 & 0 \\ 0 & 0 & 0 \\ 0 & 0 & 0 \end{bmatrix} \begin{bmatrix} T_{ws} \\ T_{vs} \\ Q \end{bmatrix} \tag{E.20}$$

E.5 Matlab functions

The matlabfunction *RC_OutputDisplay*(*xn,uTn,uQn,yUDn,yUD*) sums the outputs for the specified input parameters.

The matlabfunction *RC_makeSS*(*xn,R_X,uTn,R_UT,uQn,R_UQ,Cap,C5,D5*) constructs a state space model based on the specified input parameters.

The matlabfunction *RC_makeDiffEq*(*xn,R_X,un,uTn,R_UT,uQn,R_UQ,Cap*) constructs the differential equation notation based on the specified input parameters. This notation is used in ACADO. It also defines a range for the differential equation coefficients.

Bibliography

- [1] 11 MAART 2005 - Besluit van de Vlaamse Regering tot vaststelling van de eisen op het vlak van de energieprestaties en het binnenklimaat van gebouwen, 2005. pages 44
- [2] AKANDER, J. *The ORC method - Effective Modelling of thermal Performance of Multilayer Building Components*. PhD thesis, Kungl Tekniska Högskolan, 2000. pages 163
- [3] ANTONOPOULOS, A., VRACHOPOULOS, M., AND TZIVANIDIS, C. Experimental and theoretical studies of space cooling using ceiling-embedded piping. *Applied Thermal Engineering* 17, 4 (1997), 351–367. pages 24
- [4] ARMSTRONG, P. R., LEEB, S. B., AND NORFORD, L. K. Control with Building Mass Part I : Thermal Response Model. *ASHRAE Transactions* 112 (2006), 449–461. pages 164, 238, 247
- [5] ARMSTRONG, P. R., LEEB, S. B., AND NORFORD, L. K. Control with Building Mass Part II : Simulation. *ASHRAE Transactions* 112, Part 1 (2006), 462–473. pages 165
- [6] ASHRAE INC. *ANSI/ASHRAE Standard 55-2004: Thermal Environmental Conditions for Human Occupancy*. Atlanta, 2004. pages 11, 152, 153, 286, 289, 292
- [7] ASHRAE INC. *2008 ASHRAE Handbook - HVAC Systems and Equipment*, si edition ed. Atlanta, 2008. pages 313, 315
- [8] ASHRAE INC. *2009 ASHRAE handbook - FUNDAMENTALS*, si edition ed. Atlanta, 2009. pages 10, 31, 176, 300, 305, 312, 313, 319, 320, 321

- [9] AWBI, H., AND HATTON, A. Natural convection from heated room surfaces. *Energy and Buildings* 30, 3 (Aug. 1999), 233–244. pages 12, 13, 187, 233, 324, 325
- [10] BABIAK, J., BJARNE W. OLESEN, AND PETRAS, D. *Rehva guidebook: Low temperature heating and high temperature cooling, Embedded water based heating and cooling systems*. Rehva, Brussels, Belgium, 2007. pages 5
- [11] BABIAK, J., MINÁROVÁ, M., AND OLESEN, B. W. What is the effective thickness of a thermally activated concrete slab? In *Clima 2007 WellBeing Indoors* (Helsinki, Finland, 2007), p. 5. pages 24
- [12] BACHER, P., AND MADSEN, H. Identifying suitable models for the heat dynamics of buildings. *Energy and Buildings* 43, 7 (Feb. 2011), 1511–1522. pages 226
- [13] BALAN, R., COOPER, J., CHAO, K.-M., STAN, S., AND DONCA, R. Parameter identification and model based predictive control of temperature inside a house. *Energy and Buildings* 43, 2-3 (Feb. 2011), 748–758. pages 164
- [14] BARLOW, S., AND FIALA, D. Occupant comfort in UK offices—How adaptive comfort theories might influence future low energy office refurbishment strategies. *Energy and Buildings* 39, 7 (July 2007), 837–846. pages 155
- [15] BARTON, P., BEGGS, C. B., AND SLEIGH, P. A. A theoretical study of the thermal performance of the TermoDeck hollow core slab system. *Applied Thermal Engineering* 22 (2002), 1485–1499. pages 24
- [16] BAUMGARTNER, T., SCHWEIZER, A., GEHBAUER, H., STEINBACH, C., AND WILL, A. Thermoaktive Betondecke Neubau Büro- und Wohngebäude "Weissadlergasse" Helvetia Versicherungen. Tech. Rep. November, Frankfurter Förderprogramm Energie, Frankfurt-Am-Main, 2002. pages 5
- [17] BEAN, R., OLESEN, B. W., AND KIM, K. W. History of Radiant Heating & Cooling Systems - Part 1. *Ashrae Journal* 52, 1, 40–47. pages 3, 4

- [18] BEAN, R., OLESEN, B. W., AND KIM, K. W. History of Radiant Heating & Cooling Systems - Part 2. *Ashrae Journal* 52, 2, 50–55. pages 4
- [19] BERTAGNOLIO, S., STABAT, P., CACIOLO, M., AND CORGIER, D. IEA-ECBCS ANNEX 48 Reversible Air-Conditioning: Review of heat recovery and heat pumping solutions. Tech. rep., International Energy Agency, Energy Conservation in Buildings and Community Systems Programme, 2011. pages 175
- [20] BEST PRACTICE PROGRAMME. Energy Consumption Guide 19 : Energy Use in Offices. Tech. Rep. 2, 2000. pages 320, 322
- [21] BIANCHI, M. A. *Adaptive Modellbasierte Prädiktive Regelung einer Kleinwärmepumpenanlage*. PhD thesis, ETH Zürich, 2006. pages 162, 163, 226, 258
- [22] BRAHAM, G. D. Mechanical Ventilation and Fabric Thermal Storage. *Indoor and Built Environment* 9 (2000), 102–110. pages 5
- [23] BRAUN, J. E. Load Control Using Building Thermal Mass. *Journal of Solar Energy Engineering* 125, 3 (2003), 292. pages 35, 162, 163
- [24] BUREAU VOOR NORMALISATIE (NBN). NBN B 62-002: Thermal performance of buildings - Calculations of thermal transmittances of building components and building elements - Calculation of transmission and ventilation heat transfer coefficients, 2008. pages xl, 171
- [25] CALAY, R., HOLDO, A., AND HAMMOND, G. Natural convective heat transfer rates in rectangular enclosures. *Energy and Buildings* 27, 2 (Apr. 1998), 137–146. pages 324
- [26] CARLI, M. D., HAUSER, G., SCHMIDT, D., ZECCHIN, P., AND ZECCHIN, R. An innovative building based on active thermal slab systems. In *58th ATI National Conference*, (San Martino di Castrozza, Italy), p. 12. pages 5
- [27] CARSLAW, H., AND JAEGER, J. *Conduction of heat in solids*, 2nd ed. Oxford University Press, London, 1959. pages 16, 75, 77, 78, 83, 106
- [28] CAUSONE, F., CORGNATI, S. P., FILIPPI, M., AND OLESEN, B. W. Experimental evaluation of heat transfer coefficients between radiant ceiling and room. *Energy and Buildings* 41, 6 (June 2009), 622–628. pages 324, 325, 326

- [29] ÇENGEL, Y. A. *Introduction to Thermodynamics and Heat Transfer, 2/e*. McGraw-Hill Higher Education, University of Nevada, Reno, 2008. pages 67
- [30] CHO, S., AND ZAHEER-UDDIN, M. Predictive control of intermittently operated radiant floor heating systems. *Energy Conversion and Management* 44, 8 (May 2003), 1333–1342. pages 160, 165
- [31] CIGLER, J., AND PRIVARA, S. Subspace Identification and Model Predictive Control for Buildings. In *Int. conf. on control, Automation, Robotics and Vision* (2010), no. December, pp. 750–755. pages 163, 166
- [32] COFFEY, B., HAGHIGHAT, F., MOROFSKY, E., AND KUTROWSKI, E. A software framework for model predictive control with GenOpt. *Energy and Buildings* 42, 7 (July 2010), 1084–1092. pages 162
- [33] DAVIES, M. Wall transient heat flow using time-domain analysis. *Building and Environment* 32, 5 (Sept. 1997), 427–446. pages 163
- [34] DAVIES, M. G. Simple Models for Room Response. In *Building Heat Transfer*. John Wiley & Sons, Ltd, Chichester, 2004, ch. 14, pp. 311–334. pages 17, 163, 226, 228, 230, 323, 326
- [35] DE CARLI, M., AND OLESEN, B. Field measurements of operative temperatures in buildings heated or cooled by embedded waterbased radiant systems. *ASHRAE Transactions* 108 2 (202), 714–725. pages 5
- [36] DE DEAR, R., AND BRAGER, G. Thermal comfort in naturally ventilated buildings: revisions to ASHRAE Standard 55. *Energy and Buildings* 34, 6 (July 2002), 549–561. pages 151, 289, 290, 291, 292, 302, 303
- [37] DE DEAR, R., BRAGER, G., AND COOPER, D. Developing an Adaptive Model of Thermal Comfort and Preference. Final report ASHRAE RP-884. Tech. Rep. March, AHSRAE, Inc & Macquarie Research Ltd., 1997. pages 155, 288, 291
- [38] DOUNIS, A., AND CARAISCOS, C. Advanced control systems engineering for energy and comfort management in a building environment—A review. *Renewable and Sustainable Energy Reviews* 13, 6-7 (Aug. 2009), 1246–1261. pages 167

- [39] DUŠKA, M., LUKEŠ, J., BARTÁK, M., DRKAL, F., AND HENSEN, J. Trend in heat gains from office equipment. In *Proceedings of the 6th international conference on Indoor Climate of Buildings, Strbské Pleso* (Bratislava, 2007), pp. pp. 1–6. pages 301, 305, 320, 321
- [40] EMMERICH, S. J., MCDOWELL, T., AND ANIS, W. Investigation of the Impact of Commercial Building Envelope Airtightness on HVAC Energy Use. Tech. rep., U.S Department of Energy, Office of Building Technologies. pages 327
- [41] EUROPEAN COMMITTEE FOR STANDARDISATION. EN12831: Heating systems in buildings - Method for calculation of the heat design load, 2003. pages 181
- [42] EUROPEAN COMMITTEE FOR STANDARDIZATION. EN442-2: Radiators and convectors - Part 2, Test methods and rating, 1996. pages 70
- [43] EUROPEAN COMMITTEE FOR STANDARDIZATION. EN 15377-3 Heating systems in buildings - Design of embedded water based surface heating and cooling systems - Part 3: Optimizing for use of renewable energy sources, 2007. pages 24, 40
- [44] EUROPEAN COMMITTEE FOR STANDARDIZATION. EN15251: Indoor environmental input parameters for design and assessment of energy performance of buildings addressing indoor air quality, thermal environment, lighting and accoustics, 2007. pages xii, 152, 184, 187, 190, 286, 320, 322, 328
- [45] EUROPEAN COMMITTEE FOR STANDARDIZATION. EN 15377-1 Heating systems in buildings - Design of embedded water based surface heating and cooling systems - Part 1: Determination of the design heating and cooling capacity, 2008. pages 37
- [46] EUROPEAN PROJECT THERMCO (TECHNICAL UNIVERSITY OF DENMARK). Thermal Comfort in Transient Environments, 2009. pages 153
- [47] FERKL, L., AND SIROKY, J. Ceiling radiant cooling: Comparison of ARMAX and subspace identification modelling methods. *Building and Environment* 45, 1 (Jan. 2010), 205–212. pages 163, 166
- [48] FEUSTEL, H. E., AND STETIU, C. Hydronic radiant cooling - preliminary assessment. *Energy and Buildings* 22 (1995), 193–205. pages 326

- [49] FORT, K. Type 360 : Floor heating and hypocaust. pages 24
- [50] FRAISSE, G., VIARDOT, C., LAFABRIE, O., AND ACHARD, G. Development of a simplified and accurate building model based on electrical analogy. *Energy and Buildings 34* (2002), 1017–1031. pages 163
- [51] GAYESKI, N. T., ARMSTRONG, P. R., AND NORFORD, L. K. Predictive Pre-cooling of Thermo- Active Building Systems with Low- Lift Chillers . Part II : Experiment. *ASHRAE Journal* (2011). pages 162
- [52] GLÜCK, B. *Thermisch Bauteilaktivierung (Bauteilheizung und Bauteilkühlung)*. Rud. Otto Meyer-Umwelt-Stiftung, Hamburg, Germany, 1999. pages 24
- [53] GOUDA, M. M., DANAHER, S., AND UNDERWOOD, C. P. Building thermal model reduction using nonlinear constrained optimization. *Building and Environment 37* (2002), 1255–1265. pages 164
- [54] GRUBER, P., GWERDER, M., AND TÖDTLI, J. Predictive Control for Heating Applications. In *Proceedings of the 7th REHVA World Congress (Clima 2000/Napoli 2001)* (Napoli, Italy, 2001), p. 15pp. pages 164
- [55] GÜNTENSPERGER, W., GWERDER, M., HAAS, A., LEHMAN, B., RENGGLI, F., AND TÖDTLI, J. Control of concrete core conditioning systems. In *8th REHVA World Congress for Building Technologies (Clima 2005)* (Lausanne, Switzerland), p. 8pp. pages 34, 158
- [56] GWERDER, M., AND TÖDTLI, J. Predictive Control for Thermal Storage Management in Buildings. In *8th REHVA World Congress for Building Technologies âĂŞ CLIMA 2005*, (Lausanne, Switzerland), no. October, pp. 1–6. pages 165
- [57] GYALISTRAS, D., AND GWERDER, M. Use of Weather and Occupancy Forecasts For Optimal Building Climate Control (OptiControl): Two Years Progress Report. Tech. Rep. September, Terrestrial Systems Ecology ETH Zurich, Building Technologies Division, Siemens Switzerland Ltd., Zug, 2010. pages 260
- [58] HARRIS, N. C., AND CONDE, D. F. *Modern Air Conditioning Practice*, 2nd ed. McGraw-Hill Book Company, 1959. pages 316

- [59] HAYES, B. Why W? On the Lambert W function, a candidate for a new ‘elementary’ function in mathematics. *American Scientist* 93, 2 (2005), 104–108. pages 117
- [60] HENS, H. *Toegepaste bouwfysica : Randvoorwaarden, prestaties en materiaaleigenschappen*. Acco, Leuven, 2003. pages 16, 63
- [61] HENZE, G., PFAFFEROTT, J., HERKEL, S., AND FELSMANN, C. Impact of adaptive comfort criteria and heat waves on optimal building thermal mass control. *Energy and Buildings* 39, 2 (Feb. 2007), 221–235. pages 304
- [62] HOH, A., TSCHIRNER, T., AND MÜLLER, D. A combined thermo-hydraulic approach to simulation of active building components applying Modelica Simulating basic building behavior. In *4th International Modelica Conference* (Hamburg, Germany). pages 24
- [63] HÖNMANN, W., RECKNAGEL, H., AND SPRENGER, E. *Taschenbuch für Heizung und Klimatechnik, einschließlich Brauchwassererwärmung und Kältetechnik*. Oldenbourg Verlag, München, Wien., 1990. pages 313
- [64] HOUSKA, B., FERREAU, H. J., AND DIEHL, M. ACADO Toolkit - An Open-Source Framework for Automatic Control and Dynamic Optimization. *Optimal Control Methods and Application*. 298–312. pages 235, 250
- [65] HOWELL, J. R. Radiation Heat Transfer Configuration Factors. pages 63
- [66] HUDSON, G., AND UNDERWOOD, C. . P. A Simple building modelling procedure for MATLAB/SIMULINK. In *6th International Conference on Building Performance Simulation (IBPSA)* (Kyoto-Japan, 1999), pp. 777–783. pages 163, 164
- [67] IHM, P., AND KRARTI, M. Optimal Control Strategies for Heated Radiant Floor Systems. *ASHRAE Transactions* (2005), 535–546. pages 35, 166
- [68] INTERNATIONAL STANDARDISATION ORGANISATION. EN ISO 7730(2005) : Ergonomics of the thermal environment - Analytical determination and interpretation of thermal comfort using calculation of the PMV and PPD indices and local thermal comfort criteria., 2005. pages xxxiv, xl, xliii, 10, 39, 63, 151, 152, 153, 157, 286, 288

- [69] INTERNATIONAL STANDARDISATION ORGANISATION. EN13790 : Energy performance of buildings - Calculation of energy use for space heating and cooling, 2007. pages 320, 321, 323
- [70] ISSO KENNISINSTITUUT VOOR DE INSTALLATIESECTOR. *ISSO-Handboek Installatietechniek (2e versie)*. 2003. pages 300
- [71] J.C.COOL, F.J.SCHIJFF, AND T.J.VIERSMA. *Regeltechniek*, first ed. Agon Elsevier, Amsterdam/Brussel, 1969. pages 89
- [72] JIN, X., ZHANG, X., LUO, Y., AND CAO, R. Numerical simulation of radiant floor cooling system: The effects of thermal resistance of pipe and water velocity on the performance. *Building and Environment* 45, 11 (Nov. 2010), 2545–2552. pages 59
- [73] KAMPF, J., AND ROBINSON, D. A simplified thermal model to support analysis of urban resource flows. *Energy and Buildings* 39, 4 (Apr. 2007), 445–453. pages 163
- [74] KARLSSON, H. *Thermal system analysis of embedded building integrated heating*. PhD thesis, Chalmers University of Technology, 2006. pages 160
- [75] KELLER, B. *Klimagerechtes Bauen*. Vieweg+Teubner, Stuttgart, 1997. pages 129, 133
- [76] KHALDI, F. Master thesis: Ontwikkeling en validatie van een RC-model voor betonkernactivering. Tech. rep., KULeuven, 2007. pages 66
- [77] KHALIFA, A. Natural convective heat transfer coefficient - a review II. Surfaces in two- and three-dimensional enclosures. *Energy Conversion and Management* 42, 4 (Mar. 2001), 505–517. pages 325
- [78] KOLARIK, J., OLESEN, B. W., TOFTUM, J., AND MATTAROLO, L. Thermal Comfort, Perceived Air Quality and Intensity of SBS Symptoms During Exposure to Moderate Operative Temperature Ramps. In *Clima 2007 WellBeing Indoors* (2007). pages 153
- [79] KOLARIK, J., TOFTUM, J. R., OLESEN, B. W., AND JENSEN, K. L. Simulation of energy use, human thermal comfort and office work performance in buildings with moderately drifting operative temperatures. *Energy and Buildings* 43, 11 (July 2011), 2988–2997. pages 159

- [80] KONINKLIJK NEDERLANDS METEOROLOGISCH INSTITUUT. ww.knmi.nl, march 2008. pages 33, 294, 296
- [81] KOSCHENZ, M., AND LEHMANN, B. *Thermoaktive Bauteilsysteme tabs*. EMPA Energiesysteme/Haustechnik, Duebendorf (Switzerland), 2000. pages xxxi, xxxii, 21, 22, 23, 24, 36, 48, 51, 55, 56, 57, 62, 66, 88, 89, 151, 229, 233, 275, 325
- [82] KUHN, H. W., AND TUCKER, A. W. Nonlinear programming. In *Proceedings of the Second Berkeley Symposium on Mathematical Statistics and Probability* (Statistical Laboratory of the University of California, Berkeley, 1950), Jerzy Neyman, Ed., no. x, Univ. of Calif. Press, pp. 481–492. pages 235
- [83] KUMMERT, M. *Contribution to the application of modern control techniques to solar buildings. Simulation-based approach and experimental validation*. PhD thesis, Fondation Universitaire Luxembougoise, 2001. pages 18, 226, 258, 323
- [84] KUMMERT, M. Performance comparison of heating control strategies combining simulation and experimental results. In *Proceedings of the 9th International IBPSA conference* (Montréal, Canada, 2005), IBPSA, pp. 563–570. pages 162
- [85] LEE, K., AND BRAUN, J. Model-based demand-limiting control of building thermal mass. *Building and Environment* 43, 10 (Oct. 2008), 1633–1646. pages 164
- [86] LEE, K.-H., AND BRAUN, J. E. An Experimental Evaluation of Demand Limiting Using Building Thermal Mass in a Small Commercial Building. *ASHRAE Transactions* 112, 2002 (2006), 559–572. pages 164
- [87] LEHMANN, B., DORER, V., AND KOSCHENZ, M. Application range of thermally activated building systems tabs. *Energy and Buildings* 39, 5 (May 2007), 593–598. pages xli, 34, 40, 151, 170, 181, 184, 185, 208
- [88] LIENHARD IV, J. H., AND LIENHARD V, J. H. *A heat transfer textbook, third edition*. Phlogiston Press, Cambridge, Massachusetts, USA, 2006. pages 2, 14, 55
- [89] LIM, J., JO, J., KIM, Y., YEO, M., AND KIM, K. Application of the control methods for radiant floor cooling system in residential buildings. *Building and Environment* 41, 1 (Jan. 2006), 60–73. pages 251

- [90] MACIEJOWSKI, J. *Predictive Control with Constraints*. Pearson Education, Prentice Hall, Harlow, Essex, 2002. pages 138, 144, 162, 226
- [91] MASY, G. *Definition and validation of a simplified multizone dynamic building model connected to heating system and HVAC unit*. Doctorat en sciences de l'ingénieur, Université de Liège, 2008. pages 35, 163, 226, 230, 232, 323
- [92] MEIERHANS, R. Slab cooling and earth coupling. *ASHRAE Transactions* 99, 2 (1993), 8. pages 5, 24
- [93] MORARI, M., AND LEE, J. H. Model predictive control : past , present and future. *Computers & Chemical Engineering Engineering* 23 (1999), 667–682. pages 167, 258
- [94] NATIONAL EDUCATION NETWORK GALLERY. gallery.e2bn.org, 2011. pages 4
- [95] NEUMANN, C., AND HERKEL, S. Langzeitmonitoring der Demonstrationsgebäude im Rahmen des Forschungs- programms EnBau:MONITOR. Tech. rep., Fraunhofer ISE, Gruppe Solares Bauen, Freiburg, 2005. pages 5, 29, 31, 171
- [96] NICOL, F., AND HUMPHREYS, M. Derivation of the adaptive equations for thermal comfort in free-running buildings in European standard EN15251. *Building and Environment* 45, 1 (Jan. 2010), 11–17. pages 152, 258, 290
- [97] OLESEN, B. W. Cooling and heating of buildings by activating their thermal mass with embedded hydronic pipe systems. In *ASHRAE-CIBSE* (Dublin, Ireland, 2001), p. 19. pages 5, 158
- [98] OLESEN, B. W., CARLI, M. D., SCARPA, M., AND KOSCHENZ, M. Dynamic Evaluation of the Cooling Capacity of Thermo-Active Building Systems. *ASHRAE Transactions* 112, 2 (2006). pages 24
- [99] OLESEN, B. W., PH, D., AND SOMMER, K. Control of Slab Heating and Cooling Systems Studied by Dynamic Computer Simulations. *ASHRAE Transactions* (2002), 698–. 707. pages 34, 158, 286, 289, 291
- [100] OSELAND, N. A. Predicted and reported thermal sensation in climate chambers, offices and homes. *Energy and Buildings* 23 (1995), 105–115. pages 154, 302

- [101] PARYS, W., SAELENS, D., AND HENS, H. Coupling of dynamic building simulation with stochastic modelling of occupant behaviour in offices - a review-based integrated methodology. *Journal of Building Performance Simulation*, 933000804 (2011), 1–20. pages 130, 134, 184, 322
- [102] PASSEL, W. V., HERDT, R. D., REET, T. V., MOENSENS, N., AND SOURBRON, M. THERMAC : Handboek voor het verwarmen en natuurlijk koelen van THERmisch ACTieve gebouwen. Tech. rep., 2008. pages 29, 62
- [103] PFAFFEROTT, J., HERKEL, S., KALZ, D., AND ZEUSCHNER, A. Comparison of low-energy office buildings in summer using different thermal comfort criteria. *Energy and Buildings* 39, 7 (July 2007), 750–757. pages 154
- [104] PFAFFEROTT, J., AND KALZ, D. Thermoaktive Bauteilsysteme. Tech. rep., BINE Informationsdienst, 2007. pages 5
- [105] PRÍVARA, S., ŠIROKÝ, J., FERKL, L., AND CIGLER, J. Model predictive control of a building heating system: The first experience. *Energy and Buildings* 43, 2-3 (Feb. 2011), 564–572. pages 166
- [106] PROAKIS, J. G., AND MANOLAKIS, D. G. *Digital Signal Processing : Principles, Algorithms an Applications*, third ed. Prentice-Hall, Inc., New Jersey, 1996. pages 130, 131
- [107] REINHART, C. F. Lightswitch-2002: a model for manual and automated control of electric lighting and blinds. *Solar Energy* 77, 1 (Jan. 2004), 15–28. pages 322
- [108] REN, M. J., AND WRIGHT, J. A. Optimal Control of Fabric Thermal Storage Systems. In *Clima 2000* (Brussels, Belgium, 1997), p. 18p. pages 163
- [109] REN, M. J., AND WRIGHT, J. A. Predictive Optimal Control of Fabric Thermal Storage Systems. In *5th International IBPSA Conference* (Prague, Czech Republic, 1997), p. 8pp. pages 163
- [110] REN, M. J., AND WRIGHT, J. A. Slab Thermal Storage System. *Building and Environment* 1323, 97 (1998), 43–52. pages 24, 163
- [111] RIJKSEN, D., WISSE, C., AND A.W.M. VAN SCHIJNDEL. Reducing peak requirements for cooling by using thermally activated building systems. *Energy and Buildings* 42, 3 (Mar. 2010), 298–304. pages 159

- [112] ROULET, C. Real heat recovery with air handling units. *Energy and Buildings* 33, 5 (May 2001), 495–502. pages 179
- [113] RUSSELL, M. B., AND SURENDRAN, P. N. Influence of active heat sinks on fabric thermal storage in building mass. *Applied Energy* 70 (2001), 17–33. pages 24
- [114] SAELENS, D., PARYS, W., AND BAETENS, R. Energy and comfort performance of thermally activated building systems including occupant behavior. *Building and Environment* 46, 4 (Apr. 2011), 835–848. pages 322
- [115] SAKELLARI, D., FORSEN, M., AND LUNDQVIST, P. Investigating control strategies for a domestic low-temperature heat pump heating system. *International Journal of Refrigeration* 29, 4 (June 2006), 547–555. pages 160
- [116] SCHIAVON, S., LEE, K. H., BAUMAN, F., AND WEBSTER, T. Influence of raised floor on zone design cooling load in commercial buildings. *Energy and Buildings* 42, 8 (Aug. 2010), 1182–1191. pages 170, 171, 181
- [117] SCHIAVON, S., LEE, K. H., BAUMAN, F., AND WEBSTER, T. Simplified calculation method for design cooling loads in underfloor air distribution (UFAD) systems. *Energy and Buildings* 43, 2-3 (Feb. 2011), 517–528. pages 170
- [118] SCHILD, P., AND MYSEN, M. AIVC Technical Note 65, Recommendations on Specific Fan Power and Fan System Efficiency. Tech. rep., AIVC, 2009. pages 179
- [119] SCHILD, P. G. AIVC VIP n°6 : Air-to-Air Heat Recovery in Ventilation Systems. Tech. rep., AIVC, 2004. pages 179
- [120] SCHMIDT, D. *Methodology for the Modelling of Thermally Activated Building Components in Low Exergy Design (Doctoral Thesis)*. PhD thesis, Royal institute of Technology, 2004. pages 24
- [121] SEEM, J. E. *Modeling of heat transfer in buildings*. PhD thesis, University of Wisconsin-Madison, 1987. pages 17
- [122] SOLAR ENERGY LABORATORY. *Trnsys 16: A transient system simulation program*. University of Madison, Wisconsin, 2007. pages 23, 24, 129, 169, 299

- [123] SOLAR ENERGY LABORATORY, AND TRANSSOLAR ENERGIETECHNIK GMBH. Multizone building modeling with type 56 and TRNBUILD. In *Trnsys 16 : A transient simulation program*, 2007-02 ed. Solar Energy Laboratory, University of Wisconsin-Madison, 2007, ch. Vol. 6, p. 213. pages 193, 323, 325, 332
- [124] SOURBRON, M., DE HERDT, R., VAN REET, T., VAN PASSEL, W., BAELMANS, M., AND HELSEN, L. Efficiently produced heat and cold is squandered by inappropriate control strategies: A case study. *Energy and Buildings* 41, 10 (Oct. 2009), 1091–1098. pages 160
- [125] SOURBRON, M., AND HELSEN, L. Evaluation of adaptive thermal comfort models in moderate climates and their impact on energy use in office buildings. *Energy and Buildings* 43, 2-3 (Feb. 2011), 423–432. pages 285
- [126] SOURBRON, M., KHALDI, F., BAELMANS, M., AND HELSEN, L. Validation of a thermally activated hollow core slab RC-model with measurements and FEM simulations. In *Building Physics Symposium in honour of Professor Hugo Hens* (Leuven, 2008), S. Roels, G. Vermeir, and D. Saelens, Eds., vol. 1, Laboratory of Building Physics, University of Leuven, pp. 263–266. pages 66
- [127] SPITLER, J. D., AND REES, S. J. Quantitative Comparison of North American and U . K . Cooling Load Calculation Procedures — Methodology. *ASHRAE Transactions* 104, 2 (1998), 36–46. pages 171
- [128] SUN, J., AND REDDY, A. Optimal control of building HVAC&R systems using complete simulation-based sequential quadratic programming (CSB-SQP). *Building and Environment* 40 (2005), 657–669. pages 162
- [129] SWEDISH ENERGY AGENCY. Energy Use in Offices 2005. Tech. rep., 2005. pages xxxvii, 31, 320, 321, 322
- [130] TIAN, Z., AND LOVE, J. Radiant slab cooling: a case study of building energy performance. In *SimBuild 2006, MIT, IBPSA-USA* (Cambridge, Massachusetts, USA). pages 5
- [131] TIAN, Z., AND LOVE, J. Energy performance optimization of radiant slab cooling using building simulation and field measurements. *Energy and Buildings* 41, 3 (Mar. 2009), 320–330. pages 158

- [132] TÖDTLI, J., GWERDER, M., LEHMANN, B., RENGGLI, F., AND DORER, V. *TABS Control, Steuerung und Regelung von thermoaktiven Bauteilsystemen*. Faktor Verlag, Zurich, 2009. pages 159, 290, 323
- [133] TROCH, E. Master thesis: De invloed van bouwkundige ingrepen op de prestaties van betonkernactivering in kantoorgebouwen. Tech. rep., KULeuven, 2010. pages 332
- [134] VAES, G. Master thesis: Parameteridentificatie van een RC-model voor BKA o.b.v. CFD berekeningen en metingen. Tech. rep., KULeuven, 2008. pages 66
- [135] VANBRONKHORST, D., PERSILY, A., AND EMMERICH, S. Energy Impacts of Air Leakage in US Office Buildings. In *16th AIVC Conference* (Palm Springs, USA, 1995). pages 327
- [136] VANDERLINDEN, A., BOERSTRA, A., RAUE, A., KURVERS, S., AND DEDEAR, R. Adaptive temperature limits: A new guideline in The Netherlands, A new approach for the assessment of building performance with respect to thermal indoor climate. *Energy and Buildings* 38, 1 (Jan. 2006), 8–17. pages 286, 289
- [137] VANHOOF, J., AND HENSEN, J. Quantifying the relevance of adaptive thermal comfort models in moderate thermal climate zones. *Building and Environment* 42, 1 (Jan. 2007), 156–170. pages 156, 291, 296
- [138] VEREIND DEUTSCHE INGENIEURE. *VDI-Wärmeatlas*. 2006. pages 313, 315
- [139] VEREIND DEUTSCHER INGENIEURE. VDI2078: Berechnung der Kühllast klimatisierter Räume (VDI-Kühllastregeln), 1996. pages 181, 300, 305, 320
- [140] VERHELST, C. *Model predictive control of ground coupled heat pump systems in office buildings*. PhD thesis, 2012. pages 282
- [141] VLIET-BIS 970.389/WTCB. Kantoor 2000: studie van energieverbruik en binnenklimaat van kantoren, Eindverslag, 2001. pages 29
- [142] WAGNER, A., GOSSAUER, E., MOOSMANN, C., GROPP, T., AND LEONHART, R. Thermal comfort and workplace occupant satisfaction—Results of field studies in German low energy office buildings. *Energy and Buildings* 39, 7 (July 2007), 758–769. pages 154

- [143] WANG, S., AND XU, X. Optimal and robust control of outdoor ventilation airflow rate for improving energy efficiency and IAQ. *Building and Environment* 39, 7 (July 2004), 763–773. pages 251
- [144] WEBER, T., AND JOHANNESSON, G. An optimized RC-network for thermally activated building components. *Building and Environment* 40, 1 (Jan. 2005), 1–14. pages 23, 50, 89, 137, 140, 163
- [145] WEBER, T., JOHANNESSON, G., KOSCHENZ, M., LEHMANN, B., AND BAUMGARTNER, T. Validation of a FEM-program (frequency-domain) and a simplified RC-model (time-domain) for thermally activated building component systems (TABS) using measurement data. *Energy and Buildings* 37, 7 (July 2005), 707–724. pages 5, 23, 24, 31, 128, 129, 137
- [146] WEITZMANN, P., PITTARELLO, E., AND OLESEN, B. W. The cooling capacity of the Thermo Active Building System combined with acoustic ceiling. In *8th symposium on Building Physics in the Nordic Countries*, pp. Copenhagen, Denmark. pages 151
- [147] WEITZMANN, P., AND SVENDSEN, S. Detailed measurements and modelling of thermo active components using a room size test facility. In *7th Nordic Building Physics Symposium* (Reykjavík, Iceland, 2005). pages 25
- [148] WIMMER, R. W. *Regelung einer Wärmepumpenanlage mit Model Predictive Control*. PhD thesis, ETH Zürich, 2004. pages 163, 258
- [149] ZAHEER-UDDIN, M., G.R.ZHENG, AND CHO, S.-H. Optimal operation of an embedded-piping floor heating system with control input constraints. *Energy Conservation Managment* 38, 7 (1997), 713–725. pages 162, 163, 165
- [150] ZAHEER-UDDIN, M., ZHANG, Z. L., AND CHO, S. H. Augmented control strategies for radiant floor heating systems. *International Journal of Energy Research* 26, 1 (Jan. 2002), 79–92. pages 159
- [151] ZAHEER-UDDIN, M., AND ZHENG, G. R. Optimal control of time-scheduled heating, ventilating and air conditioning processes in buildings. *Energy Conversion and Management* 41 (2000), 49–60. pages 165

- [152] ZIMMERMAN, M., AND ANDERSSON, J. IEA ECBCS Programme Annex 28: Low Energy Cooling, Case Study Buildings. Tech. rep., EMPA ZEN, Duebendorf (Switzerland), 1999. pages 5

Curriculum

Maarten Sourbron

Rotselaarsesteenweg 5
3018 Wijgmaal
016/22 39 12 - 0472/83 32 58
Maarten.Sourbron@fulladsl.be
Belgian

Born in Duffel, September, 27th 1976

Married to Marleen Gysen

3 daughters: Kaat (°2002), Hanne (°2004) and Lena (°2007)

Career

2012: Lessius, Campus De Nayer

Guestlector for the courses “Thermodynamica 2” en “Thermotechniek en stromingsmachines” at the Faculty of Engineering Technology, KULeuven.

2007-2012: KULeuven, Department of Mechanical Engineering

Phd “Dynamic thermal behaviour of buildings with concrete core activation” (promotor prof. L. Helsen, co-promotor prof. M. Baelmans)

Starting from Februari, 2012: research engineer, European ERASME-project “GEOTABS”.

2004-2007: Hogeschool voor Wetenschap & Kunst, De Nayer Instituut

Coordinator of the IWT-TIS-project IDEG: “Integratie van Duurzame Energie in Gebouwen” (Integration of Sustainable Energy in Buildings) (until 09/2006) and research engineer, IWT-TETRA-project THERMAC: Thermisch actieve gebouwen (Thermally Activated Buildings)

2002-2004: Stabo ingenieurs (Leuven)

Design Engineer: technical installation of buildings (HVAC, electricity, lighting)

1999-2002: Hogeschool voor Wetenschap & Kunst, De Nayer Instituut
Research engineer: “Instralings simulatie en optimalisatie van thermische zonne-energie” (Solar thermal energy) and “Thermische zonne-energie, warmteterugwinning en warmtepomp als verwarmings- en/of koelconcept in residentiële woningen” (Heat pumps in dwellings)

Education 1994-1999: KULeuven

Burgerlijk Werktuigkundig-Elektrotechisch ingenieur, Mechanical Engineering, specialisation Energy Technology

1988-1994: Vita-et-Pax-college Schoten

Latin-Mathematics

Publications

Articles in internationally reviewed academic journals

Sourbron, M., Verhelst, C., Helsen, L. (2012). Building models for Model Predictive Control of office buildings with Concrete Core Activation. *Journal of Building Performance Simulation*, art.nr. TBPS-2011-0043.

Sourbron, M., Helsen, L. (2010). Evaluation of adaptive thermal comfort models in moderate climates and their impact on energy use in office buildings. *Energy and Buildings*, 43(2-3), 423-432 (citations : 1) (IF publication year : 2.05) (IF most recent : 2.05).

Sourbron, M., De Herdt, R., Van Reet, T., Van Passel, W., Baelmans, M., Helsen, L. (2009). Efficiently produced heat and cold is squandered by inappropriate control strategies: a case study. *Energy and Buildings*, 41(10), 1091-1098 (citations : 1) (IF publication year : 1.59) (IF most recent : 2.05).

Other academic books as author

Van de Meulebroecke, A., Suijkerbuik, M., Verhaert, I., Hendriksen, L., Sourbron, M., Steendam, K. (2006). *Code van goede praktijk voor warmtepompinstallaties in de woningbouw*. Belgium: Ode Vlaanderen.

Papers at international scientific conferences and symposia, published in full in proceedings

Sourbron, M., Helsen, L. (2010). *Thermally activated building systems in office buildings: impact of control strategy on energy performance and thermal comfort*. International Conference on System Simulation in Buildings. Liege, 13-15 December 2010.

Sourbron, M., Helsen, L. (2010). *Identifying appropriate thermal comfort*

criteria for buildings equipped with thermally active building systems (TABS). In : 10th REHVA WORLD CONGRESS "Sustainable Energy Use in Buildings". CLIMA 2010. Antalya, Turkey, 9-12 May 2010.

Sourbron, M., Baelmans, M., Helsen, L. (2009). *Thermal response of thermally activated building systems (TABS) in office buildings.* In : Proceedings of EFFSTOCK 2009. Effstock 2009. Stockholm, Sweden, 14-17 June 2009.

Sourbron, M., Khaldi, F., Baelmans, M., Helsen, L. (2008). *Validation of a thermally activated hollow core slab RC-model with measurements and FEM simulations.* In : Proceedings of the Symposium Building Physics. Symposium Building Physics. Leuven, Belgium, Oct 29-31, 2008.

Sourbron, M., Verhelst, C., Helsen, L. (2008). *Monitoring an office building equipped with thermally activated building systems (TABS) and a ground source heat pump.* In : Proceedings of the Heat Pump Platform Symposium. Heat Pump Platform Symposium. Sint-Katelijne-Waver, Belgium, Sep 17, 2008.

Sourbron, M., De Herdt, R., Van Reet, T., Van Passel, W., Baelmans, M., Helsen, L. (2007). *Thermal activated building systems (TABS): current practice.* In : Proceedings of the Passive House Symposium. Passive House Symposium. Brussels, Belgium, Sep 7, 2007 (pp. 303-310).

Papers at other scientific conferences and symposia, published in full in proceedings

Sourbron, M. (2007). *Aspecten van regeling met betonkernactivering.* In : Proceedings of the Duurzame energieinstallaties: thermische activering en ventilatie in gebouwen. Duurzame energie-installaties: thermische activering en ventilatie in gebouwen. Sint-Katelijne-Waver, Belgium, Sep 13, 2007.

Meeting abstracts, presented at international scientific conferences and symposia, published or not published in proceedings or journals

Sourbron, M., Helsen, L. (2011). *Thermally Activated Building Systems: Exploiting inertia.* KIC-InnoEnergy Storage. 22-23 November 2011.

Verhelst, C., Sourbron, M., Antonov, S., Helsen, L. (2011). *Towards MPC for office buildings with TABS connected to a GCHP system.* IBPSA Model Predictive Control in Buildings Workshop. Montréal: IBPSA.

Sourbron, M., Helsen, L. (2009). *Do adaptive thermal comfort models lower energy use in moderate climates?.* Strategic Energy Forum. Brussels, Belgium,

10 December 2009.

Helsen, L., Verhelst, C., Sourbron, M. (2008). *Thermal systems in buildings: a hot research topic at the Division Applied Mechanics and Energy Conversion (K.U. Leuven)*, Proceedings of the Heat Pump Platform Symposium. Heat Pump Platform Symposium. Sint-Katelijne-Waver, Belgium, Sep 17, 2008.

Sourbron, M., Helsen, L. (2008). *Monitoring of ICT3 and ICT4 office buildings Wetenschapspark Arenberg*. Annex 48 meeting. Münster, Germany, 8-9 April 2008.

Sourbron, M., Helsen, L. (2008). *The effect of control strategy on the energy efficiency of thermally activated building systems*. Strategic Energy Forum. Brussels, 16 December 2008.

Sourbron, M., Baelmans, M., Helsen, L. (2007). *How efficiently produced heat and cold is squandered by inappropriate control strategies: Analysing TABS control strategies by measurements and simulations*. Common technical briefing of ECBCS and HPP, Energy conservation in buildings and heat pump use. Brussels, Belgium, Nov 14, 2007.

Sourbron, M., De Herdt, R., Van Reet, T., Van Passel, W., Baelmans, T., Helsen, L. (2007). *Control of an office building equipped with thermally activated building systems (TABS): a case study*, Proceedings of the IEA Annex 48 Meeting. IEA Annex 48 Meeting. Luik, Belgium, Oct 1, 2007.

Meeting abstracts, presented at other scientific conferences and symposia, published or not published in proceedings or journals

Sourbron, M. (2012). *Dynamisch simuleren van Betonkernactivering*. Geotabs Workshop. Leuven, 4 June 2012.

Sourbron, M., Helsen, L. (2010). *Betonkernactivering : benutten van traagheid*. Studiedag Geothermie en Betonkernactivering. Hasselt, Belgium, 20 May 2010 <http://www.dubolimburg.be/nl/betonkern>.

Sourbron, M., Helsen, L. (2010). *De invoering van het Quest/EHPA-product label voor warmtepompen in België*. WPP Symposium. Sint-Katelijne-Waver, Belgium, 15 september 2010.

Hoogmartens, J., Sourbron, M., Helsen, L. (2009). *Energie in gebouwen: meten is weten*. VERA Overlegavond Beleidsmakers Vlaams-Brabant. Kampenhout, Belgium, 8 Oktober 2009.

Sourbron, M., Helsen, L. (2008). *ICT3 en ICT4 kantoorgebouwen Wetenschapspark Arenberg*. Interleuven. 15 April 2008.

Misc.

Hoogmartens, J., Helsen, L., Sourbron, M., Saelens, D., Parys, W., Verhelst, C. (2011). *GEOTABS: Towards optimal design and control of geothermal heat pumps combined with thermally activated building systems in offices*.

Sourbron, M. (2010). *Dynamisch gedrag van betonkernactivering : van projectonderzoek tot doctoraatsonderzoek*.

Helsen, L., Sourbron, M., Verhelst, C. (2008). *Milieutechnologie : Grondgekoppelde warmtepompen als bron voor betonkernactivering*. In: Nieuwsbrief Milieutechnologie (10-extra). Mechelen, Belgium: Kluwer.

Sourbron, M., Van Passel, W., Helsen, L. (2008). *Het belang van regelstrategie in thermisch actieve gebouwen -metingen in een kantoorgebouw met betonkernactivering*. In: De Onderneming, 848, 70-73: Distrigraph bvba.

